

---

# **Qualitative and quantitative screening of side-chain profiles of cereal grain arabinoxylans**

---

Zur Erlangung des akademischen Grades eines  
DOKTORS DER NATURWISSENSCHAFTEN

(Dr. rer. nat.)

der KIT-Fakultät für Chemie und Biowissenschaften  
des Karlsruher Instituts für Technologie (KIT)

genehmigte

DISSERTATION

von

Rachel Renae Schendel, M.Sc.

aus

Rochester, Minnesota, Vereinigte Staaten von Amerika

KIT-Dekan: Prof. Dr. Willem Klopper

Referent: Prof. Dr. Mirko Bunzel

Korreferent: Prof. Dr. Andrea Hartwig

Tag der mündlichen Prüfung: 22. Juli 2016







# Acknowledgements

---

*I thank my doctoral adviser, Professor Dr. Mirko Bunzel, for giving me the opportunity to come to Germany and pursue a doctoral degree under your supervision. Thank you for generously sharing your knowledge and scientific expertise and for always making time for your students. Thank you for working so hard to cultivate a positive team attitude among your students and for modeling that yourself. Thank you for challenging me—you always expected me to do excellent work and believed that I could meet those standards. And because you believed in me, you gave me courage to keep trying until I grew to meet those positive expectations. Thank you also for helping me make the adjustment to life in Germany, in particular for opening your home to me for that first month (thank you as well, Diana!) and for letting me speak German to you long before I was any good at it.*

*Thank you to all of my labmates and coworkers in the AK Bunzel family. You are an outstanding team, and it has been an honor to be a member. Special thanks are due to Dr. Andreas Hildebrand, who helped me navigate the bureaucratic maze of paperwork upon my arrival and was always ready to help with any problems, big or small. Thank you for helping me get settled into my new home in Germany and for making me feel welcome to the Institute right away. Thank you to Dr. Daniel Wefers and Dr. Judith Schäfer for your friendship and support, both at work and personally. Thank you for working as a team and for sharing what you had learned with me. You are both exceptional scientists, and I'm proud to have worked with you. Thank you to Martin Waterstraat for being such a good-natured office-mate and for helping me plan lots of practical jokes. Thank you to Andreas Becker, Felix Ubat, and Beate Kohn for your cheerful team spirits and the positive atmosphere in the lab. Thank you to my Institute coworkers from AK Hartwig and your kind, friendly, generous hearts. Thank you all for adopting me into the "Lemi" family.*

*Many thanks to my hard-working team of diplomand students: Andreas Becker, Marleen Meyer, Cathrin Wilms, Isabella Sackmann, Ann-Katrin Puchbauer, Cecile Karrer, Natalie Britscho, and Ute Schmitt. Thank you for the enthusiasm, diligence, and creativity you invested into our research.*

*Thank you to Prof. Dr. Andrea Hartwig for serving as second thesis examiner.*

*I thank Dr. Catrin Tyl for the capable NMR measurements of many samples and your friendship.*

*Thank you to my dear friend, Dr. Sarah Fremgaard Leuchtgens, for proofreading the thesis draft. Thank you to Brother Louie for your long-distance phone calls while I was writing the thesis that made me laugh, cheered me up, and motivated me to keep on writing.*

*Thank you to both my Kyлло and Schendel family for your love and prayers. Thank you especially to my parents, who have consistently modeled hard work, a love of learning, and lives lived to the glory of God. Thank you for homeschooling me, even when most of your friends thought you were strange because of it.*

*A thousand thanks to my loving husband, Isaac Smith Schendel, for your patience with many late nights and for always believing that I could and would succeed. Thank you for marrying me, dear sir.*

*Finally, I thank God, my Creator, for His unfailing love and the gifts of life, health, and the ability to observe and learn from His handiwork.*



# *Dedication*

---

**SOLI DEO GLORIA**



# Table of Contents

---

<i>ACKNOWLEDGEMENTS</i> .....	I
<i>DEDICATION</i> .....	III
LIST OF ABBREVIATIONS .....	X
1. LITERATURE REVIEW .....	1
1.1. Feruloylated arabinoxylans in cereal grains .....	2
1.2. Structure of feruloylated arabinoxylans in cereal grains .....	3
1.2.1. Substitution patterns in cereal grain arabinoxylans .....	4
1.2.1.1. Substitution with $\alpha$ -L-arabinofuranose .....	4
1.2.1.2. Substitution with acetyl groups .....	10
1.2.1.3. Substitution with uronic acids .....	11
1.2.1.4. Cereal grain arabinoxylans are substituted with feruloylated and coumaroylated side-chains .....	12
1.2.1.5. Substitution of cereal grain arabinoxylans with non-feruloylated or coumaroylated oligosaccharide side-chains has not been proven yet .....	15
1.2.2. Ferulate crosslinking of cereal grain arabinoxylans .....	16
1.2.2.1. Dehydrodiferulates .....	16
1.2.2.2. Cyclobutane dimers .....	18
1.2.3. Chain length of cereal grain arabinoxylans .....	18
1.3. Enzymatic fermentability of arabinoxylans is strongly affected by arabinoxylan structural differences .....	20
1.4. Arabinoxylan structural differences influence food processing outcomes .....	22
1.4.1. Arabinoxylans and bread-baking .....	22
1.4.2. Arabinoxylans and refrigerated dough quality .....	23
1.4.3. Arabinoxylans and beer brewing .....	23
1.5. Potential human health benefits are discussed for arabinoxylans .....	24
1.5.1. Arabinoxylans belong to the dietary fiber complex .....	24
1.5.2. Arabinoxylans have prebiotic properties .....	25
1.5.3. Cereal ferulates could have beneficial health effects .....	25
1.6. Biosynthesis of arabinoxylans .....	26
1.6.1. Xylan backbone synthesis .....	26
1.6.2. Xylan backbone substitution .....	28
1.6.3. Feruloylation of the arabinoxylan polymer .....	29
1.6.4. Dehydrodiferulate formation and arabinoxylan crosslinking .....	31

1.7. Arabinoxylans' role in plants.....	31
2. STUDY OBJECTIVES .....	33
3. MATERIALS AND METHODS.....	35
3.1. Plant materials.....	35
3.2. Isolation of arabinoxylans from plant materials.....	35
3.2.1. Solubilization of arabinoxylan polymers .....	35
3.2.2. Isolation of plant cell wall materials/dietary fiber .....	36
3.2.2.1. Protein correction of dietary fiber .....	37
3.3. Composition analysis of arabinoxylans .....	39
3.3.1. Monosaccharide composition .....	39
3.3.1.1. Hydrolysis methods.....	39
3.3.2. Detection methods.....	40
3.3.3. Phenolic acid profile .....	40
3.3.4. Determination of acetyl contents .....	41
3.4. Structural profiling analysis of arabinoxylans .....	42
3.4.1. Linkage patterns of arabinoxylans.....	42
3.4.1.1. Analysis of partially methylated alditol acetates .....	42
3.4.2. Side-chain profiles of arabinoxylans.....	45
3.4.2.1. Release of (non)feruloylated arabinoxylan mono-/oligosaccharides from arabinoxylans .....	45
3.4.2.2. Separation of non-feruloylated arabinoxylan mono-/oligosaccharides from feruloylated compounds .....	46
3.4.2.3. Fractionation and isolation of pure feruloylated mono- /oligosaccharides .....	47
3.4.2.4. Fractionation and isolation of pure non-feruloylated arabinoxylan oligosaccharides.....	48
3.4.2.5. Structural characterization of purified arabinoxylan oligosaccharides: Application of liquid chromatography coupled with mass spectrometric detection .....	49
3.4.2.6. Structural characterization of purified arabinoxylan oligosaccharides: Application of nuclear magnetic resonance spectroscopy .....	51
3.4.2.7. Structural characterization of purified arabinoxylan oligosaccharides: Determination of monosaccharides' chiral configurations .....	54
3.4.2.8. (Feruloylated) side-chain screening methods .....	54
4. RESULTS AND DISCUSSION: <i>CHAPTER ONE</i> .....	57
<i>Characterization of the feruloylated arabinoxylans from intermediate wheatgrass (Thinopyrum     intermedium)</i>	
4.1. Monosaccharide composition, linkage analysis, and phenolic acid profile .....	57
4.2. Isolation of feruloylated oligosaccharides from insoluble intermediate wheatgrass fiber .....	58

4.3. Identification of isolated feruloylated oligosaccharides released by mildly acidic hydrolysis.....	59
4.4. Identification of isolated feruloylated oligosaccharides released by enzymatic (Driselase) hydrolysis .....	65
4.5. Conclusion .....	66
5. RESULTS AND DISCUSSION: <i>CHAPTER TWO</i> .....	67
<i>Feruloylated side-chain profiles in cereal grain arabinoxylans: Development of a quantitative LC-DAD/MS screening approach</i>	
5.1. Isolation of feruloylated side-chain standard compounds .....	67
5.2. Reduction of feruloylated side-chain mono- /oligosaccharides.....	68
5.3. Method validation .....	69
5.4. MS <sup>2</sup> fragmentation of reduced standard compounds.....	70
5.5. Application of the chromatographic feruloylated side-chain profiling method to cereal grain materials.....	71
5.6. Method limitations.....	72
5.7. Cereal grains possess unique feruloylated side-chain profiles .....	73
6. RESULTS AND DISCUSSION: <i>CHAPTER THREE</i> .....	75
<i>Quantitative profiling of feruloylated side-chains in cereal arabinoxylans using HSQC-NMR</i>	
6.1. Method development.....	75
6.2. Method validation .....	78
6.3. Application of the method to cereal samples .....	80
6.4. Comparison of the two profiling methods.....	80
7. RESULTS AND DISCUSSION: <i>CHAPTER FOUR</i> .....	83
<i>Isolation and identification of <math>\alpha</math>-D-xylopyranosyl-(1<math>\rightarrow</math>3)-L-arabinose as a non-feruloylated oligomeric side-chain in cereal arabinoxylans</i>	
7.1. Release and isolation of non-feruloylated arabinoxylan side-chains .....	83
7.2. Structural characterization of a dimeric non-feruloylated arabinoxylan side-chain structure.....	85
7.2.1. Mass spectrometric analysis .....	85
7.2.2. Monosaccharide composition and methylation analysis.....	85
7.2.3. NMR analysis.....	85
7.3. Qualitative screening of cereal grain materials.....	87
8. COMPREHENSIVE DISCUSSION .....	89
9. SUMMARY .....	93
10. ZUSAMMENFASSUNG.....	95
11. REFERENCES.....	97

12.	APPENDICES.....	129
12.1.	Instruments.....	129
12.2.	Chemicals.....	131
12.3.	Enzymes.....	141
12.4.	Prepared reagents and solutions .....	142
12.5.	Experimental methods .....	143
12.5.1.	Preparative isolation of insoluble dietary fiber from cereal grains .....	143
12.5.2.	Drying isolated insoluble fiber samples.....	143
12.5.3.	Methods for characterization of dietary fiber samples .....	143
12.5.3.1.	Ash correction of insoluble fiber samples .....	143
12.5.3.2.	Colorimetric protein correction of insoluble fiber samples .....	143
12.5.3.3.	Determination of ester-linked phenolic acids .....	144
12.5.3.4.	Determination of monosaccharide composition of insoluble fiber materials (Saeman hydrolysis) .....	145
12.5.3.5.	Methylation analysis of insoluble fiber samples (linkage analysis via partially methylated alditol acetates) .....	146
12.5.4.	Methods for release and isolation of feruloylated oligosaccharides .....	147
12.5.4.1.	Mild acid degradation (semi-selective side-chain hydrolysis method for preparative quantities).....	147
12.5.4.2.	Enzymatic degradation (Driselase method).....	147
12.5.4.3.	Amberlite XAD-2 separation of feruloylated oligosaccharides from acidic or enzymatic hydrolysates .....	148
12.5.4.4.	Sephadex LH-20 separation of feruloylated oligosaccharides .....	148
12.5.4.5.	Semi-preparative/preparative chromatography clean-up of feruloylated oligosaccharide fractions.....	148
12.5.5.	Methods for release and isolation of non-feruloylated side-chain oligosaccharides.....	149
12.5.5.1.	Mild acid degradation (semi-selective side-chain hydrolysis method for preparative quantities).....	149
12.5.5.2.	Amberlite XAD-2 separation of non-feruloylated oligosaccharides from acidic hydrolysate .....	149
12.5.5.3.	Bio-Gel P-2 separation of non-feruloylated oligosaccharides.....	149
12.5.5.4.	Semi-preparative/preparative chromatography clean-up of non-feruloylated oligosaccharide fractions.....	150
12.5.6.	Methods for characterization of isolated (feruloylated)-oligosaccharides .....	150
12.5.6.1.	Molecular weight determination of feruloylated oligosaccharides.....	150
12.5.6.2.	PGC-ESI-MS analysis of non-feruloylated oligosaccharides .....	151
12.5.6.3.	NMR spectroscopy for structural characterization.....	151
12.5.6.4.	Determination of monosaccharide composition of soluble oligosaccharides (TFA hydrolysis) .....	151
12.5.6.5.	Determination of D/L-configuration of monosaccharides.....	152
12.5.7.	Feruloylated side-chain profiling methods .....	152
12.5.7.1.	LC-DAD/MS-based determination of feruloylated side-chain profiles.....	152

12.5.7.2. HSQC-NMR-based determination of feruloylated side-chain profiles .....	154
12.5.8. Qualitative HPAEC-PAD screening of cereal materials for non-feruloylated side-chain oligosaccharides .....	154
12.6. NMR parameters .....	156
12.6.1. Measurement and processing parameters for structural characterization.....	156
12.6.1.1. <sup>1</sup> H-NMR measurement and processing parameters.....	156
12.6.1.2. <sup>1</sup> H, <sup>1</sup> H-COSY measurement and processing parameters .....	157
12.6.1.3. <sup>1</sup> H, <sup>13</sup> C-HSQC measurement and processing parameters .....	159
12.6.1.4. HMBC measurement and processing parameters .....	161
12.6.1.5. TOCSY measurement and processing parameters .....	163
12.6.1.6. HSQC-TOCSY measurement and processing parameters .....	165
12.6.2. Measurement and processing parameters for quantitative NMR ( <sup>1</sup> H, <sup>13</sup> C-HSQC).....	167
12.7. Additional data tables .....	169
12.8. Additional figures: Chromatograms .....	172
12.9. Additional figures: Spectra .....	173
12.10. Additional data figures .....	184
CURRICULUM VITAE .....	185
PUBLICATIONS LIST .....	187

# List of Abbreviations

---

- 2,3,4-Xylp**: (1→4)- and *O*-2- and *O*-3- glycosidically linked xylopyranose  
**2,4-Xylp**: (1→4)- and *O*-2-glycosidically linked xylopyranose  
**2-Araf**: (1→2)-glycosidically linked arabinofuranose  
**2D**: Two-dimensional  
**3,4-Xylp**: (1→4)- and *O*-3-glycosidically linked xylopyranose  
**3-Araf**: (1→3)-glycosidically linked arabinofuranose  
**3-Glcp**: (1→3)-glycosidically linked glucopyranose  
**5-Araf**: (1→5)-glycosidically linked arabinofuranose  
**4,6-Glcp**: (1→4)- and *O*-6-glycosidically linked glucopyranose  
**4CL**: 4-Coumarate-CoA ligase  
**4-Glcp**: (1→4)-glycosidically linked glucopyranose  
**4-Manp**: (1→4)-glycosidically linked mannopyranose  
**4-Xylp**: (1→4)-glycosidically linked xylopyranose  
**AHCT**: Anthocyanin *O*-hydroxycinnamoyltransferase  
**Araf**: Arabinofuranose  
**Arap**: Arabinopyranose  
**AX**: Arabinoxylan  
**A/X**: Arabinose/xylose ratio  
**AXOS**: Arabinoxylan oligosaccharides  
**BEAT**: Benzylalcohol *O*-acetyltransferase  
**BAHD**: Named for first biochemically characterized members of this acyltransferase enzyme family: **BEAT**, **AHCT**, **HCBT**, and **DAT**  
**C3H**: *p*-Coumaroyl-shikimate/quininate 3-hydroxylase  
**C4H**: Cinnamate 4-hydroxylase  
**CA**: 5-*O*-*trans*-coumaroyl-L-arabinofuranose  
**CCoAOMT**: Caffeoyl-CoA *O*-methyltransferase  
**CID**: Collision-induced dissociation  
**COSY**: Correlation spectroscopy  
**DAD**: Diode array detector  
**DAT**: Deacetylvindoline 4-*O*-acetyltransferase  
**db**: Dry-basis  
**DFA**: Dehydrodiferulate  
**DMSO**: Dimethyl sulfoxide  
**DP**: Degree of polymerization  
**DUF**: Domain of unknown function  
**dXylp**: Disubstituted xylopyranose residues  
**EI**: Electron impact ionization  
**ELSD**: Evaporative light-scattering detection  
**ESI**: Electrospray ionization  
**EtOH**: Ethanol  
**FA**: 5-*O*-*trans*-feruloyl-L-arabinofuranose

**FAX:**  $\beta$ -D-xylopyranosyl-(1 $\rightarrow$ 2)-5-*O*-*trans*-feruloyl-L-arabinofuranose  
**FAXG:**  $\alpha$ -L-galactopyranosyl-(1 $\rightarrow$ 2)- $\beta$ -D-xylopyranosyl-(1 $\rightarrow$ 2)-5-*O*-*trans*-feruloyl-L-arabinofuranose  
**FAXGG:**  $\alpha$ -D-galactopyranosyl-(1 $\rightarrow$ 3)- $\alpha$ -L-galactopyranosyl-(1 $\rightarrow$ 2)- $\beta$ -D-xylopyranosyl-(1 $\rightarrow$ 2)-5-*O*-*trans*-feruloyl-L-arabinofuranose  
**FAXGX:**  $\alpha$ -D-xylopyranosyl-(1 $\rightarrow$ 3)- $\alpha$ -L-galactopyranosyl-(1 $\rightarrow$ 2)- $\beta$ -D-xylopyranosyl-(1 $\rightarrow$ 2)-5-*O*-*trans*-feruloyl-L-arabinofuranose  
**FID:** Flame ionization detector  
**Gal:** Galactose  
**GAX:** Glucuronoarabinoxylan  
**Glc:** Glucose  
**GlcA:** Glucuronic acid  
**GT:** Glycosyltransferase  
**GUX:** Glucuronyltransferase  
**GXMT:** Glucuronoxylan methyltransferase  
**HCBT:** *N*-Hydroxycinnamoyl/benzoyltransferase  
**HCT:** Hydroxycinnamoyl-CoA shikimate/quinic acid hydroxycinnamoyl transferase  
**HMBC:** Heteronuclear multiple-bond correlation spectroscopy  
**HOHAHA:** HOmonuclear HArtmann-Hahn NMR experiment  
**HPAEC-PAD:** High performance anion exchange chromatography coupled with pulsed amperometric detection  
**HPLC:** High-performance liquid chromatography  
**HPSEC-MALLS:** High-performance size exclusion chromatography coupled with multi-angle laser light scattering detection  
**HPSEC-RALLS:** HPSEC coupled with right-angle laser light scattering detection  
**HSQC:** Heteronuclear single quantum coherence spectroscopy  
**IRX:** Irregular xylem  
**IWG:** Intermediate wheatgrass (*Thinopyrum intermedium*)  
**LC-DAD-MS<sup>2</sup>:** Liquid chromatography coupled with a diode array detector and tandem mass spectrometry  
**LC-MS:** Liquid chromatography coupled with mass spectrometry  
**LOD:** Limit of detection  
**LOQ:** Limit of quantification  
**MeI:** Methyl iodide  
**MeOH:** Methanol  
**mXyl:** Monosubstituted xylopyranose residues  
***m/z*:** Mass-to-charge ratio  
**NMR:** Nuclear magnetic resonance  
**ND:** Not detected  
**NR:** Not reported  
**PAL:** Phenylalanine ammonia lyase  
**RGP:** Reversibly glycosylated protein  
**RI:** Refractive index  
**RP-HPLC:** Reversed-phase high-performance liquid chromatography  
**RWA:** Reduced wall acetylation  
**TAL:** Tyrosine ammonia lyase

**t-Araf**: Terminal arabinofuranose  
**TFA**: Trifluoroacetic acid  
**t-Galp**: Terminal galactopyranose  
**t-Glcp**: Terminal glucopyranose  
**THF**: Tetrahydrofuran  
**TOCSY**: Total correlation spectroscopy  
**t-Xylp**: Terminal xylopyranose  
**UAM**: UDP-Arap mutase  
**UDP**: Uridine diphosphate  
**UGD**: UDP-glucose dehydrogenase  
**UGE**: UDP-glucose epimerase  
**UXE**: UDP-xylose epimerase  
**UXS**: UDP-xylose synthase  
**uXyl**: Unsubstituted xylopyranose residues  
**WE-AX**: Water-extractable arabinoxylans  
**WU-AX**: Water-unextractable arabinoxylans  
**XA**:  $\alpha$ -D-xylopyranosyl-(1 $\rightarrow$ 3)-L-arabinopyranose.  
**XAT**: Xylan arabinosyltransferase  
**XAX**: Xylosyl arabinosyl substitution of xylan;  $\beta$ -(1 $\rightarrow$ 2)-xylosyl transferase  
**Xyl**: Xylose  
**Xylp**: Xylopyranose

# 1. Literature Review

---

Plant cell walls are crucial for plants' structural integrity and resilience against insects, disease, and abiotic stressors. Cell wall composition and structure varies between plant organs and at different growth stages, with fine-tuned differences enabling the plant to regulate its growth and reproduce successfully. For animals and humans, plant cell wall structures not only safeguard the foundation of our food chain, but are also a source of both fuel and fiber for paper and textiles. When consumed in human and animal diets, plant cell walls are associated with numerous health benefits as roughage, or dietary fiber.

Plant cells are surrounded by a primary cell wall, which consists of an insoluble network of cellulose microfibrils embedded in a matrix of pectic and hemicellulosic polysaccharides and permeated with an aqueous solution containing inorganic ions, soluble proteins and carbohydrates, arabinogalactan proteins, and freshly synthesized wall components (Albersheim et al., 2010). Two broad classes of primary cell walls are found in flowering plants: primary cell walls of dicots (and noncommelinid monocots), which contain high levels of xyloglucans and pectins and smaller amounts of mannans, glucomannans, and xylans; and the primary cell walls of commelinid monocots, with (glucurono)arabinoxylans replacing xyloglucans as the dominant hemicellulose, high hydroxycinnamate contents, and insignificant amounts of pectins and mannans (Vogel (2008); **Table 1**). Primary cell walls of grasses (family Poaceae) also contain mixed linkage  $\beta$ -(1 $\rightarrow$ 3,1 $\rightarrow$ 4)-glucans. Upon completion of cell expansion, some cells begin depositing a thick secondary wall. In contrast to primary walls, secondary walls contain lignin, which decreases their flexibility and water permeability.

**Table 1. Approximate composition of cell walls from grasses and dicots (% dry weight)<sup>a,b</sup>**

	Primary walls		Secondary walls	
	Grasses	Dicots	Grasses	Dicots
Cellulose	20–30	15–30	35–45	45–50
Pectins	5	20–25	– <sup>c</sup>	–
Hemicelluloses				
Glucuronoxylan	– <sup>c</sup>	–	–	20–30
(Glucurono)arabinoxylans	20–40	5	40–50	–
Mannans	2	3–5	0–5	2–8
Xyloglucans	2–5	20–25	–	–
$\beta$ -(1 $\rightarrow$ 3,1 $\rightarrow$ 4)-glucans	2–15	–	–	–
Lignin	–	–	20	7–10

<sup>a</sup>Values vary between tissues and species. Not shown: Structural protein and ash/silica contents.

<sup>b</sup>Figures taken from Vogel (2008) and Scheller and Ulvskov (2010).

<sup>c</sup>–, absent or minor

In the most commonly accepted model of plant cell wall architecture, hemicelluloses tether cellulose microfibrils together by forming hydrogen-bonding regions between multiple microfibrils and by being trapped in the microfibril as it crystallizes (Scheller and Ulvskov (2010), **Figure 1**). For primary cell walls, this “tethering glycan” role is filled principally by xyloglucans in dicots and by xylans in monocots, but in secondary cell walls, xylans are the major hemicellulose for both monocots and dicots. Importantly, the extent and pattern of substitution along the hemicellulosic backbone affects the polymer's ability to form hydrogen bonds with the cellulose microfibrils: denser substitution patterns increase solubility and limit

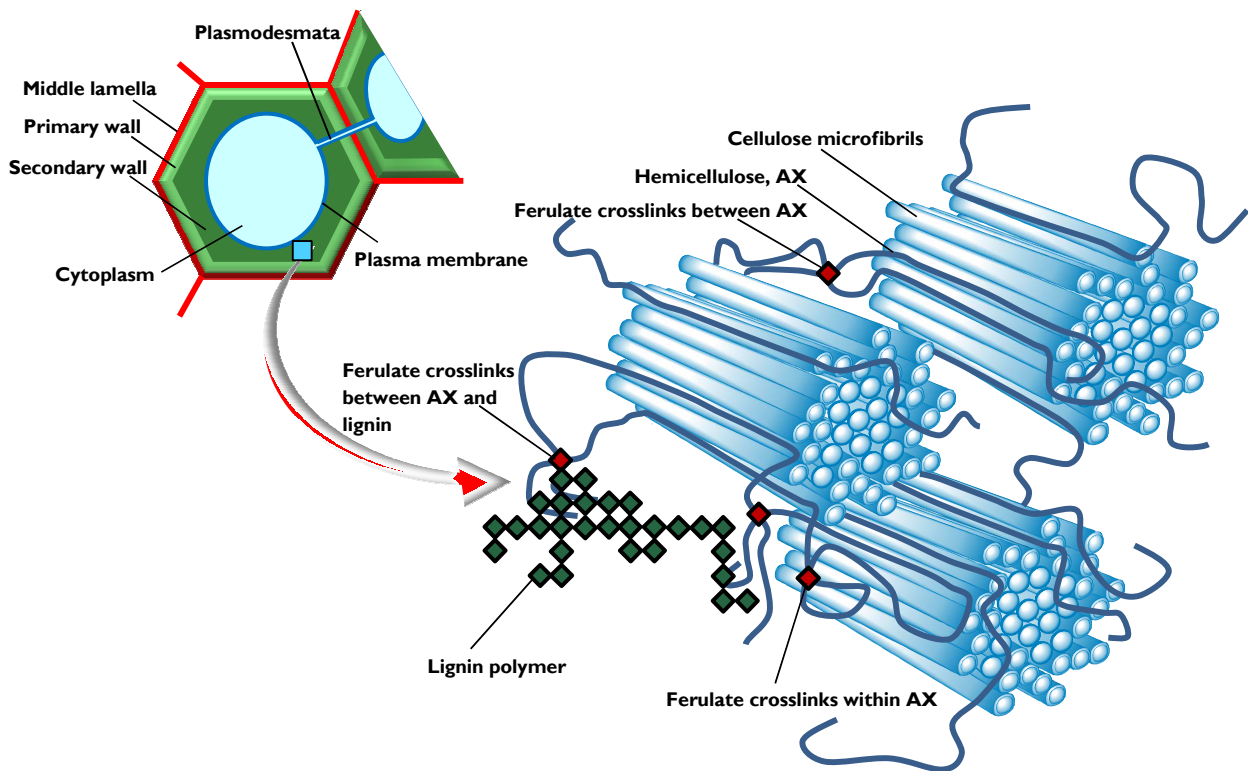


**Figure 1. Cell wall structure of grasses. Top left:** Simplified cell model showing layers produced in a horizontal tissue slice. **Bottom right:** Close-up model of a slice of the secondary cell wall showing cellulose microfibrils interacting with hemicellulosic arabinoxylans (AX) via hydrogen bonding, ferulate crosslinking between and within AX polymers, and ferulate crosslinking between AX and lignin. Red diamonds: ferulate dimers or higher oligomers; green diamonds: monolignol components of the lignin polymer.

interactions with cellulose (Saulnier et al., 2012).

Although the hemicellulosic xylans found in both monocots and dicots share the same semi-flexible  $\beta$ -(1 $\rightarrow$ 4)-linked xylopyranose backbone, their backbone substitution patterns differ. In dicots, most xylans are substituted with glucuronic acid (GlcA), 4-*O*-methyl-GlcA, and acetyl groups and are therefore sometimes termed glucuronoxylans. In commelinid monocots,  $\alpha$ -L-arabinofuranose (Araf) is the major substituent, and the polymers are called arabinoxylans (AX), or sometimes, glucuronoarabinoxylans (GAX).

Ferulic acid, the most abundant hydroxycinnamate in plant cell walls, is found esterified to AX via the *O*-5 position of the arabinose side-chains in all commelinid monocots. Ester-linked ferulic acid is also present in dicotyledonous plants from the so-called “core” Caryophyllales, where, in contrast to the commelinid monocots, it acylates pectic arabinans and galactans (Ishii, 1997; Levigne et al., 2004; Harris and Trethewey, 2010). Free radical-induced oxidative coupling of ferulates produces ferulate dimers and higher oligomers and creates inter- and intramolecular cross-links between AX chains (Ralph et al., 1994; Saulnier et al., 1999; Allerdings et al., 2005; Bunzel et al., 2008). Ferulate and diferulates also couple with lignin, resulting in AX-lignin cross-linkages (Ralph et al., 1995). These covalent ferulate crosslinks are a key contributor to the structural strength of the graminaceous cell wall matrix.

### 1.1. Feruloylated arabinoxylans in cereal grains

Livestock consume grass cell walls, and thus AX, both from vegetative (for example,

fresh grass, grass hay, and maize silage) and reproductive (grain) plant organs. Grains, on the other hand, are the primary source of graminaceous cell walls in human diets. The outer tissues of grain kernels comprise several layers (from outer to inner layers: outer pericarp, inner pericarp, seed coat, and nucellar epidermis) with very thick cell walls and high feruloylated AX contents. However, these outer grain layers are removed as bran in the refining process.

The grain endosperm is made up of the outer aleurone layer and the inner starchy endosperm. The aleurone layer cells are thick-walled and rich in heavily feruloylated AX, but the inner starchy endosperm cells have very thin cell walls and AX with low feruloylation levels (Saulnier et al., 2012). Because the aleurone layer is removed with the bran during grain refining, refined flour has far lower feruloylated AX contents compared to the bran fraction (**Table 2**). Many epidemiological studies have found positive correlations between consumption of whole grains and various health benefits, including reduced risk of cardiovascular disease (Erkkilä et al., 2005; Mellen et al., 2008), type 2 diabetes (de Munter et al., 2007; Ardisson Korat et al., 2014), and colon cancer (Schatzkin et al., 2007; Egeberg et al., 2010). Furthermore, of the whole grain components (bran, germ, and starchy endosperm), the bran constituents seem to play a leading role in the “whole grain effect” (Jensen et al., 2004; de Munter et al., 2007). The health benefits of cereal fiber and the associated feruloylated AX will be discussed in greater detail in **Section 1.5**.

**Table 2. Arabinoxylan contents of cereal grain milling fractions**

Milling fraction	AX (%) <sup>a</sup>	Reference
<i>Winter wheat</i> (131 varieties)		
refined flour	1.35-2.75	(Gebruers et al., 2008)
bran	13.2-22.1	
<i>Durum wheat</i> (10 varieties)		
refined flour	1.75-2.35	(Gebruers et al., 2008)
bran	10.9-13.7	
<i>Rye</i> (5 varieties)		
refined flour	2.95-3.30	(Shewry et al., 2010)
bran	12.14-13.34	
<i>Spelt</i> (5 varieties)		
refined flour	1.60-2.15	(Gebruers et al., 2008)
bran	11.1-13.9	
<i>Barley</i> (10 varieties)		
flour	1.69-2.24	(Andersson et al., 2008)
bran (with hull)	4.84-9.84	

<sup>a</sup>Range of arabinoxylan (AX) contents (dry matter basis) among multiple varieties, determined as 0.88 times the sum of arabinose and xylose.

## 1.2. Structure of feruloylated arabinoxylans in cereal grains

All feruloylated AX are based on a (1→4)-linked β-D-xylopyranosyl backbone structure substituted with various side-chain (branch) elements (**Figure 2**). The dominant side-chain, α-L-Araf, is found as either a mono- and/or di-substituent at the xylopyranosyl O-3 and/or O-2 positions and may be O-5-acylated with ferulic acid or other phenolic acids. GlcA, its 4-O-methyl derivative, and acetyl groups are also observed in grains as AX backbone substituents, particularly in maize and sorghum AX (Verbruggen et al., 1995; Huisman et al., 2000; Kabel et al., 2002; Appeldoorn et al., 2010; Appeldoorn et al., 2013).

Among cereal grains, structural differences in feruloylated AX are determined primarily by AX substitution patterns, ferulate cross-linking, and chain length. Wheat and rye AX have been extensively studied because of their key roles in the structures of doughs and baked goods. Barley AX have also been the subject of many structural investigations because AX structural differences affect beer brewing (wort viscosity and subsequent filtration) and beer foam stability. (The food processing implications of AX structural differences will be discussed in more detail in **Section 1.4**.) The motivation for examining AX structures from the other commonly cultivated

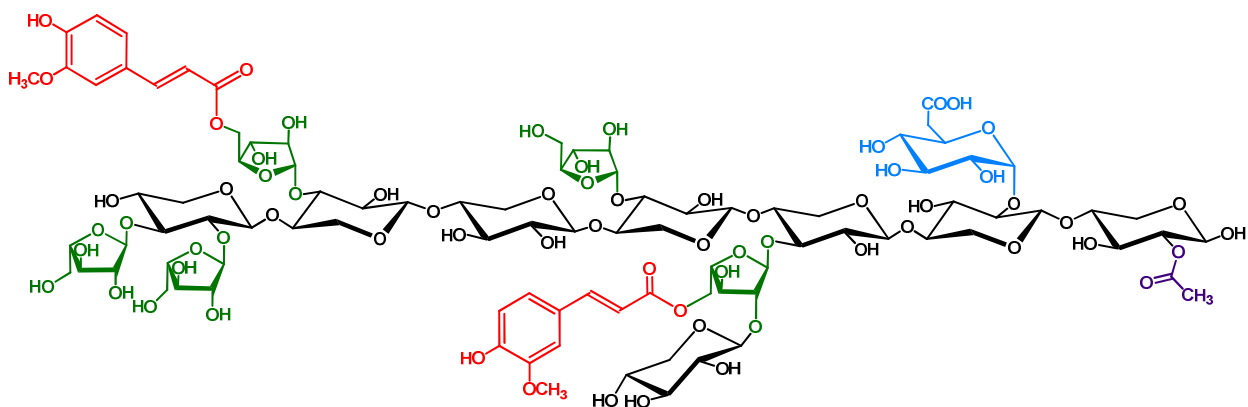


**Figure 2. Arabinoxylan structure model.** The (1→4)-linked β-D-xylopyranosyl arabinoxylan backbone is substituted with side-chains, or branch elements, including O–3 and/or O–2-linked α-L-arabinofuranose units (green), which may be acylated on the O–5 position with ferulic acid (red) to form feruloylated side-chains. Additional side-chain substituents include glucuronic acid (blue), 4-O-methyl glucuronic acid (not shown), and acetyl groups (purple).

cereal grains (maize, rice, etc) has primarily been to determine the relationships between AX structure and enzymatic fermentability. AX enzymatic fermentability directly affects the feed value of cereals in animal nutrition and biofuel yield from second generation biofuel production using cereal grain byproducts. (The relationship between AX structural differences and enzymatic fermentability will be discussed in more detail in **Section 1.3.**) In the following section, AX structural differences (substitution patterns, ferulate cross-linking, and chain length) will be examined, with a focus on the differences among cereal species.

### 1.2.1. Substitution patterns in cereal grain arabinoxylans

#### 1.2.1.1. Substitution with α-L-arabinofuranose

The ratio of arabinose to xylose (A/X ratio) following monosaccharide analysis is commonly reported as an indicator of substitution density along the xylan backbone. Methylation analysis uncovers another layer of detail in substitution patterns by showing the ratio between unsubstituted, monosubstituted, and disubstituted xylopyranose (uXylp, mXylp, and dXylp, respectively) residues in the AX backbone (**Table 3**). However, methylation analysis reveals no information about the distribution *pattern* of these variously substituted residues along the AX backbone. This additional layer of detail can be delivered by partial enzymatic hydrolysis of the AX and isolation and characterization of the released AX oligosaccharides (AXOS). Such techniques have been developed for mapping the AX structures of wheat, rye, and barley following *endo*-xylanase hydrolysis; however, these methods are not applicable to maize or rice AX because of their resistance to *endo*-xylanase hydrolysis (Saulnier and Quemener, 2010).

The two most important physicochemical and biochemical implications of arabinose substitution patterns are water-solubility and enzymatic fermentability of the AX polymer. In terms of water-solubility, AX with extended regions of unsubstituted xylose residues are prone to aggregation and are therefore more likely to be water-insoluble. Conversely, if other factors are held equal (especially ferulate cross-linking, but also polymer size), AX with greater arabinose substitution density are more likely to be water-extractable AX (WE-AX). Increased substitution density reduces AX adsorption to cellulose (Kabel et al., 2007; Köhnke et al., 2008), and reduced AX branching both increases AX adsorption to cellulose and inhibits enzymatic (cellulase) hydrolysis of cellulose (Selig et al., 2015). When considering enzymatic fermentability, densely-

**Table 3. Substitution patterns in cereal arabinoxylans as shown by methylation analysis**

Cereal grain, tissue	AX extraction method	Linkage on Xylp <sup>a</sup>						Reference
		A/X	uXyl	mXyl	dXyl	tXyl	O-3/ O-2 <sup>b</sup>	
<i>Wheat</i>								
endosperm <sup>d</sup>	water	0.43-1.02	52-70	13-22	8-33	1-2	1.8-25.1	(Gruppen et al., 1992a)
endosperm <sup>d</sup>	water	0.43-0.97	51-64	12-27	10-26	2-9	4.8-32.0	(Izydorczyk and Biliaderis, 1993)
endosperm	water	0.53	65	20	12	3	36	(Cleemput et al., 1995)
endosperm <sup>c</sup>	water	0.57	64	15	21	NR	NR	(Dervilly-Pinel et al., 2001a)
endosperm <sup>d</sup>	alkali, various	0.36-1.08	52-70	14-22	7-33	1-2	1.8-26.8	(Gruppen et al., 1992a)
aleurone	whole cell walls	0.35	75	20	5	trace	NR	(Bacic and Stone, 1981)
beeswing bran (outer pericarp)	alkali	1.14	18	30	34	19	NR	(Brillouet and Joseleau, 1987)
industrial bran	native material	1.17	28	26	29	18	NR	(Brillouet et al., 1982)
industrial bran <sup>d</sup>	mildly alkaline (0.2M NaOH)	0.57-1.07	37-18	22-34	40-35	1-12	NR	(Shiiba et al., 1993)
industrial bran	alkali (sat. Ba(OH) <sub>2</sub> )	0.71	53	18	20	12	11	(Schooneveld-Bergmans et al., 1999)
<i>Rye</i>								
endosperm	water	0.50	57	35	7	NR	NR	(Dervilly-Pinel et al., 2001a)
endosperm <sup>d</sup>	alkali (sat. Ba(OH) <sub>2</sub> )	0.40-1.04	30-65	29-36	5-34	NR	NR	(Verwimp et al., 2007)
whole grain <sup>d</sup>	water	0.48-0.55	42-50	47-52	3-6	NR	NR	(Bengtsson and Åman, 1990)
whole grain <sup>d</sup>	water	0.55-1.42	22-50	18-47	3-59	trace	0.3-37.4	(Vinkx et al., 1995a)
whole grain <sup>d</sup>	alkali (various)	0.55-1.10	17-87	8-31	3-26	3-26	7-12	(Vinkx et al., 1995b)
industrial bran	alkali (1% NH <sub>4</sub> OH)	0.78	35	28	22	16	5.2	(Ebringerová et al., 1990)
<i>Triticale</i>								
endosperm	water	0.59	63	14	22	NR	NR	(Dervilly-Pinel et al., 2001a)
<i>Rice</i>								
whole grain	water	0.87-0.88	30-40	38-51	17-20	2-3	NR	(Rao and Muralikrishna, 2007)
endosperm	alkaline (4M KOH)	0.88-0.97	14-16	78-84	2-6	trace	8	(Shibuya et al., 1983)
bran	alkaline (4M NaOH)	0.93-0.98	14-24	54-55	15-19	5-6	4.4	(Shibuya and Iwasaki, 1985)
<i>Maize</i>								
whole grain	alkali (1% Ca(OH) <sub>2</sub> )	0.57	13.4	42	20	24	6.4	(Saulnier et al., 1993)
whole grain <sup>d,e</sup>	alkali (sat. Ba(OH) <sub>2</sub> )	0.79-0.80	32-34	41-42	16-20	16-23	3.6-4.2	(Huisman et al., 2000)
bran <sup>d</sup>	alkali (various)	0.58-0.59	16-17	40-41	19-20	23	NR	(Chanliaud et al., 1995)

Cereal grain, tissue	AX extraction method	Linkage on Xylp <sup>a</sup>						Reference
		A/X	uXyl	mXyl	dXyl	tXyl	O-3/O-2 <sup>b</sup>	
<b>Sorghum</b>								
water-insoluble cell wall material from endosperm <sup>d</sup>	alkali (various)	0.83-1.16	21-43	34-60	9-18	2-17	2.6-5.5	(Verbruggen et al., 1995)
water-insoluble cell wall material from endosperm <sup>d, e</sup>	alkali (sat. Ba(OH) <sub>2</sub> )	1.12-1.26	33-39	47-51	11-13	3	3.0	(Huisman et al., 2000)
<b>Barley</b>								
endosperm <sup>c</sup>	water	0.58-0.61	52-65	8-17	20-26	NR	NR	(Dervilly-Pinel et al., 2001a)
water-insoluble cell wall material from endosperm <sup>d</sup>	alkali (1M KOH)	0.50-0.97	6-63	12-86	0-25	0-4	NR	(Ballance et al., 1986)
water-insoluble cell wall material from endosperm <sup>d</sup>	alkali (various)	0.29-1.18	32-71	19-32	9-32	0-7	1.5-4.0	(Viëtor et al., 1992)
aleurone	whole cell walls	0.52	67	24	8	1	NR	(Bacic and Stone, 1981)
whole grain <sup>c</sup>	water	NR	47-62	17-33	16-23	NR	0.8-16	(Oscarsson et al., 1996)
whole grain	water	0.64	64	14	22	NR	1.8	(Dervilly et al., 2001)
malt <sup>c</sup>	water	0.62-0.69	58-61	12-13	25-28	1-2	0.7-1.4	(Debyser et al., 1997)
malt	water	0.64	60	15	25	NR	1.5	(Dervilly et al., 2001)
malt <sup>d</sup>	alkali (various)	0.41-1.23	33-77	17-31	4-29	1-17	0.9-2.9	(Viëtor et al., 1992)

<sup>a</sup>All values were calculated as the molar percentage of the total reported Xylp residues. Total sum may not equal 100% because of rounding.

<sup>b</sup>Ratio of O-3 to O-2 monosubstituted Xylp residues. When reported, value was estimated by the relative abundance of characteristic fragment ions in the mass spectrum (typically m/z 117 or m/z 118 for O-3-substituted residues, depending on whether NaBH<sub>4</sub> or NaBD<sub>4</sub> was used for reduction, and m/z 129 for O-2-substituted residues), as the partially methylated alditol acetates for these structural moieties coelute chromatographically under most of the published conditions (Gruppen et al., 1992b).

<sup>c</sup>Average from multiple varieties.

<sup>d</sup>Data range from multiple fractions

<sup>e</sup>1→3-linked Xylp also observed in samples; value not included in total Xylp.

Abbreviations used: **AX**: arabinoxylan; **A/X**: arabinose/xylose ratio; **dXyl**: disubstituted Xylp residues; **mXyl**: monosubstituted Xylp residues; **NR**: not reported; **uXyl**: unsubstituted Xylp residues; **Xylp**: xylopyranose.

substituted AX regions resist enzymatic hydrolysis with *endo*-xylanases, which require two to three unsubstituted xylose residues for steric access to the xylan backbone (Pollet et al., 2010a). The pattern of AX substitution is also decisive for fermentability with *endo*-xylanases: a hypothetical AX with a low A/X ratio of 0.5 and an alternating pattern of single uXylp and mXylp would be completely resistant to *endo*-xylanase attack. Conversely, a hypothetical AX with a high A/X ratio of 1.00 and a repeating substitution pattern of two adjacent dXylp followed by two adjacent uXylp would be effectively broken down by *endo*-xylanases into AXOS.

AX are highly heterogeneous in their substitution patterns and density. Variations are not only observed among cereal species and tissue types, but heterogeneous AX polymers are also isolated from single tissue types using techniques such as graded ethanol (EtOH) precipitation, sequential ammonium sulfate precipitation, and/or chromatography (size exclusion and/or ion

exchange) (Gruppen et al., 1992a; Viëtor et al., 1992). For example, WE-AX isolated from wheat endosperm had an average A/X ratio of 0.55, but the A/X ratios of subfractions from this material ranged from 0.37 to 1.30 (Dervilly-Pinel et al., 2001b).

**Wheat.** Despite pronounced heterogeneity, some patterns do emerge among cereal species and tissue types. In wheat grain, AX in the aleurone layer have a very low A/X ratio with a high percentage of unsubstituted xylose residues (75% of total xylose monomers) and only 5% dXylp residues (Bacic and Stone, 1981). Because xylan chains with high levels of uXylp residues easily self-aggregate, aleurone AX are water-unextractable (WU)-AX. The bulk endosperm AX from wheat grain shows a higher average A/X ratio ( $\approx 0.55$ ) (Cleemput et al., 1995; Dervilly-Pinel et al., 2001a). This increased substitution density compared to aleurone AX is primarily due to an increase in dXylp residues in wheat endosperm. No substantial differences in arabinose substitution patterns are observed between wheat endosperm WU-AX and WE-AX (Gruppen et al., 1993b).

The outer pericarp layer of wheat contains highly substituted AX polymers (A/X ratio of 1.14 and a large percentage of dXylp residues) (Brillouet and Joseleau, 1987). Pericarp and bran AX also show a higher level of terminal xylose residues compared to endosperm or aleurone AX (Brillouet et al., 1982; Brillouet and Joseleau, 1987; Schooneveld-Bergmans et al., 1999), which arise both from the non-reducing end of the AX polymers and from oligosaccharide side-chain substituents. Most mXylp residues are substituted on the O-3 position in wheat AX, but small amounts of O-2 monosubstitution are also observed in methylation analysis results, especially in the bran fraction (Schooneveld-Bergmans et al., 1999). Overall, differences in uXylp and dXylp residues appear to mostly account for the variations in A/X ratios from various wheat fractions: mXylp residues remain relatively constant (Delcour et al., 1999).

The distribution pattern of arabinose substituents in wheat endosperm AX has been studied extensively by both *endo*-xylanase hydrolysis and periodate oxidation methods. Most experimental evidence points towards a non-random distribution of substituents along the xylan backbone (Saulnier et al., 2007). Dervilly-Pinel et al. (2004) used a statistical model to compare random distribution of variously substituted xylose residues with experimentally determined values from well-characterized wheat endosperm WE-AX. They found that the experimental values differed sharply from the random distribution model, and especially, that rates of disubstitution were much higher than predicted by random distribution. Regions of up to six contiguous substituted Xylp residues were found in small amounts in wheat endosperm WE-AX using periodate oxidation, but the majority of substituted residues were present as isolated residues ( $\approx 60$ -80%) or clusters of two or three substituted residues ( $\approx 15$ -25% and 5-15%, respectively) (Dervilly-Pinel et al., 2004). Wheat endosperm WU-AX have comparable structures to WE-AX, as seen by the AXOS profile produced by enzymatic (*endo*-xylanase) hydrolysis of WU-AX from wheat endosperm (Gruppen et al., 1992c; Gruppen et al., 1993b). Enzymatic hydrolysis of endosperm WU-AX subfractions with A/X ratios varying from 0.36 to 0.80 showed that the subfractions with low AX ratios contained up to seven contiguous uXylp residues. However, most stretches of uXylp residues were only one to four units long and were framed by single substituted Xylp residues or pairs of substituted Xylp. As the A/X ratio increased, the proportion of AXOS containing doubly substituted xylose residues increased faster than statistically predicted (Gruppen et al., 1993b). In summary, while a range of wheat endosperm AX structures exist, the substitution pattern consists mostly of one to three contiguous substituted xylose residues followed by up to seven (but usually less) unsubstituted

xylose residues. In addition, the substitution pattern favors dXylp residues, with dXylp residues increasing and uXylp residues decreasing as A/X ratios rise (Figure 3A-B).

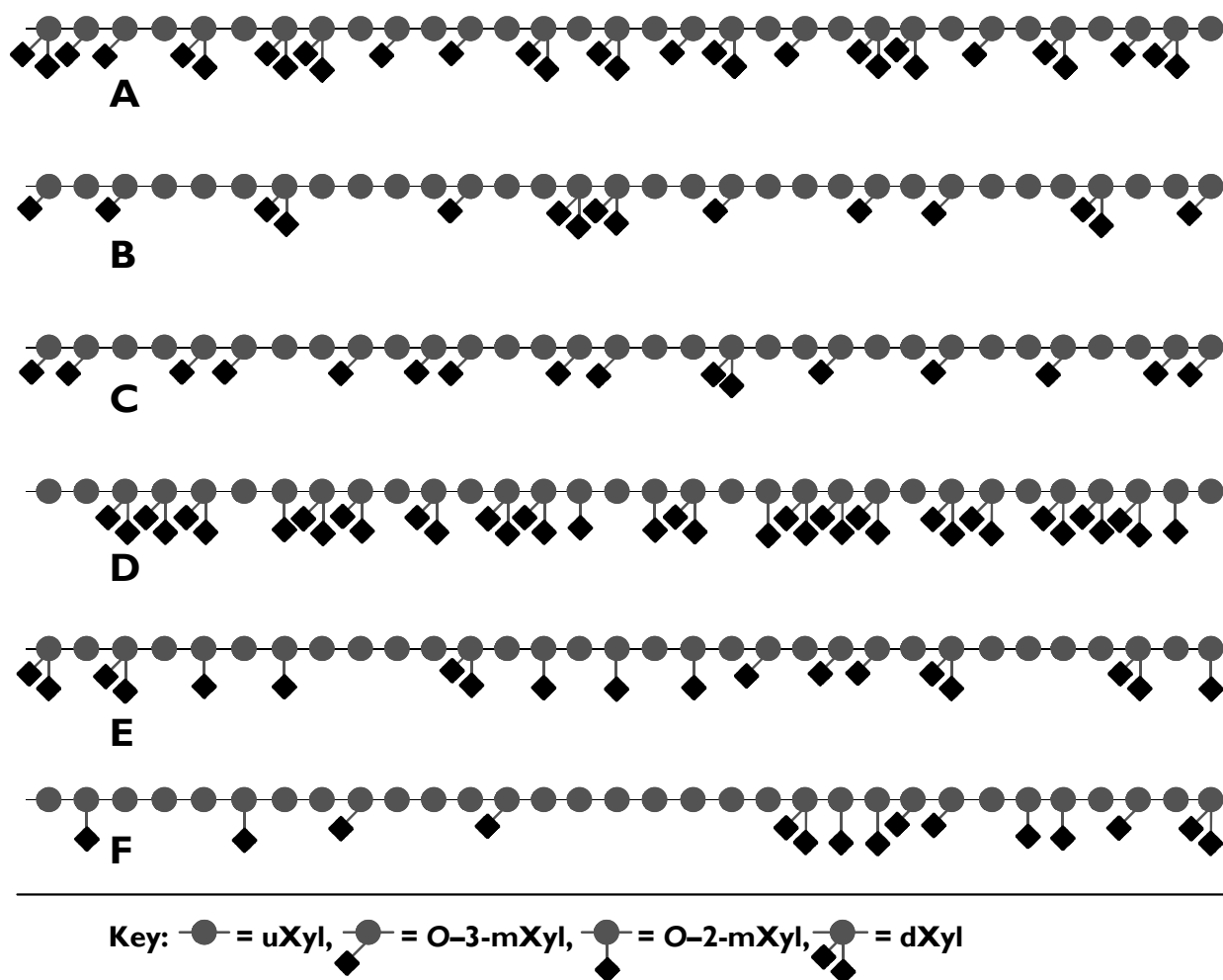


**Figure 3. Proposed models of arabinose distribution patterns in cereal arabinoxylans (AX).** **A:** Heavily-substituted water-insoluble wheat endosperm AX, based on Gruppen et al. (1993b). **B:** Less substituted water-insoluble wheat endosperm AX, based on Gruppen et al. (1993b). **C:** Rye water-soluble endosperm AXI, based on Bengtsson et al. (1992a), Vinkx et al. (1993), and Vinkx et al. (1995a). **D:** Rye water-soluble endosperm AXII, based on Bengtsson et al. (1992a), Vinkx et al. (1993), and Vinkx et al. (1995a). **E:** Barley water-insoluble AX, based on Viëtor et al. (1994b). **F:** Oat alkali-soluble AX, based on Tian et al. (2015).

*Abbreviations used:* **uXyl**: unsubstituted xylopyranose; **mXyl**: monosubstituted xylopyranose; **dXyl**: disubstituted xylopyranose.

**Triticale and Rye.** Methylation analysis shows that the endosperm AX of triticale, a hybrid of wheat and rye, are most comparable to its wheat parent (Dervilly-Pinel et al., 2001a). Compared to wheat endosperm WE-AX, rye endosperm WE-AX have a similar A/X ratio, but lower levels of uXylp and dXylp residues and more mXylp (Dervilly-Pinel et al., 2001a).

The isolation and analysis of subfractions of rye WE-AX reveal a greater range of structural extremes and a larger population density at those structural extremes compared to wheat. The presence of two disparate rye WE-AX populations was first observed by Bengtsson et al. (1992a), who suggested that rye AX could be divided into two distinct polymers or polymeric regions based on the analysis of the *endo*-xylanase hydrolysate of rye endosperm AX and the enzyme-resistant residue. The first, rye AXI, is a lightly substituted polymer with

occasional monosubstituted xylose residues and very little disubstitution, and the second, rye AXII, was proposed to be a heavily substituted polymer with mostly disubstituted and unsubstituted residues. Using <sup>1</sup>H-nuclear magnetic resonance (NMR) analysis to assign anomeric protons to either AXI or AXII, Bengtsson et al. (1992b) estimated that the contents of these two polymers ranged between 1.4-1.7% (AXI) and 0.6-1.0% (AXII) of rye dry matter. Other work, however, showed that although relatively pure rye WE-AX subfractions with similar characteristics to Bengtsson's AXI and AXII were isolated (Bengtsson and Åman, 1990; Vinkx et al., 1993; Vinkx et al., 1995a), other, intermediate WE-AX polymers were also present, indicating that Bengtsson's binary model was too simplistic (Vinkx et al., 1993). The contrast between the WE-AX polymers at rye's structural extremes is nevertheless fascinating: the AXI-like polymer had an A/X ratio of 0.55 and contained almost no dXylp residues (3%) and nearly equal proportions of mXylp and uXylp residues (47% and 50%, respectively). Periodate analysis of this polymer showed that the substituted xylose residues were mostly distributed along the xylan backbone as individual residues or pairs (**Figure 3C**, Åman and Bengtsson (1991)). In contrast, the AXII-like polymer was built predominantly from dXylp residues (59%) and smaller amounts of mXylp and uXylp (18% and 36%, respectively) and had an A/X ratio of 1.42. In addition, most of the mXylp residues in the AXII-like polymer were *O*-2-substituted (**Figure 3D**, Vinkx et al. (1995a)).

WU-AX from rye whole meal fall into three broad classes: an AX with a very low A/X ratio ( $\approx 0.2$ ) and low levels of disubstitution which likely stems from the aleurone layer; a heavily substituted AX (A/X ratio  $\approx 1.1$ , 26% dXylp residues, 31% mXylp residues) which likely stems from the pericarp; and a third, intermediate AX structure with an A/X ratio between 0.55 and 0.79, likely from the endosperm (Vinkx et al., 1995b; Vinkx and Delcour, 1996). The WU-AX structures of rye differ strongly from rye WE-AX, and no evidence of AXI-like or AXII-like structures is seen in the WU-AX (Verwimp et al., 2007). Rather, WU-AX from rye endosperm are very comparable to wheat endosperm WU-AX. Graded EtOH precipitation of rye endosperm WU-AX produces fractions with A/X ratios ranging between 0.40 and 1.04. Like wheat endosperm WU-AX, the level of mXylp residues remains relatively constant throughout these fractions, although the overall level of mXylp is higher in rye (between 29 and 36%). Also like wheat, the levels of dXylp in rye endosperm WU-AX rise with increasing A/X ratio (from 5% to 34%) (Verwimp et al., 2007). However, no *endo*-xylanase fingerprinting analysis has been performed on rye endosperm WU-AX, so the distribution pattern of these residues compared to wheat is unknown. Based on methylation analysis, Vinkx and Delcour (1996) also concluded that no appreciable differences are seen between the WU-AX from rye and wheat bran.

**Barley.** Like wheat and rye, barley endosperm AX are heterogeneous (Viëtor et al., 1992). The overall methylation analysis profiles of barley WE-AX are comparable to those from wheat and rye (Dervilly-Pinel et al., 2001a). *Endo*-xylanase fingerprinting of barley WU-AX led Viëtor et al. (1994b) to propose a block-like substitution pattern model, where blocks of four or more unsubstituted residues alternate with enzyme-resistant blocks. The blocks resistant to *endo*-xylanase hydrolysis were not heavily substituted, and were therefore proposed to consist of substituted (both mono- and disubstituted) xylose residues either alone or in pairs and followed by single uXylp residues. Besides these differences in substituent distribution, barley AX also contain a greater proportion of *O*-2-monosubstituted xyloses compared to wheat and rye (**Figure 3E**, Viëtor et al. (1994a)). Barley aleurone AX have a greater A/X ratio than seen in wheat aleurone, with the increased arabinose substituents stemming from mXylp residues (Bacic and

Stone, 1981). No appreciable differences in substitution pattern are seen between barley and malt AX (Viëtor et al., 1992; Viëtor et al., 1994b).

**Oats.** Oat AX have been less extensively studied than wheat, rye, and barley AX, and no methylation analysis of oat AX has been published. <sup>1</sup>H-NMR analysis of oat WE-AX showed both disubstituted and *O*-3-monosubstituted xylose residues (Westerlund et al., 1993), and enzymatic fingerprinting of oat materials also released AXOS with *O*-2-monosubstituted xyloses (Pastell et al., 2009; Tian et al., 2015). Oat AX are very sparsely substituted (A/X ratios in the literature range from 0.20 for total alcohol-insoluble residues (Tian et al., 2015) to between 0.47 and 1.0 for various alkali-soluble fractions, with the majority of the dissolved material showing an A/X ratio of  $\approx 0.6$  (Virkki et al., 2005)). Enzymatic fingerprinting of the alkali-soluble AX from whole grain oat cell wall material indicates that their substituent distribution pattern is most similar to the block pattern observed in barley AX. However, compared to barley, the stretches of unsubstituted residues are likely much longer in oats. Oats also contain regions with scattered substituted xylose residues, in addition to blocks of densely substituted, *endo*-xylanase-resistant regions (**Figure 3F**, Tian et al. (2015)).

**Rice.** Rice endosperm AX have a higher average A/X ratio compared to wheat endosperm AX. Interestingly, the arabinose substituents are found almost exclusively on mXylp residues, and only a fraction of xylose residues in rice endosperm are disubstituted (Shibuya et al., 1983). In contrast, highly substituted subfractions of wheat endosperm AX contain up to 33% dXylp residues (Gruppen et al., 1993a). Another unique characteristic of rice AX is that although the A/X ratios of rice endosperm and bran AX are very similar, the ratio of mXylp to dXylp residues changes, with more dXylp residues in bran (Shibuya et al., 1983; Shibuya and Iwasaki, 1985).

**Maize.** Maize AX show an intermediate level of arabinose substitution (greater than wheat, rye, and barley, and less than rice). Importantly, the A/X ratio of maize AX is much lower than rice; however, because of the high levels of terminal xylose residues in maize AX, the A/X ratio is not a good indicator of their complexity. The substantial percentage of terminal xylose residues points towards extensive oligosaccharide side-chain substituents in maize AX. Maize AX also display substantial amounts of non-arabinose substituents (acetyl groups and uronic acids), as discussed in the following sections, meaning that their total backbone substitution profile is very complex.

**Sorghum.** Sorghum AX have a very high A/X ratio ( $\approx 1.1$ ). However, the isolation and characterization of AXOS containing short arabinose oligosaccharide side-chains means that the A/X ratio, which assumes that all arabinose units are directly attached to the xylan backbone, somewhat overestimates the substitution complexity (Verbruggen et al., 1998). Compared to maize, sorghum AX contain far fewer terminal xylose residues, indicating fewer oligosaccharide side-chains ending in xylose (Huisman et al., 2000).

#### 1.2.1.2. *Substitution with acetyl groups*

Graminaceous AX are also partly acetylated on the xylan backbone, although to a lesser extent than hardwood xylans. This aspect of cereal grains' AX structures, however, has been largely ignored in the literature and a comprehensive survey of acetyl contents in cereal grains has not been performed. A summary of the reported literature values is provided in **Table 4**.

The degree of acetylation appears to vary substantially among species as well as tissue types. Maize bran, for example, contained 3.6% acetic acid by dry weight (Saulnier et al., 1995a), whereas wheat bran's content was far lower (0.4%) (Kabel et al., 2002). Analysis of wheat aleurone cell walls showed an acetic acid content of 4.9%, over ten times greater than in

bran (Rhodes et al., 2002). In some cereal materials (maize, sorghum, and oats), acetyl groups contribute substantially to the overall substitution complexity of the AX backbone and molar ratios of acetyl groups to xylose residues  $\geq 0.20$  are observed.

In grain kernels, acetylation is assumed to occur on both the xylose *O*-2 and *O*-3 positions along the xylan backbone. Separate MALDI-TOF-analyses of AX oligosaccharides (AXOS) in enzymatic hydrolysates detected *O*-acetylated structures in both barley and wheat AX (Kabel et al., 2003b; Sørensen et al., 2007). To the best of our knowledge, only one report of fully characterized acetylated AX structures isolated specifically from cereal grains exists in the literature. These complex structures from maize grain contained di-substituted xylose monomers which were both *O*-2-acetylated and *O*-3-substituted with feruloylated side-chains (Appeldoorn et al., 2013). Migration of the acetyl group within a sugar monomer (for example, between position *O*-2 and *O*-3 of a (1→4)-linked-xylose monomer as well as to the *O*-4 position of a non-reducing terminal xylose) readily occurs in xylooligosaccharides (Kabel et al., 2003a; Puchart and Biely, 2015). Acetyl group migration is an intramolecular transesterification reaction and proceeds by nucleophilic acyl substitution. A hydroxyl group adjacent to the acetyl ester serves as the attacking nucleophile, and a cyclic *ortho*-acid ester intermediate is produced (Bonner, 1959). This rearrangement complicates exact assignment of the native acetylation position in isolated oligosaccharides. *O*-2-Acetylation of the arabinose substituents in feruloylated side-chains was also reported in the vegetative structures of grasses, including sugarcane and bamboo (Azuma et al., 1990; Ishii, 1991).

**Table 4. Reported acetyl contents of cereal grain materials**

Cereal material	Acetyl content (% w/w, db)	acetyl/Xyl <sup>a</sup>	Reference
<b>Wheat</b>			
bran, milling fraction	0.8%	0.07	(Kabel et al., 2002)
alcohol-insoluble residue of bran (milling fraction)	0.5%	0.04	(Mandalari et al., 2005)
aleurone, destarched cell wall material	4.9%	NR	(Rhodes et al., 2002)
<b>Barley</b>			
brewers spent grains	0.9%	0.08	(Mandalari et al., 2005)
brewers spent grains	0.8%	0.17	(Kabel et al., 2002)
<b>Oats</b>			
whole oat grain, hulled	0.8%	0.20	(Tian et al., 2015)
<b>Sorghum</b>			
endosperm, destarched, water-insoluble material	NR	0.26	(Verbruggen et al., 1993)
<b>Maize</b>			
whole grain, destarched water-insoluble cell wall material	4.9%	0.36	(Huisman et al., 2000)
corn cobs	4.3%	0.49	(Van Dongen et al., 2011)
corn bran, crude milling fraction	3.6%	NR	(Saulnier et al., 1995a)
corn bran, destarched	3.9%	0.26	(Agger et al., 2010)
corn bran, crude milling fraction	3.2%	NR	(Van Eylen et al., 2011)

<sup>a</sup>(mol)/(mol) ratio of acetyl groups to Xylp (xylopyranose) residues.

Abbreviations used: **db**: dry basis; **NR**: not reported.

### 1.2.1.3. Substitution with uronic acids

Considerable amounts of GlcA and its 4-*O*-methyl derivative are observed in maize and sorghum grain (8-9% (w/w, d.b) of the insoluble cell wall material (Huisman et al., 2000)). Isolated AX from rice grain endosperm and bran also contain up to 10% GlcA by weight

(Shibuya et al., 1983; Shibuya and Iwasaki, 1985). Smaller amounts of uronic acids are detected in all major cereal grains, including wheat (Bergmans et al., 1996), rye (Vinkx et al., 1995b), barley (Kabel et al., 2002), and oats (Tian et al., 2015). Montgomery et al. (1956) showed via partial acidic hydrolysis of corn hull hemicelluloses that  $\alpha$ -D-GlcA *O*-2-linked to xylose is present in cereal grains. Enzymatic hydrolysis of sorghum AX and the isolation and two-dimensional (2D)-NMR characterization of the released acidic AXOS has proven that  $\alpha$ -D-GlcA is *O*-2-linked to the cereal grains' AX backbone (Verbruggen et al., 1998). In sorghum, GlcA-substituted xylose residues are found both as isolated moieties and adjacent to Araf-substituted residues. Galacturonic acid is generally assumed not to be a constituent of graminaceous AX. It is sometimes present in cereal grain material, but is assigned to pectin.

#### 1.2.1.4. Cereal grain arabinoxylans are substituted with feruloylated and coumaroylated side-chains

**Table 5. Phenolic acid contents of insoluble fiber from whole cereal grain released by alkaline hydrolysis ( $\mu\text{g/g}$ ).**

Cereal	<i>trans</i> -ferulic acid	<i>cis</i> -ferulic acid	<i>trans-p</i> -coumaric acid	sinapic acid
Wheat	5952	423	166	79
Rye	6338	611	353	89
Spelt	7281	231	165	53
Barley	4675	378	481	95
Oats	4249	197	309	160
Sorghum	7619	656	298	trace
Maize	24622	213	2157	89
Rice	7512	444	2169	185
Wild rice	4358	167	175	445

Data taken from (Bunzel, 2001).

A distinguishing feature of graminaceous cell wall material is the presence of ester-linked phenolic acids. *Trans*-ferulic acid is the dominant phenolic acid released after alkaline hydrolysis of cereal grain cell wall material (**Figure 4, Table 5**), and *cis*-ferulic, sinapic, and *trans*- and *cis-p*-coumaric acids are present in smaller amounts (Bunzel, 2001; Vitaglione et al., 2008). The alkaline hydrolysates of some cereals also contain caffeic and *iso*-ferulic acids (Guo and Beta, 2013).

Mildly acidic hydrolysis of cereal grain cell wall material semi-selectively cleaves the furanosidic linkage between

Araf substituents and the AX backbone. These mildly acidic hydrolysates contain most of the cell

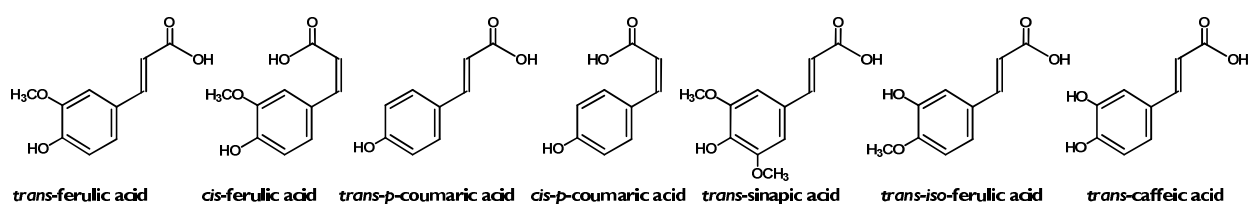


**Figure 4. Major phenolic acids released from cereal grain cell wall material with alkaline hydrolysis.**

wall materials' ferulates (Saulnier et al., 1995c). Isolation and characterization of compounds from the hydrolysates shows *O*-5-acylation of a portion of the Araf residues with ferulic acid, creating feruloylated side-chains.

In addition to the ubiquitous 5-*O-trans*-feruloyl-L-arabinofuranose (FA) structure, some grasses produce more complex feruloylated side-chains. The feruloylated disaccharide,  $\beta$ -D-xylopyranosyl-(1 $\rightarrow$ 2)-5-*O-trans*-feruloyl-L-arabinofuranose (FAX) has been identified in the leaves of various grasses (Wende and Fry, 1997) as well as rye, maize, and wild rice grains (Saulnier et al., 1995c; Bunzel et al., 2002; Steinhart and Bunzel, 2003). In maize grain,

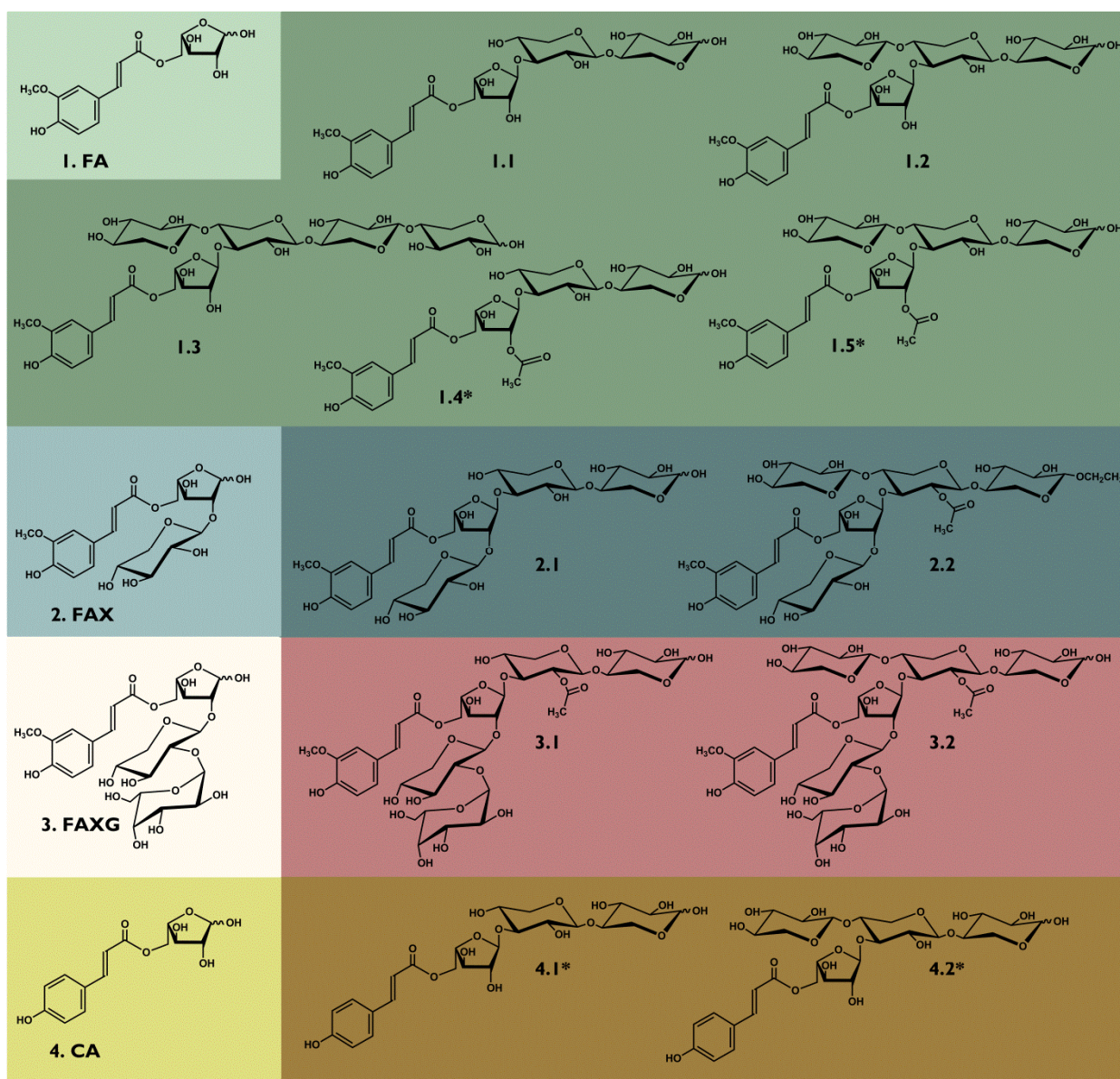


**Figure 5. Fully-characterized feruloylated mono-, di-, and trisaccharide side-chain structures isolated from cereals. Left, light-colored boxes:** Side-chain structures. **Right, dark-colored boxes:** Feruloylated oligosaccharides isolated after enzymatic hydrolysis, showing attachment of the respective side-chain structures to the arabinoxylan backbone. *Abbreviations used:* **CA:** 5-*O*-*trans*-coumaroyl-L-arabinofuranose; **FA:** 5-*O*-*trans*-feruloyl-L-arabinofuranose; **FAX:**  $\beta$ -D-xylopyranosyl-(1 $\rightarrow$ 2)-5-*O*-*trans*-feruloyl-L-arabinofuranose; **FAXG:**  $\alpha$ -L-galactopyranosyl-(1 $\rightarrow$ 2)- $\beta$ -D-xylopyranosyl-(1 $\rightarrow$ 2)-5-*O*-*trans*-feruloyl-L-arabinofuranose. \*Isolated from vegetative structures (straw or shoots).

substantial amounts of the feruloylated trisaccharide,  $\alpha$ -L-galactopyranosyl-(1 $\rightarrow$ 2)- $\beta$ -D-xylopyranosyl-(1 $\rightarrow$ 2)-5-*O*-*trans*-feruloyl-L-arabinofuranose (FAXG) were detected (Saulnier et al., 1995c; Allerdings et al., 2006). Additionally, acidic hydrolysis of maize grain fiber releases a coumaroylated side-chain: 5-*O*-*trans*-coumaroyl-L-arabinofuranose (CA) (Allerdings et al., 2006). The structures of FA, FAX, FAXG, and CA are provided in **Figure 5**, as well as all fully-characterized structures of enzymatically released feruloylated/coumaroylated oligosaccharides described in the literature. *Endo*-xylanase hydrolysis of cereal grain materials followed by isolation and characterization of the released oligosaccharides has proven that FA, FAX, and FAXG are attached to AX (Gubler et al., 1985; Bunzel et al., 2002; Appeldoorn et al., 2013). The attachment of CA to AX has not been shown yet in cereal grain materials, but oligosaccharides

containing this side-chain moiety were isolated from barley straw and bamboo shoots (oligosaccharides 4.1 and 4.2, **Figure 5**) (Mueller-Harvey et al., 1986; Ishii, 1997).

Several enzymatically-released oligosaccharides containing the FA moiety have been fully characterized and described in the literature (**Figure 5**). Oligosaccharide 1.1 is a ubiquitous product of *endo*-xylanase hydrolysis and has been isolated from barley, maize, wheat, rye, and wild rice (Gubler et al., 1985; McCallum et al., 1991; Ohta et al., 1994; Ralet et al., 1994a; Bunzel et al., 2002; Steinhart and Bunzel, 2003). The isolation of oligosaccharide 1.2, representing an isolated FA moiety, has been reported from wheat bran and rye (Lequart et al., 1999; Steinhart and Bunzel, 2003). Oligosaccharide 1.3 has been reported in wheat bran (Lequart et al., 1999). Oligosaccharides 1.4 and 1.5 are identical to oligosaccharides 1.1 and 1.2, except that the *Araf* *O*-2 positions of 1.4 and 1.5 are acetylated. These structures have, to date, only been isolated from vegetative structures of graminaceous plants (bamboo shoot and sugarcane bagasse) (Azuma et al., 1990; Ishii, 1991).

Enzymatically-released oligosaccharides containing the FAX side-chain structure have been reported in wild rice and maize (Bunzel et al., 2002; Appeldoorn et al., 2013). In maize, a structure has been isolated showing *O*-2-acetylation of the same backbone xylose moiety carrying the FAX side-chain (oligosaccharide 2.2, **Figure 5**), indicating that side-chain substitution presents no hindrance for backbone acetylation.

To date, the FAXG structure has only been isolated from maize. Two enzymatically released oligosaccharides containing the FAXG side-chain have been fully characterized in the literature (oligosaccharides 3.1 and 3.2, **Figure 5**). Like oligosaccharide 2.2, these structures display *O*-2-acetylation of a side-chain-substituted xylose moiety and underline the elaborate and dense substitution pattern of maize AX compared to other cereal grains.

Two additional feruloylated side-chains have been isolated from maize grain. These feruloylated tetrasaccharides are the most complex feruloylated side-chains reported to date (structures provided in **Figure 6**):  $\alpha$ -D-galactopyranosyl-(1 $\rightarrow$ 3)- $\alpha$ -L-galactopyranosyl-(1 $\rightarrow$ 2)- $\beta$ -D-xylopyranosyl-(1 $\rightarrow$ 2)-5-*O*-*trans*-feruloyl-L-arabinofuranose (FAXGG) and  $\alpha$ -D-xylopyranosyl-(1 $\rightarrow$ 3)- $\alpha$ -L-galactopyranosyl-(1 $\rightarrow$ 2)- $\beta$ -D-xylopyranosyl-(1 $\rightarrow$ 2)-5-*O*-*trans*-feruloyl-L-arabinofuranose (FAXGX) (Allerdings et al., 2006). An enzymatically-released oligosaccharide showing an FAXGX-like moiety attached to xylobiose was tentatively identified by ESI-MS<sup>n</sup> analysis (Appeldoorn et al., 2013), but unequivocal NMR confirmation of the attachment of these structures to AX has not been provided yet.

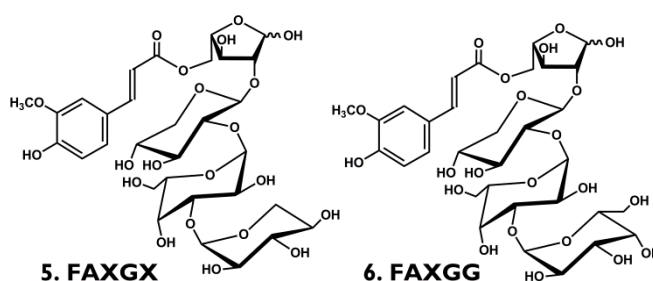


**Figure 6. FAXGX and FAXGG side-chain structures isolated from maize.**

Abbreviations used: **FAXGG**:  $\alpha$ -D-galactopyranosyl-(1 $\rightarrow$ 3)- $\alpha$ -L-galactopyranosyl-(1 $\rightarrow$ 2)- $\beta$ -D-xylopyranosyl-(1 $\rightarrow$ 2)-5-*O*-*trans*-feruloyl-L-arabinofuranose; **FAXGX** =  $\alpha$ -D-xylopyranosyl-(1 $\rightarrow$ 3)- $\alpha$ -L-galactopyranosyl-(1 $\rightarrow$ 2)- $\beta$ -D-xylopyranosyl-(1 $\rightarrow$ 2)-5-*O*-*trans*-feruloyl-L-arabinofuranose.

No AXOS containing sinapic acid have been isolated yet, so the proof of sinapic acid's attachment to AX is still lacking. A hint of its connection to cereal grain cell wall polysaccharides was provided, however, when wild rice grain insoluble cell wall material was treated with a mixture of polysaccharide-cleaving enzymes and the resulting hydrolysate contained sinapic acid (Bunzel et al., 2002).

### 1.2.1.5. Substitution of cereal grain arinoxylans with non-feruloylated or coumaroylated oligosaccharide side-chains has not been proven yet

Methylation analysis shows that many cereal grains contain, in addition to terminal Araf, 1→5-, 1→3-, and 1→2-linked Araf (Viëtor et al., 1992; Izydorczyk and Biliaderis, 1993; Vinkx et al., 1995b). Based on these results, it is widely assumed in the literature that cereal grains' AX are substituted with short non-feruloylated oligosaccharides in addition to feruloylated side-chains. However, confirmation of this assumption requires isolation and characterization of enzymatically-released AXOS containing such structural units from cereal grain material that has not been exposed to alkaline conditions. Alkaline conditions would cleave the ester linkage between the ferulate and saccharide moieties in feruloylated side-chains, creating non-feruloylated oligosaccharide side-chains which are merely experimental artefacts.

AXOS containing 1→5-linked Araf have not been reported, and the 1→5-linked Araf observed in methylation analysis likely arise from traces of pectic arabinans. Similarly, no AXOS containing 1→3-linked Araf have been reported, but this structural unit is unlikely to arise from arabinans, which have been described to contain branching on the Araf O-3-position but no linear 1→3-linked Araf residues (Wefers et al., 2015). Montgomery et al. (1957) isolated a disaccharide from alkali-extracted corn hull hemicellulose via mildly acidic hydrolysis and reported its structure as  $\alpha$ -D-xylopyranosyl-(1→3)-L-arabinose. However, no NMR data are available to confirm the structure, and this structural moiety has not been reported since.

In addition to its presence in the feruloylated side-chains series, 1→2-linked Araf occurs as part of arabinobiose side-chains substituting the xylan backbone of sorghum grain (**Figure 7**, oligosaccharides 7.1 and 7.2) (Verbruggen et al., 1998) and switchgrass biomass (Mazumder and York, 2010) (**Figure 7**, oligosaccharide 7.3). The complex AXOS identified in sorghum display both substitution with the arabinobiose side-chain and  $\alpha$ -D-GlcA on the xylan backbone, with either an unsubstituted Xylp or O-3-mXylp separating the two elements. Unfortunately, the AX materials used in these studies were extracted under alkaline conditions (concentrated Ba(OH)<sub>2</sub> and 1M KOH, respectively), meaning that it is impossible to rule out that one or both of the Araf was feruloylated in the native material. However, until now no feruloylated arabinobiose side-chain structure has been described in the literature.

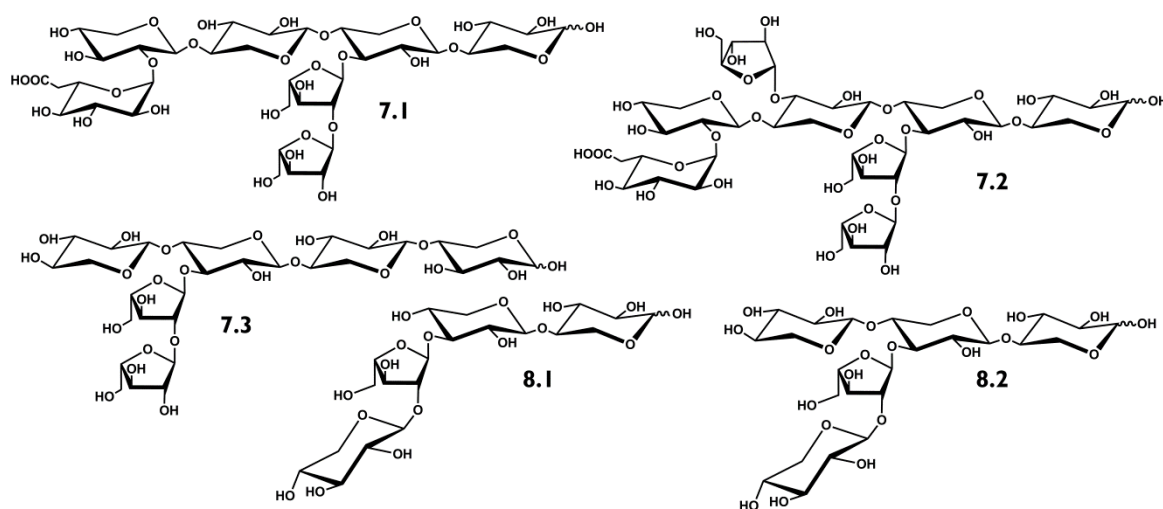


**Figure 7. Enzymatically-released arinoxylan (AX)\* oligosaccharides containing non-feruloylated side-chain oligosaccharides.** \*The AX materials used as the substrates for these enzymatic hydrolyses were isolated under alkaline extraction conditions, which would cleave ester-linked ferulates.

Non-feruloylated AXOS containing 1→2-linked *Araf* in the form of a β-D-xylopyranosyl-(1→2)-L-arabinofuranose side-chain have been reported in oat spelts, corn cobs, barley husks, rice husks, wheat straw, and switchgrass (**Figure 7**, oligosaccharides 8.1 and 8.2) (Ebringerová et al., 1992; Höjje et al., 2006; Pastell et al., 2009; Bowman et al., 2014; Bowman et al., 2015). Oligosaccharides 8.1 and 8.2 are the non-feruloylated analogues of oligosaccharides 1.1 and 1.2 (**Figure 5**). However, all of the AX materials producing this structure were alkali-extracted, and these structures therefore arose, at least partially, from de-feruloylation of FAX.

Both terminal galactopyranosyl (*Galp*) and 1→4-linked *Galp* residues are also observed in methylation analyses of some cereal materials (Huisman et al., 2000), which has led to speculation in the literature that terminal *Galp* residues may be found directly linked to the AX backbone, although no hard evidence for this linkage exists. It is probable that at least a portion of these residues arise from small amounts of pectic galactans. Terminal *Galp* would also arise from the FAXG side-chain moiety during methylation analysis, but this structural unit has only been directly observed in maize. However, LC-MS-based analyses of enzymatic (*endo*-xylanase) hydrolysates of alkali-extracted oat and barley AX have revealed oligosaccharides containing one hexose plus multiple pentose units, meaning that *Galp* is possibly part of these cereal grain AX as well (Tian et al., 2015; Coelho et al., 2016).

In summary, although it is widely assumed that cereal AX are substituted with non-feruloylated oligosaccharide side-chains, the isolation and unequivocal characterization of an AXOS containing such a structure from material not handled under alkaline conditions has yet to be performed. Therefore, definitive proof of non-feruloylated side-chain oligosaccharides as AX substituents is still lacking.

## 1.2.2. Ferulate crosslinking of cereal grain arabinoxylans

### 1.2.2.1. Dehydrodiferulates

Free-radical-induced oxidative coupling of ferulates produces dehydrodiferulates (DFAs) (**Figure 8A**), which stabilize cereal grains' cell walls by covalently cross-linking AX to each other and lignin (Allerdings et al., 2005; Bunzel, 2010). In insoluble cell wall material from cereal grains, the molar percentage of total DFAs as percentage of the sum of monomeric ferulates and dimeric DFAs ranges between 26% (spelt) and 45% (oats) (Bunzel, 2001).

Several DFA regioisomers are described according to the coupling position of the ferulate units: 8–5, 8–*O*–4, 5–5, 8–8 (cyclic (c), non-cyclic (nc), and tetrahydrofuran (THF)), and 4–*O*–5 (**Figure 8B**) (Bunzel, 2010). Analysis of the 8–5-coupled regioisomer after alkaline hydrolysis, acidification, and extraction with organic solvents such as diethyl ether or ethyl acetate gives rise to three 8–5-coupled dimers: the 8–5c, 8–5nc, and, depending on the conditions, 8–5 decarboxylated (dc) DFAs. Whereas the esterified 8–5c-dimer is presumed to be the native form in the plant, the other dimers can be formed as free acids during food processing steps involving alkaline conditions. For example, the pretreatment of cereal brans with alkali, which has been proposed as a method for potentially enhancing the bioavailability of (di)ferulates (Guo et al., 2011), results in a mixture of 8–5c, 8–5nc, and 8–5dc DFA.

In contrast to 8–5-DFA, it is assumed that all three 8–8-DFA regioisomers could naturally occur *in planta*. Esters of each of the three 8–8-linked compounds yield only their respective acids upon alkaline hydrolysis, acidification, and extraction (Ralph et al., 2004; Schatz et al., 2006). To further complicate the analytical spectrum, there are up to six potential stereoisomeric forms of the 8–8-DFA-THF regioisomer.

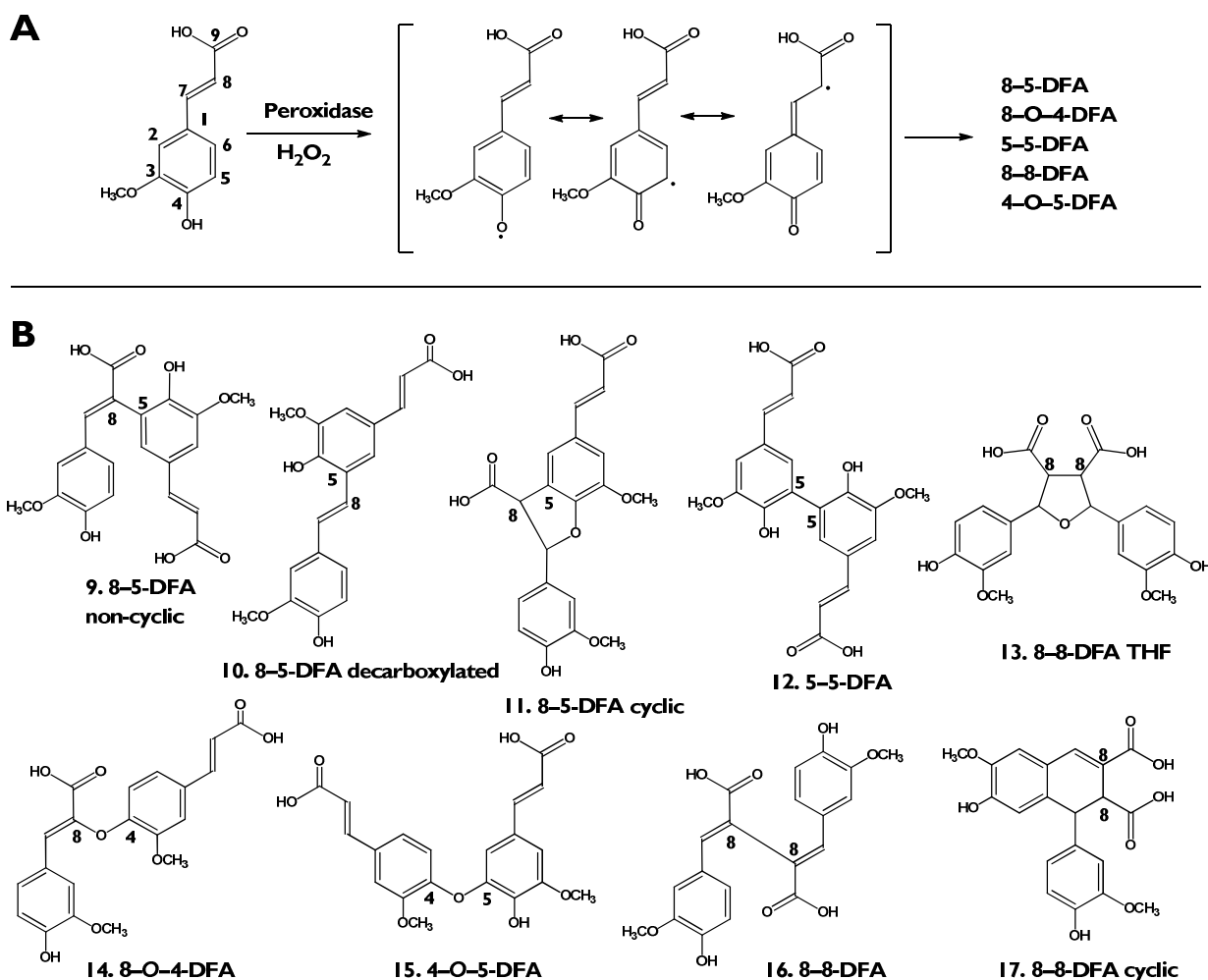


**Figure 8. (A): Formation of dehydrodiferulates (DFA) by free-radical-induced oxidative coupling. (B): DFA regioisomers present in cereal grains.**

*Abbreviations used:* THF: tetrahydrofuran.

Proof of DFAs' attachment to cereal AX has been supplied by partial degradation of cereal cell wall material (for example, mildly acidic hydrolysis) and isolation and characterization of released DFA-containing saccharides. Oligosaccharides have been isolated from maize bran containing the 5-5-DFA (Saulnier et al., 1999), 8-O-4-DFA (Allerdings et al., 2005; Bunzel et al., 2008), and 8-8-DFA (cyclic) regioisomers (Bunzel et al., 2008). Several characterized structures (**Figure 9**) contain the FAX side-chain, proving that this structural element is not sterically hindered from participating in oxidative cross-linking reactions. No 8-5-DFA-, 4-O-5-DFA-, 8-8-(non-cyclic)-DFA or 8-8-THF-DFA-saccharides have been isolated yet, so definitive proof of their attachment to cell wall polysaccharides is lacking.

Besides the dimeric DFAs, oxidatively-coupled ferulate trimers and tetramers have been identified in cereal grains (Bunzel et al., 2003a; Funk et al., 2005; Bunzel et al., 2006). The alkaline hydrolysate of popcorn flour contained the largest quantities of ferulate trimers in a screening study of various whole grain flours (Jilek and Bunzel, 2013), but trimers were found in all tested cereals (grain maize, wheat, rye, barley, and oats) and pseudocereals (buckwheat and amaranth) in the study.

Traces of sinapate dehydrodimers (8-8c and 8-8nc) are present ( $\approx 1\%$  of total ferulate DFAs) in most cereal grains. Crossed sinapate-ferulate (8-8, 8-5, and potentially 8-O-4) dimers are also formed in some cereals (Bunzel et al., 2003b).

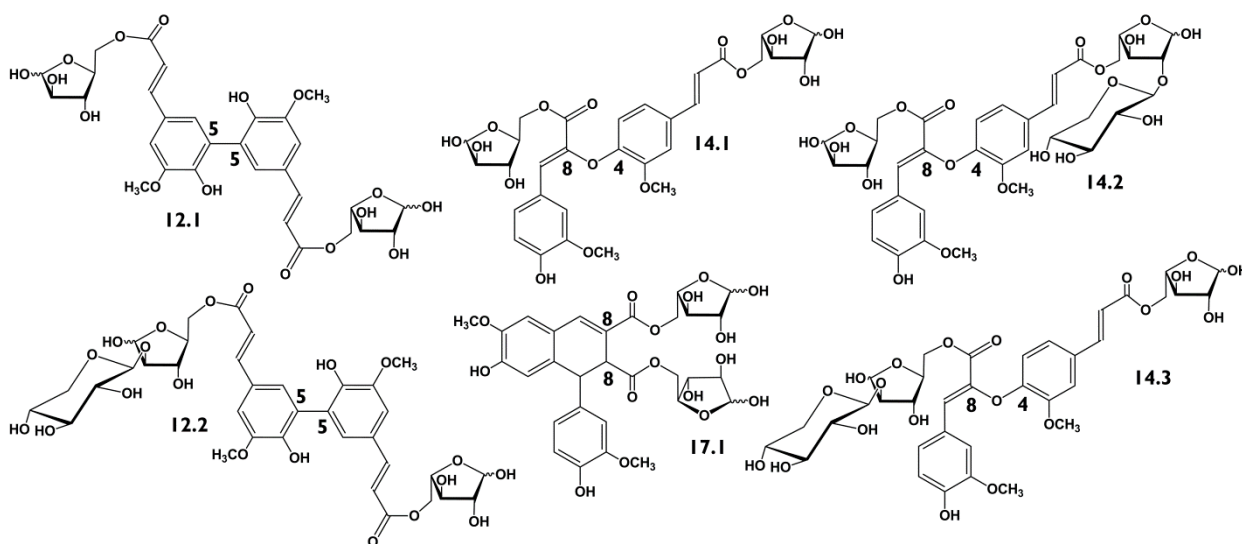


**Figure 9. Dehydrodiferulate (DFA)-oligosaccharides isolated from maize bran.**

#### 1.2.2.2. Cyclobutane dimers

In tissues exposed to UV light, phenolic acid dimers can also form via a photochemically-driven [2+2]-cycloaddition (**Figure 10**). Homodimers (ferulate-ferulate and coumarate-coumarate) and heterodimers (ferulate-coumarate) are reported (Bunzel, 2010). Multiple potential stereoisomers of the resulting cyclobutane ring exist for both the truxinic (head-to-head formation) and truxillic (head-to-tail) acids. Multiple cyclobutane ferulate and coumarate homodimers and heterodimers were present in apparently substantial amounts in the alkaline extracts of corn stover (Dobberstein and Bunzel, 2010b). However, quantification methods for these compounds have yet to be developed and validated, so it is difficult to estimate their contribution to the total dimer population in cereal grains.

AX cross-linking is important for both plant physiological processes and utilization of graminaceous cell walls. Increased ferulate cross-linking in plant materials enhances their resistance to enzymatic degradation, thus decreasing forage digestibility for livestock and impeding breakdown of forage and grain byproduct materials during second-generation biofuel production (Grabber et al., 1998; Lam et al., 2003; Chundawat et al., 2011; Jung et al., 2012b). In food processing, AX cross-linking drastically reduces the water-solubility of the AX polymer, and removal of ferulates via alkaline extraction renders the majority of AX soluble (Gruppen et al., 1992b). In their native, cross-linked state, insoluble AX still have considerable water-binding capacities and therefore exert the detrimental effect of immobilizing water in doughs and baked goods (Courtin et al., 1999). In the plant, cross-linking is suggested to be involved in cessation of

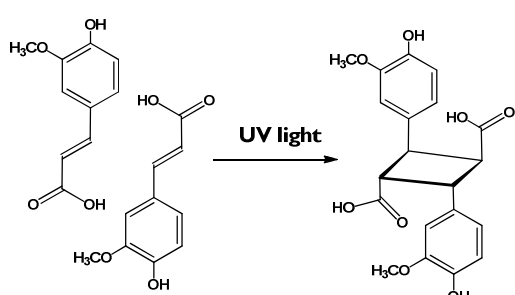


**Figure 10. Example of a ferulate cyclobutane head-to-tail (truxillic acid) homodimer.**

cell extension by increasing the cell wall's stiffness (Kamisaka et al., 1990), thus also improving plants' disease and insect resistance (Buanafina, 2009; Buanafina and Fescemyer, 2012).

#### 1.2.3. Chain length of cereal grain arabinoxylans

AX polymer sizes in cereal grains vary widely. Variability appears not only among cereal species and tissues (**Table 6**), but also varieties and growing season (Izydorczyk and Biliaderis, 1993; Buksa et al., 2014). However, additional variability has been added

**Table 6. Arabinoxylan (AX) molecular weight**

Cereal grain, tissue	AX extraction method	$M_w \times 10^{-3}^a$ (g/mol)	Analytical method	Reference
<b>Wheat</b>				
Endosperm	water-soluble AX, deferuloylated (1M NaOH, 2 h)	215-285	HPSEC-MALLS	(Dervilly-Pinel et al., 2001b)
Endosperm	water-soluble	65	sedimentation equilibrium ultracentrifugation	(Andrewartha et al., 1979)
Endosperm	water-soluble	134-201	measured apparent viscosity to calculate intrinsic viscosity, $M_w$	(Rattan et al., 1994)
Endosperm	alkaline (Ba(OH) <sub>2</sub> )	260-850	HPSEC-MALLS	(Gruppen et al., 1992a)
Whole grain flour	water-soluble	255	HPSEC-RI, dextran calibration	(Girhammar and Nair, 1992a)
Industrial bran	water soluble	two fractions: 5 and 50	gel filtration, RI detection, dextran calibration	(Maes and Delcour, 2002)
Industrial bran	mildly alkaline (0.2M NaOH)	300-350	HPSEC-RI, dextran calibration	(Shiiba et al., 1993)
Industrial bran	alkaline (H <sub>2</sub> O <sub>2</sub> in NaOH)	two fractions: 5-10 and 100-140	gel filtration, RI detection, dextran calibration	(Maes and Delcour, 2002)
<b>Barley</b>				
Endosperm	water-soluble	237-255	HPSEC-MALLS	(Dervilly-Pinel et al., 2001a)
Whole grain	water-soluble	340	HPSEC-MALLS	(Dervilly et al., 2001)
Malt	water-soluble	250	HPSEC-MALLS	(Dervilly et al., 2001)
<b>Rye</b>				
Endosperm	water-soluble	288	HPSEC-MALLS	(Dervilly-Pinel et al., 2001a)
Endosperm	alkaline (Ba(OH) <sub>2</sub> )	137-1306	HPSEC-RI, dextran calibration	(Verwimp et al., 2007)
Whole grain flour	water-soluble	770	HPSEC-RI, dextran calibration	(Girhammar and Nair, 1992a)
Whole grain flour	water-soluble	200	HPSEC-MALLS	(Andersson et al., 2009)
Whole grain flour	water-soluble	140-263	HPSEC-RI, dextran calibration	(Bukša et al., 2014)
Whole grain flour	alkaline	244-309	HPSEC-RI, dextran calibration	(Bukša et al., 2014)
Wholegrain sourdough bread	water-soluble	70	HPSEC-MALLS	(Andersson et al., 2009)
<b>Triticale</b>				
Whole grain flour	water-soluble	569	HPSEC-RI, dextran calibration	(Girhammar and Nair, 1992b)
Endosperm	water-soluble	239	HPSEC-MALLS	(Dervilly-Pinel et al., 2001a)
<b>Maize</b>				
Bran	alkaline	220-230	HPSEC-RI, dextran calibration	(Chanliaud et al., 1995)
Endosperm	alkaline	171-400	HPSEC-RALLS	(Huisman et al., 2000)

<sup>a</sup> Weight average molecular weight. When given, ranges show variations among different fractions, varieties, or planting year.

Abbreviations used: **HPSEC-MALLS**: high-performance size exclusion chromatography coupled with multi-angle laser light scattering detection; **HPSEC-RALLS**: HPSEC coupled with right-angle laser light scattering detection; **RI**: refractive index.

to the literature by the analytical challenges inherent to measuring AX chain length, including polydispersity, aggregation, and uncertain conformation. Relative measurement techniques such as calibration of gel permeation columns with dextran (pullulan) standards are especially problematic since dextrans are more flexible than AX. Therefore, the hydrodynamic volumes and column retention times of the two polymers are different, leading to overestimation of AX size. If dextran calibration is to be used, values should be reported as “relative to dextran” and not as absolute values. Finally, measurement of WU-AX chain length requires bringing the insoluble AX into solution. This may be partially accomplished by alkaline extraction, which hydrolyzes ferulate crosslinks. Ferulate crosslinks are also present in small amounts in WE-AX, which increases their measured weight-average molecular weight (Dervilly-Pinel et al., 2000).

The physicochemical and physiological consequences of variations in AX chain length differ depending on whether or not the given AX polymer is water-soluble. For WE-AX polymers, the most important effect of increased chain length is greater solution viscosity. AX solution viscosity has direct implications for human and animal nutrition and food processing. In human nutrition, consumption of viscous, soluble fibers may help to moderate the glycemic response to carbohydrates and lower plasma cholesterol (Gray (2006)). In animal nutrition, increased intestinal viscosity is linked with decreased ileal starch digestibility and therefore, decreased feed-to-gain ratios (Meng et al., 2005). Finally, in food processing, the desirability of WE-AX viscosity depends on the process. For example, viscosity conferred by WE-AX is assumed to be at least partially responsible for their positive dough-stabilizing effects in bread baking (Goesaert et al., 2005). When the WE-AX sizes of rye and wheat, the two major cereals used in bread-baking, are directly compared in the same study, the molecular weights of rye WE-AX are higher (Girhammar and Nair, 1992a; Dervilly-Pinel et al., 2001a). In contrast to bread-baking, increased AX molecular weight is a negative characteristic in beer brewing, where viscous WE-AX decrease the wort membrane filterability (Lu and Li, 2006).

As described previously, AX substitution patterns directly influence the water solubility of the polymer and therefore contribute to the relative viscosity of an aqueous extract from a given cereal source by altering the AX concentration in solution. However, relative viscosity is not only a function of polymer concentration but also of the intrinsic viscosities of the individual polymers in the solution. Early researchers proposed that increased arabinose substitution along the xylan backbone resulted in a fully extended, rigid AX polymer (Andrewartha et al., 1979). Compared to more flexible polymers, rigid polymers have greater hydrodynamic volumes and therefore, greater intrinsic viscosities. However, later work with homogenous AX solutions has shown that AX polymers have a “semi-flexible random-coil” conformation in solution and that intrinsic viscosity of AX polymers is solely determined by the xylan chain length, not degree of backbone substitution (Dervilly-Pinel et al., 2000; Dervilly-Pinel et al., 2001b). Given the large natural variability of AX chain lengths among cereal grains, WE-AX concentration alone cannot predict the relative viscosity of an aqueous grain extract (Saulnier et al., 1995b).

AX size also influences the extent of AX adsorption to cellulose: adsorption increases with AX chain length (Kabel et al., 2007). Both WE- and WU-AX adsorb to cellulose and inhibit the enzymatic hydrolysis of cellulose by cellulase in model systems (Zhang et al., 2012).

### **1.3. Enzymatic fermentability of arabinoxylans is strongly affected by arabinoxylan structural differences**

Feruloylated AX are depolymerized by a variety of enzymes, including *endo*-1,4- $\beta$ -

xylanases and the accessory enzymes,  $\beta$ -xylosidases,  $\alpha$ -L-arabinofuranosidases,  $\alpha$ -glucuronidases, feruloyl esterases, acetylxylan esterases, and  $\alpha$ -galactosidases (Crepin et al., 2004; Pollet et al., 2010a; Biely et al., 2014; Lagaert et al., 2014). These enzymes work synergistically, i.e. simultaneous treatment with an enzymatic cocktail breaks down AX more effectively than consecutive treatment with individual enzymes (de Vries et al., 2000). The enzymatic degradability of AX is influenced by many structural factors, including the degree of substitution along the xylan backbone, presence of oligosaccharide side-chains, *O*-5-feruloylation of *Araf* backbone substituents, and ferulate-governed crosslinking of xylan strands (Grabber et al., 1998; Beaugrand et al., 2004b; Jung et al., 2012a; Neumüller et al., 2014; Snelders et al., 2014b).

*Endo*- $\beta$ -(1,4)-D-xylanases (EC 3.2.1.8) cleave the internal  $\beta$ -(1 $\rightarrow$ 4)-linkages between xylose residues in the AX backbone, producing low molecular weight oligosaccharides. Four separate glycoside hydrolase (GH) families are registered in the Carbohydrate-Active Enzymes (CAZy) database: GH5, GH8, GH10, and GH11. This discussion will focus on the GH10 and GH11 families, which make up the majority of identified xylanases (Pollet et al., 2010a).

The smallest hydrolysis products of GH10 and GH11 xylanases are xylobiose and xylotriose, respectively. Further breakdown of these oligosaccharides to xylose monomers requires  $\beta$ -xylosidases. GH10 xylanases are less hampered by backbone substitution than their GH11 counterparts and require only two consecutive unsubstituted xylose residues for hydrolysis, compared to three for GH11 xylanases (Pollet et al., 2010a). However, both enzymes are incapable of completely solubilizing densely-substituted regions along the AX backbone. Therefore, xylanase-resistant residues remaining after xylanase hydrolysis have higher A/X ratios than the original AX material (Beaugrand et al., 2004a; Beaugrand et al., 2004b; Marcotuli et al., 2016).

GH10 xylanases can cleave the glycosidic linkage on the non-reducing end of a xylose substituted with either arabinose or methyl-GlcA, whereas GH11 xylanases cannot (Pollet et al., 2010a). AX backbone substitution with acetyl groups appears to partially hinder *endo*-xylanases in a comparable manner to *Araf* or methyl-GlcA substitution (Selig et al., 2009; Biely et al., 2013). GH10 and GH11 xylanases can release acetylated AXOS (Veličković et al., 2014), showing that these enzymes are not totally blocked by acetyl residues. GH10 *endo*-xylanases can accommodate acetylated xyloses in the -III, +I, +III, and +IV subsites but are hindered by acetylation in the -II, -I, and +II subsites (Biely et al., 2013). Agger et al. (2010) compared addition of either acetyl xylan esterase or feruloyl esterase (or both) to a minimalistic enzyme mixture containing a GH10 xylanase and an  $\alpha$ -L-arabinofuranosidase on the breakdown of maize bran. The addition of acetyl xylan esterase, which removes blocking acetyl groups on the backbone, resulted in a greater release of soluble xylose than the feruloyl esterase alone. A synergistic effect was observed when both esterases were used, resulting in a greater release of soluble xylose than either esterase alone. Similar results have been reported by other research groups, who found that the addition of acetyl xylan esterase to hemicellulolytic preparations enhanced the breakdown of wheat WU-AX (Tong et al., 2015) and water-unextractable solids from maize silage (Neumüller et al., 2014).

$\alpha$ -L-Arabinofuranosidases, which cleave the *O*-2- and *O*-3-glycosidic bonds between *Araf* substituents and the AX backbone, are found in glycoside hydrolase (GH) families 3, 43, 51, 54, and 62 (Lagaert et al., 2014). Arabinofuranosidases are typically hindered by *O*-5-feruloylation of *Araf* (Hespell and O'Bryan, 1992; Luonteri et al., 1999; Panagiotou et al., 2003;

Remond et al., 2008), and only one arabinofuranosidase capable of cleaving 5-*O*-*trans*-feruloyl-L-arabinofuranose (FA) from a xylan or xylooligosaccharide backbone is described in the literature (Wood and McCrae, 1996). Arabinofuranosidases are also unable to cleave xylose-substituted arabinoses, regardless of whether or not these arabinoses are feruloylated (Bowman et al., 2014; Bowman et al., 2015). Therefore, for complete enzymatic breakdown of AX substituted with the FAX structural moiety, both feruloyl esterase and  $\beta$ -xylosidase are necessary to remove the ferulic acid and terminal xylose, respectively. Reports on the ability of  $\beta$ -xylosidases to cleave terminal xylose from an oligosaccharide side-chain moiety are mixed. Although Wende and Fry (1997) described the conversion of free FAX to FA with  $\beta$ -xylosidase, Bowman et al. (2014) were unable to cleave the side-chain xylose of a  $\beta$ -D-xylopyranosyl-(1 $\rightarrow$ 2)-L-arabinofuranose side-chain with  $\beta$ -xylosidase when it was linked to a xylotetrasaccharide backbone remnant. For the cleavage of the terminal  $\alpha$ -Gal units found in the FAXG and FAXGG structural moieties, an  $\alpha$ -galactosidase should be required. However, specific studies on the action of this enzyme against either FAXG or FAXGG have not yet been performed.

## **1.4. Arabinoxylan structural differences influence food processing outcomes**

### **1.4.1. Arabinoxylans and bread-baking**

With their large water-holding capacities and ability to form viscous solutions (Girhammar and Nair, 1992b; Vanhamel et al., 1993), AX strongly influence dough and bread characteristics. In the case of rye flour, for example, whose ability to form a gluten network is marginal compared with wheat, native WE-AX are essential for successful bread baking (Verwimp et al., 2012). Supplementing rye doughs with additional WE-AX further improves bread and dough structures (Buksa et al., 2015).

The overall effect of AX on dough and bread structure strongly depends on their water extractability and molecular weight. In general, WE-AX with a high molecular weight (>200,000) exert positive effects on dough and bread, whereas WE-AX with lower molecular weights and WU-AX decrease dough and bread quality (Goesaert et al., 2005). Several mechanisms are discussed for the positive effects of high-molecular-weight WE-AX on bread and dough structures. First, WE-AX increase the viscosity of the aqueous phase surrounding gas bubbles in bread dough, which slows down the diffusion of carbon dioxide and promotes gas retention. Second, at high concentrations, WE-AX can form gel-like structures, which could serve as a secondary, complementary network stabilizing the primary gluten network. WE-AX-mediated stabilization results in improved loaf volume and crumb structure. Furthermore, AX slow bread staling, either by sterically hindering starch associations or by altering water distribution.

WU-AX are generally associated with a reduction in dough and bread quality, and several mechanisms are discussed for this effect (Courtin and Delcour, 2002; Goesaert et al., 2005). First, WU-AX immobilize large amounts of water, which is then unavailable for protein hydration and gluten formation. Second, WU-AX can act as a physical barrier between proteins, thus hindering gluten development. Finally, WU-AX may perforate gas cells, thus destabilizing the gluten network.

The addition of *endo*-xylanase enzymes to dough is a processing tool often applied to enhance the positive effects of AX in bread-baking. Importantly, such treatments are most effective when the enzymes preferentially attack WU-AX over WE-AX and are active during the

mixing stage. This maintains the positive effects of WE-AX throughout the baking process and provides additional solubilized AX for the dough fermentation stage, while reducing the negative effects of WU-AX (Courtin et al., 1999; Dornez et al., 2011). Enzyme dosage is also important: excessive levels of *endo*-xylanases release too much water and produce sticky doughs (Courtin and Delcour, 2002).

Based on the proven prebiotic and potential antioxidative human health benefits of feruloylated AXOS (see **Section 1.5**), bread supplemented with these compounds has been proposed as a functional food in human diets. Snelders et al. (2014a) investigated the effects of feruloylated AXOS on bread and dough characteristics and found that adding AXOS with high levels of ferulates or the same amount of ferulates as free ferulic acid both significantly increased dough extensibility and produced unmanageable doughs above an AXOS concentration of 2% (dry matter basis). Conversely, adding AXOS low in ferulates produced stiff, dry doughs with a high resistance to extension. Whereas the effects of low-ferulate AXOS were attributed to increased water absorption by the carbohydrate portion of the AXOS, thus reducing gluten hydration, the dough-relaxing effects of both esterified ferulates and free ferulic acid could not be explained. Jackson et al. showed that endogenous ferulates present in the soluble fraction of dough were depleted during mixing and contributed to breakdown of overmixed gluten-starch doughs (Jackson and Hosney, 1986b). These researchers also provided evidence for formation of a covalent cysteine-ferulate adduct in a model dough system (Jackson and Hosney, 1986a). However, in the baking study by Snelders, neither loss of cysteine nor ferulic acid was observed (Snelders et al., 2014a). Although ferulate addition noticeably affected dough properties, no effects on loaf volume were observed, meaning that feruloylated AXOS supplementation of bread is technologically feasible.

#### **1.4.2. Arabinoxylans and refrigerated dough quality**

In contrast to bread-baking, where *endo*-xylanase solubilization of WU-AX is desirable, the steady solubilization of WU-AX by endogenous or microbial *endo*-xylanases during storage of refrigerated doughs is responsible for the refrigerated dough defect called “syruping”, or release of water (Gys et al., 2003). To avoid this defect, the food industry has tested three solutions: first, adding additional xylans to the product to make up for their partial loss during storage; second, adding xylanase inhibitors to refrigerated dough products; and third, debranning flour before milling, which reduces the *endo*-xylanase content of flour (Courtin et al., 2006).

#### **1.4.3. Arabinoxylans and beer brewing**

During mashing, WE-AX are brought into solution and some of the WU-AX may be solubilized enzymatically. High levels of WE-AX in the wort increase its viscosity and reduce filtration volumes. This effect is especially pronounced in wheat beers, which have higher AX contents than barley-based beers (Lu and Li, 2006). Although AX contents in beer are negatively associated with wort filterability, some evidence points towards an enhancing effect of AX on protein-stabilized beer foam, presumably by increasing the viscosity of the liquid phase (Evans et al., 1999; Husband et al., 2009).

To address the problem of poor wort filtration, brewers may add enzyme mixtures during mashing which target both AX and  $\beta$ -glucan. Beers produced with these enzymes contain higher levels of free ferulic acid or soluble, ester-linked ferulates than non-treated beers (Szwajgier et al., 2005; Szwajgier et al., 2007), although naturally-occurring *endo*-xylanases in wort also contribute to release of water-soluble ferulates. These feruloylated, water-soluble AXOS are prime substrates for the naturally-occurring feruloyl esterases in wort (Vanbeneden et al., 2007).

Besides variations in *endo*-xylanase activity, differences in the AX structures used in the cereal malts or adjuncts alter enzymatic degradability (as discussed in **Section 1.3**) and therefore also affect the free ferulic acid concentration in beers (Vanbeneden et al., 2008). In addition to the prebiotic potential of feruloylated AXOS, both feruloylated AXOS and free ferulic acid are highly bioavailable sources of ferulates (see discussion in **Section 1.5** regarding potential human health implications). Furthermore, free ferulic acid in wort is metabolized by yeast to 4-vinyl guaiacol, an important flavor impact compound in certain beers. Another important sensory aspect of AXOS in beer is their positive contribution to mouthfeel (Aerts et al., 2010).

## **1.5. Potential human health benefits are discussed for arabinoxylans**

Besides the general health benefits ascribed to dietary fiber, AXOS display exceptional prebiotic properties. Ferulates could also potentially act as dietary antioxidants following their release from the AX polymer in the gut. Importantly, the health-promoting properties of feruloylated AX are structure-dependent, which further underlines the importance of being able to detect and describe structural differences in the AX from different cereal sources.

### **1.5.1. Arabinoxylans belong to the dietary fiber complex**

The American Association of Cereal Chemists International recommends the following definition for dietary fiber:

*“Dietary fiber is the edible parts of plants or analogous carbohydrates that are resistant to digestion and absorption in the human small intestine with complete or partial fermentation in the large intestine. Dietary fiber includes polysaccharides, oligosaccharides, lignin, and associated plant substances. Dietary fibers promote beneficial physiological effects including laxation, and/or blood cholesterol attenuation, and/or blood glucose attenuation.”* (AACCI, 2001)

National definitions of dietary fiber vary slightly between the health authorities of different nations (Jones, 2014). The major source of disagreement arose from a similar definition provided by the Codex Alimentarius in 2009, which explicitly defined dietary fiber as “carbohydrate polymers with 10 or more monomeric units” (CODEX, 2010) and left the decision of whether or not smaller oligosaccharides with a degree of polymerization (DP) between 3 and 9 should be considered dietary fiber open to the individual national authorities (Jones, 2014). Although the Codex definition first appears to limit dietary fiber to “carbohydrate polymers” (which would exclude ferulates and lignin), a footnote to the definition states:

*“When derived from a plant origin, dietary fibre may include fractions of lignin and/or other compounds associated with polysaccharides in the plant cell walls. These compounds also may be measured by certain analytical method(s) for dietary fibre.”* (CODEX, 2010)

The compounds classified as “dietary fiber” have extremely diverse compositions and physicochemical properties. Many health benefits are ascribed to dietary fiber, but these health benefits are structure-specific (Gray, 2006). For example, viscous polysaccharide fibers such as guar gum have the positive effect of slowing down gastric emptying and moderating blood glucose levels after a meal. Non-viscous fibers such as cellulose have no effect on gastric emptying, but seem to relieve symptoms of diverticulitis more effectively than viscous fibers.

As the dominant hemicelluloses in whole cereal grains, feruloylated AX are major contributors to the dietary fiber complex in diets containing whole grains. Numerous epidemiological studies have shown that consumption of whole grains is associated with various

health benefits, including reduced risk and/or slowed progression of cardiovascular disease (Erkkilä et al., 2005; Mellen et al., 2008), type 2 diabetes (de Munter et al., 2007; Ardisson Korat et al., 2014), and colon cancer (Schatzkin et al., 2007; Egeberg et al., 2010). Several health-promoting mechanisms are linked to consumption of cereal grain fiber, including faecal bulking and reduction of constipation, fermentation by the colonic microflora and resulting production of health-promoting short-chain fatty acids, and reduced risk of obesity (Topping, 2007).

### **1.5.2. Arabinoxylans have prebiotic properties**

To qualify as a prebiotic, compounds must meet several criteria: first, they must be non-digestible (i.e. resistant to stomach acids, human digestive enzymes, or absorption in the small intestine); second, they must be fermentable by the gut microbiota; and third, they must selectively stimulate the growth of the intestinal bacteria which positively influence health and well-being (Anadón et al., 2010). Both AX and AXOS clearly meet these three criteria, as reviewed by Broekaert et al. (2011). AXOS are stable against acidic hydrolysis under simulated gastric conditions (Courtin et al., 2009), and Sanchez et al. (2009) showed that AXOS were resistant to *in vitro* simulation of the human stomach and small intestine. Numerous studies (including *in vitro*, animal, and human models) have shown that both AX and AXOS are fermented by the gut microbiota and selectively increase propionate and/or butyrate levels (Sanchez et al., 2009; Damen et al., 2011; Damen et al., 2012; Van den Abbeele et al., 2013). Finally, both AX and AXOS are bifidogenic in humans (Cloetens et al., 2010; Maki et al., 2012).

The fermentation profiles and resulting prebiotic effects of feruloylated AX differ based on their cereal source and AX structure. A particular benefit of using these AX structures, which are gradually fermented throughout the colon, thus delivering fermentable carbohydrates to the distal colon, is discussed in the literature. The localization of fermentation to the distal colon is believed to limit protein fermentation, which is associated with negative health consequences, by providing carbohydrate-fermenting bacteria with their substrates. AXOS with an average DP of 29 were associated with extended fermentation, distal colon fermentation, and reduced markers of protein fermentation in a human intestinal model (Sanchez et al., 2009). Shorter AXOS were primarily fermented in the proximal colon. AX cross-linking also slows AX fermentation in humans (Hopkins et al., 2003). Potential synergisms have been shown, i.e. mixtures of AXOS, WU-AX, and WE-AX have a stronger bifidogenic effect and reduce markers of protein metabolism more than the sums of their individual parts (Damen et al., 2011).

### **1.5.3. Cereal ferulates could have beneficial health effects**

Of the whole grain components (bran, germ, and starchy endosperm), the bran constituents seem to play a leading role in the “whole grain effect” (Jensen et al., 2004; de Munter et al., 2007). The ester-linked hydroxycinnamates concentrated in the cereal bran fraction have been hypothesized to be partially responsible for these observed health benefits, following their release from the dietary fiber complex by the concerted action of bacterial xylanases and esterases in the large intestine (Vitaglione et al., 2008).

Cinnamoyl esterases are produced by the human small intestine (Andreasen et al., 2001b), but their activity against hydroxycinnamate esters is very inefficient compared to that of the human intestinal microbiota, which are capable of releasing ester-linked ferulate monomers and DFAs from both model compounds and cereal bran (Andreasen et al., 2001a; Andreasen et al., 2001b). DFAs were rapidly absorbed into the plasma of rats following an oral dose of the free DFAs (Andreasen et al., 2001a). In contrast, no DFAs were detected in human plasma after consumption of a bran-rich cereal (Kern et al., 2003), indicating that DFAs ingested in their

native environment (ester-linked to AX) are metabolized by intestinal microbiota or excreted. Ferulate monomers, on the other hand, are detected in human plasma along with microbial metabolites after consumption of whole-grain cereal products (Kern et al., 2003; Anson et al., 2011). Ferulate bioavailability can be increased through modifications to cereal products, such as enzymatic processing of whole grain ingredients (Anson et al., 2011; Pekkinen et al., 2014). However, the amount of ferulaes absorbed as such (i.e. without microbial transformation) is relatively small ( $\approx 3\%$ ) (Kern et al., 2003). Therefore, although free ferulates or feruloylated AXOS were demonstrated to exert potential health benefits in isolated *in vitro* situations, such as free radical reduction (Russell et al., 2005; Snelders et al., 2013) and inhibition of LDL oxidation (Andreasen et al., 2001c), a relevant discussion of the physiological effects of ferulates must include their susceptibility to microbial metabolism and the physiological effects of these metabolites.

## 1.6. Biosynthesis of arabinoxylans

AX are synthesized in the Golgi apparatus and carried to the cell wall in membrane-bound vesicles. Until recently, little was known about the exact enzymes in the AX synthesis machinery of feruloylated AX. However, the completion of genome sequencing for both rice and *Arabidopsis* (*Arabidopsis thaliana*) enabled the direct comparison of a grass with a dicot genome. By assuming that genes involved in AX biosynthesis would be expressed at much higher levels in rice than *Arabidopsis*, Mitchell et al. (2007) used bioinformatics to identify likely candidate genes for involvement in AX assembly (glycosyltransferases (GT) from the GT43, GT47, and GT 61 families) and feruloylation (a subgroup of the CoA-acyl transferase superfamily). This unleashed an explosion of laboratory research, which has largely confirmed Mitchell's results, although many details of AX synthesis remain unknown (see reviews by Rennie and Scheller (2014) and Saulnier et al. (2012)). The key enzymes involved in AX assembly are glycosyltransferases (GTs), and most are found in the Golgi as Type II membrane-bound proteins (containing a single transmembrane region, with the N-terminal anchor extending into the cytosol and the C-terminal region containing the catalytic domain positioned in the Golgi lumen). However, some of the enzymes needed for synthesis of intermediates are located in the cytosol, meaning specific transporters are likely required for shuttling the products of these enzymes into the Golgi (Oikawa et al., 2013).

The nucleotide sugar, uridine diphosphate (UDP)-glucose (Glc), is the starting point for AX biosynthesis (**Figure 11**). UDP-Glc is oxidized to UDP-GlcA by UDP-Glc dehydrogenase (UGD), which is moved into the Golgi via an unknown transporter. In the Golgi, UDP-GlcA may either be transferred onto the xylan backbone by glucuronyltransferase (GUX) or converted to UDP-Xylose (Xyl) by a membrane-bound enzyme, UDP-Xyl synthase (UXS) (Saulnier et al., 2012). Cytosolic UXS isoforms have also been described, and a Golgi-localized UDP-Xyl transporter shuttling UDP-Xyl between the cytosol and Golgi was identified in *Arabidopsis* (Rennie and Scheller, 2014; Ebert et al., 2015).

### 1.6.1. Xylan backbone synthesis

Xylans in conifers and dicots display a unique reducing end sequence:  $\beta$ -D-Xylp-(1 $\rightarrow$ 4)- $\beta$ -D-Xylp-(1 $\rightarrow$ 3)- $\alpha$ -L-Rhap-(1 $\rightarrow$ 2)- $\alpha$ -D-GalAp-(1 $\rightarrow$ 4)-D-Xylp. The function of this sequence is debated, with some researchers suggesting that it serves as a primer, whereas others hypothesize it may act as a terminator for chain elongation (Scheller and Ulvskov, 2010). This reducing end oligosaccharide has not been detected in grasses (Kulkarni et al., 2012), although to date, only



and low xylan contents in mutant plants. The xylosyltransferases IRX9 (GT family 43), IRX10 (GT family 47), and IRX14 (GT family 43) are all involved in extension of the xylan chain, with the IRX10 ortholog showing the highest relative expression of the three genes in wheat endosperm (Pellny et al., 2012). Inhibition of the genes coding IRX9 and IRX10 results in reduced AX content, chain length, and extract viscosity in wheat (Lovegrove et al., 2013; Freeman et al., 2016). Xylosyltransferases appear to exist in the Golgi as part of a multi-protein xylan synthase complex (Zeng et al., 2010), where they function interdependently (Jiang, 2015). Lee et al. (2012) found that simultaneous expression of IRX9 and IRX14 in tobacco BY2 cells induced xylan synthesis, whereas expression of either IRX9 or IRX14 alone had little effect.

### 1.6.2. Xylan backbone substitution

In cereal grain AX,  $\alpha$ -L-Araf is the dominant substituent, being found as a mono- and/or di-substituent at the xylopyranosyl *O*-3 and/or *O*-2 positions (Izydorczyk and Biliaderis, 1995). Two biosynthetic routes for arabinose exist *in planta*. The first, a membrane-bound UDP-Xyl 4-epimerase (UXE), catalyzes the freely reversible interconversion of UDP-Xyl and UDP-arabinopyranose (Arap) in the Golgi and has been identified in both *Arabidopsis* and barley (*Hordeum vulgare*) (Burget et al., 2003; Zhang et al., 2010). UXE show a strong preference for UDP-Xyl and UDP-Arap (Zhang et al., 2010; Sogaard et al., 2012). The second, a cytosolic UDP-glucose epimerase (UGE) with broad substrate specificity (substantial activity against UDP-Xyl and UDP-Arap in addition to UDP-Glc and UDP-Gal) has been characterized in *Arabidopsis*, meaning UDP-Xyl in the cytosol could possibly be converted to UDP-Arap (Kotake et al., 2009). However, although grasses also express multiple UGEs, this cytosolic biosynthetic route may be less significant in grasses than dicots: for example, barley UGEs showed little activity against UDP-Xyl (Zhang et al., 2006).

Importantly, although the pyranosyl configuration of arabinose is more thermodynamically stable than the furanosyl configuration (Mackie and Perlin, 1966; Angyal and Pickles, 1967; Conner and Anderson, 1972), arabinose is incorporated into the AX polymer of monocots (and the pectic arabinans of dicots) as Araf. It was originally speculated that UDP-Arap is the sugar donor, and that the pyranose to furanose tautomerization was catalyzed by the arabinosyltransferase during arabinose addition to the xylan backbone. Indeed, supplying intact Golgi bodies from wheat (*Triticum aestivum*) seedlings with radiolabeled UDP-Arap in the presence of non-labeled UDP-Xyl resulted in the incorporation of radioactivity into an AX-like (susceptible to hydrolysis by xylanases and arabinofuranosidases) product (Porchia et al., 2002). However, UDP-Araf was clearly shown to be a sugar donor for the synthesis of arabinan oligosaccharides in mung beans (Konishi et al., 2006), pointing to the possibility that plants express a separate enzyme catalyzing the conversion of UDP-Arap to UDP-Araf. An UDP-Arap mutase (UAM) from GT family 75 was first successfully identified and characterized in rice and catalyzed the reversible interconversion of UDP-Arap and UDP-Araf, with a thermodynamic pyranose:furanose equilibrium of ~90:10 (Konishi et al., 2007). Enzymatic activity was concentrated in the cytosolic fraction, and the protein was assigned to the Reversibly Glycosylated Proteins (RGP) family: plant-specific, soluble cytosolic proteins which are often associated with the Golgi body (Konishi et al., 2007; Rautengarten et al., 2011). It is currently believed that UAM is associated, but not membrane-bound, with the Golgi membrane on its cytosolic side, which would necessitate the transport of UDP-Araf into the Golgi for arabinosylation of the xylan backbone (Oikawa et al., 2013). Very recent work indicates that a cytosolic RGP forms part of the multi-enzyme xylan synthase complex (which also successfully

substitutes xylans with *Araf* when supplied with UDP-*Arap*) in wheat (Jiang, 2015). The importance of UAM for normal AX synthesis has been shown by down-regulating gene expression coding for this protein in rice, which produced stunted, infertile plants with reduced arabinose, ferulic acid, and *p*-coumaric acid contents in their cell walls (Konishi et al., 2011). Similar cell wall composition results (reduced arabinose, ferulate, and coumarate) were observed in the grass species *Brachypodium distachyon* following reduced UAM expression (Rancour et al., 2015), but in contrast to the report from rice, plant vitality was not affected. Several UAM have also been identified in barley (Hsieh et al., 2016).

A GT61 family member was shown to be responsible for  $\alpha$ -(1→3)-arabinosyl substitution of xylan and named xylan arabinosyltransferase (XAT) (Anders et al., 2012). Heterologous expression of wheat and rice XAT gene orthologs in the dicot *Arabidopsis* had the gain-of-function effect of inducing xylan arabinosylation. Furthermore, knocking down XAT expression drastically reduced  $\alpha$ -(1→3)-arabinose monosubstitution in wheat endosperm, but had no effect on levels of disubstitution, indicating that additional enzymes are likely responsible for  $\alpha$ -(1→2)-arabinose substitution and  $\alpha$ -(1→3)-arabinose substitution on dXylp residues. Interestingly XAT suppression reduced both the average AX chain length and the content of WE-AX in wheat (Anders et al., 2012; Freeman et al., 2016).

Little is known about the biosynthesis of oligosaccharide side-chain substituents. Chiniqy et al. (2012) described a GT61 xylosyltransferase in rice which modified  $\alpha$ -(1→3)-linked arabinose substituents with  $\beta$ -(1→2)-xylosyl units. The enzyme was designated xylosyl arabinosyl substitution of xylan 1 (XAX1). Loss-of-function mutants not only lacked the  $\beta$ -Xylp-(1→2)- $\alpha$ -*Araf*-(1→3)- structural feature but also had reduced ferulate and coumarate contents compared to wild-type plants. These results were surprising, given the current hypothesis for AX feruloylation: UDP-feruloyl arabinose has been proposed as the xylan feruloylation substrate (Buanafina (2009); see below). If that were the case, however, and the side-chain xylose residue is added by XAX1 after feruloylation, one would not expect to see a reduction in ferulate content in the *xax1* mutant plants. Biosynthetic pathways for the more complex AX side-chain substituents have not been described. Complex side-chains have been described containing, in addition to the  $\beta$ -(1→2)-Xylp- $\alpha$ -(1→3)-*Araf* moiety, both  $\alpha$ -Galp and  $\alpha$ -Xylp components, meaning that two more GTs may be necessary for synthesis of complex AX side-chains.

Other backbone decorations such as GlcA, its 4-*O*-methyl derivative, or acetate esters are also observed (although to a lesser extent than arabinose or oligosaccharide side-chains) in grasses, particularly in maize and sorghum AX (Verbruggen et al., 1995; Huisman et al., 2000; Kabel et al., 2002; Appeldoorn et al., 2010; Appeldoorn et al., 2013). GlcA may be attached to the xylan backbone by GUX (GT8 family) via UDP-GluA. A GT47 GUX that functions as an integral member of a xylan synthase complex has also been identified in wheat (Jiang, 2015). The GlcA residues may be modified by 4-*O*-methyl groups, which are transferred by glucuronoxylan methyltransferase (GXMT) from *S*-adenosyl-methionine. The biosynthetic mechanism for AX acetylation is not completely clarified, although it is known that acetyl-CoA is the acetate donor, that both DUF231 (Domain of unknown function) and Reduced Wall Acetylation (RWA) proteins are involved, and that acetylation occurs in the Golgi (Rennie and Scheller, 2014).

### 1.6.3. Feruloylation of the arabinoxylan polymer

Hydroxycinnamates originate from the phenylpropanoid pathway (**Figure 11**), which utilizes the amino acids phenylalanine and, in grasses, tyrosine and also produces the monolignol

precursors of lignin. The esterification of cell wall polymers with hydroxycinnamates is ubiquitous to the commelinid monocots and also observed in the core Caryophyllales members (Harris and Trethewey, 2010). In grasses, feruloylation of AX is a distinguishing feature.

Mitchell et al. (2007) used a bioinformatics approach to compare gene expression in grasses (rice) to dicots (*Arabidopsis*), successfully singling out 12 loci from the Pfam family PF02458 as candidates for AX feruloylation. These genes belong to the BAHD acyl transferase superfamily, which was named after its first four biochemically characterized members: **BEAT**, **AHCT**, **HCBT**, and **DAT** (BEAT: Benzylalcohol *O*-acetyltransferase; AHCT: Anthocyanin *O*-hydroxycinnamoyltransferase; HCBT: *N*-Hydroxycinnamoyl/benzoyltransferase; and DAT: Deacetylindoline 4-*O*-acetyltransferase) and whose proteins utilize CoA thioesters as acyl donors. The proteins encoded by Mitchell's candidate genes were found to be expressed in all tissues of *Brachypodium distachyon* (Molinari et al., 2013). Downregulation of gene transcription produced lower ferulate levels in rice (Piston et al., 2009), and upregulation increased ferulate levels in *Brachypodium* (Buanafina et al., 2015). Some of the proteins from the Mitchell clade are highly specific: for example, two separate proteins contribute precisely to coumaroylation of AX (Bartley et al., 2013) and acylation of monolignols with *p*-coumaric acid (Withers et al., 2012; Marita et al., 2014; Petrik et al., 2014), respectively.

Feruloylation occurs intracellularly (Fry et al., 2000; Obel et al., 2003), specifically, in the Golgi. Some research also indicates that polysaccharide feruloylation may occur both in the Golgi and also directly at the cell wall (Mastrangelo et al., 2008). The BAHD acyltransferases are cytoplasmic (D'Auria, 2006), meaning that a feruloylated intermediate must be transferred into the Golgi apparatus for Golgi-localized feruloylation.

Specific mechanistic studies involving the BAHD proteins which are responsible for AX feruloylation have not been performed yet, and therefore, the intermediate steps and acceptor molecules are unknown. Feruloyl-CoA is assumed to serve as the acyl donor for the BAHD proteins driving AX feruloylation, but this has not been explicitly proven. Fry et al. (2000) treated maize suspension cultures with [<sup>14</sup>C]-labeled cinnamate and observed rapid formation of [<sup>14</sup>C]-labeled coumarate, followed by an unidentified compound suggested to be a breakdown product of feruloyl CoA and finally, intraprotoplasmic incorporation of radiolabeled ferulates into polysaccharides. Yoshida-Shimokawa et al. (2001) showed that the cytosolic fraction of rice cells catalyzed the transfer of ferulic acid from feruloyl-CoA to the *O*-5 position of Ara<sub>f</sub> in α-L-Ara<sub>f</sub>-(1→3)-β-D-Xyl<sub>p</sub>-(1→4)-β-D-Xyl<sub>p</sub>, but these results stem from crude cell fractions and not purified proteins, meaning that the feruloyl CoA could have been transformed into an unidentified intermediate en route to the final product. Additionally, AXOS are likely not present in the cytosol to serve as acceptor molecules in a cellular environment, further weakening the model's relevance. UDP-Ara<sub>f</sub> is the current leading candidate for acceptor molecule (Buanafina, 2009), with UDP-feruloyl-Ara<sub>f</sub> then being transported into the Golgi and attached to the xylan via an unknown enzyme. To date, however, this theory is purely speculative.

In a competing theory, Obel et al. (2003) fed radiolabeled [<sup>14</sup>C]-ferulate to suspension-cultured wheat cells and observed rapid production of 1-*O*-feruloyl-β-D-glucose that paralleled feruloylated AX appearance, leading them to propose this compound "as a substrate or precursor for arabinoxylan formation." Although the ferulic acid glucose ester is indeed an activated compound with high group transfer potential, its formation in this experiment also potentially represents a metabolic detoxification strategy for the cell to mark excess ferulates for storage in the vacuole and avoid intracellular ferulate accumulation (Jones and Vogt, 2001).

#### **1.6.4. Dehydrodiferulate formation and arabinoxylan crosslinking**

The free-radical induced coupling of ferulates to create dehydrodiferulates (DFAs) is catalyzed by peroxidases/laccases in the presence of hydrogen peroxide. DFA formation is already detected intraprotoplasmically (Fry et al., 2000; Obel et al., 2003; Lindsay and Fry, 2008; Mastrangelo et al., 2008), meaning that AX are delivered to the cell wall in a cross-linked form. Whereas Obel et al. (2003) surmised that only the 8–5-DFA regioisomer was formed in the Golgi, later work by Lindsay and Fry (2008) described the intraprotoplasmic formation of several DFA regioisomers.

Further oxidative cross-linking of the AX polymer occurs after polysaccharide deposition in the cell wall (Lindsay and Fry, 2008). Thus, although ferulate incorporation into the cell wall is relatively constant throughout plant maturation (Hatfield et al., 2008), older, mature plant tissues are more extensively cross-linked than younger cell walls, with levels of AX-lignin cross-linking specifically increasing with age (Lam et al., 1992).

#### **1.7. Arabinoxylans' role in plants**

The tissue-specific structural differences between AX enable them to play tissue-specific roles in plants. In particular, evidence suggests that plants use AX to help control their tissue hydration levels and adjust the level of substitution on the AX polymer to permit or restrict water diffusion, with higher substitution levels permitting more water diffusion (Saulnier et al., 2012). During maturation, the degree of both arabinose and acetyl substitution of the AX backbone in grain gradually decreases (Veličković et al., 2014). Although some exceptions appear in the literature (Saulnier et al., 2012), drought-stressed plants generally produce more AX overall, and these AX have a lower degree of substitution than well-watered plants (Rakszegi et al., 2014).

Ferulate cross-linking is suggested to be involved in cessation of cell extension by increasing the cell wall's stiffness (Kamisaka et al., 1990), thus also improving plants' disease and insect resistance (Buanafina, 2009; Buanafina and Fescemyer, 2012). DFA crosslinking provides structural support, and therefore structural tissues such as stems have higher ferulate levels than leaves (Piston et al., 2009). Differing effects of drought and osmotic stress on plants' ferulate levels are described. Osmotically stressed maize cell roots had higher ferulate levels (monomers and oligomers) and were smaller than non-stressed plants (Vuletić et al., 2014), whereas osmotically-stressed rice internodes had clearly decreased ferulate levels (Sasayama et al., 2011).



## 2. Study Objectives

---

Clear structure-function relationships are being established for several quantifiable features of cereal grain AX, such as ferulate dimers. However, some well-known structural elements, such as acetyl substituents and feruloylated side-chains, have not been quantified yet in cereal materials, and their proposed structure-function relationships in plant physiology, food and biomaterials processing, and human and animal nutrition therefore remain mostly theoretical. In the case of feruloylated side-chains, no quantitative methods even exist. Additionally, some structural aspects of feruloylated side-chains, such as their localization within the xylan backbone, remain unknown. Other structural features of cereal grain AX, such as non-feruloylated oligosaccharide side-chains, have been proposed to occur, but their presence has not been definitively proven. The objectives of this study are therefore threefold: first, to gain more structural information about feruloylated side-chains in cereal grains; second, to develop, validate, and test rapid methods for quantitatively screening the feruloylated side-chain profiles of cereal materials; and third, to investigate cereal grain AX for the existence of non-feruloylated side-chain oligosaccharides.

To accomplish these objectives, two complementary hydrolysis methods will be used which either semi-specifically release side-chains (mildly acidic hydrolysis method) or release oligosaccharides containing side-chains attached to a xylan backbone fragment (enzymatic hydrolysis method) from cereal materials. Various chromatographic techniques will be employed to isolate both known structural elements (feruloylated side-chains FA, FAX, and FAXG) as standard compounds for development of quantitative screening methods as well as novel feruloylated and non-feruloylated AXOS. Advanced structural characterization techniques for the unequivocal characterization of isolated components will be utilized, including 1D- and 2D-NMR, LC-MS, and methylation analysis.

Various analytical approaches for quantitative and qualitative screening of feruloylated and non-feruloylated AX side-chain substituents will be tested. All quantitative methods will be validated and tested on cereal materials, and an emphasis will be placed on developing methods which are both analytically sound and rapid, allowing them to be used as quantitative screening methods for comparison of various cereal materials, plant tissues, etc.

Non-feruloylated side-chain compounds will be studied in cereal materials which have not been exposed to alkaline conditions. The unequivocal characterization of isolated non-feruloylated side-chains will enable the comparison of their structures to the oligosaccharide moieties of feruloylated side-chains. Qualitative screening of cereal materials for specific non-feruloylated structural elements will be performed.

This work will provide the foundation for determining evidence-based structure-function relationships of AX side-chains in various fields.



# 3. Materials and Methods

---

## 3.1. Plant materials

Maize (*Zea mays* L.) middlings were a gift from Cornexo GmbH (Freimersheim, Germany) and used for isolation of feruloylated side-chain standard compounds. Intermediate wheatgrass (*Thinopyrum intermedium*) grain was kindly shared by Dr. Lee DeHaan from The Land Institute (Salina, Kansas, USA). Wholegrain maize flour (*Zea mays* L.) was a gift from Mühle Beck (Keltern, Germany). Wild rice (*Zizania aquatica* L.), long-grain brown rice (*Oryza sativa* L.), rye (*Secale cereale* L.), kamut (*Triticum turanicum* Jakubz.), wheat (*Triticum aestivum* L.), spelt (*Triticum spelta* L.), popcorn (*Zea mays* L. var. *evarta*), oat (*Avena sativa* L.) (dehulled), barley (*Hordeum vulgare* L.) (dehulled), and proso millet (*Panicum miliaceum* L.) whole grains were purchased from local grocery stores.

Before isolation of the plant cell wall materials containing AX (dietary fiber), all materials were defatted with acetone and milled to <0.5 mm (method details are provided in Section 12.5.1).

## 3.2. Isolation of arabinoxylans from plant materials

Many different methods for the isolation of AX polymers from cereal materials are described in the literature. These methods may be divided into two types: 1) The solubilization of AX polymers from cereal materials with various solvents, which usually entails the separation of AX from other cell wall polysaccharides, starch, proteins, and fats; and 2) The isolation of plant cell wall materials or dietary fiber determination, which results in the removal of fat, starch, and non-structural proteins, but retains other cell wall polysaccharides.

### 3.2.1. Solubilization of arabinoxylan polymers

Most of the methods to isolate pure AX polymers are chemical/enzymatic methods. For selective extraction of WE-AX, fat and soluble protein may be first removed from the finely ground material (<0.5 mm) (for example, by Soxhlet extraction with *n*-hexane to defat the material and adsorption of soluble proteins with bentonite clay or silica gel, respectively). The remaining material is suspended in water, centrifuged, and the supernatant is treated with  $\alpha$ -amylase and amyloglucosidase to remove soluble starch fragments (Izydorczyk et al., 1990; Maes and Delcour, 2002). Alternatively, the destarching step may be performed at the beginning of isolation. Finally, some researchers add treatment steps with  $\beta$ -glucan-hydrolyzing enzymes ((1 $\rightarrow$ 3, 1 $\rightarrow$ 4)- $\beta$ -glucan 4-glucanohydrolase and  $\beta$ -glucosidase) because  $\beta$ -glucans are partially water-soluble and therefore co-extracted with WE-AX (Dervilly-Pinel et al., 2001a).

For the isolation of WU-AX, alkaline solutions are the most common extraction solutions. The effectiveness of alkaline solutions lies in their ability to both cleave ferulate esters in AX and disrupt hydrogen bonds between AX and cellulose. Various alkaline solutions have been tested and compared in the literature, including saturated barium or calcium hydroxide with sodium borohydride (Bergmans et al., 1996), alkaline hydrogen peroxide (pH 11.5, 2% hydrogen peroxide) (Maes and Delcour, 2002), and dilute solutions of either sodium or potassium hydroxide (Chanliaud et al., 1995). The addition of sodium borohydride to alkaline extraction solutions helps prevent alkaline peeling, although AX are less susceptible to this breakdown

reaction than other hemicelluloses (Wang et al., 2015). Alkaline peeling is a polysaccharide degradation reaction which occurs under alkaline conditions: the aldehyde functional group on the reducing sugar is isomerized to a ketose via an 1,2-enediol intermediate. Following formation of a 2,3-enediol,  $\beta$ -alkoxy-elimination cleaves the glycosidic linkage on the *O*-4-position of the backbone, creating a new reducing end. The same series of reactions is repeated, and the monomers are removed one by one from the backbone's reducing end. Reduction of the reducing end to a sugar alcohol blocks the start of this degradation process and protects the polymer. In addition to preventing alkaline peeling, sodium borohydride enhances the selectivity of alkaline extractions, although the mechanism of this effect is unknown (Gruppen et al., 1991).

Hydrogen peroxide is added in some alkaline AX extractions described in the literature because of its delignifying (“bleaching”) effect (Zhang et al., 2014). Both extraction selectivity and yield also appear to be influenced by the cation of the alkaline solutions, but the mechanism behind these experimental observations is unknown. For example, barium hydroxide was far more selective for AX compared to calcium hydroxide (fewer co-extracted  $\beta$ -glucans) and produced higher AX yields (Bergmans et al., 1996), and potassium hydroxide had superior extraction yields compared to sodium hydroxide (Chanliaud et al., 1995). Sonication during both aqueous and alkaline AX extraction increases extraction yields and reduces extraction time (Hromádková et al., 1999), but may lead to cleavage of covalent bonds in the material.

The advantage of alkaline extraction methods is the production of relatively pure AX materials with good yields. The hydrolysis of ester-linkages, however, makes these extraction methods unsuitable for studying feruloylated AX in their native form. In particular, distinguishing between feruloylated and non-feruloylated side-chains is impossible.

To avoid the hydrolysis of ester-linkages that occurs during alkaline extraction, solvent extractions of AX with dimethyl sulfoxide (DMSO) or 4-methylmorpholine-4-oxide have also been tested. Although DMSO and DMSO-water mixtures are good solvents for alkali-extracted AX (Ebringerova et al., 1994), DMSO itself is a very poor extraction solvent for releasing AX from the cell wall matrix (Holloway, 1985). 4-Methylmorpholine-4-oxide, on the other hand, was successfully used to solubilize almost all of the non-starch polysaccharides from destarched barley and barley malt (Voragen et al., 1987). The clear advantage of this solvent, which breaks down hydrogen bonding networks, over alkaline extraction is its non-destructiveness. Compared to alkaline extraction though, it is completely non-selective. Anhydrous 4-methylmorpholine-4-oxide has a very high melting point (176°C), so mixtures of the anhydrous compound and its monohydrate (melting point of 76°C) are sometimes used. Alternatively, 4-methylmorpholine-4-oxide may be mixed with DMSO; heating this mixture at 120°C produces an effective polysaccharide solvent. Some procedures mix 4-methylmorpholine-4-oxide with a small amount of water, but this creates an alkaline environment, which will cleave ester linkages. When handled properly, for research questions where solubilization of the entire milieu of native cell wall polymers is needed, 4-methylmorpholine-4-oxide extraction is an outstanding technique.

### **3.2.2. Isolation of plant cell wall materials/dietary fiber**

To study native AX, non-destructive methods are imperative. When the original AX structure is needed for a study, but the solubilization of the whole AX polymer is not desirable (for example, for enzymatic fermentation studies of native cereal materials), the simple isolation of plant cell wall materials is preferred. Here, the cereal material is finely ground (<0.5 mm), washed with 80% EtOH to remove free monosaccharides and oligosaccharides, defatted, and destarched (thermostable  $\alpha$ -amylase digestion followed by amyloglucosidase). The material may

be partially deproteinized using proteases. For isolation of total cell wall material, soluble polymers in the enzymatic hydrolysate are precipitated with 80% EtOH, and the precipitate is combined with the insoluble residue.

The approved methods for dietary fiber isolation are based on the technique for isolation of plant cell wall materials. The methods have been steadily modified to better mimic human digestion and to capture all of the saccharidic material resistant to human digestive enzymes (fiber) while eliminating all digestible material (non-fiber). Because the spectrum of material classified as dietary fiber is very diverse, this method is quite complex. One of the first official methods, AOAC 985.29, differentiates between insoluble and soluble fiber by separating the insoluble residue remaining after  $\alpha$ -amylase, amyloglucosidase, and protease digestion (insoluble fiber) and then precipitating the soluble polysaccharides in the enzymatic hydrolysate with EtOH (soluble fiber). Both the insoluble and soluble fibers are corrected for residual protein and ash because these components are not included in the definition of dietary fiber. A main advantage of the 985.29 method includes the use of a thermostable, fungal  $\alpha$ -amylase, which enables starch digestion to be performed near 100 °C. Native starch granules swell and gelatinize at these temperatures, resulting in swift and efficient digestion by the amylase.

Unfortunately, the efficient, thorough starch digestion characterizing the 985.29 method is also one of its primary disadvantages: human digestion takes place at lower temperatures and the resulting starch digestion is less efficient. Starch that is not susceptible to human digestion is termed resistant starch and is classified as dietary fiber. To better mimic human digestion, AOAC 2009.01, which uses a porcine  $\alpha$ -amylase and an incubation temperature of 37 °C, was developed. This method also added a column chromatography step to quantify the non-digested oligosaccharides remaining in solution after precipitation of soluble fiber (McCleary et al., 2012). The method has clear drawbacks, including an inordinately long incubation time (16 h) and poor chromatographic separation of the dietary fiber oligosaccharides from the internal standard. A further-modified method has been developed to address these issues (McCleary et al., 2015), but has not yet been accepted as an official method.

For this work, a slightly modified version of the AOAC 985.29 method was selected in order to ensure that data could be expressed in terms of insoluble, non-starch polysaccharides. The digestion parameters of the 985.29 method ensured that the starch-rich cereal materials studied here were efficiently destarched. Exact details of the method used are provided in **Section 12.5.1**. Following isolation of insoluble fiber, the material was thoroughly dried (see **Section 12.5.2**).

### 3.2.2.1. *Protein correction of dietary fiber*

Although the definition of dietary fiber permits the inclusion of “compounds associated with polysaccharides in the plant cell walls” (CODEX, 2010), the proteins resistant to human digestive enzymes are not included in the dietary fiber complex because they do not produce the “beneficial physiological effects” required of dietary fiber components (AACCI, 2001). All dietary fiber values must therefore be corrected for residual protein. Diverse protein quantification methods have been developed, and these can be grouped into colorimetric and nitrogen-determination methods. The most common colorimetric methods are summarized in **Table 7**.

The primary drawbacks to colorimetric methods are their variability in absorption response between different proteins, their sensitivity to absorption interferences (e.g. turbid solutions, non-protein sample components absorbing at measurement wavelength), and the fact

**Table 7. Common colorimetric protein quantification methods**

Method name	Principle	Advantages	Disadvantages <sup>1</sup>	Reference
<b>Biuret</b>	Complexation of peptide bonds with cupric ions under alkaline extraction conditions to form purple color, absorbance read at 540 nm.	No detection of nonprotein nitrogen, rapid	Insensitive, <b>carbohydrates produce interfering pigments under alkaline extraction conditions</b> , incomplete protein extraction requires standardization against known protein	(Jennings, 1961)
<b>Lowry</b>	Folin-Ciocalteu phenol reagent reduces tryptophan and tyrosine residues to form bluish color, absorbance read at 750 nm	More sensitive than Biuret method, rapid	<b>Interference by reducing compounds</b> , different amino acid compositions of different proteins result in quantification errors	(Lowry et al., 1951)
<b>Bradford</b>	Coomassie Brilliant Blue G-250 dye binds to protein, absorption maximum of bound dye is shifted relative to unbound dye, absorbance read at 595 nm	More sensitive than both Biuret and Lowry methods, rapid	Color varies among different proteins and the <b>bovine serum albumin used to create standard curves is not comparable to cereal proteins</b>	(Bradford, 1976)

<sup>1</sup>The disadvantages especially relevant for protein content determination in dietary fiber samples are bolded.

that they are not absolute methods (quantification necessitates standardization against known protein). Additionally, they are unsuitable for insoluble proteins. Their advantage over the classic nitrogen-determination methods (at least for the Lowry and Bradford methods) is their sensitivity. Compared to colorimetric methods, the Kjeldahl and Dumas methods determine the absolute nitrogen content in a sample. This value is converted to crude protein in the sample through multiplying by a factor. This factor has been empirically set at 6.25 for protein correction in dietary fiber (McCleary et al., 2012), making the assumption that the proteins in dietary fiber contain 16% nitrogen by weight. An automatic error is thereby introduced, because the correct factor for cereal fibers, based on their amino acid composition, is higher than 6.25 (Müller, 2015). Both the Kjeldahl and Dumas methods are also susceptible to error introduced by non-protein nitrogen.

The principle behind the Dumas method of protein quantification involves sample combustion at very high temperatures (700-1000°C). Nitrogen in the sample is released as N<sub>2</sub> and nitrogen oxides. Following reduction of the nitrogen oxides to N<sub>2</sub> in a copper reduction chamber and absorption of CO<sub>2</sub> and water, the nitrogen is quantified in a thermal conductivity conductor. Although the method is rapid and requires no harsh chemicals (both strong advantages compared to the Kjeldahl method), the Dumas instrument itself is expensive (high initial costs) and challenging to maintain.

In the Kjeldahl method, samples are digested with concentrated sulfuric acid, producing ammonium sulfate. With the classic quantification method, the digest is neutralized; the ammonia formed is distilled into a boric acid solution containing indicators; and the borate formed is titrated with HCl. The titration method requires large sample quantities and is therefore not ideal for dietary fiber samples. A modified colorimetric quantification method for small sample quantities was developed by Willis et al. (1996), whereby the ammonia in the Kjeldahl digest is converted to a colored complex which absorbs at 685 nm with sodium salicylate and hypochlorite. With slight modifications to Willis's original method, highly comparable results to titration are produced (Müller, 2015).

Willis's method, although both accurate and appropriate for small sample quantities, is time-consuming. Use of an ammonium electrode, which directly measures the ammonia content

in Kjeldahl digests (the pH must be adjusted to strongly alkaline), offers a more rapid measurement alternative. In addition, compared to the Willis method, the ammonium electrode method is not disturbed by sample turbidity. However, the method requires the purchase of specific equipment. Because an ammonium electrode was not available at the beginning of this work, protein content in isolated fiber samples was determined by the Willis method following Kjeldahl digestion (see **Section 12.5.3.2** for the exact method).

### **3.3. Composition analysis of arabinoxylans**

#### **3.3.1. Monosaccharide composition**

##### *3.3.1.1. Hydrolysis methods*

Acidic hydrolysis of polysaccharides to their monosaccharide constituents is the first step towards determining the monosaccharide composition of plant cell wall polysaccharides. Trifluoroacetic acid (TFA), H<sub>2</sub>SO<sub>4</sub>, and methanolic HCl are the primary reagents used for this purpose, with the ideal acid depending on the sample characteristics. Proper hydrolysis conditions (temperature, acid concentration, and hydrolysis time) are critical, although no single set of hydrolysis conditions is ideal for all polysaccharides in a cell wall sample and a compromise must be met between complete polysaccharide hydrolysis and degradation of the released monosaccharides under the acidic conditions. Some authors attempt to correct for degradation losses by subjecting monosaccharide standards to the same hydrolysis conditions and then calculating the percent recovery of the monosaccharide standards (Viëtor et al., 1992), but the decomposition of free monosaccharide standards is likely greater than in the polysaccharide samples, where monosaccharides are released throughout the hydrolysis, so this method will overestimate monosaccharide contents in the samples. Fructose is unstable under all of the commonly used hydrolysis methods, with losses of 100%, 90%, and 95% observed during experimental conditions typically used for methanolysis, TFA hydrolysis, and H<sub>2</sub>SO<sub>4</sub> hydrolysis, respectively, of cell wall samples. Fructose contents, if desired, must therefore be quantified separately using milder hydrolysis conditions (Nguyen et al., 2009).

Soluble polysaccharides and oligosaccharides are easily hydrolyzed with TFA, which has the advantage of being volatile and therefore easily removed after hydrolysis. Albersheim et al. (1967) investigated the effect of hydrolysis time on sugar release and degradation during a 2M TFA hydrolysis at 121°C and found that a one-hour hydrolysis time produced the highest concentrations of released Xyl, Gal, Rha, and Fuc, but that Ara concentrations had already declined compared to shorter hydrolysis times. Man and Glc concentrations continued to climb with increased hydrolysis times. Based on these results, a one-hour hydrolysis time is recommended as the best compromise between hydrolysis and degradation for the TFA hydrolysis of plant cell wall polysaccharides (see **Section 12.5.6.4** for the exact method used in this work).

Cellulose is not hydrolyzed under the conditions of the TFA hydrolysis, and therefore, insoluble plant cell wall material must be hydrolyzed under the Saeman hydrolysis conditions (Selvendran et al., 1979). Here, the material is wetted with 72% H<sub>2</sub>SO<sub>4</sub> and hydrolyzed at room temperature, then diluted with water to 2M and hydrolyzed for 2-3 hours at 100°C (see **Section 12.5.3.4** for the exact method used in this work).

The glycosidic linkages involving uronic acids are more resistant to hydrolysis by either 2M TFA or the Saeman hydrolysis conditions than those of neutral sugars. However, when the

H<sub>2</sub>SO<sub>4</sub> hydrolysis conditions are intensified, significant decomposition of the uronic acids occurs, which negates any enhanced hydrolysis (Selvendran et al., 1979). Methanolysis followed by TFA hydrolysis offers a solution to uronic acid analysis in soluble polysaccharides.

Methanolysis (treatment with methanolic HCl) is best suited for soluble polysaccharides or oligosaccharides. Compared to the aqueous conditions of the TFA and Saeman hydrolysis, very little decomposition of neutral monosaccharides and uronic acids occurs under the methanolysis conditions (Chambers and Clamp, 1971). Neutral monosaccharides are released as their respective methyl glycosides, whereas uronic acids are released as the methyl glycoside 6-methyl esters (both GlcA and galacturonic acid) and as the methyl glycoside of glucurono-3,6-lactone (only GlcA; galacturonic acid does not undergo lactonization) (Cheetham and Sirimanne, 1983; Bleton et al., 1996). Derivatization at this point (usually trimethylsilylation) to permit gas chromatographic analysis produces up to four peaks for each sugar (the  $\alpha$ - and  $\beta$ -methylpyranosides and  $\alpha$ - and  $\beta$ -methylfuranosides) and therefore, a complex chromatogram. Alternatively, the methyl groups may be cleaved with a TFA hydrolysis, and the free sugars and uronic acids separated and detected by high performance anion exchange chromatography (HPAEC) coupled with pulsed amperometric detection (PAD). Because the 4-*O*-methyl-GlcA found as a substituent of (arabino)xylans (in addition to  $\alpha$ -GlcA) is not commercially available, quantification of this substituent requires purification of the standard compound from plant material or chemical synthesis.

### 3.3.2. Detection methods

Besides the advantage of being able to avoid a derivatization step, HPAEC-PAD separation and detection of neutral sugars and uronic acids is very sensitive. GC-separation and detection with a flame-ionization detector following derivatization (for neutral sugars, typically reduction with sodium borohydride, acetylation of alditols with acetic anhydride and methylimidazole as catalyst, and extraction with organic solvent) is significantly more time-consuming, but is a time-proven alternative for laboratories without the expensive HPAEC-PAD equipment. GC-FID analysis cannot be used for analysis of fructose, as the fructose monomer is reduced to a mixture of glucitol and mannitol during derivatization. An alternative detection method is UV-absorption in combination with high-performance liquid chromatography (HPLC) separation and either pre- or post-column derivatization of the sugars with a UV-active marker. In this work, HPAEC-PAD separation and detection were used (see **Section 12.5.3.4** for the exact method).

### 3.3.3. Phenolic acid profile

Phenolic acids in cereal grains are bound via ester linkages to AX and either ester or ether linkages to lignin. Determination of the ester-linked phenolic acids is typically performed with an alkaline hydrolysis, acidification of the hydrolysate to protonate the released acids, extraction of the protonated acids with organic solvent, and analysis. Many different sets of hydrolysis parameters are described in the literature, including acidic hydrolyses (Barberousse et al., 2008), but 2M NaOH for 18 h at room temperature is the most common. To reduce oxidative degradation and *cis-trans* isomerization, samples should be sparged with nitrogen gas at the beginning of hydrolysis and protected from light. Ferulic acid is stable under these conditions (Vaidyanathan and Bunzel, 2012), but even with nitrogen sparging, caffeic acid is extensively degraded. Excellent recoveries of caffeic acid were achieved by the addition of ascorbic acid during alkaline hydrolysis (Nardini et al., 2002; Nardini and Ghiselli, 2004). However, the hydrolysis time used in this method (30 min) was much shorter than the recommended 18 h for cereal samples.

Release of phenolic acids ether-linked to lignin requires much harsher hydrolysis conditions (4M NaOH, 170°C, 2 h) (Barberousse et al., 2008).

Extraction of the released phenolic acids may be performed with either ethyl acetate or diethyl ether following acidification, as both of these solvents quantitatively recover free phenolic acids (Vaidyanathan and Bunzel, 2012). The extracts are dried and then may be either resolubilized in a polar solvent for RP-HPLC separation or derivatized (trimethylsilylation) for GC analysis. For liquid chromatography of the phenolic acids, C8 or C18 column phases are often described, although phenyl-hexyl phases, which permit  $\pi$ - $\pi$ -interactions with the phenolic moieties, offer greater selectivity than C8 or C18 phases (Dobberstein and Bunzel, 2010a).

Detection is most commonly based on UV absorption (Barberousse et al., 2008), but fluorescence detection is also a possibility for sensitive detection of the primary monomeric phenolic acids found in cereals (ferulic, *p*-coumaric, sinapic, and caffeic acids) following chromatographic separation. Mass spectrometric detection offers both sensitive and specific detection, with stable isotope dilution analysis representing the gold standard for accurate quantification. Guth and Grosch (1994) used stable isotope dilution to quantify ferulic and caffeic acids in oats, and Langos et al. (2015) recently published a stable isotope dilution analysis method for caffeic, cinnamic, *p*-coumaric, ferulic, sinapic, and vanillic acids. However, to date, no stable isotope dilution quantification method has been described for diferulates or higher oligomers. Alternatively, Neumüller et al. (2013) published a quantification method for ferulic and *p*-coumaric acids whereby the alkaline hydrolysis was performed in NaOD and D<sub>2</sub>O, which enabled the direct analysis and quantification of the hydrolysate by <sup>1</sup>H-NMR.

For diferulates, HPLC-UV, LC-MS, GC-MS, and GC-FID quantification methods have been described (Bunzel et al., 2001; Dobberstein and Bunzel, 2010a; Jilek and Bunzel, 2013), whereas for ferulate trimers, only LC-MS and HPLC-UV methods have been published (Dobberstein and Bunzel, 2010a; Jilek and Bunzel, 2013). Derivatized trimers and larger oligomers have limited volatility and therefore require high-temperature GC equipment for GC analysis. An additional challenge in quantification of ferulate oligomers is the lack of commercially available standard substances, which means they must either be isolated from plant materials or synthesized before a quantification method can be established in a particular laboratory.

Both *o*-coumaric acid or caffeic acid are suggested as internal standards for phenolic acid monomers (Dobberstein and Bunzel, 2010a). However, caffeic acid is detected following alkaline hydrolysis of many cereal products (Guth and Grosch, 1994; Guo and Beta, 2013), so it cannot be universally used. Mono-methylated 5–5 dehydrodiferulate has been used as a standard for ferulate dimer quantification in various detection methods, including HPLC-UV, LC-MS, and GC-FID + GC-MS (Bunzel et al., 2001; Dobberstein and Bunzel, 2010a; Jilek and Bunzel, 2013). For this work, which focused primarily on monomeric ferulates, an alkaline hydrolysis method was used, followed by acidification and extraction into diethyl ether. Phenolic monomers were quantified by HPLC-UV, using *o*-coumaric acid as an internal standard. The exact method is provided in **Section 12.5.3.3**.

### **3.3.4. Determination of acetyl contents**

Both acidic and alkaline hydrolyses are described in the literature for releasing acetyl esters from plant cell wall materials (Voragen et al., 1986; Kenji et al., 1994). When performed in D<sub>2</sub>SO<sub>4</sub> and D<sub>2</sub>O or NaOD and D<sub>2</sub>O, direct analysis of the hydrolysate by <sup>1</sup>H-NMR is possible (Kenji et al., 1994; Neumüller et al., 2013). Alternatively, a HPLC method was described using a

protonated cation exchange column (acidic eluent) with detection by the universal refractive index (RI) detector (Voragen et al., 1986). This method permits the simultaneous quantification of methoxyl (from esterified uronic acids) and acetate groups in a sample. Acetic acid can also be separated and detected by GC-FID. The acetic acid contents of the cereal materials investigated in this study were not determined.

### 3.4. Structural profiling analysis of arabinoxylans

#### 3.4.1. Linkage patterns of arabinoxylans

##### 3.4.1.1. Analysis of partially methylated alditol acetates

The formation and analysis of partially methylated alditol acetates to determine the linkage patterns of a polysaccharide is commonly known as “methylation analysis” and is a proven member of the carbohydrate analysis method portfolio. With this approach, which was conceived in its complete form by Björndal and coworkers (1967b; 1967a), the free hydroxyl groups in intact polysaccharides are methylated, and the polysaccharide is cleaved into its constituents, now partially-methylated monosaccharides, via acidic hydrolysis. The monomers are reduced to partially methylated alditols, and finally, the hydroxyl groups exposed upon cleavage of the glycosidic linkages and ring opening are acetylated (**Figure 12A**). The resulting partially methylated alditol acetates are separated via GC (**Figure 12B**) and detected with FID or MS. Fragmentation in an electron impact (EI) source and MS detection results in typical fragmentation patterns (**Figure 12C**), which, together with retention times, are used to identify peaks by comparison with authentic standards.

The EI fragmentation patterns of partially methylated alditol acetates are documented for all known sugars and their linkage patterns (Jansson et al., 1976; Pettolino et al., 2012). Primary fragmentation between two methoxylated carbons is preferred, followed by fragmentation between methoxylated and acetoxyated carbons, and finally, between two acetoxyated carbons. Secondary fragments arise from loss of acetic acid, MeOH, ketene, and formaldehyde (Björndal et al., 1967a).

If sufficient amounts of pure standards are available for all potential sugars and linkage patterns, quantification may be done via GC-MS. Alternatively, quantification may be performed by re-injecting the samples onto a GC-FID system and calculating the concentration of individual partially methylated alditol acetates using the effective carbon response factors calculated by Sweet et al. (1975). With this approach, the contribution of each individual carbon type (for example, carbonyl and ether) to the flame response is determined, and the total response factor for a given sugar derivative is computed by summing the contributions of the carbon atoms in that molecule. In this way, the type and amount of individual linkage patterns in a polysaccharide or plant cell wall sample can be determined. However, methylation analysis is unable to provide any information about the anomeric configuration or position of the individual monomers within their respective polymers.

The methylation step uses methyl iodide (MeI) as the methylation reagent in the presence of a strong base to deprotonate the hydroxyl groups. Two methods are commonly used to provide the base: either sodium hydride mixed in DMSO to generate methylsulfinyl carbanion, or solid NaOH in DMSO (Pettolino et al., 2012). Solid NaOH in DMSO generates cleaner chromatograms and is less prone to under-methylation than the methylsulfinyl reagent (Ciucanu and Kerek, 1984). Even under these conditions under-methylation is still a prevalent cause of

analysis failure and can either be caused by incomplete dissolution of the polysaccharide material in DMSO during methylation or moisture contamination, which decomposes the MeI reagent.

Following extraction of the methylated polysaccharides into dichloromethane, they are

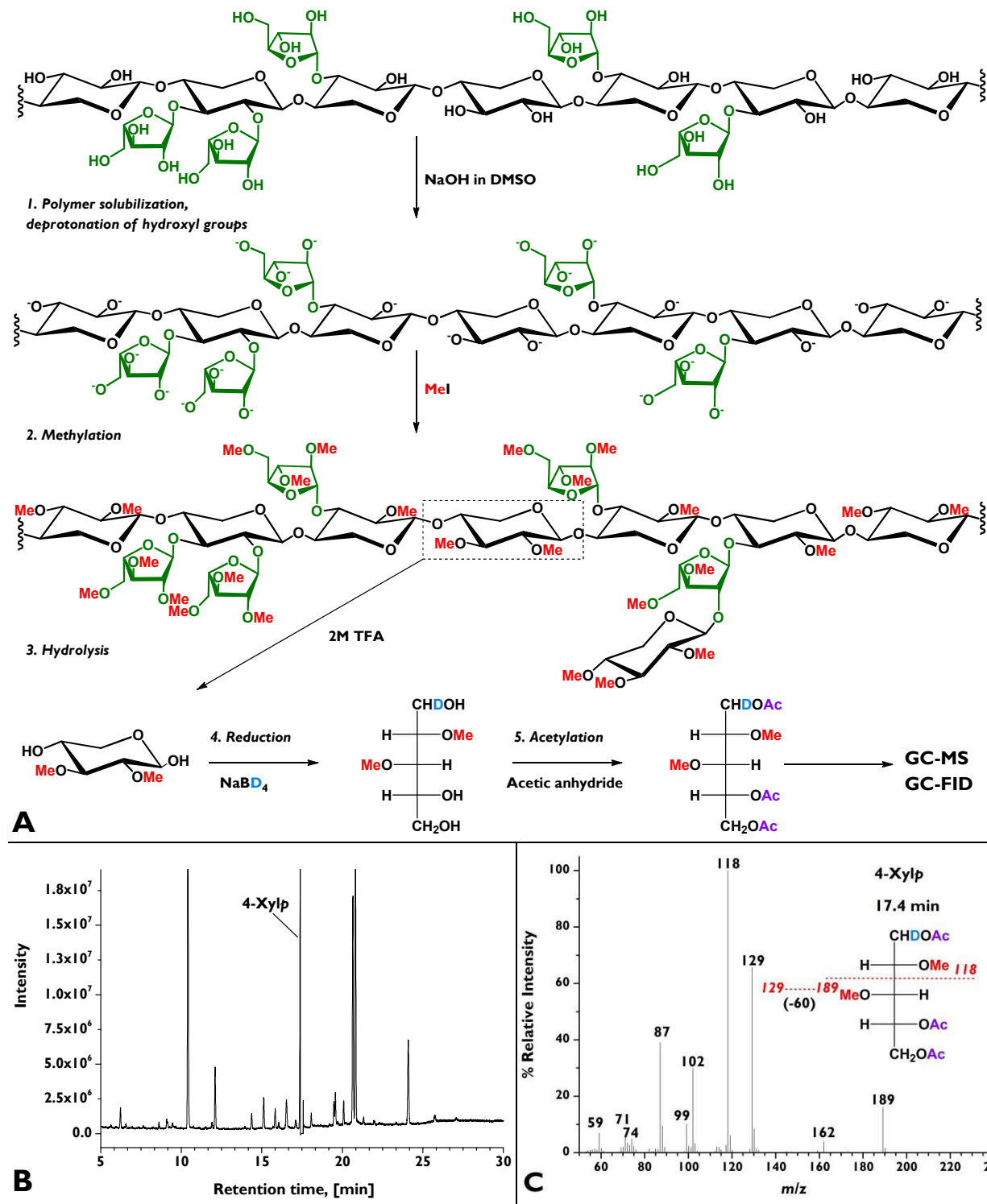


**Figure 12. Methylation analysis of arabinoxylyans. [A]:** Solubilization; methylation, acid hydrolysis, reduction, and acetylation steps. **[B]:** GC-MS separation of partially methylated alditol acetates. **[C]:** Fragmentation of 4-Xylp following electron impact (EI) ionization.

*Abbreviations used:* **4-Xylp**: partially methylated alditol acetate arising from (1→4)-linked xylopyranose; **DMSO**: dimethyl sulfoxide; **GC-FID**: gas chromatography coupled with flame ionization detection; **GC-MS**: gas chromatography coupled with mass spectrometric detection; **MeI**: methyl iodide; **m/z**: mass-to-charge ratio; **TFA**: trifluoroacetic acid.

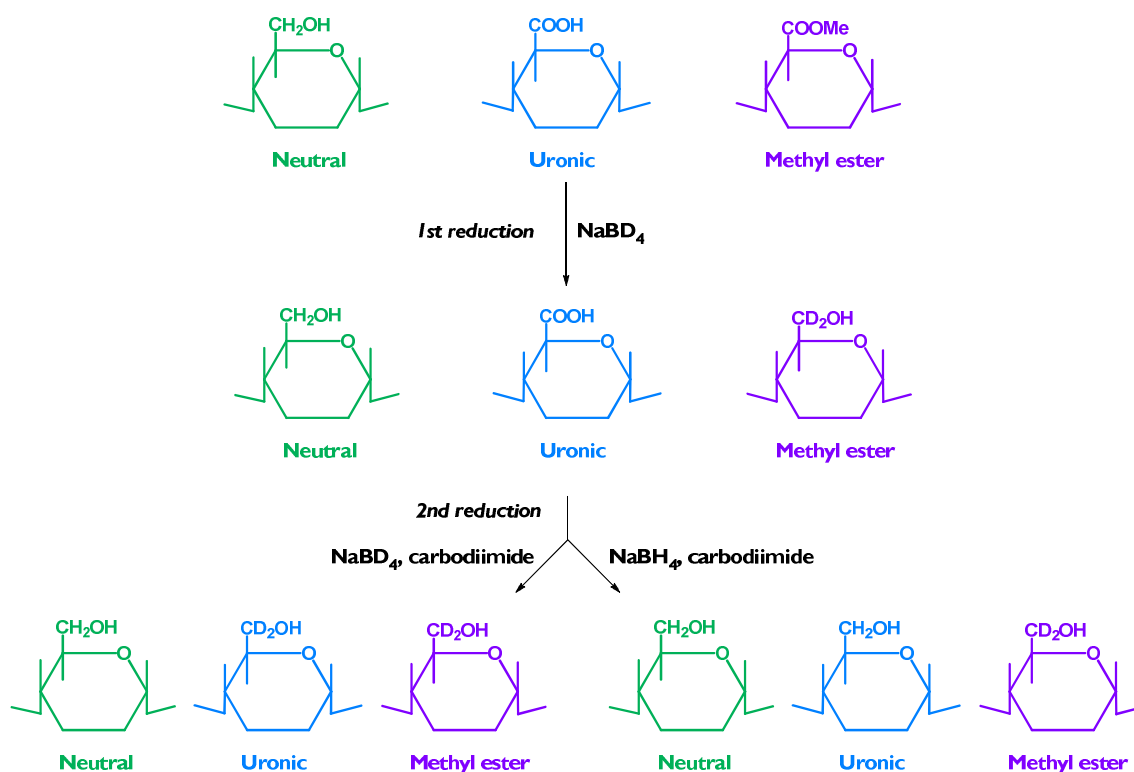


**Figure 13. Selective reduction and labeling of uronic acid substituents and their methyl esters.** *Figure modified from Pettolino et al (2012).*

hydrolyzed with a TFA hydrolysis. Reduction of the released monomers is performed in  $\text{NaBD}_4$  to mark the reducing end with a deuterium atom, and the partially methylated alditols are acetylated with acetic anhydride.

Under these conditions, uronic acids will not be detected because they resist acidic hydrolysis. However, the carboxylic acid functional group may be reduced prior to methylation. Methyl-esterified uronic acids, such as those found in pectins, are susceptible to reduction by sodium borohydride (Maness et al., 1990), but non-esterified uronic acid moieties require activation with carbodiimide in order to be reduced with  $\text{NaBH}_4$ . This differing susceptibility to reduction can be used to differentiate between esterified and non-esterified uronic acids in plant cell wall materials by sequentially reducing cell wall material first with  $\text{NaBD}_4$  (thus marking the non-reducing end with deuterium), splitting the sample, and reducing a second time with  $\text{NaBH}_4$  and  $\text{NaBD}_4$ , respectively, in the presence of the carbodiimide activator (reducing the free acids to non-deuterated neutral sugars, **Figure 13**) (Kim and Carpita, 1992; Pettolino et al., 2012). However, the 4-*O*-methyl GlcA found as a substituent of AX cannot be separately quantified from GlcA with methylation analysis, because methylation of terminally-linked GlcA and 4-*O*-methyl-GlcA produces identical derivatives.

Choosing the proper column phase for separation of the partially methylated alditol acetates is critical for accurate results. Typically, for the best overall separation of the complex mixture of partially methylated alditol acetates resulting from a cell wall sample, polar to mid-polar phases provide the best separation (for example, DB1701, DB225, SP-1000, SP-2330, or SP-2340 are all described in the literature in relation to AX analysis). However, none of these listed phases are able to separate the partially methylated alditol acetates corresponding to *O*-2- and *O*-3-monosubstituted xylose. Therefore, many researchers have resorted to an elaborate estimation of the ratio of these two components using the intensity of fragments corresponding to the two units (Gruppen et al., 1992b). Chesson et al. (1983) solved this problem by measuring all

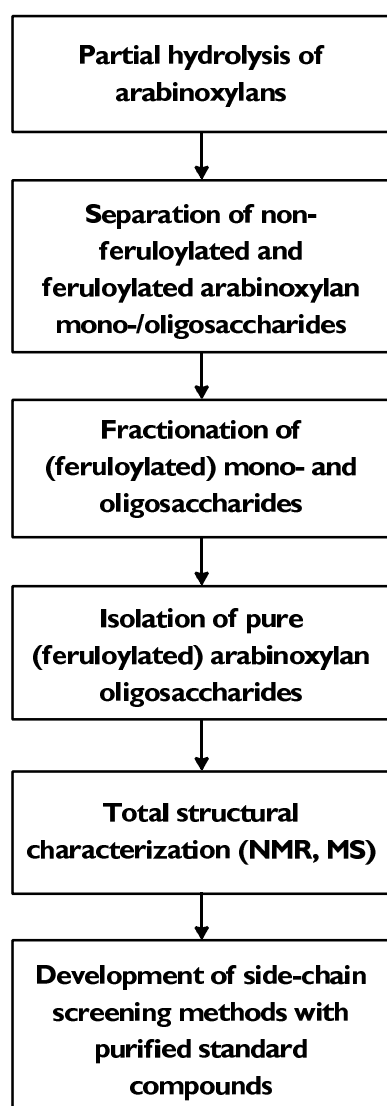


Figure 14. Method steps for development of arabinoxylan side-chain profiles.

Abbreviations used: MS: mass spectrometry; NMR: nuclear magnetic resonance.

samples twice: once with the polar SP-1000 phase and again with a non-polar OV-1 column phase, which separated *O*-2- and *O*-3-monosubstituted xylose but gave poorer resolution for the other sample components compared to the SP-1000 column phase.

The methylation analysis method used in this work is provided in Section 12.5.3.5.

### 3.4.2. Side-chain profiles of arabinoxylans

Although methylation analysis provides an excellent first look at the overall linkage patterns of AX, it cannot supply crucial information about the substitution patterns of various AX side-chain elements within the xylan backbone and the backbone environment (i.e. neighboring substituents) surrounding AX structural elements. Additionally, because methylation analysis contains steps with alkaline conditions, all information about substitution with ester-linked compounds such as phenolic acids or acetyl groups is lost. This missing information can be gained through partial hydrolysis of AX, isolation, purification, and characterization of the released AXOS as standard compounds, and the development of qualitative or quantitative screening methods with these compounds (Figure 14). In the following sections, applicable methods for this process will be discussed for the development of both feruloylated and non-feruloylated side-chain profiles.

#### 3.4.2.1. Release of (non)feruloylated arabinoxylan mono-/oligosaccharides from arabinoxylans

The release of AX fragments may either be performed chemically (mildly acidic hydrolysis) or enzymatically. Saulnier et al. (1995) developed and optimized a mildly acidic hydrolysis method which semi-specifically releases side-chains attached to the xylan backbone via *Araf* by capitalizing on the greater acid lability of glycosidic linkages involving furanoses compared to glycosidic linkages involving pyranoses. The recommended hydrolysis conditions (50 mM TFA, 100°C, 2 h) balance maximized cleavage of *Araf*-based side-chains with minimal degradation of ferulate ester bonds. Minimizing ferulate ester bond degradation is important to ensure good yields of feruloylated side-chain standard compounds, to prevent the isolation and characterization of non-feruloylated side-chains which are only experimental artefacts (i.e. compounds which were feruloylated in the original material), and to avoid altering the side-chain profile of a material. Oxalic acid (32 mM, 100°C) has also been used for selective release of feruloylated side-chains and produces similar results to 50 mM TFA (Saulnier et al., 1995c). Finally, acetic acid was also tested for this purpose, but proved ineffective. Compared to 50 mM TFA, acetic acid (concentrations ranging from 0.5 to 4M; hydrolysis times ranging from 2 to 6 h) released fewer side-chains and produced a lower side-chains: free ferulates ratio, indicating relatively more

ferulate ester bond degradation (Meyer, 2013). The TFA hydrolysis method developed by Saulnier's group was used in this work; a detailed description of the method is provided in **Section 12.5.4.1** (release of feruloylated side-chains) and **Section 12.5.5.1** (release of non-feruloylated side-chains).

The main drawbacks with chemical hydrolysis are the incomplete liberation and partial degradation of side-chains under the mildly acidic hydrolysis conditions and, even more importantly, the loss of information about the placement of the side-chains within the xylan backbone. Enzymatic approaches to directly release the side-chains from the AX backbone (e.g. arabinofuranosidases) could theoretically address the issue of incomplete liberation and also eliminate side-chain degradation. However, this approach is practically unfeasible because most, but not all, arabinofuranosidases are unable to cleave feruloylated *Araf* units from the xylan backbone (Wood and McCrae, 1996; Luonteri et al., 1999; Remond et al., 2008), and no reports of arabinofuranosidases that can release the more complex feruloylated side-chains are found in the literature. Arabinofuranosidases are also unable to cleave non-feruloylated side-chain oligosaccharides from the xylan backbone (Verbruggen et al., 1998; Pastell et al., 2009).

*Endo*-xylanase AX hydrolysis offers a complementary approach to mildly acidic hydrolysis by providing information about the backbone environment (in particular, neighboring substituents) surrounding the feruloylated side-chains. However, this information is limited to the backbone region which is accessible to the xylanase enzymes. Both pure *endo*-xylanases and enzymatic mixtures such as Driselase have been used to release feruloylated AXOS (Ralet et al., 1994a; Lequart et al., 1999; Bunzel et al., 2002) and non-feruloylated AXOS from AX materials (Gruppen et al., 1992c; Ordaz-Ortiz et al., 2005; Höije et al., 2006; Appeldoorn et al., 2010). Enzymatic mixtures may provide a better yield of AXOS by breaking down other cell wall polysaccharides and exposing more AX to enzymatic cleavage. Pure *endo*-xylanases, on the other hand, have the advantage of specificity for cleaving within the xylan backbone and reduce the risk that the backbone region surrounding the feruloylated and non-feruloylated side-chains will be altered by other enzymatic activity, such as removal of arabinose units by arabinofuranosidases. Regardless of whether *endo*-xylanases are used alone or as part of a cocktail of carbohydrate hydrolases, it is imperative that the enzyme preparation is free of feruloyl esterase activity, which would alter both the feruloylated and non-feruloylated side-chain profiles of the released compounds. Driselase, for example, has been shown to lack feruloyl esterase activity (Micard et al., 1994) and was therefore used in this work for enzymatic release of feruloylated AXOS (see **Section 12.5.4.2** for a detailed method description).

#### 3.4.2.2. *Separation of non-feruloylated arabinoxylan mono-/oligosaccharides from feruloylated compounds*

Following either mildly acidic or *endo*-xylanase hydrolysis, the released feruloylated and non-feruloylated oligosaccharides may be separated from each other, for example with Amberlite XAD-2 resin or C18 column chromatography. This step is helpful for accumulating or concentrating feruloylated standard compounds and also permits the application of targeted chromatography techniques that are specific for feruloylated compounds or non-feruloylated oligosaccharides in the following fractionation steps. Amberlite XAD-2 has been extensively used in the literature to isolate aromatic compounds from crude aqueous extracts (Rosler and Goodwin, 1984); however, the adsorption mechanism is dominated by van der Waals forces, and the material is therefore not specifically selective for aromatic compounds (Supelco, 1997). Tomás-Barberán et al. (1992) described recoveries of over 70% for both flavonoid aglycones and

flavonoid glycosides using Amberlite XAD-2, and the material has been used by several research groups to isolate feruloylated oligosaccharides (Saulnier et al., 1995c; Allerdings et al., 2006). Non-feruloylated monosaccharides and oligosaccharides do not bind to the Amberlite XAD-2 material and are washed from the column with water. This method appears to work best with mildly acidic hydrolysates, which primarily contain released side-chains (and therefore, mostly ferulates esterified with oligosaccharides of DP4 or less). The non-polar, ferulate component of these AXOS is significant enough to force their retention on the Amberlite XAD-2 material. Bunzel et al. (2002) reported a breakthrough of ferulates into the aqueous Amberlite XAD-2 eluate of only 7% for acidic hydrolysates of AXOS, but in enzymatic hydrolysates, which contain feruloylated AXOS with a greater DP, 75% of the released ferulates eluted in the aqueous fraction.

C18 material provides better recoveries of feruloylated oligosaccharides than Amberlite XAD-2 (Krause, 2014) and is therefore the better choice for quantitative isolation of feruloylated oligosaccharides. However, for routine preparative isolations, Amberlite XAD-2 is preferred because of its low cost, better durability, and longer working life. A detailed description of the Amberlite XAD-2-based preparative isolation methods used in this work are provided in **Section 12.5.4.3** (isolation of feruloylated mono-/oligosaccharides from mildly acidic or enzymatic hydrolysates) and **Section 12.5.5.2** (isolation of non-feruloylated oligosaccharides from mildly acidic hydrolysates).

#### 3.4.2.3. *Fractionation and isolation of pure feruloylated mono-/oligosaccharides*

The process of separation of mixtures of feruloylated oligosaccharides into individual pure compounds is often started with gel chromatography. Sephadex LH-20 material has been used effectively in the literature to separate feruloylated oligosaccharides with pure water (Bunzel et al., 2002; Allerdings et al., 2006), water-methanol (MeOH) (Saulnier et al., 1995c), or water-EtOH eluents and UV detection (Saulnier et al., 1999). This is possible because the Sephadex LH-20 material is made up of hydroxypropylated cross-linked dextran beads that have both hydrophilic and lipophilic characteristics and swell both in water and organic solvents. Therefore, a hybrid separation mechanism of size-exclusion chromatography, partition chromatography, and adsorption chromatography is possible (Henke, 1994). Stepwise elution with increasing levels of organic modifier enables the separation of oligosaccharides acylated with monomeric ferulates, which elute with pure water, from oligosaccharides acylated with dimeric ferulates, which elute when low percentages (15-20%) of MeOH or EtOH are added to the eluent (Saulnier et al., 1999; Allerdings et al., 2005). Alternatively, Bio-Gel P-2 chromatography may be used as the first clean-up step (Appeldoorn et al., 2013). Compared to Sephadex LH-20, the separation mechanism of the Bio-Gel P-2 gel material (polyacrylamide beads) is almost exclusively size exclusion chromatography. However, feruloyl groups appear to interact with the polyacrylamide matrix (Guillon and Thibault, 1989; Ralet et al., 1994b; Appeldoorn et al., 2013) and therefore elute later than expected based on molecular weight alone. In this work, initial separation of feruloylated oligosaccharide mixtures was performed with Sephadex LH-20 gel chromatography (pure water eluent; see **Section 12.5.4.4** for exact method details).

Further clean-up and purification of Sephadex LH-20 fractions can be performed with (semi)preparative RP-HPLC (C18, water-MeOH gradient) or Bio-Gel P-2 size-exclusion gel chromatography (water eluent) (Allerdings et al., 2006). RP-HPLC clean-up is hampered by on-column mutarotation between the  $\alpha$ - and  $\beta$ -anomers of the reducing sugar under the aqueous

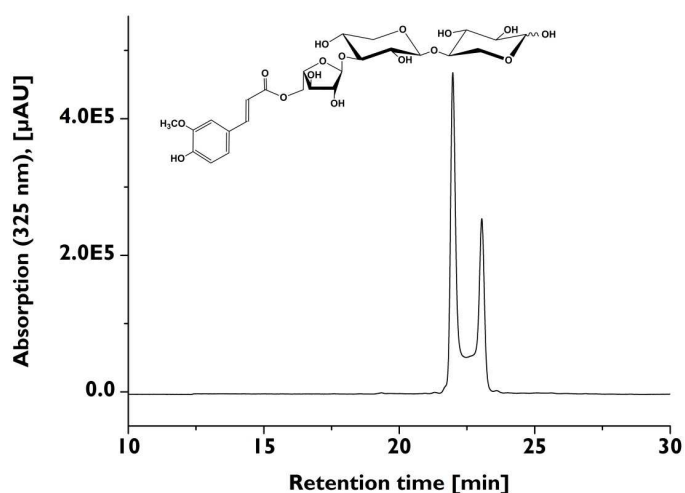


**Figure 15.** Typical partially-split peak produced by a single, pure feruloylated oligosaccharide compound under RP-HPLC conditions.

Abbreviations used: **RP-HPLC**: reversed-phase high-performance liquid chromatography.

#### 12.5.4.5).

#### 3.4.2.4. Fractionation and isolation of pure non-feruloylated arabinoxylan oligosaccharides

Bio-Gel P-2 gel chromatography has been extensively used to fractionate non-feruloylated AXOS (Bengtsson et al., 1992a; Gruppen et al., 1992c; Viëtor et al., 1994a; Pastell et al., 2009). Higher temperatures improve separation (BeMiller et al., 1993), and methods using a column temperature of up to 65°C are described in the literature (Viëtor et al., 1994a). Successful AXOS separation up to DP10 has been reported for Bio-Gel P-2 chromatography (Gruppen et al., 1992c), and the “typical fractionation range” of the material given by the manufacturer is 100-1800 daltons. However, some researchers have coupled Bio-Gel P-4 (typical fractionation range of 800 to 4000 daltons) and Bio-Gel P-2 columns for better separation of oligosaccharides in the upper working range of the Bio-Gel P-2 material (oligosaccharides with DP 7 and higher) (Pollet et al., 2010b). Although Bio-Gel P-2 is the most commonly applied size-exclusion gel chromatography material for preparative-scale AXOS separation, other gels have also been applied, including Fractogel TSK HW 40 (fractionation range from 100 to 5000 daltons) (Verbruggen et al., 1998). Because non-feruloylated AXOS are UV-inactive, universal detection methods such as RI or evaporative light-scattering detection (ELSD) are used for monitoring the eluent.

Preparative HPLC may also be used for preparative-scale separation of non-feruloylated oligosaccharides or for further clean-up and purification of gel chromatography fractions. Oligosaccharides can be separated on C18 column phases using pure water as the eluent; linear oligosaccharides interact most with the C18 stationary phase under these conditions (El Rassi, 1996). A drawback for this method is that some C18 phases are not stable under aqueous conditions. The porous graphitized carbon (PGC) phase, which shows excellent retention of polar analytes, is another reversed-phase option for preparative clean-up of oligosaccharide fractions. On-column mutarotation between the  $\alpha$ - and  $\beta$ -configurations of the reducing oligosaccharides may be reduced by heating the column to >70°C (Westphal et al., 2010). Increased temperature enhances analyte retention, in contrast to other reversed phases, and also produces sharper peak shapes (El Rassi, 1996). Preparative PGC columns are commercially

conditions of typical gradients (El Rassi, 1996), which results in very broad or partially-split peaks (**Figure 15**) and, in the case of mixtures of compounds, complex chromatographs. However, compared to Bio-Gel P-2 separations, where compounds are mainly separated based on their hydrodynamic volume, (semi)preparative C18-based-RP-HPLC provides better separation of feruloylated AXOS with similar sizes but different substitution patterns. In this work, (semi)-preparative RP-HPLC was used to clean up Sephadex LH-20 fractions of feruloylated AXOS (method details are provided in **Section**

available, but costly.

Alternatively, if a HPAEC system is available, preparative HPAEC-PAD separation and detection is possible. With its exceptional resolution, preparative HPAEC is a powerful option for separation of oligosaccharides and has been applied to AXOS (Viëtor et al., 1994a; Verbruggen et al., 1998; Bowman et al., 2012). Neutralization/desalting of the alkaline eluent after detection is necessary to prevent Lobry de Bruyn-van Ekenstein aldose-ketose transformation of the reducing sugar, and current HPAEC instrumental configurations include an optional in-line desalter. This component must be carefully installed and maintained to avoid damaging the detector cell with excessive back pressure. Like PGC chromatography, the primary disadvantage of this approach is the high cost of preparative columns.

In this work, Bio-Gel P-2 gel chromatography was used for initial fractionation of non-feruloylated AXOS (see **Section 12.5.5.3** for method details). Bio-Gel P-2 fractions were further purified with C18-based semi-preparative HPLC using pure water as eluent (see **Section 12.5.5.4** for exact method).

#### 3.4.2.5. *Structural characterization of purified arabinoxylyan oligosaccharides: Application of liquid chromatography coupled with mass spectrometric detection*

LC-MS techniques are information-rich and extensively used for analyses of oligosaccharides. LC-MS-based analysis of oligosaccharides has the clear advantage over GC-MS techniques of permitting analysis of native, underivatized oligosaccharide compounds. GC analysis of these polar analytes requires derivatization with functional groups to increase analyte volatility and, with normal GC conditions, is limited to oligosaccharides with DP5 or less. High-temperature GC equipment permits the analysis of permethylated oligosaccharides up to DP11 (Zaia, 2004). However, not only does derivatization add an extra laboratory step, but most of the standard derivatization procedures for oligosaccharides (for example, permethylation) are performed under alkaline conditions, which makes them unsuitable for analysis of feruloylated and/or acetylated oligosaccharides. The AX oligosaccharides purified in this work were therefore analyzed with LC-MS.

Ionization was done via electrospray ionization (ESI), a soft ionization technique which results in relatively little fragmentation. During ESI-ionization, the eluent is pumped through a steel microcapillary which is maintained at several kilovolts compared to a cylindrical electrode surrounding the needle and results in a spray of charged droplets. A stream of inert gas (desolvation spray) helps evaporate the solvent until the charged droplets become so small that the droplets' surface tension can no longer support the charge and the droplets are torn apart (Coulombic explosion). ESI-ionization may be performed either in positive or negative mode, and both positive and negative modes have been used for analysis of AXOS (Quemener and Ralet, 2004; Quemener et al., 2006; Vismeh et al., 2013). Positive-mode ESI ionization of oligosaccharides primarily results in various quasimolecular ions such as sodium, potassium, or ammonium adducts, which complicates correct assignment of a compound's molecular weight. Some researchers therefore add a small amount of salt (25  $\mu$ M) to the aqueous eluent when using positive ionization to ensure the formation of only one adduct type. Lithium chloride (resulting in Li adducts) has been successfully used in various studies (Wefers et al., 2014), and sodium acetate has also been used to promote Na adducts (Westphal et al., 2010). Although negative ionization results in fewer adducts (the  $[M-H]^-$  quasimolecular ion predominates in the first-order mass spectrum) and spectra are thus easier to interpret, oligosaccharides are more readily ionized in the positive mode (Vismeh et al., 2013), producing a better signal-to-noise (S/N) ratio

than negative mode measurements. Positive ionization was used in this work.

Several types of mass analyzers, which separate charged particles, have found common use for MS analysis of oligosaccharides, including time-of-flight, quadrupoles, and ion-trap instruments (Zaia, 2004). For this work, both a linear ion-trap and triple quadrupole system were available for use, and therefore the principle of each instrument and their comparative advantages and disadvantages will be briefly discussed.

Linear ion-trap MS instruments function by receiving and simultaneously trapping ions with a broad range of mass-to-charge ( $m/z$ ) ratios within a set of quadrupole rods and electrodes at the entrance and exit which serve as endcaps to the quadrupole configuration. A 2D radio-frequency field is created with the quadrupole rods which confines the ions in the radial direction, and the potentials on the end electrodes confine the ions in the axial direction. Trapped ions are injected sequentially in mass order into an ion detector during scanning. Collision-induced dissociation (CID) may be performed on ions with a particular  $m/z$  in the trap, followed by ejection and detection of the daughter ions to produce a  $MS^2$  spectrum. Alternatively, this process may be repeated on one of the daughter fragments within the trap, leading to a  $MS^3$  spectrum. Ion trap instruments have fast scanning speeds and, because of their ability to receive and trap ions with a range of  $m/z$  ratios, their sensitivity in the full-scan mode is exceptional. However, this ability to capture all the ions in a given  $m/z$  range at any time also makes ion-trap instruments less able to handle samples with a heavy matrix load: the ion trap has a finite charge capacity, and a heavy concentration of co-eluting matrix components can thus overflow the ion trap and prevent detection of a less-concentrated analyte.

A quadrupole MS analyzer uses a set of quadrupole rods, to which AC and DC voltages are supplied. Charged ions enter the quadrupole from the ESI interface and begin oscillating in the x,y plane. The frequency and amplitude of these oscillations depend both on the ion's  $m/z$  value and the AC and DC voltage. At a specific AC and DC voltage combination, a given  $m/z$  will oscillate stably within the quadrupole, drift down the rod assembly, and enter the detector. All other ions with other  $m/z$  values will have unstable oscillations, strike the quadrupoles, and be discharged. The limitation of only being able to stabilize and guide one  $m/z$  value at a time into the detector means that a quadrupole's sensitivity in full-scan mode is much lower than an ion-trap instrument. In a triple-quadrupole configuration, the first quadrupole filters out a desired precursor mass which is then fragmented in a separate collision cell. This is followed by a second quadrupole filter which selects the desired fragment ion. Thus, in comparison to the fragmentation in an ion-trap MS analyser, which occurs in the same sequential process but uses the same trap electrode for precursor selection, CID, and product ion selection, the process of MS/MS fragmentation in a triple-quadrupole MS is distributed spatially between three separate electrode structures. Therefore, the hardware requirements and resulting cost of a triple-quadrupole MS system are greater than those of an ion-trap.

In this work, feruloylated mono-/oligosaccharides were separated on a C18 phase with a 0.1% aqueous formic acid and acetonitrile (or MeOH) gradient. The eluent was monitored with a diode array detector (DAD) coupled with an ion trap-MS system operating in the full-scan mode, which enabled the acquisition of a compound's UV absorption spectrum and molecular weight in one measurement (see **Section 12.5.6.1** for exact method). Non-feruloylated oligosaccharides were separated on a heated PGC column with a gradient of aqueous LiCl (25  $\mu$ M) and acetonitrile. Following positive ESI ionization, they were analyzed and fragmented on a triple-quadrupole MS system. Please note that the reason for choosing the triple-quadrupole MS system in this case was a series of lengthy repairs on the ion-trap MS system, which is a better

choice for analysis of relatively pure compounds, as detailed above. The exact method is described in **Section 12.5.6.2**.

Besides determination of the molecular weight, analysis of fragmentation patterns, especially the fragments arising from cross-ring fragmentation, permits the assignment of coupling positions (Quemener and Ralet, 2004). Some researchers derivatize the reducing end of oligosaccharides (for example, by permethylation) to facilitate spectra analysis (Mazumder and York, 2010), but underivatized oligosaccharides also produce informative spectra (Quemener et al., 2006). MS fragmentation patterns have even been used to determine the anomeric conformation of disaccharides (Mulrone et al., 1995). However, determination is based on intensity ratios of fragments which are present in both  $\alpha$ - and  $\beta$ -configured compounds and is therefore error-prone. As discussed in the following section, NMR analysis is a better choice for both determination of oligosaccharide coupling positions and the anomeric conformation of individual sugars.

#### 3.4.2.6. *Structural characterization of purified arabinoxylan oligosaccharides: Application of nuclear magnetic resonance spectroscopy*

NMR spectroscopy, in particular 2D-NMR, provides a wealth of information about an isolated structure and single-handedly enables the total characterization of many molecules. NMR was employed extensively in this work for the structural characterization of isolated compounds. This section will therefore briefly describe the basic principles of the 1D- and 2D-NMR-experiments used in this work.

Atom nuclei with odd mass numbers possess angular momentum and nuclear spin: they rotate about an axis. This spinning movement of positive charge generates a small magnetic field, rendering these nuclei magnetic and NMR-active. The NMR-active nuclei most relevant for structural characterization of (feruloylated) AXOS are  $^1\text{H}$  and  $^{13}\text{C}$ , which is why they are the only ones considered in this discussion. In the absence of an external magnetic field, the magnetic moments of these nuclei are randomly oriented, but when these nuclei are placed in the field of a larger magnet, they twist and orient themselves so that their magnetic moments are aligned either with or against the external field. Alignment with the external field ( $\alpha$ -spin state) is a slightly lower energy state than alignment against the external field ( $\beta$ -spin state). In a given sample of the same molecule, slightly more nuclei will be in the  $\alpha$ -spin state than in the  $\beta$ -spin state, leading to a small net energy difference in the sample. This energy difference, which is directly proportional to the strength of the external magnetic field, can be detected by applying electromagnetic radiation with the exact frequency needed to make a nucleus flip its spin direction. This leads to a small net absorption of energy in the sample because of the slight excess of nuclei in the  $\alpha$ -spin state. Directly following this absorption, the nuclei are said to be “in resonance” and move to re-establish the equilibrium state by emitting the absorbed energy as electromagnetic radiation. This emission is the NMR signal which is created and detected as a free-induction decay (FID) in an NMR spectrometer and converted via Fourier transformation into an NMR spectrum.

Different nuclei in a molecule will experience a slightly different magnetic field depending on their environment and magnetic shielding by electrons. These slight differences in the effective magnetic field experienced by the nuclei in a molecule result in the emission of electromagnetic radiation with slightly different frequencies and multiple signals in a spectrum. The resonance frequencies of these signals are reported not as their absolute values (in Hz), but as chemical shift values relative to a common standard such as trimethylsilane (in ppm; the trimethylsilane proton signal is set as exactly 0 ppm). In the past, a small amount of trimethylsilane

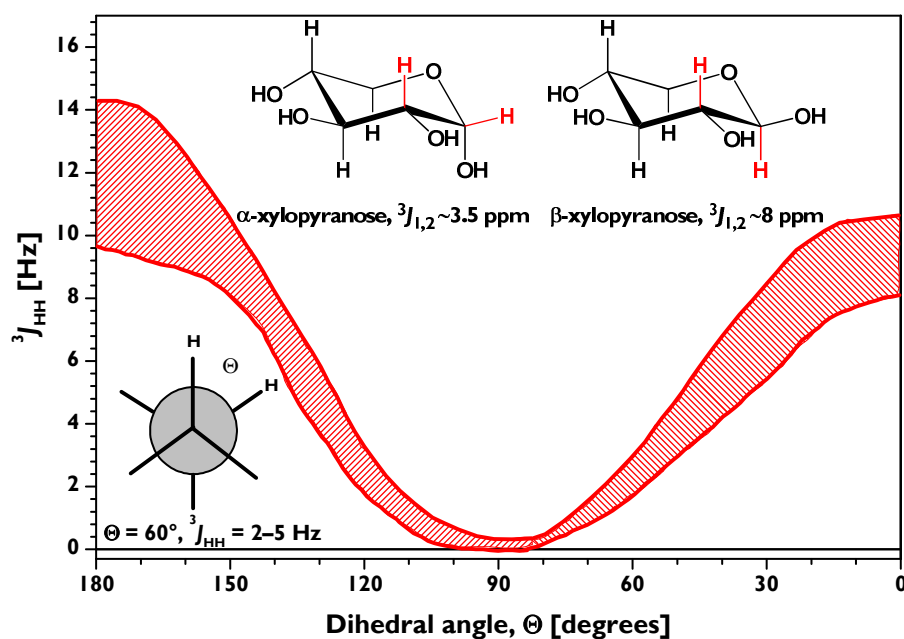


Figure 16. Karplus equation relationship between dihedral angle and  $^3J_{\text{HH}}$  coupling constants of pyranoses.

Many deuterated solvents are available, and feruloylated oligosaccharides readily dissolve in both  $\text{D}_2\text{O}$  and  $\text{DMSO-}d_6$ . However, the ferulate ester bond appears to be more stable in  $\text{DMSO-}d_6$  than in  $\text{D}_2\text{O}$  (see discussion in **Section 6.1**), making it the preferred solvent for feruloylated oligosaccharides. The proton chemical shifts of oligosaccharides may be divided into the anomeric chemical shifts (typically 4.4-5.5 ppm), which are shifted downfield relative to the non-anomeric protons (found typically in the 3-4 ppm range). The aromatic proton chemical shifts of the ferulate component of feruloylated AXOS are found downfield of the oligosaccharide signals (between  $\approx 6.5$  and 8 ppm). The integrals of  $^1\text{H-NMR}$  resonance signals are proportional to the number of nuclei, which permits quantitative assessment of the ratios of compound mixtures by comparison of their signal integrals.

Resonance signals in a spectrum often also exhibit signal fine structure, or signal splitting, which arise as a result of interactions between neighboring nuclei. These spin-spin-couplings can occur between nuclei of the same chemical species (homonuclear) and between nuclei of different elements (heteronuclear). The number of signal splittings (i.e. doublet, triplet, quadruplet, and multiplet signals) is directly related to the number of coupled nuclei. The size of the coupling is described through the coupling constant,  $J$ , and is given in Hz. Proton coupling constants provide information about the relative orientation of two neighboring protons to each other; for example, the H7 and H8 protons in *trans*-ferulic acid have a coupling constant of  $\approx 16$  Hz, whereas the *cis*-configuration of these same protons in *cis*-ferulic acid have a coupling constant of  $\approx 12$  Hz. In pyranose sugar moieties, the Karplus equation, which relates the theoretical dependence of vicinal proton coupling constants to their dihedral angle (Lemieux et al., 1958; Karplus, 1959), is used to predict coupling constants (Coxon, 2009). Because the relationship depends on the cosine of the dihedral angle, the Karplus equation predicts that coupling constants of vicinal pyranose protons will be greater when they are both in an axial configuration than when they are in an axial-equatorial or equatorial-equatorial configuration (**Figure 16**).

For structural analysis of (feruloylated) AXOS, the 1D- $^1\text{H-NMR}$  experiment thus yields information about the isomer form of the ferulate moiety and the anomeric conformation of

would be added to every measurement as a calibration standard, but today the signal of the residual solvent is mostly used. Tables of the  $^1\text{H}$  and  $^{13}\text{C}$  chemical shifts of many solvents in various deuterated NMR solvents are available for reference (Gottlieb et al., 1997). NMR measurement is performed in deuterated solvents because deuterium is not NMR-active and therefore does not produce an NMR signal.

xylopyranoses in the sample (via the  $^3J_{\text{H,H}}$  coupling constant) and the ratio of compounds to each other. However, severe signal overlap occurs in the non-anomeric carbohydrate region of the spectrum, and it is impossible to assign all signals or determine coupling positions. 2D-NMR experiments fill these gaps and enable the unequivocal structural characterization of complex feruloylated AXOS.

2D-NMR experiments have two frequency scales: a direct frequency measurement (via Fourier transformation of the FID on the horizontal scale) and an indirect second frequency measurement on the vertical scale. To create the second dimension, a series of 1D spectra are recorded. In each measurement the evolution time in the pulse sequence is lengthened. This incremented delay is a second, indirect time domain which can be converted by Fourier transformation to the second frequency scale. Signal intensity is the third dimension.

Several 2D-NMR experiments were applied to the characterization of (feruloylated) oligosaccharides:  $^1\text{H}$ - $^1\text{H}$ -correlation spectroscopy (COSY),  $^1\text{H}$ - $^1\text{H}$ -total correlation spectroscopy (TOCSY),  $^1\text{H}$ - $^{13}\text{C}$ -heteronuclear single quantum coherence (HSQC) spectroscopy,  $^1\text{H}$ - $^{13}\text{C}$  heteronuclear multiple-bond correlation (HMBC) spectroscopy, and HSQC-TOCSY. An illustration of the pulse programs of the individual 2D-NMR experiments and the measurement and processing parameters used in this work for these experiments are provided in **Section 12.6.1**.

In the COSY experiment, the scalar couplings between  $^1\text{H}$  on adjacent carbon atoms are measured. For structural characterization of (feruloylated) AXOS, this experiment is especially useful for assigning non-anomeric proton signals within a sugar ring by spreading the highly overlapped non-anomeric carbohydrate chemical shift region into a second dimension.

The TOCSY NMR experiment (which is referred to in the older literature as HOHAHA for HOmonuclear HArtmann-Hahn spectroscopy), a COSY-like spectrum is created. However, instead of only showing correlations between the  $^1\text{H}$  on adjacent carbon atoms, the  $^1\text{H}$  correlations in an entire spin-system are visible. Because the presence of oxygen disrupts the TOCSY magnetization transfer, each sugar ring is a defined spin system. This experiment is therefore helpful for grouping individual proton signals into their corresponding sugars when a compound contains many sugar monomers.

In the HSQC experiment, heteronuclear correlations between  $^1\text{H}$  and directly attached  $^{13}\text{C}$  are measured. This experiment enables the determination of the  $^{13}\text{C}$  signals of all carbon nuclei directly coupled to hydrogens in the molecule. Because the proton magnetization is transferred to the carbon nucleus and back during this pulse sequence, the intensity of the cross-peak signals is roughly based upon the number of protons. This is a significant advantage over direct measurement of the  $^{13}\text{C}$  chemical shifts via a 1D- $^{13}\text{C}$  experiment, whose signal intensity is very weak compared to  $^1\text{H}$  experiments due to the lower natural abundance of  $^{13}\text{C}$  compared to  $^1\text{H}$  and the lower gyromagnetic ratio (the ratio of an atom's angular momentum to magnetic momentum; higher gyromagnetic ratios are correlated with a stronger NMR response) of  $^{13}\text{C}$  compared to  $^1\text{H}$ . The HSQC experiment also permits the rapid determination of the sugars present in an oligosaccharide compound via the distinctive anomeric cross-peaks.

HSQC-TOCSY spectra correlate the chemical shift of a  $^{13}\text{C}$  heteronucleus to all proton shifts in a spin-spin system. Like the TOCSY experiment, this experiment helps group signals from complex oligosaccharides into their respective sugar ring systems.

Like the HSQC experiment, the HMBC experiment arises via heteronuclear  $^1\text{H}$ - $^{13}\text{C}$  couplings. However, instead of measuring directly linked nuclei, the experiment measures

couplings over two to four bonds. In the analysis of (feruloylated) oligosaccharides, this experiment enables the confirmation of the ferulate ester linkage to arabinose (HMBC cross-peak between the ferulate carbonyl  $^{13}\text{C}$  shift and the  $^1\text{H}$  shifts of the H5 protons of Araf), the ring form of sugars (furanose vs. pyranose), and the coupling positions of the sugars and their substituents.

Details of sample preparation for the NMR structural characterization experiments performed in this work are provided in **Section 12.5.6.3**.

#### 3.4.2.7. *Structural characterization of purified arabinoxylan oligosaccharides: Determination of monosaccharides' chiral configurations*

Neither NMR nor MS approaches provide information about the absolute chiral configuration of the monosaccharides in an isolated compound, so this was determined separately. Two main approaches are described in the literature: separation on a chiral stationary phase or derivatization with a chiral reagent (Ruiz-Matute et al., 2011). The latter approach produces diastereomeric derivatives, which can be separated on standard non-chiral stationary phases. Whereas the first approach (direct separation on a chiral phase) requires less laboratory preparation steps, chiral phases are expensive and fragile. Therefore, for this work, derivatization with a chiral reagent was selected (see **Section 12.5.6.5** for the exact method description). The monosaccharide composition of isolated AXOS was confirmed by TFA hydrolysis and HPAEC-PAD separation and detection of the released monosaccharides (see **Section 12.5.6.4** for the method description).

#### 3.4.2.8. *(Feruloylated) side-chain screening methods*

Following the successful isolation of pure AX side-chain standard compounds, these may be used to develop rapid side-chain screening methods.

For example, several HPAEC-PAD methods have been described in the literature which screen for the major non-feruloylated AXOS released upon *endo*-xylanase hydrolysis (Ordaz-Ortiz et al., 2005; Saulnier and Quemener, 2010; Makaravicius et al., 2012). These methods have been used to classify cereal varieties based on AX structural differences (Ordaz-Ortiz et al., 2005), develop structural models for cereal AX (Tian et al., 2015), and compare the action of different enzymatic preparations on cereal biomass (Makaravicius et al., 2012), among others. In this work, HPAEC-PAD was used to develop a qualitative screening technique for a novel non-feruloylated side-chain isolated from cereal grain AX (see discussion in **Section 7**; the experimental details of the method are provided in **Section 12.5.8**). However, HPAEC-PAD screening cannot be used for feruloylated AX side-chains because the alkaline conditions necessary for anion-exchange chromatography of carbohydrates cleave ferulate ester linkages.

Numerous methods exist for the quantification of total esterified ferulates and other phenolic acids in plant materials; however, only a few approaches discriminate between different ferulate populations in plant materials and/or localize the ferulates' position in cell wall polymers. Vaidyanathan and Bunzel (2012) described an approach which divided a plant material's total monomeric ferulates into four populations: ester-linked to insoluble fibers, ester-linked to soluble fibers, ester-linked to oligosaccharides, and free ferulic acid. This method does not, however, provide information about the distribution of ferulates among the potential side-chain structures. Philippe et al. (2007) created an elegant method for investigating local deposits of FA within the cell using a polyclonal antibody. However, the researchers did not investigate deposition of the other, more complex feruloylated side-chains.

To date, information about ferulate incorporation into more complex AX side-chains is based on NMR spectroscopic characterization of preparatively isolated feruloylated AX fragments (for example, Saulnier et al. (1995c), Bunzel et al. (2002), Allerdings et al. (2006), and Appeldoorn et al. (2013)). This preparative approach works well for the qualitative assessment of plant materials rich in a specific structural element but is time-consuming for plant materials low in a specific structural unit. Additionally, quantitative information about the various side-chains is lacking.

Rapid screening methods for feruloylated AX side-chains have not been developed yet. HPAEC-PAD screening following enzymatic hydrolysis, which has been effectively used for non-feruloylated AXOS, cannot be used for feruloylated AX side-chains because the alkaline conditions necessary for anion-exchange chromatography of carbohydrates cleave ferulate ester linkages. Reversed-phase HPLC separations present an alternative to the alkaline HPAEC conditions, but separations are hampered by on-column mutarotation between  $\alpha$ - and  $\beta$ -configurations of the reducing sugar in the feruloylated AXOS compounds. This problem was addressed in this work by reducing the feruloylated AXOS to their respective sugar alcohols, which permitted the successful development and validation of a quantitative LC-DAD-MS<sup>2</sup>-based screening method for feruloylated side-chain profiles in cereal grain AX (the method development, validation, and application are presented in **Section 5**; the exact method procedure is provided in **Section 12.5.7.1**).

Besides chromatography-based methods, <sup>1</sup>H-NMR-spectroscopy-based methods have been used for both qualitative and quantitative screening of substitution patterns (*O*-3-monosubstitution with *Araf*, *O*-2-monosubstitution with *Araf*, disubstitution with *Araf*, *uXylp*, etc.) of cereal grain AX (Hoffmann et al., 1992; Höije et al., 2006; Toole et al., 2012). <sup>1</sup>H-NMR has also been used to qualitatively screen AX materials for a non-feruloylated disaccharide side-chain (2-*O*- $\beta$ -D-xylopyranosyl- $\alpha$ -L-arabinofuranose) (Höije et al., 2006), but no quantitative NMR screening methods for AX side-chains have been developed. Additionally, until now, all of the NMR-based screening methods in the literature have only screened for non-feruloylated structural moieties, and feruloylated side-chains have been ignored.

A serious drawback to the <sup>1</sup>H-NMR-based screening methods is the significant signal overlap in complex samples. Therefore, we chose to develop and validate a quantitative HSQC-NMR screening method for feruloylated side-chains in cereal AX (method development, validation, and application are presented in **Section 6**; the exact method procedure is provided in **Section 12.5.7.2**). The HSQC method permits the dispersion of the crowded carbohydrate region of the <sup>1</sup>H frequency axis over the <sup>13</sup>C frequency scale and reduces signal overlap. Quantitative HSQC-NMR has not yet been applied to AX, but has been finding increasing use in analytical food chemistry (Pauli et al., 2012). HSQC cross-peak intensities are influenced by several factors, including variations in <sup>13</sup>C-<sup>1</sup>H coupling constants (<sup>1</sup>*J*<sub>C,H</sub>), differing polarization transfer efficiency, and relaxation time (*T*<sub>1</sub> and *T*<sub>2</sub>) differences. However, external or internal calibration corrects for these potential differences and permits quantitative work. In this work, caffeine was used as an internal calibration standard.



# 4. Results and Discussion: *Chapter One*

---

## *Characterization of the feruloylated arabinoxylans from intermediate wheatgrass (Thinopyrum intermedium)*

Grain production worldwide is exclusively dominated by annual crop species. When compared with annual plants, perennials better utilize water, soil nutrients, and solar energy because of their deeper root systems and longer growing seasons (Gash et al., 1997; Wallace, 2000; Cox et al., 2006; Dohleman and Long, 2009). Cultivation of perennial crops can therefore reduce chemical inputs and tillage requirements and improve soil health and erosion control compared to annual crops (Gantzer et al., 1990). The possibility of more sustainable grain harvests, particularly from marginal agricultural land, is driving research initiatives to integrate perennial grains into cropping and food processing systems (Glover et al., 2010). Intermediate wheat grass (IWG, *Thinopyrum intermedium*), a member of the Triticeae tribe of Pooideae and a close perennial relative of annual wheat, was selected as the most promising candidate for grain crop development in a screening study of nearly 100 cool-season perennial grass species (Wagoner and Schauer, 1990). An extensive, multidisciplinary research effort is working to develop IWG as a cost-effective grain crop, to characterize IWG grain, and to identify the best applications for IWG in food products. In this study, the structures of IWG's feruloylated AX were investigated using the conventional approach: preparative isolation and structural characterization of diagnostic oligosaccharides following partial hydrolysis of IWG AX.

### 4.1. Monosaccharide composition, linkage analysis, and phenolic acid profile

The neutral monosaccharide composition of IWG insoluble fiber following Saeman hydrolysis was 52.5% Xyl, 19.1% Ara, 1.7% Gal, and 26.7% Glc. Trace amounts of Man were also detected. IWG's A/X ratio of 0.36 indicates a low degree of AX backbone substitution. Slightly higher A/X ratios were reported for annual wheat and rye (0.49 and 0.43, respectively) insoluble fibers (Bunzel, 2001).

Further structural insights into IWG insoluble AX were provided by methylation analysis (see **Table 8**). The majority (nearly 80%) of the recovered xylose residues were non-substituted. For comparison, 60% of the xylanase-extractable xylose residues from annual

**Table 8: Methylation analysis results (arabinose and xylose) of intermediate wheat grass insoluble fiber**

Linkage type	Mean <sup>a</sup>	Standard deviation
t-Araf	19.32	0.23
2-Araf	0.80	0.05
3-Araf	1.76	0.08
5-Araf	1.68	0.08
t-Xylp	3.23	0.13
4-Xylp	57.43	0.44
2,4/3,4-Xylp <sup>b</sup>	11.18	0.35
2,3,4-Xylp	4.62	0.26

<sup>a</sup>  $n = 4$ ; values are presented as relative molar percentages, with the sum of the recovered amounts of xylose (Xyl) and arabinose (Ara) derivatives being set to 100%.

<sup>b</sup> 2,4-Xylp and 3,4-Xylp were co-eluted. Value represents the sum of both linkage types.

Abbreviations used: **t-Araf**: terminal arabinofuranose; **2-Araf**, etc: *O*-2-glycosidically-linked arabinofuranose; **t-Xylp**: terminal xylopyranose; **2,4-Xylp**:(1→4)- and *O*-2-glycosidically linked xylopyranose; **3,4-Xylp**:(1→4)- and *O*-3-glycosidically linked xylopyranose; **2,3,4-Xylp**:(1→4)- and *O*-2- and *O*-3-glycosidically linked xylopyranose; **4-Xylp**:(1→4)-glycosidically linked xylopyranose.

**Table 9: Phenolic acid content of intermediate wheatgrass insoluble fiber**

Phenolic acid	Mean ( $\mu\text{g/g}$ insoluble fiber) <sup>a</sup>	Standard deviation ( $\mu\text{g/g}$ insoluble fiber)
Caffeic acid	141.3	17.5
<i>trans-p</i> -Coumaric acid	180.0	7.6
<i>cis-p</i> -Coumaric acid	24.2	0.3
<i>trans</i> -Ferulic acid	6750.3	139.0
<i>cis</i> -Ferulic acid	1123.5	78.9
Sinapic acid	87.4	1.4
<i>iso</i> -Ferulic acid	ND <sup>b</sup>	-

<sup>a</sup>*n* = 4, values corrected for residual protein and ash.

<sup>b</sup>ND = not detected.

could arise either from (1→2)-linked arabinose side-chains such as those isolated from sorghum (Verbruggen et al., 1998) or from feruloylated side-chains containing a xylose substituent on the *O*-2 position of arabinose. Small amounts of arabinans from pectic polysaccharides in the IWG insoluble fiber are indicated by the recovery of 5-Araf. Finally, 3-Araf could also arise from pectic arabinan side-chains, but it is also possible that IWG AX contain side-chains linked via the *O*-3 position of arabinose. The GC-MS chromatogram of the partially methylated alditol acetates is provided in **Section 12.8** of the appendix (**Figure 35**); EI-MS fragmentation spectra of the individual peaks are found **Section 12.9** in the appendix (**Figures 36-43**).

The ester-linked phenolic acid profile of IWG insoluble fiber is shown in **Table 9**.

*Trans*-ferulic acid was the most abundant phenolic acid (6750  $\mu\text{g/g}$  corrected insoluble fiber), with a comparable concentration to those reported from insoluble wheat and rye fibers (Bunzel, 2001). The concentration of *cis*-ferulic acid was unusually high (over 1100  $\mu\text{g/g}$  corrected insoluble fiber, or more than 16 % of the *trans*-isomer level). In contrast, *cis*-ferulic acid levels of 0.4-4 % of the *trans*-isomer were reported for annual wheat (McCallum and Walker, 1991). Although exposure to UV light was avoided during extraction and handling, it is possible that a portion of the detected *cis*-ferulic acid levels arose from the limited light exposure during sample preparation. *Iso*-ferulic acid was not detected, in contrast to data from annual wheat reported by Guo and Beta (2013).

#### **4.2. Isolation of feruloylated oligosaccharides from insoluble intermediate wheatgrass fiber**

Feruloylated oligosaccharides were liberated from insoluble IWG fiber with two complementary hydrolysis methods. The mildly acidic (50 mM TFA) hydrolysis developed by Saulnier et al. (1995c) semi-selectively cleaves furanosidic linkages in AX while mostly preserving ferulate ester bonds. Feruloylated side-chains were thus cleaved from the polysaccharide backbone and subsequently separated from released non-feruloylated side-chains using adsorption of the feruloylated mono-/oligosaccharides to Amberlite XAD-2 residue. In contrast to the mildly acidic hydrolysis, which favors release of feruloylated oligosaccharides with arabinose as the reducing end, enzymatic hydrolysis with Driselase, a fungal enzyme preparation containing several carbohydrate hydrolases but lacking feruloyl esterase, primarily releases oligosaccharides with xylose as the reducing end (Micard et al., 1994). Mild acidic hydrolysis thus provides a feruloylated side-chains profile of the analyzed material, whereas Driselase hydrolysis provides information about the AX backbone environment surrounding

wheat were unsubstituted (Ordaz-Ortiz and Saulnier, 2005).

Approximately a third of the remaining IWG xylose residues were di-substituted and two-thirds were mono-substituted. The majority of the recovered arabinose residues were terminal (82%), but a portion were substituted, pointing towards the presence of oligosaccharide side-chains on the AX backbone. The 2-Araf moiety

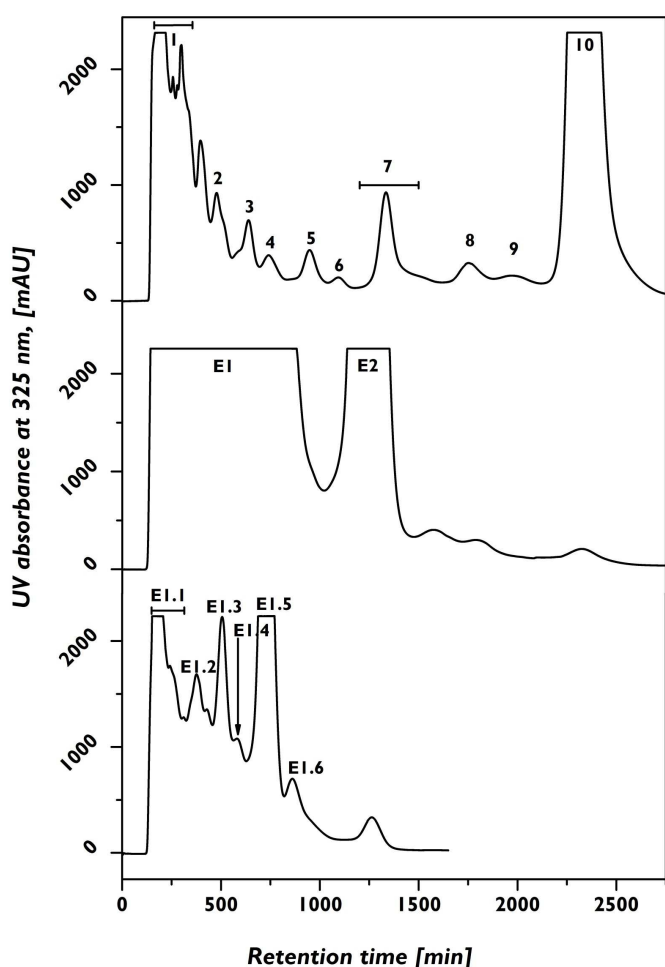


Figure 17: Sephadex LH-20 separation of feruloylated oligosaccharides from acidic (top) and enzymatic hydrolysates (middle) from intermediate wheat grass insoluble fiber, and re-injection of enzymatic peak E1 (bottom).

enzymatic fraction E1.5 contained two peaks: E1.5.1 and E1.5.2 (abbreviated as E5.1 and E5.2). The acidic hydrolysate fractions A4 and A5 each produced two peaks upon RP-HPLC separation: A4.1 and A4.2, and A5.1 and A5.2, respectively.

### 4.3. Identification of isolated feruloylated oligosaccharides released by mildly acidic hydrolysis

Acidic hydrolysate fractions A10 and A7 both had the same sodium adduct ions following ESI-positive ionization ( $m/z$  349  $[M+Na]^+$ ), which was consistent with a molecule made up of ferulic acid plus one pentose. The UV spectrum of A10 was consistent with *trans*-ferulic acid; the compound was unambiguously identified via NMR as the previously described 5-*O-trans*-feruloyl-L-arabinofuranose (FA; see **Figure 18** for isolated structures). FA is a ubiquitous feruloylated side-chain in cereal grains and has been previously isolated from maize bran, wheat bran, rye flour, and wild rice (Ralet et al., 1994a; Saulnier et al., 1995c; Bunzel et al., 2002; Steinhart and Bunzel, 2003).  $^1H$ -NMR analysis of A7 showed two doublets with  $J_{7,8} = 12$  Hz coupling constants, which indicated that the compound contained *cis*-ferulic acid. Additionally, the anomeric  $^1H$  shifts for  $\alpha$ - and  $\beta$ -reducing arabinose were clearly present, and A7 was thus identified as 5-*O-cis*-feruloyl-L-arabinofuranose (*cis*-FA). The molecular weight of A8 was 458

these structural moieties.

Following clean-up with Amberlite XAD-2, the acidic and enzymatic hydrolysates were separated using Sephadex LH-20 gel chromatography (see **Figure 17**). Two Sephadex LH-20 runs were performed from the acidic hydrolysates. Nearly identical chromatograms arose from these duplicate runs, and the matching fractions (A1-A10) were combined. One Sephadex LH-20 run was performed from the enzymatic hydrolysate. Peak E1 of the enzymatic hydrolysate was collected, reduced in volume, and divided into three aliquots. These were individually re-separated on the Sephadex LH-20 as fractions E1.1-E1.6. Collected fractions were screened by reversed phase C18-HPLC-DAD/ESI-MS for purity, and when necessary, fractions were further purified by semi-preparative or preparative RP-HPLC.

RP-HPLC separation of enzymatic fraction E1.3 resulted in five peaks: E1.3.1-E1.3.5 (abbreviated in further discussion as E3.1-E3.5). The

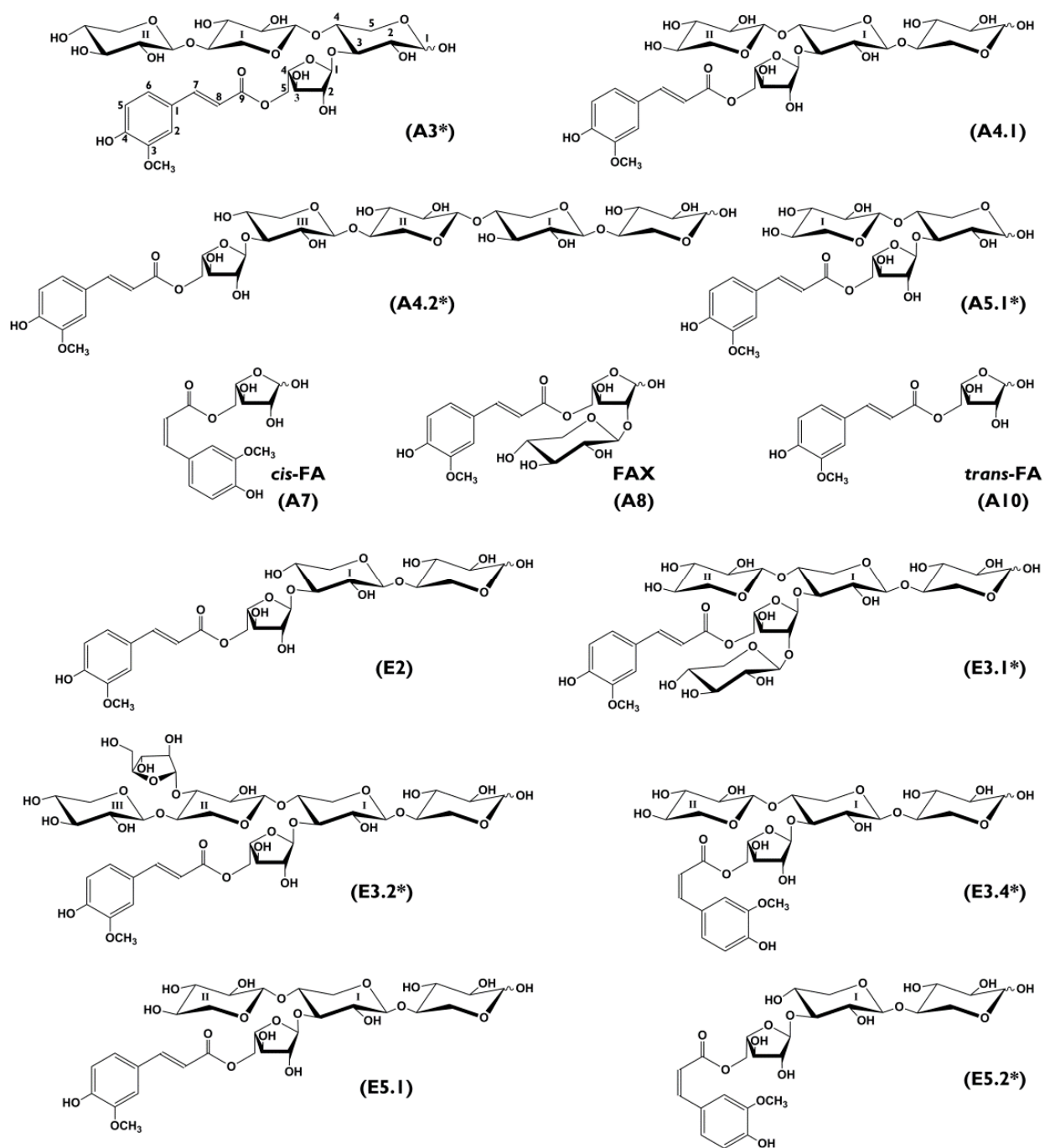


**Figure 18: Feruloylated oligosaccharide structures isolated from mildly acidic and enzymatic hydrolysates of intermediate wheatgrass insoluble fiber.**

\*Novel structure described for the first time in this work.

<sup>i, ii, iii</sup> Roman numeral notation is used to differentiate non-reducing xylose moieties originating from the arabinoxylan backbone (notation is also applied in **Tables 10** and **11**).

Abbreviations: **FA**: 5-*O*-*trans*-feruloyl-L-arabinofuranose; **FAX**:  $\beta$ -D-xylopyranosyl-(1 $\rightarrow$ 2)-5-*O*-*trans*-feruloyl-L-arabinofuranose.

(measured in ESI negative mode,  $m/z$  457 [M-H]<sup>-</sup>), indicating ferulic acid plus two pentoses. Although NMR measurement showed that the fraction was not pure and not all signals could be assigned, the presence of a second commonly described feruloylated side-chain in cereals (rye, maize, and wild rice),  $\beta$ -D-xylopyranosyl-(1 $\rightarrow$ 2)-5-*O*-*trans*-feruloyl-L-arabinofuranose (FAX), was clearly identified (Ralet et al., 1994a; Saulnier et al., 1995c; Bunzel et al., 2002; Steinhart and Bunzel, 2003).

**Table 10. <sup>1</sup>H NMR data of feruloylated oligosaccharides/monosaccharides (in D<sub>2</sub>O).** Coupling constants *J* in Hz; chemical shifts δ<sub>H</sub> in ppm; spectra calibrated against acetone (0.5 μL, δ<sub>H</sub> = 2.22 ppm, δ<sub>C</sub> = 30.89 ppm).

	H1	H2	H3	H4	H5		H6	H7	H8	OMe
	( <i>J</i> <sub>1,2</sub> )				( <i>J</i> <sub>5,6</sub> )	( <i>J</i> <sub>7,8</sub> )				
	H5 <sub>eq</sub>	H5 <sub>ax</sub>								
<b>(A3):</b> β-xylopyranosyl-(1→4)-β-xylopyranosyl-(1→4)-[5- <i>O-trans</i> -feruloyl-α-arabinofuranosyl-(1→3)]-xylopyranose										
α-Xylose, reducing	5.17 (3.5)	3.67	nd	nd	3.83	3.76	-	-	-	-
β-Xylose, reducing	4.62 (7.8)	3.39	3.69	3.77	4.06	3.39	-	-	-	-
β-Xylose <sup>I</sup>	4.30 (7.7)	3.19	3.32	3.54	3.78	3.10	-	-	-	-
β-Xylose <sup>II</sup>	4.41 (7.6)	3.29	3.50	3.67	4.02	3.31	-	-	-	-
α-Arabinose	5.34	4.21	3.98	4.54	4.49	4.33	-	-	-	-
<i>trans</i> -Ferulic acid	-	7.32	-	-	6.94 (7.9)	7.21	7.74 (15.9)	6.48	3.91	
<b>(A4.2):</b> 5- <i>O-trans</i> -feruloyl-α-arabinofuranosyl-(1→3)-β-xylopyranosyl-(1→4)-β-xylopyranosyl-(1→4)-β-xylopyranosyl-(1→4)-xylopyranose										
α-Xylose, reducing	5.17 (3.8)	3.54	nd	nd	3.82	3.74	-	-	-	-
β-Xylose, reducing	4.58 (7.7)	3.25	3.55	3.78	4.06	3.37	-	-	-	-
β-Xylose <sup>I</sup>	4.47	3.29	3.54	3.78	4.10	3.35	-	-	-	-
β-Xylose <sup>II</sup>	4.47	3.29	3.54	3.78	4.10	3.35	-	-	-	-
β-Xylose <sup>III</sup>	4.48	3.41	3.59	3.70	3.99	3.33	-	-	-	-
α-Arabinose	5.35	4.21	4.06	4.41	4.51	4.34	-	-	-	-
<i>trans</i> -Ferulic acid	-	7.30	-	-	6.93 (8.4)	7.20	7.76 (15.9)	6.45	3.90	
<b>(A5.1):</b> β-xylopyranosyl-(1→4)-[5- <i>O-trans</i> -feruloyl-α-arabinofuranosyl-(1→3)]-xylopyranose										
α-Xylose, reducing	5.17 (3.0)	3.68	nd	3.88	3.84	3.78	-	-	-	-
β-Xylose, reducing	4.62 (7.7)	3.40	3.71	3.78	4.07	3.40	-	-	-	-
β-Xylose <sup>I</sup>	4.41 (7.4)	3.27	3.39	3.59	3.90	3.25	-	-	-	-
α-Arabinose	5.40	4.21	3.98	4.56	4.51	4.33	-	-	-	-
<i>trans</i> -Ferulic acid	-	7.32	-	-	6.93 (8.4)	7.21	7.74 (16.0)	6.48	3.90	
<b>(E3.1):</b> (β-xylopyranosyl-(1→4)-{β-xylopyranosyl-(1→2)-[5- <i>O-trans</i> -feruloyl-α-arabinofuranosyl-(1→3)]}-β-xylopyranosyl-(1→4)-xylopyranose										
α-Xylose, reducing	5.18 (3.5)	nd	nd	nd	3.81	3.74	-	-	-	-
β-Xylose, reducing	4.58	3.30	3.54	3.77	4.05	3.37	-	-	-	-
β-Xylose <sup>I</sup>	4.50	3.43	3.69	3.81	4.12	3.41	-	-	-	-
β-Xylose <sup>II</sup>	4.41	3.29	3.40	3.56	3.91	3.25	-	-	-	-
β-Xylose ( <i>side-chain</i> )	4.55	3.25	3.43	3.58	3.95	3.32	-	-	-	-
α-Arabinose	5.56	4.29	4.13	4.57	4.51	4.35	-	-	-	-
<i>trans</i> -Ferulic acid	-	7.33	-	-	6.95 (7.5)	7.22	7.73 (15.5)	6.48	3.91	

**Table 10.** <sup>1</sup>H NMR data of feruloylated oligosaccharides/monosaccharides (in D<sub>2</sub>O). Coupling constants *J* in Hz; chemical shifts δ<sub>H</sub> in ppm; spectra calibrated against acetone (0.5 μL, δ<sub>H</sub> = 2.22 ppm, δ<sub>C</sub> = 30.89 ppm).

	H1	H2	H3	H4	H5		H6	H7	H8	OMe
	( <i>J</i> <sub>1,2</sub> )				( <i>J</i> <sub>5,6</sub> )	( <i>J</i> <sub>7,8</sub> )				
					H5 <sub>eq</sub>	H5 <sub>ax</sub>				
<b>(E3.2):</b> β-xylopyranosyl-(1→4)-[α-arabinofuranosyl-(1→3)]-β-xylopyranosyl-(1→4)-[5- <i>O</i> - <i>trans</i> -feruloyl-α-arabinofuranosyl-(1→3)]-β-xylopyranosyl-(1→4)-xylopyranose										
α-Xylose, reducing	5.18	3.54	3.74	3.79	3.80	3.74	-	-	-	-
β-Xylose, reducing	4.58	3.24	3.53	3.75	4.05	3.36	-	-	-	-
β-Xylose <sup>I</sup>	4.62	3.55	3.79	3.85	4.11	3.39	-	-	-	-
β-Xylose <sup>II</sup>	4.45	3.30	3.56	3.77	4.12	3.40	-	-	-	-
β-Xylose <sup>III</sup>	4.41	3.27	3.39	3.59	3.91	3.24	-	-	-	-
α-Arabinose ( <i>esterified with ferulic acid</i> )	5.29	4.21	3.99	4.61	4.51	4.32	-	-	-	-
α-Arabinose ( <i>not esterified with ferulic acid</i> )	5.23	4.15	3.95	4.13	3.81	3.71	-	-	-	-
<i>trans</i> -Ferulic acid	-	7.31	-	-	6.92	7.19	7.72 (15.4)	6.47	3.89	
<b>(E3.4):</b> β-xylopyranosyl-(1→4)-[5- <i>O</i> - <i>cis</i> -feruloyl-α-arabinofuranosyl-(1→3)]-β-xylopyranosyl-(1→4)-xylopyranose										
α-Xylose, reducing	5.18	3.54	3.75	nd	3.80	3.74	-	-	-	-
β-Xylose, reducing	4.57 (6.7)	3.25	3.54	3.75	4.04	3.36	-	-	-	-
β-Xylose <sup>I</sup>	4.41 (6.8)	3.25	3.40	3.58	3.90	3.25	-	-	-	-
β-Xylose <sup>II</sup>	4.49	3.43	3.72	3.80	4.11	3.38	-	-	-	-
α-Arabinose	5.34	4.16	3.88	4.47	4.29	4.43	-	-	-	-
<i>cis</i> -Ferulic acid	-	7.37	-	-	6.92	7.10	7.06 (13.5)	5.96	3.86	
<b>(E5.2):</b> 5- <i>O</i> - <i>cis</i> -feruloyl-α-arabinofuranosyl-(1→3)-β-xylopyranosyl-(1→4)-xylopyranose										
α-Xylose, reducing	5.18 (3.5)	3.54	3.74	3.73	3.79	3.73	-	-	-	-
β-Xylose, reducing	4.58 (7.8)	3.25	3.53	3.77	4.04	3.36	-	-	-	-
β-Xylose <sup>I</sup>	4.44 (7.9)	3.38	3.50	3.63	3.97	3.29	-	-	-	-
α-Arabinose	5.28	4.17	3.95	4.32	4.42	4.25	-	-	-	-
<i>cis</i> -Ferulic acid	-	7.34	-	-	6.86 (8.3)	7.03	6.98 (12.8)	5.89	3.82	

<sup>I, II, III</sup> Roman numeral notation is used to differentiate non-reducing xylose moieties originating from the arabinoxylan backbone (compare Figure 18).

Abbreviations used: **nd**: not determined; **NMR**: nuclear magnetic resonance.

**Table 11.** <sup>13</sup>C NMR data of feruloylated oligosaccharides/monosaccharides (in D<sub>2</sub>O). Chemical shifts δ<sub>C</sub> in ppm; spectra calibrated against acetone (0.5 μL, δ<sub>H</sub> = 2.22 ppm, δ<sub>C</sub> = 30.89 ppm); data taken from HSQC<sup>1</sup>.

	C1	C2	C3	C4	C5	C6	C7	C8	C9	OMe
<b>(A3):</b> β-xylopyranosyl-(1→4)-β-xylopyranosyl-(1→4)-[5- <i>O</i> - <i>trans</i> -feruloyl-α-arabinofuranosyl-(1→3)]-xylopyranose										
α-Xylose, reducing	92.7	72.3	nd	nd	59.9	-	-	-	-	-
β-Xylose, reducing	97.0	74.7	79.7	74.8	63.6	-	-	-	-	-
β-Xylose <sup>I</sup>	102.3	73.4	74.4	77.6	63.7	-	-	-	-	-
β-Xylose <sup>II</sup>	102.6	73.5	76.3	69.5	65.6	-	-	-	-	-
α-Arabinose	108.9	81.4	78.6	82.3	65.0	-	-	-	-	-
<i>trans</i> -Ferulic acid	126.8	112.3	148.3	149.8	116.5	124.4	147.5	114.7	169.8	56.7

**Table 11.**  $^{13}\text{C}$  NMR data of feruloylated oligosaccharides/monosaccharides (in  $\text{D}_2\text{O}$ ). Chemical shifts  $\delta_{\text{C}}$  in ppm; spectra calibrated against acetone (0.5  $\mu\text{L}$ ,  $\delta_{\text{H}} = 2.22$  ppm,  $\delta_{\text{C}} = 30.89$  ppm); data taken from HSQC<sup>1</sup>.

	C1	C2	C3	C4	C5	C6	C7	C8	C9	OMe
<b>(A4.2):</b> 5- <i>O</i> - <i>trans</i> -feruloyl- $\alpha$ -arabinofuranosyl-(1 $\rightarrow$ 3)- $\beta$ -xylopyranosyl-(1 $\rightarrow$ 4)- $\beta$ -xylopyranosyl-(1 $\rightarrow$ 4)- $\beta$ -xylopyranosyl-(1 $\rightarrow$ 4)-xylopyranose										
$\alpha$ -Xylose, reducing	92.6	71.8	nd	nd	59.2	-	-	-	-	-
$\beta$ -Xylose, reducing	97.1	74.6	nd	78.4	63.4	-	-	-	-	-
$\beta$ -Xylose <sup>I</sup>	102.3	73.3	74.4	77.0	63.5	-	-	-	-	-
$\beta$ -Xylose <sup>II</sup>	102.3	73.3	74.4	77.0	63.5	-	-	-	-	-
$\beta$ -Xylose <sup>III</sup>	102.3	73.4	82.1	68.2	65.9	-	-	-	-	-
$\alpha$ -Arabinose	108.8	81.7	77.3	82.1	64.4	-	-	-	-	-
<i>trans</i> -Ferulic acid	126.8	112.1	148.7	149.1	116.6	124.3	147.3	114.5	169.9	56.6
<b>(A5.1):</b> $\beta$ -xylopyranosyl-(1 $\rightarrow$ 4)-[5- <i>O</i> - <i>trans</i> -feruloyl- $\alpha$ -arabinofuranosyl-(1 $\rightarrow$ 3)]-xylopyranose										
$\alpha$ -Xylose, reducing	92.9	72.3	nd	76.6	59.6	-	-	-	-	-
$\beta$ -Xylose, reducing	97.0	75.8	79.0	74.5	63.6	-	-	-	-	-
$\beta$ -Xylose <sup>I</sup>	102.4	73.6	76.2	69.8	66.0	-	-	-	-	-
$\alpha$ -Arabinose	108.7	81.5	78.4	82.5	65.0	-	-	-	-	-
<i>trans</i> -Ferulic acid	127.1	112.2	148.3	149.5	116.6	124.4	147.6	114.6	169.9	56.7
<b>(E3.1):</b> $\beta$ -xylopyranosyl-(1 $\rightarrow$ 4)-{ $\beta$ -xylopyranosyl-(1 $\rightarrow$ 2)-[5- <i>O</i> - <i>trans</i> -feruloyl- $\alpha$ -arabinofuranosyl-(1 $\rightarrow$ 3)]}- $\beta$ -xylopyranosyl-(1 $\rightarrow$ 4)-xylopyranose										
$\alpha$ -Xylose, reducing	92.7	nd	71.7	nd	59.7	-	-	-	-	-
$\beta$ -Xylose, reducing	97.2	73.6	74.6	76.7	63.7	-	-	-	-	-
$\beta$ -Xylose <sup>I</sup>	103.5	75.8	75.9	69.9	65.9	-	-	-	-	-
$\beta$ -Xylose <sup>II</sup>	102.3	74.0	79.0	74.5	63.5	-	-	-	-	-
$\beta$ -Xylose ( <i>side-chain</i> )	102.4	73.5	76.2	70.0	65.8	-	-	-	-	-
$\alpha$ -Arabinose	107.4	89.5	77.0	82.1	64.7	-	-	-	-	-
<i>trans</i> -Ferulic acid	nd	112.2	nd	nd	116.4	124.1	147.3	114.8	nd	56.7
<b>(E3.2):</b> $\beta$ -xylopyranosyl-(1 $\rightarrow$ 4)-[ $\alpha$ -arabinofuranosyl-(1 $\rightarrow$ 3)]- $\beta$ -xylopyranosyl-(1 $\rightarrow$ 4)-[5- <i>O</i> - <i>trans</i> -feruloyl- $\alpha$ -arabinofuranosyl-(1 $\rightarrow$ 3)]- $\beta$ -xylopyranosyl-(1 $\rightarrow$ 4)-xylopyranose										
$\alpha$ -Xylose, reducing	92.7	72.1	71.7	74.6	59.4	-	-	-	-	-
$\beta$ -Xylose, reducing	97.2	74.4	74.6	77.1	63.7	-	-	-	-	-
$\beta$ -Xylose <sup>I</sup>	100.5	74.5	79.1	74.5	63.5	-	-	-	-	-
$\beta$ -Xylose <sup>II</sup>	102.3	73.7	79.4	76.7	63.6	-	-	-	-	-
$\beta$ -Xylose <sup>III</sup>	102.3	73.5	76.3	69.9	65.8	-	-	-	-	-
$\alpha$ -Arabinose ( <i>esterified with ferulic acid</i> )	109.1	81.4	78.5	82.4	65.0	-	-	-	-	-
$\alpha$ -Arabinose ( <i>not esterified with ferulic acid</i> )	109.4	81.8	77.4	85.2	61.9	-	-	-	-	-
<i>trans</i> -Ferulic acid	127.1	111.9	148.5	149.3	116.3	124.4	147.4	114.6	169.8	56.5
<b>(E3.4):</b> $\beta$ -xylopyranosyl-(1 $\rightarrow$ 4)-[5- <i>O</i> - <i>cis</i> -feruloyl- $\alpha$ -arabinofuranosyl-(1 $\rightarrow$ 3)]- $\beta$ -xylopyranosyl-(1 $\rightarrow$ 4)-xylopyranose										
$\alpha$ -Xylose, reducing	92.8	71.1	71.7	nd	59.6	-	-	-	-	-
$\beta$ -Xylose, reducing	97.3	74.8	74.4	77.2	63.5	-	-	-	-	-
$\beta$ -Xylose <sup>I</sup>	102.4	73.7	76.2	69.8	65.7	-	-	-	-	-
$\beta$ -Xylose <sup>II</sup>	102.4	74.0	78.5	74.4	63.5	-	-	-	-	-
$\alpha$ -Arabinose	108.6	81.4	78.2	82.4	64.9	-	-	-	-	-
<i>cis</i> -Ferulic acid	127.8	114.5	147.4	147.2	115.8	125.2	145.6	116.9	169.1	56.6

**Table 11.**  $^{13}\text{C}$  NMR data of feruloylated oligosaccharides/monosaccharides (in  $\text{D}_2\text{O}$ ). Chemical shifts  $\delta_{\text{C}}$  in ppm; spectra calibrated against acetone (0.5  $\mu\text{L}$ ,  $\delta_{\text{H}} = 2.22$  ppm,  $\delta_{\text{C}} = 30.89$  ppm); data taken from HSQC<sup>1</sup>.

	C1	C2	C3	C4	C5	C6	C7	C8	C9	OMe
<b>(E5.2):</b> 5- <i>O</i> - <i>cis</i> -feruloyl- $\alpha$ -arabinofuranosyl-(1 $\rightarrow$ 3)- $\beta$ -xylopyranosyl-(1 $\rightarrow$ 4)-xylopyranose										
$\alpha$ -Xylose, reducing	92.7	71.6	71.6	77.3	59.6	-	-	-	-	-
$\beta$ -Xylose, reducing	97.3	74.7	74.6	77.0	63.6	-	-	-	-	-
$\beta$ -Xylose <sup>1</sup>	102.5	73.7	82.4	68.7	65.8	-	-	-	-	-
$\alpha$ -Arabinose	109.0	81.8	77.5	82.0	64.5	-	-	-	-	-
<i>cis</i> -Ferulic acid	127.6	114.3	147.2	146.4	115.8	125.1	146.0	116.7	168.9	56.4

<sup>1</sup>When reported, C1, C3, C4, and C9 phenolic acid shifts were taken from HMBC.

<sup>i, ii, iii</sup> Roman numeral notation is used to differentiate non-reducing xylose moieties originating from the arabinoxylan backbone (compare **Figure 18**).

Abbreviations used: **HSQC**: heteronuclear single quantum coherence spectroscopy; **nd**: not determined; **NMR**: nuclear magnetic resonance.

Fraction A3 was measured in ESI negative mode and produced a quasi-molecular ion indicative of a ferulic acid moiety plus four pentose molecules ( $m/z$  721  $[\text{M}-\text{H}]^-$ ). NMR data (see **Tables 10** and **11**) identified the compound as  $\beta$ -xylopyranosyl-(1 $\rightarrow$ 4)- $\beta$ -xylopyranosyl-(1 $\rightarrow$ 4)-[5-*O*-*trans*-feruloyl- $\alpha$ -arabinofuranosyl-(1 $\rightarrow$ 3)]-xylopyranose. NMR data are listed here for those compounds that have not been isolated and/or NMR spectroscopically described before; NMR data for previously described compounds are provided in the appendix (**Section 12.7**; **Tables 38** and **39**).

Fractions A4.1 and 4.2 produced quasi-molecular ions of  $m/z$  745  $[\text{M}+\text{Na}]^+$  and  $m/z$  877  $[\text{M}+\text{Na}]^+$ , respectively, in ESI-positive mode, which was consistent with a ferulate moiety plus four and five pentose molecules, respectively. A4.1 was identified from NMR measurements as the previously described  $\beta$ -xylopyranosyl-(1 $\rightarrow$ 4)-[5-*O*-*trans*-feruloyl- $\alpha$ -arabinofuranosyl-(1 $\rightarrow$ 3)]- $\beta$ -xylopyranosyl-(1 $\rightarrow$ 4)-xylopyranose (Bunzel et al., 2002; Steinhart and Bunzel, 2003). However, NMR data (see **Tables 10** and **11**) for A4.2 revealed a novel compound: a xylotetrasaccharide singly substituted with 5-*O*-*trans*-feruloyl-arabinofuranose at the non-reducing terminal end (5-*O*-*trans*-feruloyl- $\alpha$ -arabinofuranosyl-(1 $\rightarrow$ 3)- $\beta$ -xylopyranosyl-(1 $\rightarrow$ 4)- $\beta$ -xylopyranosyl-(1 $\rightarrow$ 4)- $\beta$ -xylopyranosyl-(1 $\rightarrow$ 4)-xylopyranose). The signals from the two internal, non-reducing  $\beta$ -xylose units overlapped almost perfectly in both their  $^1\text{H}$  and carbon shifts, but integration of the  $^1\text{H}$  signals clearly showed the presence of two xylose molecules. Although the compound was unambiguously identified, the possibility that it may represent a hydrolysis artefact (i.e., that the xylotetrasaccharide was substituted with additional arabinose moieties *in planta* that were cleaved during the mild acidic hydrolysis) cannot be ignored.

Fractions A5.1 and A5.2 produced quasi-molecular ions of  $m/z$  613  $[\text{M}+\text{Na}]^+$  and  $m/z$  745  $[\text{M}+\text{Na}]^+$  in ESI positive mode, corresponding to a ferulate moiety plus three and four pentose molecules, respectively. NMR analysis of A5.1 (see **Tables 10** and **11**) clearly identified the isolated compound as  $\beta$ -xylopyranosyl-(1 $\rightarrow$ 4)-[5-*O*-*trans*-feruloyl- $\alpha$ -arabinofuranosyl-(1 $\rightarrow$ 3)]-xylopyranose. The isolated amount of A5.2 was not sufficient for 2D-NMR analysis, so this compound was not further characterized.

FA (both *cis*- and *trans*-) and FAX were the only feruloylated side-chains isolated from the acidic hydrolysate, indicating that the feruloylated side-chain profile of IWG's AX is dominated by simple side-chains, with little to no appreciable amounts of the complex, Gal-containing side-chains present in large quantities in maize AX (Allerdings et al., 2006). Some of the structures isolated from the acidic hydrolysate contained pieces of the xylan backbone,

demonstrating that the hydrolysis conditions used were, as expected, not completely specific for furanosidic linkages. However, the gravimetric amounts of the backbone-containing fractions (A3, A4.1, A4.2, and A5.1) isolated from approximately 40 g of IWG insoluble fiber were all less than 1 mg, whereas the isolated gravimetric amount of the major feruloylated side-chain, *trans*-FA, was approximately 15 mg. These amounts must be approached as approximate estimates of the compounds in the acidic hydrolysate because the number of semi-preparative RP-HPLC clean-up runs, which are prone to compound losses, varied between fractions. Nevertheless, the relative specificity of the hydrolysis conditions to cleave furanosidic linkages is evident.

#### 4.4. Identification of isolated feruloylated oligosaccharides released by enzymatic (Driselase) hydrolysis

The most abundant fraction in the enzymatic hydrolysate, E2, was unambiguously identified as the previously described 5-*O-trans*-feruloyl- $\alpha$ -arabinofuranosyl-(1 $\rightarrow$ 3)- $\beta$ -xylopyranosyl-(1 $\rightarrow$ 4)-xylopyranose. Positive-mode ESI ionization produced  $m/z$  613 [M+Na]<sup>+</sup>, indicating a structure containing a ferulate moiety and three pentoses. NMR analysis confirmed the structure of this ubiquitous product of *endo*-xylanase hydrolysis of cereal grain cell walls, which has been isolated from barley, maize, wheat, rye, and wild rice (Gubler et al., 1985; McCallum et al., 1991; Ohta et al., 1994; Ralet et al., 1994a; Bunzel et al., 2002; Steinhart and Bunzel, 2003).

E3.1 had a quasi-molecular ion of  $m/z$  877 [M+Na]<sup>+</sup>, consistent with a ferulate moiety and five pentoses. NMR analysis (Tables 10 and 11) showed that the compound consisted of a xylotrisaccharide substituted with an FAX side-chain ( $\beta$ -xylopyranosyl-(1 $\rightarrow$ 4)-{ $\beta$ -xylopyranosyl-(1 $\rightarrow$ 2)-[5-*O-trans*-feruloyl- $\alpha$ -arabinofuranosyl-(1 $\rightarrow$ 3)]}- $\beta$ -xylopyranosyl-(1 $\rightarrow$ 4)-xylopyranose). The C2 of arabinose was substantially shifted downfield (89.5 ppm compared to  $\approx$ 81 ppm for a comparable arabinose not substituted with a side-chain xylose). In addition, a clear HMBC coupling was seen between the C2 of arabinose to H1 of the side-chain xylose.

ESI-positive ionization and MS analysis of E3.2 showed a quasi-molecular ion of  $m/z$  1009 [M+Na]<sup>+</sup>, indicative of a structure built from ferulic acid and six pentose units. HSQC-NMR analysis revealed seven anomeric signals: signals from two non-reducing arabinose units, three non-reducing xylose units, and  $\alpha$ - and  $\beta$ - signals from the reducing xylose unit. C4/H1 coupling between neighboring xylose molecules observed in the HMBC spectrum showed a linear xylotetrasaccharide chain. Both the first and second non-reducing xylose molecules (counting from the reducing end) were substituted with an *Araf* at their *O*-3 positions. This was shown by two separate HMBC cross-peaks representing couplings between the respective xylose C3 carbons and the anomeric protons of the two arabinose molecules. HMBC data also clearly showed that one of the arabinose molecules was *O*-5-esterified with *trans*-ferulic acid. The final structure was unambiguously assigned as  $\beta$ -xylopyranosyl-(1 $\rightarrow$ 4)-[ $\alpha$ -arabinofuranosyl-(1 $\rightarrow$ 3)]- $\beta$ -xylopyranosyl-(1 $\rightarrow$ 4)-[5-*O-trans*-feruloyl- $\alpha$ -arabinofuranosyl-(1 $\rightarrow$ 3)]- $\beta$ -xylopyranosyl-(1 $\rightarrow$ 4)-xylopyranose (see Tables 10 and 11 for complete NMR data).

E3.3, E3.4, and E3.5 all resulted in the same quasi-molecular ion of  $m/z$  745 [M+Na]<sup>+</sup> following ESI-positive ionization and MS analysis, which indicated that the structures contained single ferulate moieties plus 4 pentoses. NMR analyses of the three fractions showed that E3.3 and E3.5 were not pure; these compounds were not further characterized. E3.4 was successfully characterized by NMR as the ferulate *cis*-isomer of  $\beta$ -xylopyranosyl-(1 $\rightarrow$ 4)-[5-*O-feruloyl*- $\alpha$ -

arabinofuranosyl-(1→3)]-β-xylopyranosyl-(1→4)-xylopyranose (see **Tables 10** and **11**).

E5.1 and E5.2 had quasi-molecular ions of  $m/z$  745  $[M+Na]^+$  and  $m/z$  613  $[M+Na]^+$ , consistent with structures composed of ferulic acid and four and three pentose molecules, respectively. E5.1 was clearly identified by NMR as being identical to a compound already isolated from the acid hydrolysate: β-xylopyranosyl-(1→4)-[5-*O-trans*-feruloyl-α-arabinofuranosyl-(1→3)]-β-xylopyranosyl-(1→4)-xylopyranose. NMR revealed that E5.2 was a mixture of *cis*- and *trans*- isomers in an approximately 3:1 ratio. The *cis*-compound was characterized as 5-*O-cis*-feruloyl-α-arabinofuranosyl-(1→3)-β-xylopyranosyl-(1→4)-xylopyranose.

The structures isolated after enzymatic hydrolysis further underline the relatively simple feruloylated side-chain profile of IWG AX. A structure containing a xylose substituted with a feruloylated side-chain and adjacent to another substituted xylose (E3.2) was isolated for the first time, which shows that the presence of a neighboring arabinose substituent does not hinder feruloylation of an adjacent arabinose substituent. Although methylation analysis found that around one-fourth of the substituted xylose molecules are di-substituted, no feruloylated compounds were isolated containing a di-substituted xylose, which may indicate that feruloylation of these structures is sterically hindered or that the theoretical di-substituted xylose molecules carrying feruloylated side-chains are found only in heavily substituted regions of the AX backbone which are inaccessible to enzymes. Additionally two compounds were isolated from the enzymatic hydrolysate which were esterified with *cis*-ferulic acid.

#### 4.5. Conclusion

This study examined the structure of feruloylated AX from IWG, a perennial cereal grain. IWG AX have a low backbone substitution rate and a similar phenolic acid profile to annual wheat and rye, with the exception of *cis*-ferulic acid, where substantially higher values were found in IWG. Thirteen feruloylated oligosaccharides were isolated (eight of these structures were described for the first time) and identified by LC-ESI-MS and NMR. FA and FAX were the only feruloylated side-chains identified in IWG using this conventional approach of hydrolysis, preparative isolation, and characterization. This indicates that the feruloylated side-chain profile of IWG AX is comparable to the profile of annual rye and less complex than that of maize. IWG feruloylated AX may therefore be described as relatively simple, with similarities to annual wheat and rye. It is not possible to make quantitative conclusions about the overall content and distribution of the individual feruloylated side-chains in IWG AX from this qualitative approach; however, several new structural components of cereals' feruloylated AX were identified.

## 5. Results and Discussion: *Chapter Two*

---

### *Feruloylated side-chain profiles in cereal grain arabinoxylans: Development of a quantitative LC-DAD/MS screening approach*

Growing evidence points towards the possibility that the effects of feruloylated AX, particularly those related to enzymatic digestibility, are mediated not only by ferulate dimers/higher oligomers' crosslinking of cell wall polymers, but also by the degree and complexity of their monomeric feruloylated side-chain substituents. Many arabinofuranosidases cannot cleave feruloylated arabinose from the xylan backbone (Wood and McCrae, 1996; Luonteri et al., 1999; Remond et al., 2008). Feruloylation of AXOS limited their fermentability by human colon microbiota compared to non-feruloylated AXOS (Snelders et al., 2014b). Yang et al. (2013) observed differing short chain fatty acid profiles following *in vitro* fermentation with human fecal microbiota of autohydrolysates from wheat and maize brans and suggested that these differences may have been caused by the materials' divergent feruloylated side-chain profiles. In a study examining the maize grain material resistant to mild acid pretreatment and subsequent enzymatic saccharification with an enzyme cocktail, feruloylated oligosaccharides made up 39% of the enzyme-resistant oligosaccharides. Structural characterization of these feruloylated oligosaccharides showed that most contained the FAXG or FAX structural moiety (Appeldoorn et al., 2013). In some contexts, such as lignocellulosic biofuel production, slower rates of enzymatic digestion or recalcitrance to digestion are an economical and processing drawback, although in other situations, this may be beneficial. For example, in human diets, a more slowly digested AX serves as a potential delivery source of fermentable carbohydrates to the distal colon, which may positively influence colon health.

Until now, however, no methods have been developed which quantitatively describe the distribution of ferulates into various feruloylated side-chains. Information about ferulate incorporation into AX side-chains has been based on NMR spectroscopic characterization of preparatively isolated feruloylated AX fragments (e.g. Saulnier et al. (1995c) and Allerdings et al. (2006)). This qualitative approach works well for plant materials rich in a specific structural element but is extremely laborious for plant materials with low levels of these specific structural units (see first results chapter in **Section 4**). Therefore, in this project an efficient, robust, and sensitive screening method was developed which enabled the quantitative comparison of feruloylated side-chain profiles in cell wall materials. The approach was developed and validated using the authentic standard compounds FA, FAX, and FAXG (**Figure 5**) and tested on twelve cereal materials. The final procedure consisted of a mildly acidic hydrolysis, C18-SPE clean-up, reduction under aprotic conditions, and LC-DAD/MS separation and detection.

#### **5.1. Isolation of feruloylated side-chain standard compounds**

The standard compounds FA, FAX, and FAXG were isolated in preparative quantities from insoluble maize fiber following the mildly acidic hydrolysis of Saulnier et al. (1995c). The feruloylated mono- and oligosaccharides were absorbed on Amberlite XAD-2 material and

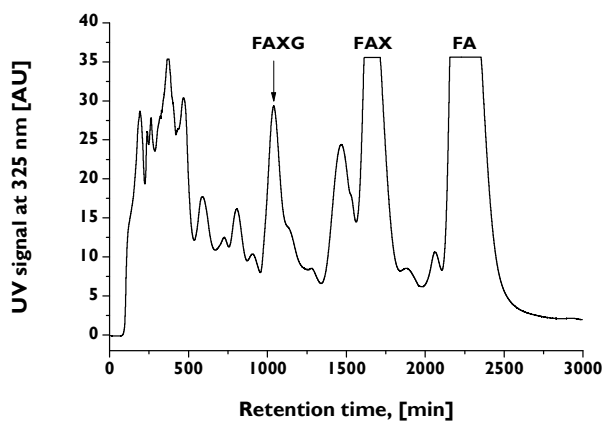


**Figure 19. Sephadex LH-20 separation of feruloylated side-chain standard compounds from mildly acidic hydrolysate of insoluble maize fiber.**

*Abbreviations used:* **FA:** 5-*O*-*trans*-feruloyl-L-arabinofuranose; **FAX:**  $\beta$ -D-xylopyranosyl-(1 $\rightarrow$ 2)-5-*O*-*trans*-feruloyl-L-arabinofuranose; **FAXG:**  $\alpha$ -L-galactopyranosyl-(1 $\rightarrow$ 2)- $\beta$ -D-xylopyranosyl-(1 $\rightarrow$ 2)-5-*O*-*trans*-feruloyl-L-arabinofuranose.

slightly. This rules out chromatographic separation of the native feruloylated side-chains standard compounds (FA, FAX, and FAXG) under the primarily aqueous conditions applied in C18-based HPLC, where on-column mutarotation produces broad, tailing, split peaks (see **Figure 20**). FAX was especially problematic and spawned a peak over 4 min wide. Reducing the standard compounds to their respective sugar alcohols with sodium borohydride in the aprotic solvent DMSO resulted in sharp, baseline-separated peaks on an analytical C18-RP-HPLC column with a binary gradient made up of acidified water and acetonitrile. The *cis*- and *trans*-isomers of each compound were also resolved (see **Figure 20**).

Several challenges had to be addressed during the development of the reduction method. First, when the reduction was performed in a protic solvent (MeOH, EtOH, or DMSO-H<sub>2</sub>O mixtures), additional peaks appeared in the chromatogram with the same *m/z* ratio as the reduced standard compounds (see **Figure 20**). A base-catalyzed Lobry de Bruyn-van Ekenstein rearrangement of the reducing arabinose to other sugars via an enediol intermediate was assumed to be responsible. The use of DMSO, an aprotic solvent, during reduction resulted in one chromatographic peak per standard compound. Nevertheless, it is still imperative to avoid inadvertently introducing water into the system during the reduction reaction. Because both DMSO and sodium borohydride are strongly hygroscopic, the reducing solution should be freshly prepared in a sealed container and the individual samples should be tightly sealed during reduction. Furthermore, the acidic workup at the end of reduction should be performed as quickly as feasible without allowing the sample to foam over: excessive time spent in completing the acid addition creates a temporarily alkaline, protic environment and facilitates the transformation reaction.

A second, sporadically recurring, hurdle during the reduction method development was the sometimes incomplete reduction, especially of the standard compound FA, over a range of reduction times and sodium borohydride concentrations. Under the final reduction conditions (2 mL of a 30 mg NaBH<sub>4</sub>/mL DMSO solution, 18 h, 30°C), the incidence of incomplete

fractionated with preparative Sephadex LH-20 gel chromatography (**Figure 19**), followed by preparative RP-HPLC cleanup of desired fractions.

## 5.2. Reduction of feruloylated side-chain mono- /oligosaccharides

Oligosaccharide profiling approaches are often based on HPAEC-PAD separation and detection (Ordaz-Ortiz et al., 2005; Tian et al., 2015). However, due to the ester-linkages between ferulic acid and the carbohydrate moiety of FA, FAX, and FAXG, the alkaline conditions that are necessary to separate carbohydrates with HPAEC are not applicable. Thus, RP-HPLC separation of the feruloylated standard compounds was tested.

The chromatographic retention factors of reducing sugars'  $\alpha$ - and  $\beta$ -anomers differ

slightly.

reduction was decreased, but not entirely eliminated. However, when occurring, the amount of unreduced FA was negligible (only  $\approx 5\%$  of the total FA in the samples) and may, therefore, be disregarded.

### 5.3. Method validation

The validation parameters for FA, FAX, and FAXG are summarized in **Table 12**. All three standard compounds were calibrated in triplicate, and linear standard curves and correlation coefficients ( $R^2$ ) were calculated. The limit of detection (LOD) and limit of quantification (LOQ) were determined as the standard compound concentrations producing signal-to-noise ratios of 3:1 and 9:1, respectively. FAXG's especially sharp peak form pushed its LOD and LOQ below those of FAX and FA, but all three compounds had LOQs in the single-digit micromolar range. Recoveries, which were determined by subjecting standard compound solutions to the sample preparation procedure beginning at SPE-clean-up, were above 93% for all three compounds. The method was robust and reproducible over time, as illustrated in **Figure 21**, which depicts six separate calibration curves prepared and analyzed four months apart, with each calibration curve originating from its own freshly prepared stock solution of standard compounds. Quantification of the feruloylated side-chains via a free ferulic acid standard curve was tested and rejected because the free acid's UV response was greater per mole than those

of the feruloylated standard compounds (see **Figure 51** in **Section 12.10** in the appendix). This produces the practical limitation for research laboratories of needing to initially isolate the standard compounds for accurate quantification. Nonetheless, once standard compounds have been secured, the method affords a sensitive, reproducible, accurate possibility to quantify the major feruloylated AX side-chain compounds in cereals and grass cell walls.

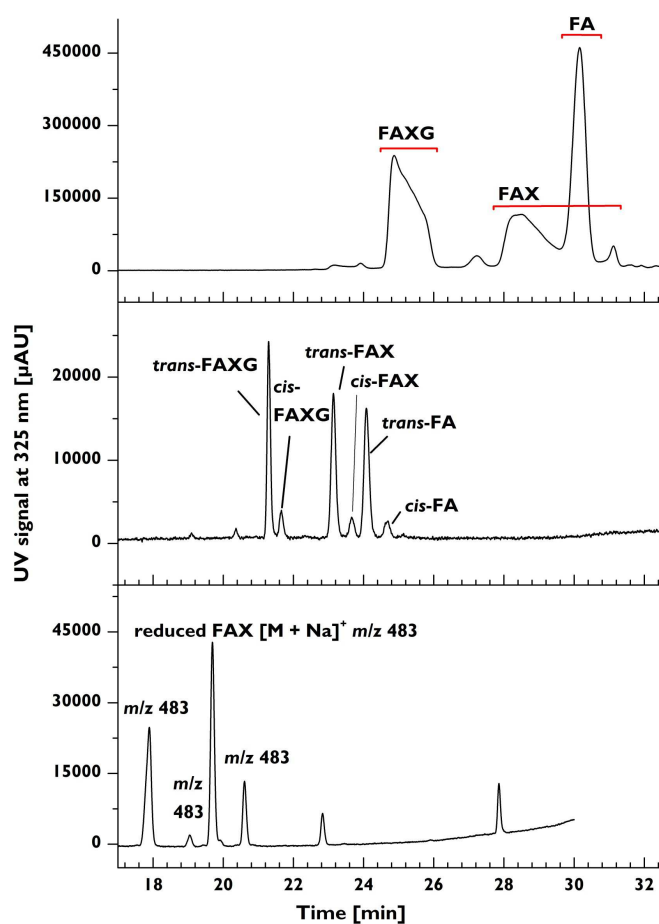


**Figure 20. Chromatography and peak forms of feruloylated side-chain standard compounds before and after reduction in various solvents.** [Top]: Broad, tailing, split peaks resulting from native (unreduced) feruloylated side-chain standard compounds. [Middle]: Narrow, symmetrical peaks resulting from reduction in aprotic solvent (DMSO) of feruloylated side-chain standard compounds to their respective sugar alcohols. [Bottom]: Lobry de Bruyn–van Ekenstein rearrangement of FAX in a protic solvent (here: EtOH) during reduction results in several isomers. Note: Bottom chromatogram was obtained using a different gradient.

Abbreviations used: **FA**: 5-*O*-*trans*-feruloyl-L-arabinofuranose; **FAX**:  $\beta$ -D-xylopyranosyl-(1 $\rightarrow$ 2)-5-*O*-*trans*-feruloyl-L-arabinofuranose; **FAXG**:  $\alpha$ -L-galactopyranosyl-(1 $\rightarrow$ 2)- $\beta$ -D-xylopyranosyl-(1 $\rightarrow$ 2)-5-*O*-*trans*-feruloyl-L-arabinofuranose; *m/z*: mass-to-charge ratio.

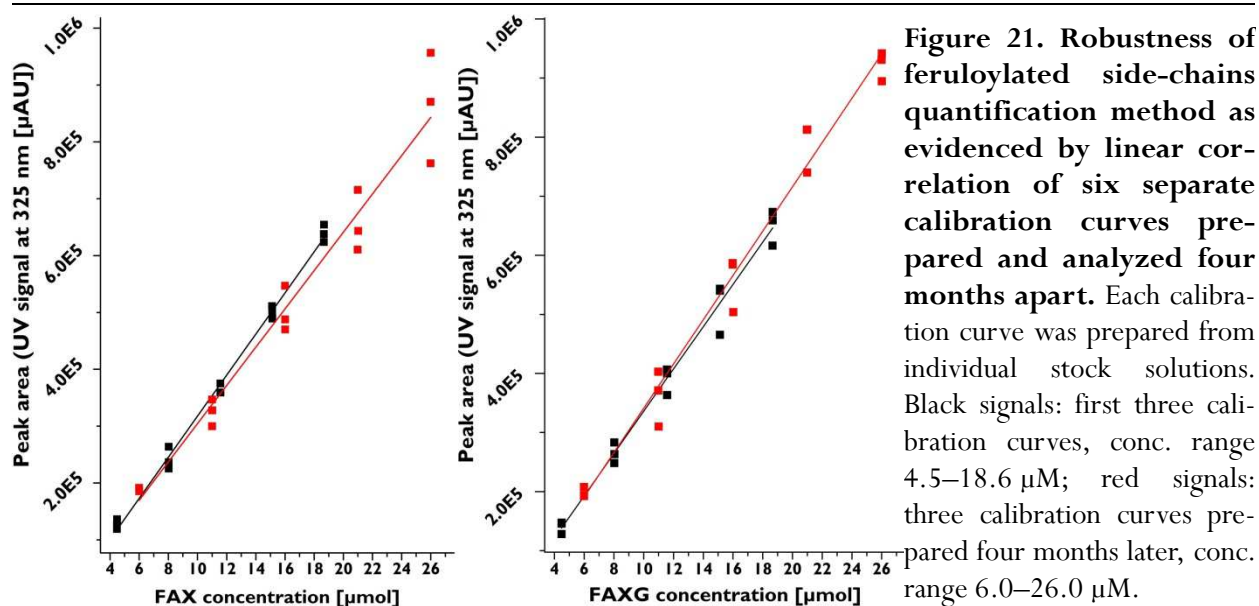
**Table 12. Calibration equations<sup>a</sup>, correlation coefficients, limits of detection (LOD), limits of quantification (LOQ), and % recovery for FA, FAX, and FAXG**

	range tested ( $\mu\text{M}$ )	linear calibration equation	correlation coefficients	LOD ( $\mu\text{M}$ )	LOQ ( $\mu\text{M}$ )	Recovery (% $\pm$ SD) <sup>b</sup>
FA	10–260	$y = 26806x - 190178$	0.9812	1.4	4.2	$93.5 \pm 5.8$
FAX	6–26	$y = 33194x - 29998$	0.9607	0.8	2.4	$98.7 \pm 7.8$
FAXG	6–26	$y = 37649x - 37727$	0.9813	0.6	1.8	$93.4 \pm 5.3$

<sup>a</sup> Calibration equations and correlation coefficients were calculated from three separate calibrations.

<sup>b</sup>  $n = 3$

Abbreviations used: **FA**: 5-*O*-*trans*-feruloyl-L-arabinofuranose; **FAX**:  $\beta$ -D-xylopyranosyl-(1 $\rightarrow$ 2)-5-*O*-*trans*-feruloyl-L-arabinofuranose; **FAXG**:  $\alpha$ -L-galactopyranosyl-(1 $\rightarrow$ 2)- $\beta$ -D-xylopyranosyl-(1 $\rightarrow$ 2)-5-*O*-*trans*-feruloyl-L-arabinofuranose; **SD**: standard deviation



Abbreviations used: **FAX**:  $\beta$ -D-xylopyranosyl-(1 $\rightarrow$ 2)-5-*O*-*trans*-feruloyl-L-arabinofuranose; **FAXG**:  $\alpha$ -L-galactopyranosyl-(1 $\rightarrow$ 2)- $\beta$ -D-xylopyranosyl-(1 $\rightarrow$ 2)-5-*O*-*trans*-feruloyl-L-arabinofuranose.

## 5.4. MS<sup>2</sup> fragmentation of reduced standard compounds

Although quantification was performed by UV absorbance at 325 nm, MS<sup>2</sup> screening of the eluate via a linear ion-trap mass spectrometer (coupled to the DAD) was used to confirm peak identity in the chromatograms. This detail was unnecessary for analysis of pure standard compounds, but analysis of plant materials following mildly acidic TFA hydrolysis and reduction produced more complex chromatograms (**Figure 22**). The sodium adducts of the reduced standard compounds FA, FAX, and FAXG produced characteristic daughter fragments (see **Figure 44** in **Section 12.9** in the appendix). Fragmentation of the sodium adduct of reduced FA ( $[\text{M} + \text{Na}]^+$   $m/z$  351) resulted in an  $m/z$  333 daughter ion, which represents the loss of one water molecule (the sodium adduct of  $[\text{M} - 18]^+$ ). One major and one minor daughter ion arose from fragmentation of the sodium adduct of reduced FAX ( $[\text{M} + \text{Na}]^+$   $m/z$  483):  $m/z$  351, representing the sodium adduct of the ion formed upon loss of the Xyl unit, and  $m/z$  465, representing the sodium adduct of  $[\text{M} - 18]^+$  (loss of one water molecule). MS<sup>2</sup> fragmentation of the sodium adduct of reduced FAXG ( $[\text{M} + \text{Na}]^+$   $m/z$  645) produced one major daughter ion:  $m/z$  483, the sodium adduct of the ion created after loss of the Gal unit. Two minor daughter ions were also observed:  $m/z$  627, the sodium adduct of  $[\text{M} - 18]^+$  (loss of one water molecule) and  $m/z$  351, the sodium adduct of the ion formed after loss of both the Gal and Xyl units.

**Table 13. Total ester-linked ferulic acid contents of insoluble grain fibers<sup>a</sup>**

Grain	Mean ( $\mu\text{g/g}$ insoluble fiber) <sup>b</sup>	Standard deviation ( $\mu\text{g/g}$ insoluble fiber)
Barley	6895	242
Grain maize	33109	652
Intermediate wheatgrass	6672	43
Kamut	6141	105
Long grain rice	8991	241
Oats	2294	537
Popcorn maize	30117	456
Proso millet	9840	79
Rye	6240	178
Spelt	8799	408
Wheat	6925	510
Wild rice	2426	223

<sup>a</sup> Values determined via alkaline hydrolysis (2M NaOH, 18 h)

<sup>b</sup>  $n = 3$ ; values corrected for residual protein and ash in the insoluble fiber material

amples required an SPE-C18 clean-up step following mildly acidic hydrolysis (50 mM TFA, 2 h). Without this clean-up step, many hydrolysates formed gels during reduction, which in turn exhibited strong foam-building capacities during the work-up step and rendered quantitative work very difficult. Following mildly acidic hydrolysis, SPE-C18 clean-up, reduction, and LC-DAD/MS<sup>2</sup> separation and detection, the quantitative distribution of the monomeric ferulates into unique feruloylated side-chain profiles was determined for each cereal grain. Two sample chromatograms are shown in **Figure 22**. FA was the most abundantly liberated feruloylated side-chain

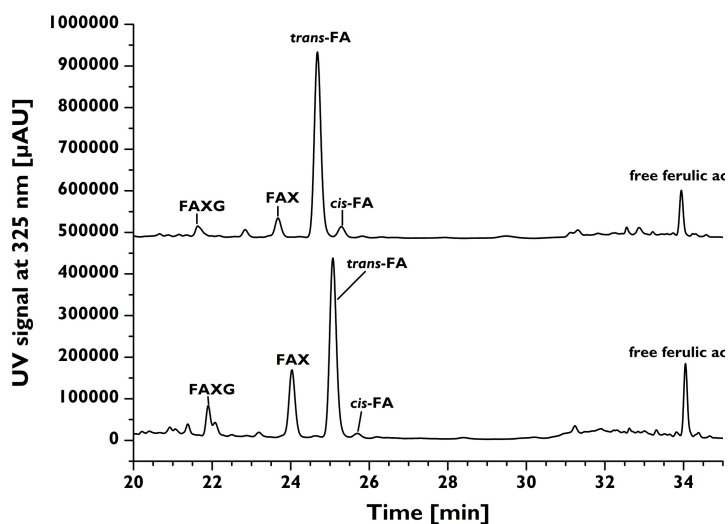


**Figure 22. Chromatographic separation of feruloylated side-chains and free ferulic acid in the TFA hydrolysates from insoluble long-grain rice (upper trace) and popcorn maize (lower trace) fibers following reduction.**

*Abbreviations used:* **FA:** 5-*O*-*trans*-feruloyl-L-arabinofuranose; **FAX:**  $\beta$ -D-xylopyranosyl-(1 $\rightarrow$ 2)-5-*O*-*trans*-feruloyl-L-arabinofuranose; **FAXG:**  $\alpha$ -L-galactopyranosyl-(1 $\rightarrow$ 2)- $\beta$ -D-xylopyranosyl-(1 $\rightarrow$ 2)-5-*O*-*trans*-feruloyl-L-arabinofuranose; **TFA:** trifluoroacetic acid.

## 5.5. Application of the chromatographic feruloylated side-chain profiling method to cereal grain materials

The contents of total esterified ferulic acid (as determined by alkaline hydrolysis with 2 M NaOH for 18 h, acidification of the hydrolysate, and extraction into organic solvent) of the insoluble fiber materials isolated from twelve cereal grains were determined and ranged from about 2.3 (oats) to 33.0 mg/g insoluble fiber (grain maize) (**Table 13**).

The developed profiling approach was applied to study the distribution of these ferulates into AX side-chains. Plant cell wall sam-

ple chain in all of the samples, with concentrations varying between 4.97 (oats) and 100.23 (grain maize)  $\mu\text{mol}$  FA/g insoluble fiber. FAX was also present in all of the sample hydrolysates, but in lower concentrations than FA (**Table 14**). MS<sup>2</sup> fragmentation of the hydrolysates and comparison of retention times with the FAXG standard compound confirmed the presence of FAXG in all twelve cereal grains screened in this study. Furthermore, this complex feruloylated side-chain could be quantified in ten out of twelve cereals (**Table 14**). Over 70% of the total monomeric ferulates as determined by alkaline hydrolysis were quantitatively captured in the respective side-chain profiles of most of the cereals, with values over

90% for several cereals (wheat, spelt, kamut, and wild rice). The values for proso millet, popcorn maize, and IWG were lower, but still above 50%. Free ferulic acid was present in all TFA hydrolysates, but its quantities were small (<10%) compared to the sum of ferulates captured with the screening method (Table 14).

**Table 14. Application of the quantitative LC-DAD/MS<sup>2</sup> feruloylated side-chain profiling method to insoluble fibers from whole grains.**

Grain	$\mu\text{moles}$ FA/g insoluble fiber <sup>a</sup>	$\mu\text{moles}$ FAX/g insoluble fiber <sup>a</sup>	$\mu\text{moles}$ FAXG/g insoluble fiber <sup>a</sup>	$\mu\text{moles}$ free ferulic acid released in TFA hydrolysis/g insoluble fiber <sup>a</sup>	FA:FAX ratio	sum of ferulates quantified in side-chain profiling method ( $\mu\text{mol/g}$ corrected insoluble fiber) <sup>a</sup>	% of total ferulates quantified in side-chain profiling method <sup>b</sup>
Barley	23.74 $\pm$ 4.04	2.10 $\pm$ 0.41	— <sup>c</sup>	2.29 $\pm$ 0.58	11.36	28.13 $\pm$ 5.04	78.91 $\pm$ 11.19
Grain maize	100.23 $\pm$ 2.75	12.70 $\pm$ 0.73	3.78 $\pm$ 0.28	9.86 $\pm$ 1.20	7.90	126.57 $\pm$ 4.89	74.27 $\pm$ 3.56
Intermediate wheatgrass	20.27 $\pm$ 3.77	0.47 $\pm$ 0.05	0.14 $\pm$ 0.004	1.29 $\pm$ 0.36	42.45	22.18 $\pm$ 4.15	64.57 $\pm$ 12.26
Kamut	26.78 $\pm$ 0.91	0.87 $\pm$ 0.07	0.21 $\pm$ 0.01	2.46 $\pm$ 0.15	30.88	30.32 $\pm$ 1.03	95.97 $\pm$ 5.28
Long grain rice	27.58 $\pm$ 4.10	2.21 $\pm$ 0.24	0.71 $\pm$ 0.03	1.66 $\pm$ 0.56	12.45	32.16 $\pm$ 4.91	69.30 $\pm$ 8.42
Oats	4.97 $\pm$ 1.61	1.10 $\pm$ 0.41	— <sup>c</sup>	— <sup>d</sup>	4.58	6.06 $\pm$ 2.02	50.85 $\pm$ 5.87
Popcorn maize	56.75 $\pm$ 10.20	20.05 $\pm$ 3.51	4.70 $\pm$ 0.79	6.54 $\pm$ 2.00	2.83	88.07 $\pm$ 16.25	56.92 $\pm$ 11.37
Proso millet	26.82 $\pm$ 1.55	1.25 $\pm$ 0.05	0.25 $\pm$ 0.005	0.75 $\pm$ 0.14	21.47	29.07 $\pm$ 1.70	57.35 $\pm$ 2.80
Rye	21.59 $\pm$ 6.30	1.11 $\pm$ 0.25	0.15 $\pm$ 0.03	1.84 $\pm$ 0.66	19.26	24.69 $\pm$ 7.23	76.67 $\pm$ 21.39
Spelt	38.17 $\pm$ 3.18	0.99 $\pm$ 0.06	0.17 $\pm$ 0.02	3.09 $\pm$ 0.43	38.62	42.43 $\pm$ 3.63	94.00 $\pm$ 11.87
Wheat	29.82 $\pm$ 1.47	0.72 $\pm$ 0.09	0.18 $\pm$ 0.008	2.43 $\pm$ 0.23	41.55	33.14 $\pm$ 1.69	93.61 $\pm$ 11.98
Wild rice	9.47 $\pm$ 1.16 <sup>e</sup>	2.39 $\pm$ 0.51 <sup>e</sup>	0.64 $\pm$ 0.08 <sup>e</sup>	— <sup>d</sup>	4.47	12.20 $\pm$ 1.55 <sup>e</sup>	91.86 $\pm$ 13.12

<sup>a</sup> Average  $\pm$  standard deviation from triplicate determinations, except where indicated. Values corrected for protein and ash.

<sup>b</sup> [(Sum of ferulates quantified from TFA hydrolysis / total ferulates as determined by alkaline hydrolysis)  $\times$  100]  $\pm$  standard deviation.

<sup>c</sup> Detected, but could not be quantified due to co-elution with a matrix component.

<sup>d</sup> Detected, but not quantified due to low concentration

<sup>e</sup> n = 2

Abbreviations used: FA: 5-O-trans-feruloyl-L-arabinofuranose; FAX:  $\beta$ -D-xylopyranosyl-(1 $\rightarrow$ 2)-5-O-trans-feruloyl-L-arabinofuranose; FAXG:  $\alpha$ -L-galactopyranosyl-(1 $\rightarrow$ 2)- $\beta$ -D-xylopyranosyl-(1 $\rightarrow$ 2)-5-O-trans-feruloyl-L-arabinofuranose; LC-DAD-MS<sup>2</sup>: Liquid chromatography coupled with a diode array detector and tandem mass spectrometry; TFA: trifluoroacetic acid.

## 5.6. Method limitations

Incomplete liberation of feruloylated AX side-chains is the major shortcoming of this approach. Enzymatic approaches are inappropriate because the studied structural elements hinder

enzymatic cleavage. Chemical approaches are often only semi-specific and need to be optimized for liberation versus destruction of specific building blocks of polymers. The mildly acidic hydrolysis method applied in this study was optimized earlier by Saulnier et al. (1995c) for semi-specific release of feruloylated AX side-chains and capitalizes on the greater acid lability of furanosidic compared to pyranosidic linkages. The recommended hydrolysis conditions (50 mM TFA, 100 °C, 2 h), which were used in this study, simultaneously balance the maximized cleavage of Araf-based side-chains with minimal degradation of ferulate ester bonds. However, the non-esterified ferulic acid detected in the hydrolysates (**Table 14**) is clearly a hydrolysis artefact, because any free ferulic acid naturally occurring in the plant materials is removed by washing steps at the end of the insoluble fiber isolation. Although the method is not quantitative in the absolute sense (the reported side-chain concentrations should not be construed as the absolute total in the material, but rather the portion released under the hydrolysis conditions), the method offers the possibility for a quantitative comparison of feruloylated side-chain profiles in different cell wall materials.

### 5.7. Cereal grains possess unique feruloylated side-chain profiles

As expected, feruloylated side-chain contents mirrored the total ferulate (alkaline hydrolysis) data: grains with higher total ferulate levels (for example, popcorn maize and grain maize) showed the highest concentration of feruloylated side-chains and grains with lower total ferulate contents (such as oats and wild rice) produced the lowest concentration of ferulate-bearing side-chains. Interestingly, however, total feruloylated side-chain concentration did not predict the side-chain profile complexity, as determined by the FA:FAX ratio. For example, although oats had the lowest total feruloylated side-chain concentration of the twelve grains screened in this study, they had the third-lowest FA:FAX ratio (demonstrating that larger portions of their ferulates are involved in more complex side-chains), being topped only by wild rice and popcorn maize. The simplest side-chain profile was produced by IWG (FA:FAX ratio over 42), which confirmed the simple feruloylated side-chains pattern predicted by the qualitative screening of IWG's AX described earlier in this work. The three tested *Triticum* species (wheat, spelt, and kamut) had similar profiles to each other and low levels of side-chain complexity (FA:FAX ratios between 30 and 40). The amount of total monomeric ferulates captured in their side-chain profiles was over 90%, which indicates that nearly all of the monomeric ferulates in these species are bound to AX in the form of the simplest possible feruloylated side-chain, FA. The FA:FAX ratio of 2.83 from popcorn maize, on the other hand, represents a high level of side-chain complexity: every third feruloylated side-chain substituent in popcorn AX is FAX. Compared to popcorn maize, grain maize had a larger concentration of total side-chains, but a simpler complexity profile. Barley and long grain rice produced similar profiles, with moderate levels of both FA and FAX. As already mentioned, oats, but also wild rice, had the surprising combination of low absolute total side-chain levels and high relative values of side-chain complexity. Another surprising result of our screening was the discovery of low levels of FAXG, which had previously only been described in maize (Allerdings et al., 2006), in all tested cereals. Although maize grain cell walls clearly have larger sheer FAXG quantities than other cereals, FAXG biosynthesis in grain cell walls seems to be ubiquitous within the Poaceae family.

The side-chain profiling method quantified less than 70% of the total ester-linked monomeric ferulate populations for IWG, oats, popcorn maize, and proso millet. It is possible that biosynthesis in these cereals directs a greater portion of alkali-hydrolysable monomeric

ferulates into other structural depots resistant to the mild TFA hydrolysis conditions in this study, such as ester-linked to lignin or other polyphenolic or polyaliphatic compounds such as suberin-type polymers. 2D-NMR analysis of the TFA hydrolysis-resistant residues could be a tool to investigate this possibility.

## 6. Results and Discussion: *Chapter Three*

---

### *Quantitative profiling of feruloylated side-chains in cereal arabinoxylans using HSQC-NMR*

The LC-DAD/MS<sup>2</sup> feruloylated side-chains screening method described in the previous results chapter illustrates the power of the side-chain screening approach for quantitatively describing and comparing feruloylated side-chain profiles in cereal grain materials. One weakness of the LC-based approach, however, is the need to reduce the released side-chain compounds to sugar alcohols before analysis. The developed reduction method is accurate and reproducible, but requires operator practice to achieve good results and is time-consuming to perform. We therefore developed an alternative quantitative profiling method to eliminate the reduction step.

NMR has been used to quantitatively rank different structural elements in AX. Many reports use <sup>1</sup>H-NMR (Viëtor et al., 1994a), but signal overlap presents a challenge for some samples (Hoffmann et al., 1992). 2D-NMR techniques provide increased resolution by dispersing signals from a potentially crowded proton dimension ( $f_2$ ) into a second dimension ( $f_1$ ). Both homonuclear (both the  $f_1$  and  $f_2$  dimensions are in the proton scale) and heteronuclear methods (the  $f_1$  dimension is based on couplings to the nucleus of another NMR-active atom, such as <sup>13</sup>C, <sup>15</sup>N, or <sup>31</sup>P) are possible. We chose to develop a semi-quantitative HSQC method based on the increased chemical shift dispersion of <sup>13</sup>C-based heteronuclear methods. HSQC, which shows couplings between a <sup>1</sup>H nucleus vs. the nucleus of the carbon to which the proton is directly bonded, has been used qualitatively for structural characterization for decades. HSQC cross-peak intensities are influenced by several factors, including variations in <sup>13</sup>C-<sup>1</sup>H coupling constants ( $^1J_{C,H}$ ), differing polarization transfer efficiency, and relaxation time ( $T_1$  and  $T_2$ ) differences. However, external or internal calibration corrects for these potential differences and permits quantitative work.

#### **6.1. Method development**

Several key parameters were optimized, in particular choice of NMR solvent, internal standard, quantification cross-peaks, and measurement time. D<sub>2</sub>O was tested and rejected as a potential solvent because spontaneous cleavage of some of the ester linkages in the feruloylated side-chain standard compounds was observed (**Figure 23**). No direct cause for the degradation could be determined, but its onset was rapid (within hours of dissolving the dried standard compounds) and its extent increased in proportion to the amount of time the sample remained in solution. In contrast, feruloylated standard compounds dissolved in DMSO-*d*<sub>6</sub> were stable over long periods of time (the longest tested storage time was four weeks). Individual HSQC-spectra of the three standard compounds in DMSO-*d*<sub>6</sub> are provided in **Figures 45-47** in **Section 12.8** in the appendix.

Requirements for a suitable internal standard compound included the presence of clear, easily-integrated cross-peaks which did not overlap with the signals from the feruloylated side-chain standard compounds. Additionally, the internal standard compound must be soluble in

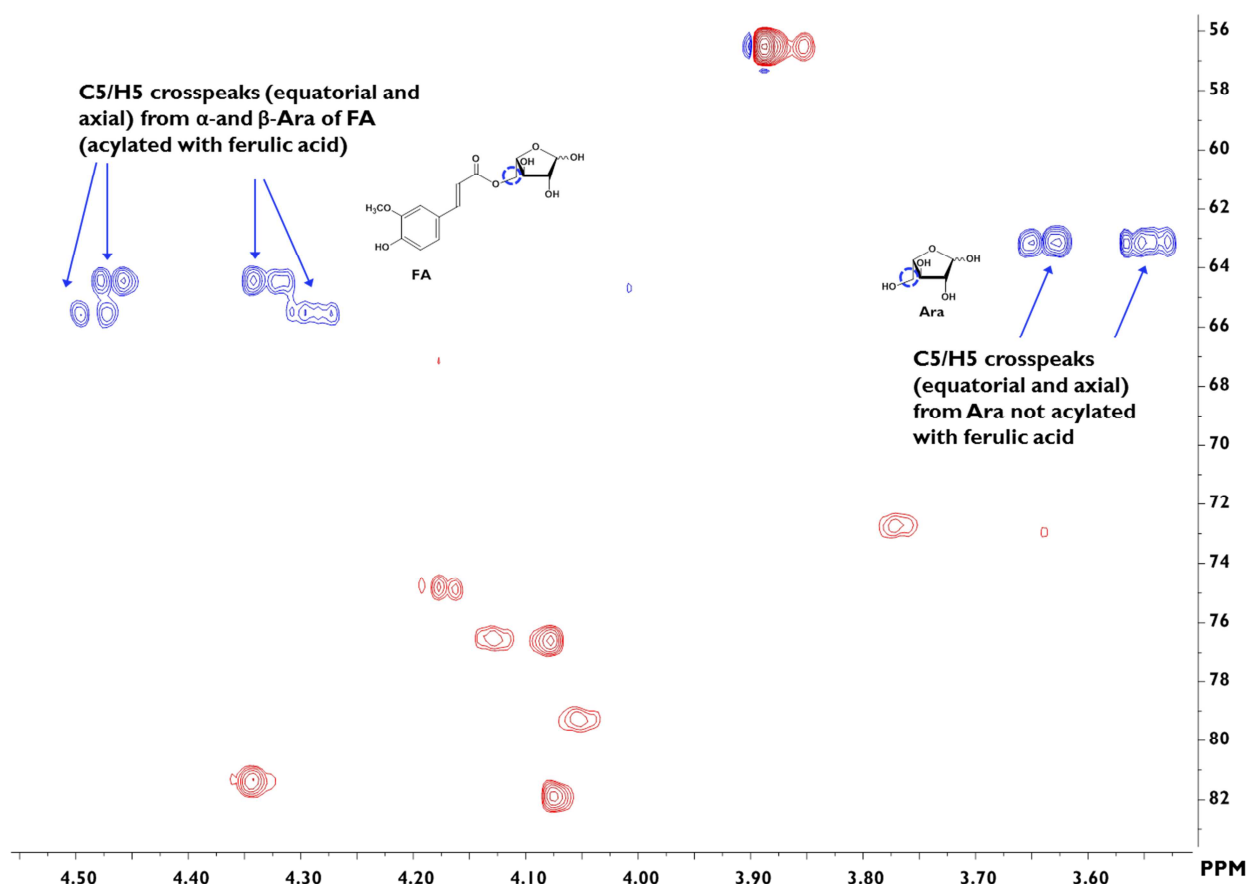


**Figure 23.** HSQC-NMR spectrum showing degradation of the feruloylated standard compound FA in D<sub>2</sub>O.

Abbreviations used: **Ara**: arabinose; **FA**: 5-*O*-*trans*-feruloyl-L-arabinofuranose; **HSQC**: heteronuclear single quantum coherence spectroscopy; **NMR**: nuclear magnetic resonance.

DMSO, must not react with the feruloylated side-chain compounds, and preferably, be a solid at room temperature to facilitate weighing in of exact amounts. Caffeine fulfilled all of these requirements and was therefore chosen as the internal standard compound. The most downfield methyl cross-peak signal was chosen for volume integration in all samples, and the ratios of the chosen sample signal volumes to the internal standard signal volume were determined and used for calibration and quantification.

For simultaneous quantification of the individual feruloylated side-chain compounds in the same NMR tube, compound-specific cross-peak signals were selected for integration and

**Table 15.** HSQC cross-peak signals selected for quantification.

Standard compound and selected cross-peak signal	Chemical shifts of quantification signals in DMSO- <i>d</i> <sub>6</sub> <sup>a</sup>			
	H (from $\alpha$ -monomer compound)	C (from $\alpha$ -monomer compound)	H (from $\beta$ -monomer compound)	C (from $\beta$ -monomer compound)
FA Ara C2/H2	3.76	82.4	3.71	76.5
FAX Ara C2/H2	3.93	89.3	3.85 <sup>b</sup>	83.0 <sup>b</sup>
FAXG Gal C5/H5	3.90	71.0	4.02 <sup>b</sup>	71.0 <sup>b</sup>

<sup>a</sup>Spectra were calibrated against residual DMSO signal (<sup>1</sup>H = 2.50 ppm; <sup>13</sup>C = 39.52 ppm).

<sup>b</sup>Calibration curves for FAX and FAXG were prepared using only the cross-peaks from the  $\alpha$ -monomer compound.

Abbreviations used: **FA**: 5-*O*-*trans*-feruloyl-L-arabinofuranose; **FAX**:  $\beta$ -D-xylopyranosyl-(1 $\rightarrow$ 2)-5-*O*-*trans*-feruloyl-L-arabinofuranose; **FAXG**:  $\alpha$ -L-galactopyranosyl-(1 $\rightarrow$ 2)- $\beta$ -D-xylopyranosyl-(1 $\rightarrow$ 2)-5-*O*-*trans*-feruloyl-L-arabinofuranose; **HSQC**: heteronuclear single quantum coherence spectroscopy; **NMR**: nuclear magnetic resonance.

calibration (**Table 15, Figure 24**). The cross-peaks for H2/C2 of the Ara<sub>f</sub> in FA were chosen because the signals were easily differentiated from cross-peaks from the more complex side-chains. Importantly, because these compounds are

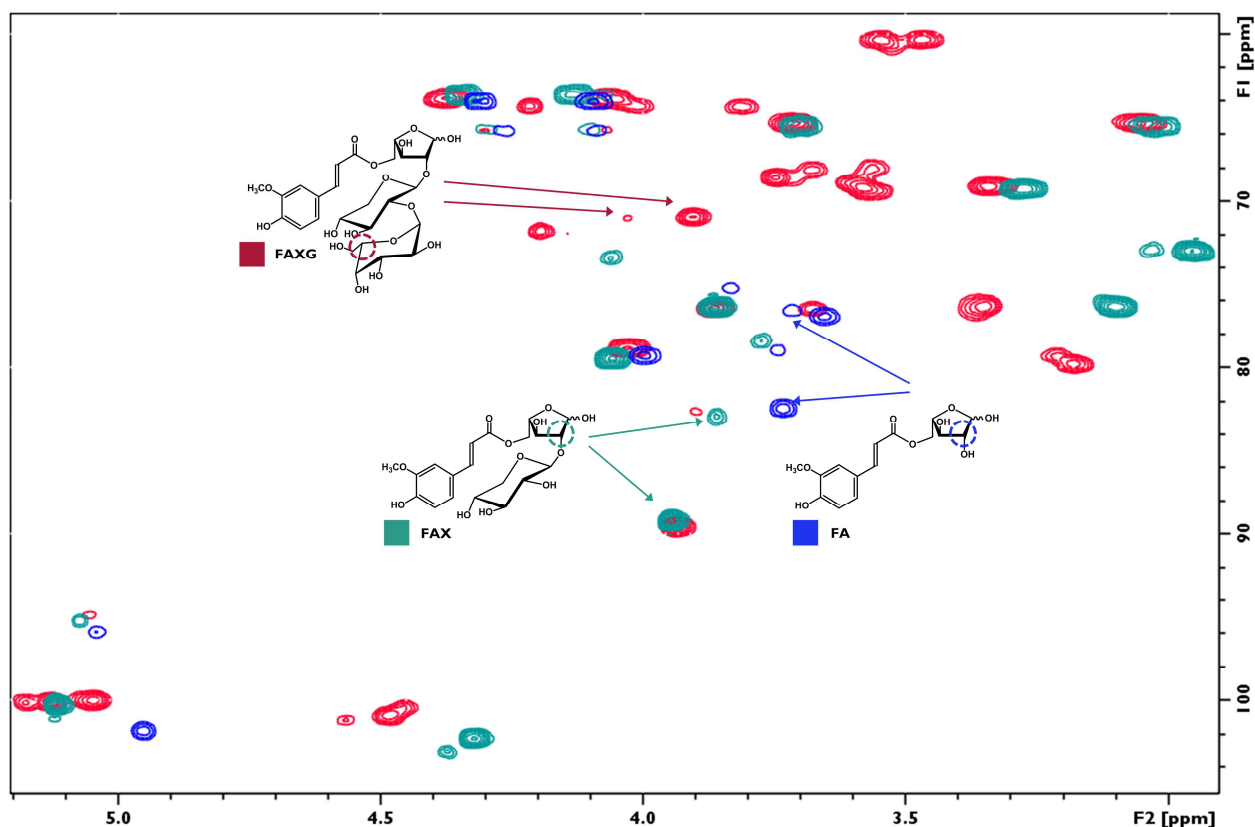


**Figure 24. Overlaid HSQC-NMR spectra of FA, FAX, and FAXG showing selected cross-peaks\* for quantification.** Spectra were measured in DMSO-*d*<sub>6</sub> and calibrated against residual DMSO signal (<sup>1</sup>H = 2.50 ppm; <sup>13</sup>C = 39.52 ppm). \*Note: Only the signals corresponding to the  $\alpha$ -monomer compound were integrated for the FAX and FAXG calibration curves.

Abbreviations used: **FA**: 5-*O*-*trans*-feruloyl-L-arabinofuranose; **FAX**:  $\beta$ -D-xylopyranosyl-(1 $\rightarrow$ 2)-5-*O*-*trans*-feruloyl-L-arabinofuranose; **FAXG**:  $\alpha$ -L-galactopyranosyl-(1 $\rightarrow$ 2)- $\beta$ -D-xylopyranosyl-(1 $\rightarrow$ 2)-5-*O*-*trans*-feruloyl-L-arabinofuranose; **HSQC**: heteronuclear single quantum coherence spectroscopy; **NMR**: nuclear magnetic resonance.

found in solution in equilibrium between their  $\alpha$ - and  $\beta$ - anomers, and the chemical shifts of other carbons and protons in the molecule are affected by the anomeric position, two unique signals are observed for this cross-peak from the  $\alpha$ - and  $\beta$ -anomers of FA. The average equilibrium percent ratios between the  $\alpha$ - and  $\beta$ -anomers of FA was 76:24, but ranged from 73:27 to 87:13. Therefore, because the equilibrium ratio is not constant between samples, more accurate results will be obtained by the sum volume integral of the two cross-peaks than by integrating only the cross-peak of the  $\alpha$ -anomer.

FAX was also quantified via its H2/C2 cross-peak of Araf, which is substantially downfield-shifted in the carbon dimension compared to FA (**Table 15**). The Araf H2/C2 cross-peak of FAXG directly overlaps, so integration of this signal represents the sum of FAX, FAXG, and likely, any more complex side-chains (such as FAXGX or FAXGG; see **Figure 6** in **Chapter 1.2.1.4** for structures). FAXG is specifically quantified via its H5/C5 cross-peak of  $\alpha$ -galactose (**Table 15**); this value is subtracted from the sum value of FAX + FAXG to obtain the concentration of FAX. Separate quantification of FAX and FAXG via their respective Xylp anomers is easily performed in mixtures of FAX and FAXG standard compounds. This is, however, impossible in plant hydrolysates, which always include some feruloylated (and acetylated) oligosaccharides containing fragments of the xylan backbone. The anomeric cross-peaks from these backbone Xylp moieties overlap with the side-chain Xylp cross-peaks.

Importantly, just as in the case of FA, the chemical shifts of the cross-peaks chosen as quantification signals for FAX and FAXG differ slightly depending on whether the reducing Ara<sup>f</sup> in the molecule is in the  $\alpha$ - and  $\beta$ -anomeric configuration. However, because FAX and FAXG levels are quite low in many plant samples, only the quantification signals corresponding to the  $\alpha$ -anomer were detected in many hydrolysates at the beginning of method development. Therefore, the calibration curves for FAX and FAXG were prepared using only the integrals from the  $\alpha$ -anomer cross-peak signals.

The final key method parameter choice was the number of measurement scans. Because we wanted to keep the method accessible as a routine-screening method, it was important to balance method sensitivity with a realistic total measurement time. We chose 20 scans, which resulted in a measurement time of  $\approx 2.25$  h but permitted quantification of both FAX and FA in the hydrolysates resulting from 200 mg or less of cereal fibers, as the best compromise between measurement speed and sensitivity.

## 6.2. Method validation

The linear calibration curve (in triplicate) for FA is shown in **Figure 25A**. Linearity was assessed by inspecting the residual plot (**Figure 25B**) and correlation coefficient (**Table 16**). The LOD and LOQ were calculated from the calibration curve according to the DIN 32645 guidelines (2008).

The triplicate linear calibration curves and residual plots for FAX and FAXG are shown in **Figures 25C-F**. Compared to the calibration curve for FA, which was prepared using the sum integral of the quantification cross-peaks representing the  $\alpha$ - and  $\beta$ -anomers, the linear relationships of the FAX and FAXG calibration curves are much weaker (**Table 16**). The weaker linearity of the concentration: signal volume relationship is due to the variability in the  $\alpha$ : $\beta$  anomer ratios of these compounds. This was shown by preparing a separate calibration curve using the ferulate methoxy cross-peak from these same measurements instead of the quantification cross-peaks for FAX and FAXG.

**Table 16. Calibration equations<sup>a</sup>, correlation coefficients, limits of detection (LOD), and limits of quantification (LOQ) for FA, FAX, and FAXG using HSQC-NMR detection.**

	range tested ( $\mu\text{M}$ )	linear calibration equation	correlation coefficients	LOD ( $\mu\text{M}$ )	LOQ ( $\mu\text{M}$ )
FA	470–2400	$y = 94872x - 0.0101$	0.9829	252	837
FAX	120–440	$y = 102034x - 0.0044$	0.8578	75	197
FAXG	120–350	$y = 110243x - 0.0076$	0.7165	99	224

<sup>a</sup> Calibration equations and correlation coefficients calculated from three separate calibrations.

*Abbreviations used:* **FA:** 5-*O*-*trans*-feruloyl-L-arabinofuranose; **FAX:**  $\beta$ -D-xylopyranosyl-(1 $\rightarrow$ 2)-5-*O*-*trans*-feruloyl-L-arabinofuranose; **FAXG:**  $\alpha$ -L-galactopyranosyl-(1 $\rightarrow$ 2)- $\beta$ -D-xylopyranosyl-(1 $\rightarrow$ 2)-5-*O*-*trans*-feruloyl-L-arabinofuranose; **HSQC:** heteronuclear single quantum coherence spectroscopy; **NMR:** nuclear magnetic resonance.

These calibration curves, which were not affected by the  $\alpha$ : $\beta$  anomer ratios in the various samples have a much stronger linear relationship, showing that the samples were pipetted and handled correctly. The FAX and FAXG sample concentrations determined using the calibration curves containing only the volume integral of the cross-peak corresponding to the  $\alpha$ -anomer must, based on the limited linearity of these calibration curves, be treated as semi-quantitative results. An excellent recovery rate (103%) for the method was exemplified by subjecting standard solutions of FA to the sample preparation procedure beginning at SPE-clean-up.

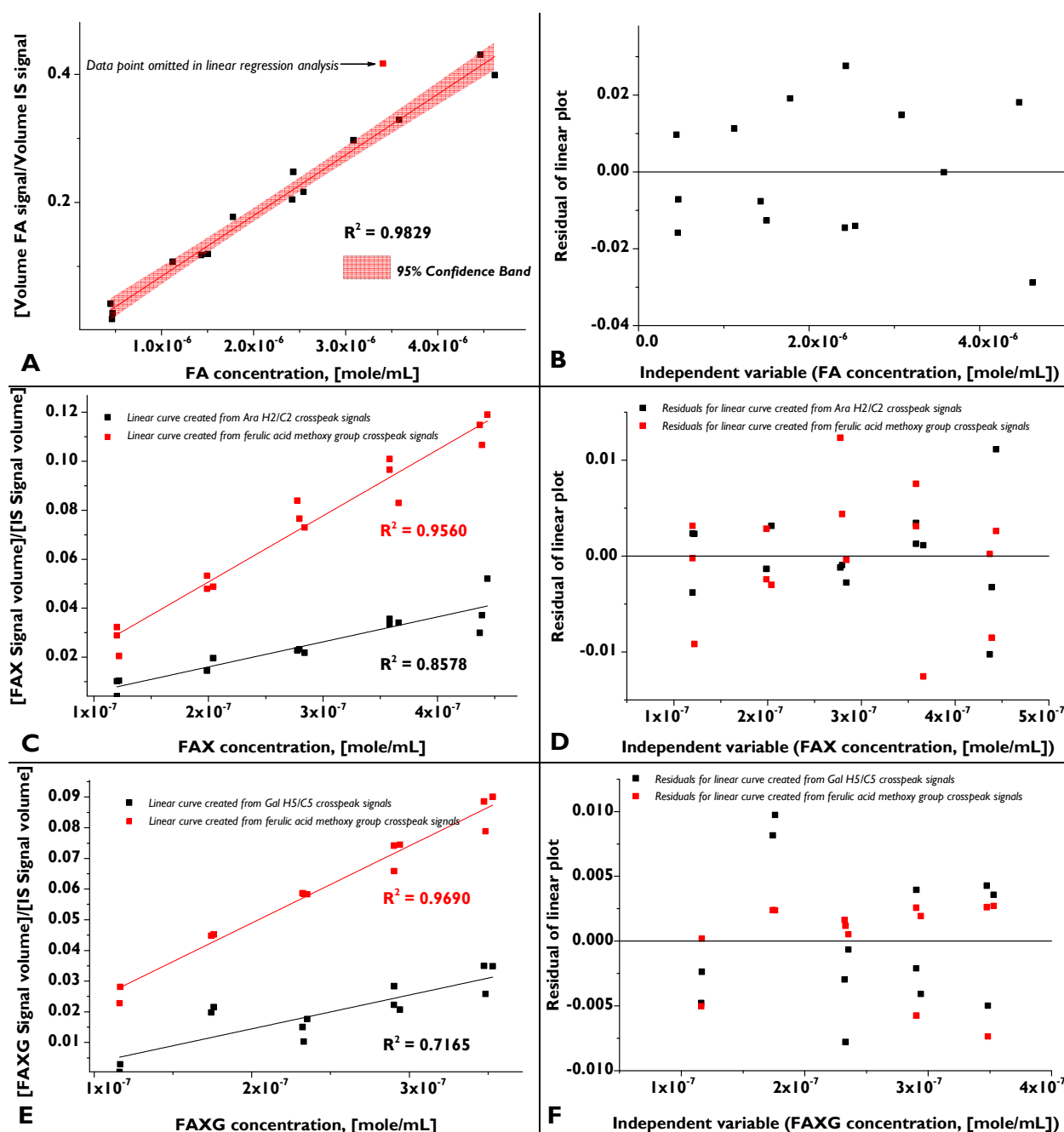


**Figure 25. Linear calibration curves (in triplicate) and corresponding residual plots of feruloylated side-chain standard compounds following volume integration of selected HSQC cross-peaks. [A]:** Linear calibration curve for FA. **[B]:** Residual plot for FA calibration curve. **[C]:** Linear calibration curve for FAX (black) created from the quantification cross-peak signal and the curve created from the ferulate methoxy cross-peak signal (red). **[D]:** Residual plots for FAX calibration curve (black) created from the quantification cross-peak signal and for the curve created from the ferulate methoxy cross-peak signal (red). **[E]:** Linear calibration curve for FAXG (black) created from the quantification cross-peak signal and the curve created from the ferulate methoxy cross-peak signals (red). **[F]:** Residual plots for FAXG calibration curve (black) created from the quantification cross-peak signal and for the curve created from the ferulate methoxy cross-peak signal (red).

*Abbreviations used:* **FA:** 5-*O*-*trans*-feruloyl-L-arabinofuranose; **FAX:**  $\beta$ -D-xylopyranosyl-(1 $\rightarrow$ 2)-5-*O*-*trans*-feruloyl-L-arabinofuranose; **FAXG:**  $\alpha$ -L-galactopyranosyl-(1 $\rightarrow$ 2)- $\beta$ -D-xylopyranosyl-(1 $\rightarrow$ 2)-5-*O*-*trans*-feruloyl-L-arabinofuranose; **HSQC:** heteronuclear single quantum coherence spectroscopy.

### 6.3. Application of the method to cereal samples

The feruloylated side-chain profiles of popcorn, oats, wheat, and wild rice insoluble fibers were determined using the developed HSQC-NMR quantification method (Table 17). The same sample preparation was used as for the LC-based method, except that after SPE-C18 clean-up and drying down of the MeOH eluates, the samples were directly dissolved in DMSO-*d*<sub>6</sub>-caffeine solution, transferred to 5 mm NMR tubes, and measured. A sample spectrum from wild rice hydrolysate is shown in Figure 26; the spectra from the other three grain species are provided in Section 12.9 in the appendix (Figures 48-50).

FA and FAX were detected and quantified in all four cereals. FAXG was only quantified or detected in popcorn. The FA concentrations in hydrolysates resulting from ≈200 mg of insoluble popcorn and wheat fibers were outside the calibration range, so these samples were diluted by 1:20 and 1:5, respectively, and measured again. The percent of total ferulates quantified via the NMR side-chain profiling method was over 55% for oats, popcorn, and wheat. Wild rice was an exception, with only 39% of its total ferulates being captured in the side-chain profile.

**Table 17. Application of the quantitative HSQC-NMR feruloylated side-chain profiling method to insoluble fibers from whole grains.**

Grain	μmoles FA/g insoluble fiber <sup>a</sup>	μmoles FAX/g insoluble fiber <sup>a,b</sup>	μmoles FAXG/g insoluble fiber <sup>a</sup>	FA:FAX ratio	sum of ferulates quantified in side-chain profiling method (μmol/g corrected insoluble fiber) <sup>a</sup>	% of total ferulates quantified in side-chain profiling method <sup>c</sup>
Oats	5.39 ± 2.68	1.15 ± 0.15	ND	4.67	6.54 ± 2.58	56.34 ± 21.88
Popcorn maize	75.00 ± 0.10	25.33 ± 4.35	11.18 ± 0.75 <sup>d</sup>	2.05	111.51 ± 4.85	71.92 ± 3.61
Wheat	27.39 ± 5.66	1.33 ± 0.23	ND	20.53	28.73 ± 5.89	82.02 ± 24.94
Wild rice	7.21 ± 0.41	2.12 ± 0.98	ND	3.40	9.32 ± 1.33	38.97 ± 3.65

<sup>a</sup> Average ± standard deviation from triplicate determinations. All values corrected for residual protein and ash.

<sup>b</sup> FAXG values subtracted. Average ± standard deviation from triplicate determinations. All values corrected for residual protein and ash.

<sup>c</sup> [(Sum of ferulates quantified from TFA hydrolysis / total ferulates as determined by alkaline hydrolysis) × 100] ± standard deviation.

<sup>d</sup> Determined from diluted popcorn sample; concentration was between LOD and LOQ.

Abbreviations used: FA: 5-*O*-*trans*-feruloyl-L-arabinofuranose; FAX: β-D-xylopyranosyl-(1→2)-5-*O*-*trans*-feruloyl-L-arabinofuranose; FAXG: α-L-galactopyranosyl-(1→2)-β-D-xylopyranosyl-(1→2)-5-*O*-*trans*-feruloyl-L-arabinofuranose; HSQC: heteronuclear single quantum coherence spectroscopy; LOD: limit of detection; LOQ: limit of quantification; ND: not detected; NMR: nuclear magnetic resonance.

### 6.4. Comparison of the two profiling methods

Because the same batches of insoluble fiber materials were used to test both the LC- and NMR-based profiling methods for popcorn, wheat, and oats, the concentrations determined by the two methods may be directly compared for these materials (Figure 27A-B). The wild rice fiber samples used for testing the two methods were not identical and are therefore not compared. The FA concentrations for wheat and oats determined by the two methods are identical, but the FA concentration determined for popcorn was higher using the NMR method than the LC-based method. This aberration is likely caused by the detection and quantification of all feruloylated oligosaccharides containing the FA moiety attached to a backbone remnant. In

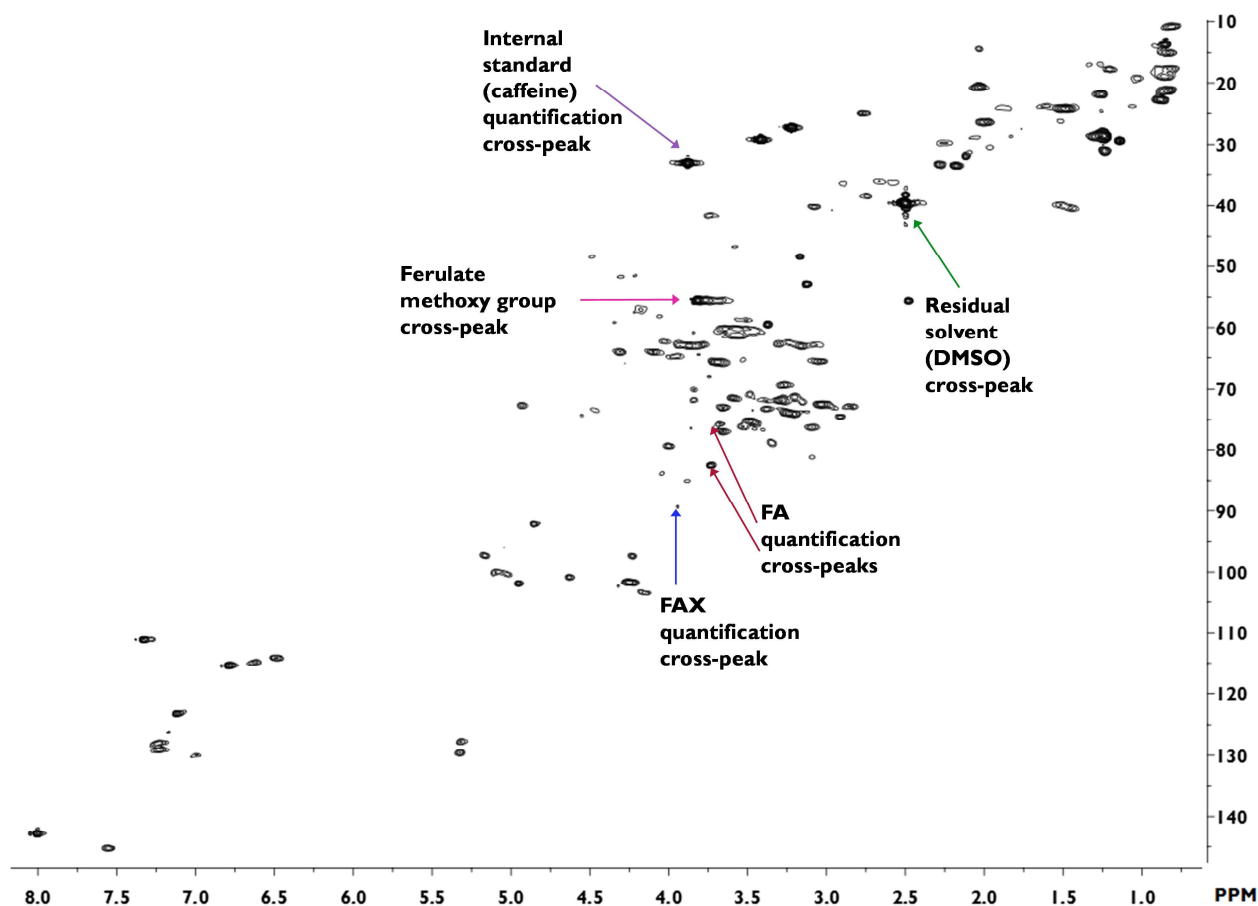


**Figure 26.** HSQC-NMR spectrum of wild rice hydrolysate. Spectra were measured in DMSO-*d*<sub>6</sub> and calibrated against the residual DMSO signal (<sup>1</sup>H = 2.50 ppm; <sup>13</sup>C = 39.52 ppm).

*Abbreviations used:* **DMSO**: dimethyl sulfoxide; **FA**: 5-*O*-*trans*-feruloyl-L-arabinofuranose; **FAX**: β-D-xylopyranosyl-(1→2)-5-*O*-*trans*-feruloyl-L-arabinofuranose; **FAXG**: α-L-galactopyranosyl-(1→2)-β-D-xylopyranosyl-(1→2)-5-*O*-*trans*-feruloyl-L-arabino-furanose; **HSQC**: heteronuclear single quantum coherence spectroscopy; **NMR**: nuclear magnetic resonance.

the LC-based remnant, these compounds are chromatographically separated, and the FA moieties contained in them remain undetermined. In contrast, with the NMR-based method, these FA moieties are quantified. In samples that contain high levels of FA (such as popcorn), the minor fraction of backbone-containing oligosaccharides is large enough to be noticeable.

A comparison of the FAX levels determined by the two methods is provided in **Figure 27B**. Here it is important to note that popcorn was the only of these three samples which contained detectable amounts of FAXG, which was quantified and subtracted from the FAX value determined via NMR. Therefore, for oats and wheat, the NMR values for FAX are inflated by FAXG. This is especially apparent in the FA:FAX ratio for wheat from the NMR data (20.53), which is much higher than the value determined by the LC-based method (41.55). Because the FAX level in wheat is so low, even small amounts of inflation by FAXG will skew this parameter. Therefore, it will be more meaningful to discuss an FA: [more complex side-chains] ratio rather than focusing specifically on the FA:FAX ratio. Additionally, it must be remembered that the FAX data from the NMR method are only semi-quantitative due to the margin of error in their linear calibration curve.

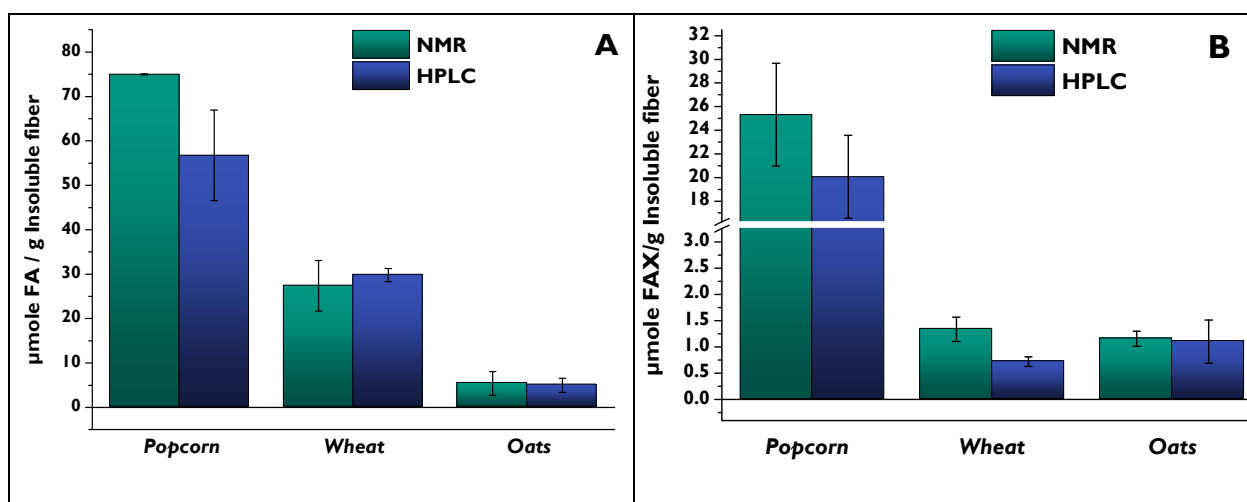


**Figure 27. Comparison of quantities of feruloylated side-chain compounds determined from identical insoluble fiber lots of whole cereal grains using the two quantification methods developed in this work. [A]: FA; [B]: FAX. Values represent the average  $\pm$  standard deviation from triplicate determinations.**

*Abbreviations used:* **FA:** 5-*O*-*trans*-feruloyl-L-arabinofuranose; **FAX:**  $\beta$ -D-xylopyranosyl-(1 $\rightarrow$ 2)-5-*O*-*trans*-feruloyl-L-arabinofuranose; **HPLC:** high-performance liquid chromatography; **NMR:** nuclear magnetic spectroscopy.

Overall, the two methods provide comparable data. Because the NMR method is less sensitive than the LC method, we were only able to detect and quantify FAXG in popcorn. However, FA and FAX were easily quantified in all samples without prior reduction or chromatography. Both methods offer the ability to quantitatively compare the feruloylated side-chains profile in plant cell wall samples. The choice between the NMR and LC-based methods depend on which instruments are available to the analyst and also the sample quantities. The increased sensitivity of the LC-based method compared to the NMR method makes it the better choice for limited sample quantities, whereas the time savings offered by the NMR method make it attractive for samples with sufficient starting material.

## 7. Results and Discussion: *Chapter Four*

### *Isolation and identification of $\alpha$ -D-xylopyranosyl-(1 $\rightarrow$ 3)-L-arabinose as a non-feruloylated oligomeric side-chain in cereal arabinoxylans*

Whereas feruloylated side-chain oligosaccharide substituents are now recognized as a distinctive feature of cereal grains' AX, less is known about the potential non-feruloylated oligosaccharide side-chain substituents. Definitive confirmation of the presence of these structures within cereal AX demands isolation and characterization of such structural units from material which has not been exposed to alkaline conditions. Alkaline conditions cleave the ester linkage between the ferulate and glycosidic moieties in feruloylated side-chains, producing non-feruloylated oligosaccharide side-chains which are only artefacts of the alkaline conditions.

In addition to its presence in FAX and other feruloylated side-chains, Araf substituted in its *O*-2 position was found as part of arabinobiose side-chains substituting the xylan backbone of sorghum grain (Verbruggen et al., 1998) and switchgrass biomass (Mazumder and York, 2010). A non-feruloylated  $\beta$ -D-xylopyranosyl-(1 $\rightarrow$ 2)-L-arabinofuranose side-chain has been reported in oat spelts, corn cobs, barley husks, rice husks, wheat straw, and switchgrass (Figure 28) (Ebringerová et al., 1992; Höjje et al., 2006; Pastell et al., 2009; Bowman et al., 2014; Bowman et al., 2015). Unfortunately, the AX materials used in these studies were extracted under alkaline conditions, and it is impossible to rule out that the Araf may have been feruloylated in the native material. Nevertheless, it is now widely assumed in the literature that cereal AX are, first, substituted with non-feruloylated oligosaccharide side-chain substituents, and, second, that the structural details of these components mirror their feruloylated counterparts. To test this assumption, we isolated and characterized the non-feruloylated disaccharide side-chains from maize AX.

#### 7.1. Release and isolation of non-feruloylated arabinoxylan side-chains

Insoluble maize fiber was hydrolyzed under mildly acidic conditions (50 mM TFA,

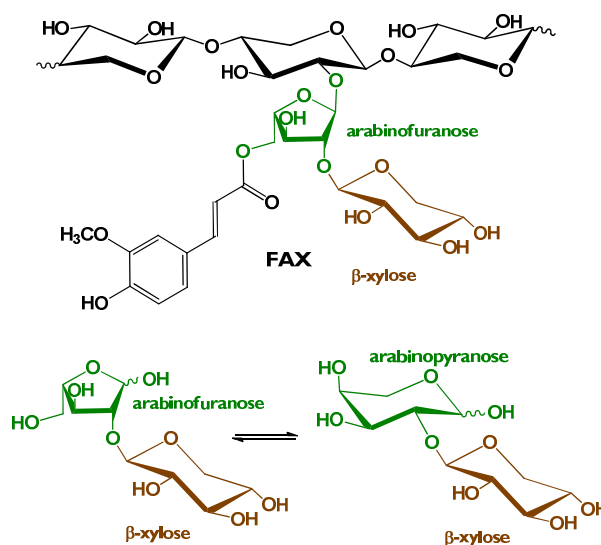
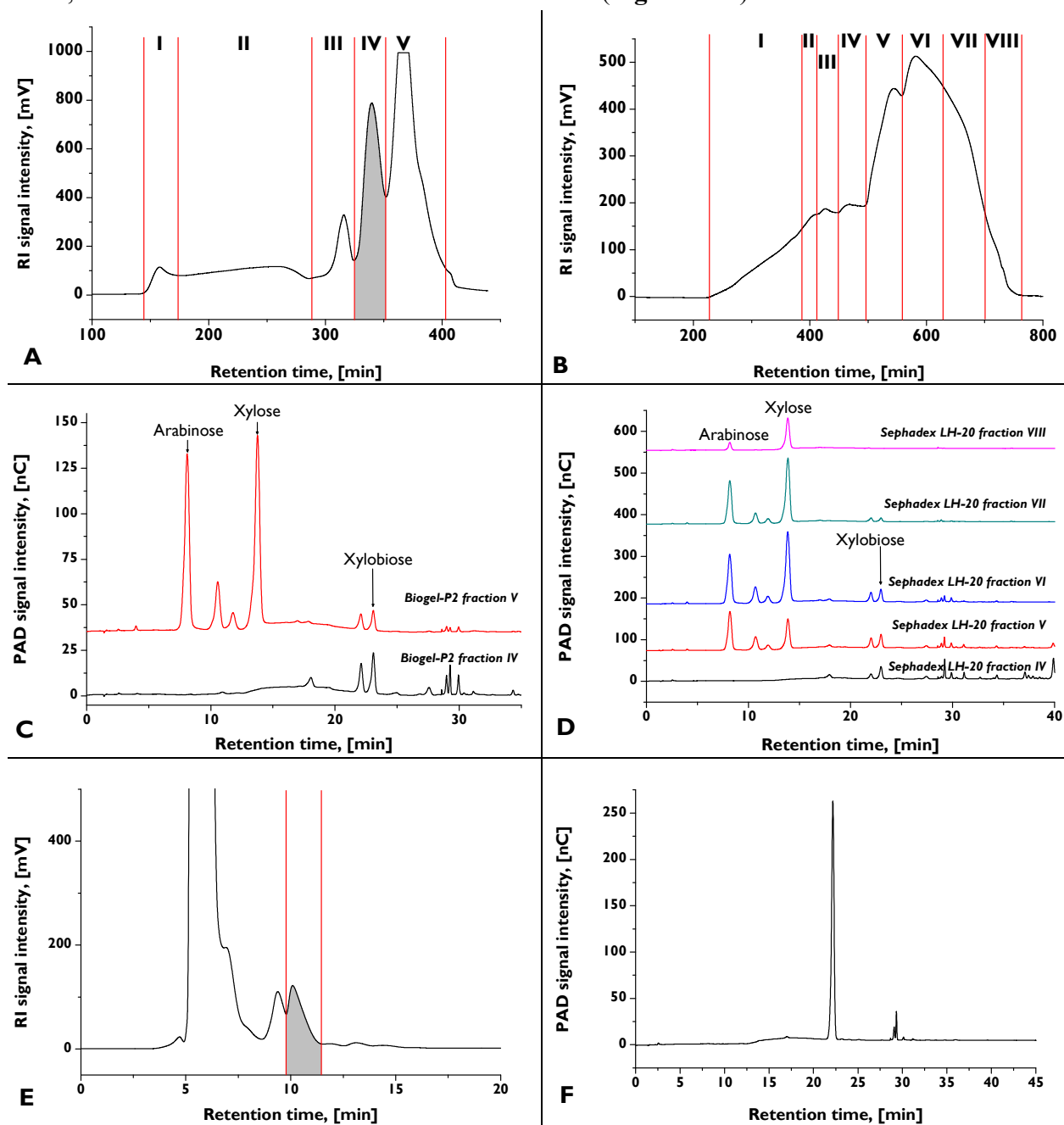


Figure 28. Feruloylated arabinoxylan side-chain structure (top, FAX attached to xylan backbone) and structures of comparable non-feruloylated disaccharide side-chains isolated from alkali-extracted materials (bottom). Upon release from the xylan backbone, the resulting equilibrium between arabinofuranose and arabinopyranose in the non-feruloylated side-chain will favor the pyranose configuration. Abbreviations used: FAX:  $\beta$ -D-xylopyranosyl-(1 $\rightarrow$ 2)-5-*O*-*trans*-feruloyl-L-arabinofuranose.

100°C, 3 h) which semi-specifically cleave the glycosidic linkages of furanoses (Saulnier et al., 1995c) and release AX side-chains. Non-feruloylated and feruloylated saccharides were separated on an Amberlite XAD-2 column; non-feruloylated oligosaccharides were eluted with pure water. Aliquots ( $\approx 700$  mg) were preparatively separated on a Bio-Gel P-2 column with pure water, and the eluate was monitored with RI detection (**Figure 29A**).



**Figure 29. Separation and purification of non-feruloylated oligosaccharides isolated from maize fiber.** [A]: Preparative separation of the aqueous Amberlite XAD-2 eluate with Bio-Gel P-2 gel chromatography (RI detection); [B]: Preparative separation of the aqueous Amberlite XAD-2 eluate with Sephadex LH-20 gel chromatography (RI detection); [C-D]: HPAEC separation (PAD detection) of aliquots of individual fractions arising from Bio-Gel P-2 [C] and Sephadex LH-20 [D] separation, showing the cleaner separation of monosaccharides and oligosaccharides of the Bio-Gel P-2 material; [E]: Semi-preparative separation of Fraction IV from the Bio-Gel P-2 separation using a chilled RP-HPLC-C18 column and pure water; [F]: HPAEC-PAD separation and detection of an aliquot of the marked fraction from [E], showing it consists of a pure compound.

Abbreviations used: **HPAEC**: high-performance anion-exchange chromatography; **PAD**: pulsed amperometric detection; **RI**: refractive-index; **RP-HPLC**: reversed-phase high-performance liquid chromatography.

Preparative Sephadex LH-20 chromatography was also tested as an alternative separation method (**Figure 29B**; pure water was used as eluent). Although the separation range was broader with Sephadex LH-20 material, a cleaner separation of monosaccharides from disaccharides was achieved with the Bio-Gel P-2 material (**Figures 29C-D**).

Aliquots (5-10 mg) from fraction IV from the Bio-Gel P-2 separations were semi-preparatively separated on a chilled (5°C) RP-HPLC-C18 column with 100% water (**Figure 29E**). One of the resulting sub-fractions was shown to be pure (**Figure 29F**), and the separation procedure was repeated until several milligrams of this compound had been isolated for structural characterization.

## 7.2. Structural characterization of a dimeric non-feruloylated arabinoxylan side-chain structure

### 7.2.1. Mass spectrometric analysis

LC-ESI-MS analysis (using an eluent containing lithium) of the purified compound revealed a molecular weight of 282 (quasimolecular ion of  $m/z$  289,  $[M+Li]^+$ ), which corresponds to a disaccharide made up of two pentose units. MS/MS fragmentation of the quasimolecular ion (**Figure 30**) produced typical fragments arising from loss of water ( $m/z$  271, loss of 18 mass units) and cleavage of the glycosidic linkage ( $m/z$  139 and  $m/z$  157).

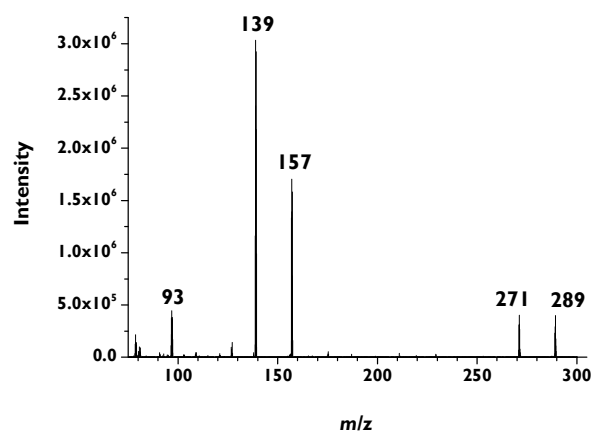


**Figure 30.** Mass spectrum resulting from fragmentation of the Li-adduct ( $m/z$  289,  $[M+Li]^+$ ) of the side-chain disaccharide purified from maize grain.

Abbreviations used:  $m/z$ : mass-to-charge ratio.

### 7.2.2. Monosaccharide composition and methylation analysis

TFA hydrolysis of the purified compound and HPAEC-PAD separation and detection of the released monosaccharides revealed arabinose and xylose in a 1:1 ratio. Derivatization of the released monosaccharides with (*R*)-2-octanol, followed by silylation and GC-MS separation and detection showed that the arabinose and xylose were present in the L- and D-configurations, respectively. Methylation analysis of the compound produced partially methylated alditol acetates corresponding to terminal Xylp and (1→3)-linked Arap (**Figure 31**).

### 7.2.3. NMR analysis

To complete the unequivocal structural characterization of this compound, 1D- ( $^1H$ ) and 2D- (COSY, HMQC, HMBC, TOCSY, and HSQC-TOCSY) NMR experiments were performed (**Tables 18-19**). The HSQC spectrum (**Figure 32**) revealed three anomeric carbon signals: signals representing the  $\alpha$ - and  $\beta$ -anomers of Arap and a signal from  $\alpha$ -Xylp. The  $\alpha$ -configuration of xylose was indicated both by the downfield shift of its anomeric proton signal (5.07-5.08 ppm) compared to typical anomeric shifts for  $\beta$ -Xyl ( $\approx$ 4.6 ppm) and its coupling constant (3.2 Hz;  $\beta$ -Xyl has a coupling constant  $\approx$ 8 Hz.) This confirms the methylation analysis results, which indicated that the arabinose unit was reducing. The  $\alpha$ -linkage of the Xylp unit was unexpected and shows that this Xyl-Ara side-chain structure is different than the oligosaccharide portion of the feruloylated disaccharide side-chain, FAX, which contains a  $\beta$ -linked Xylp unit.

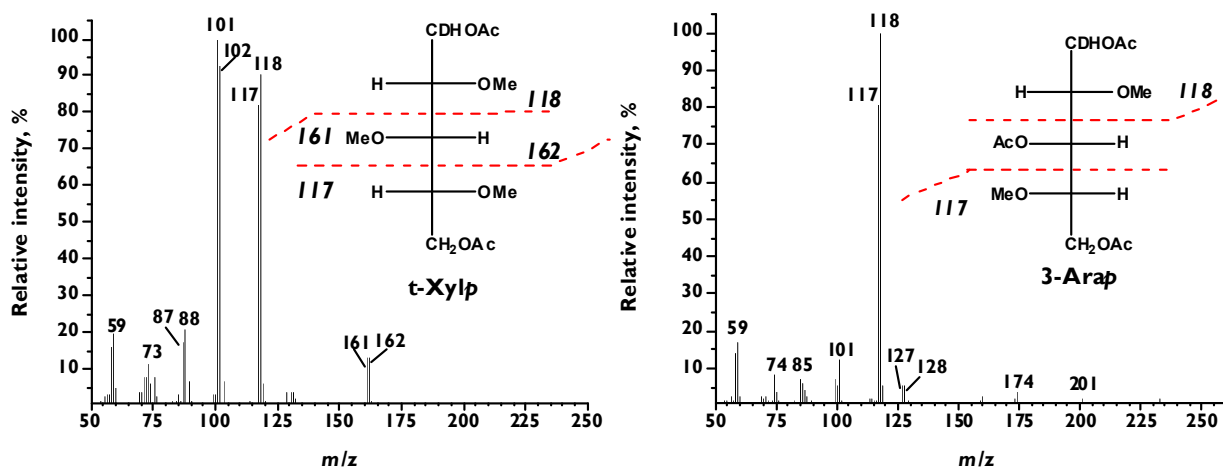


**Figure 31.** GC-MS spectra of partially methylated alditol acetates (EI ionization) of the side-chain disaccharide purified from maize grain.

Abbreviations used: **Arap**: arabinopyranose; **EI**: electron impact; **GC-MS**: gas chromatography coupled with mass spectrometry;  $m/z$ : mass-to-charge ratio; **tXylp**: terminal xylopyranose.

HMBC analysis confirmed the pyranose configuration of both sugar moieties (coupling cross peaks between H1 and C5 were observed in each ring system). HMBC analysis also showed a cross-peak corresponding to the H1 proton of  $\alpha$ -Xylp and C3 of Arap, indicating that the  $\alpha$ -xylose unit was (1 $\rightarrow$ 3)-linked to Arap. This confirms the partially methylated alditol acetate profile obtained with methylation analysis and was, once again, a surprising result since the “expected” linkage position, based on the structure of FAX, was the O-2 position of arabinose. The complete, unequivocally characterized structure is therefore  $\alpha$ -D-xylopyranosyl-(1 $\rightarrow$ 3)-L-arabinopyranose (**Figure 32**), abbreviated in the following text as XA. Montgomery et al. (1957) isolated a disaccharide from alkali-extracted corn hull hemicellulose via mildly acidic hydrolysis and reported its structure as  $\alpha$ -D-xylopyranosyl-(1 $\rightarrow$ 3)-L-arabinose. However, no NMR data were available to confirm the structure, and this structural moiety has not been reported since. Additionally, because the structure was isolated from alkali-extracted material, it is not possible to judge whether it was a non-feruloylated oligosaccharide in the native material.

**Table 18.**  $^1\text{H}$  NMR data of  $\alpha$ -D-xylopyranosyl-(1 $\rightarrow$ 3)-L-arabinopyranose (in  $\text{D}_2\text{O}$ ). Coupling constants  $J$  in Hz; chemical shifts  $\delta_{\text{H}}$  in ppm; spectra calibrated against acetone (0.5  $\mu\text{L}$ ,  $\delta_{\text{H}} = 2.22$  ppm,  $\delta_{\text{C}} = 30.89$  ppm).

	H1 ( $J_{1,2}$ )	H2	H3	H4	H5 ( $J_{5,6}$ )	
					H5 <sub>eq</sub>	H5 <sub>ax</sub>
$\alpha$ -Arabinopyranose, reducing	4.55 (7.9)	3.62	3.71	4.14	3.94	3.64
$\beta$ -Arabinopyranose, reducing	5.27 (-)	3.94	3.93	4.20	4.00	3.69
$\alpha$ -Xylose	5.07 (3.2) <sup>a</sup> 5.09 (3.2) <sup>a</sup>	3.57	3.73	3.63	nd	nd

**Table 19.**  $^{13}\text{C}$  NMR data of  $\alpha$ -D-xylopyranosyl-(1 $\rightarrow$ 3)-L-arabinopyranose (in  $\text{D}_2\text{O}$ ). Coupling constants  $J$  in Hz; chemical shifts  $\delta_{\text{H}}$  in ppm; spectra calibrated against acetone (0.5  $\mu\text{L}$ ,  $\delta_{\text{H}} = 2.22$  ppm,  $\delta_{\text{C}} = 30.89$  ppm).

	C1	C2	C3	C4	C5
$\alpha$ -Arabinopyranose, reducing	97.60	70.96	78.3	65.77	66.58
$\beta$ -Arabinopyranose, reducing	93.48	67.60	74.90	66.01	62.67
$\alpha$ -Xylose	96.30 <sup>a</sup> 96.45 <sup>a</sup>	72.18	73.68	70.07	nd

<sup>a</sup> Doublet peaks due to anomers.

Abbreviations used: **nd**: not determined; **NMR**: nuclear magnetic resonance.

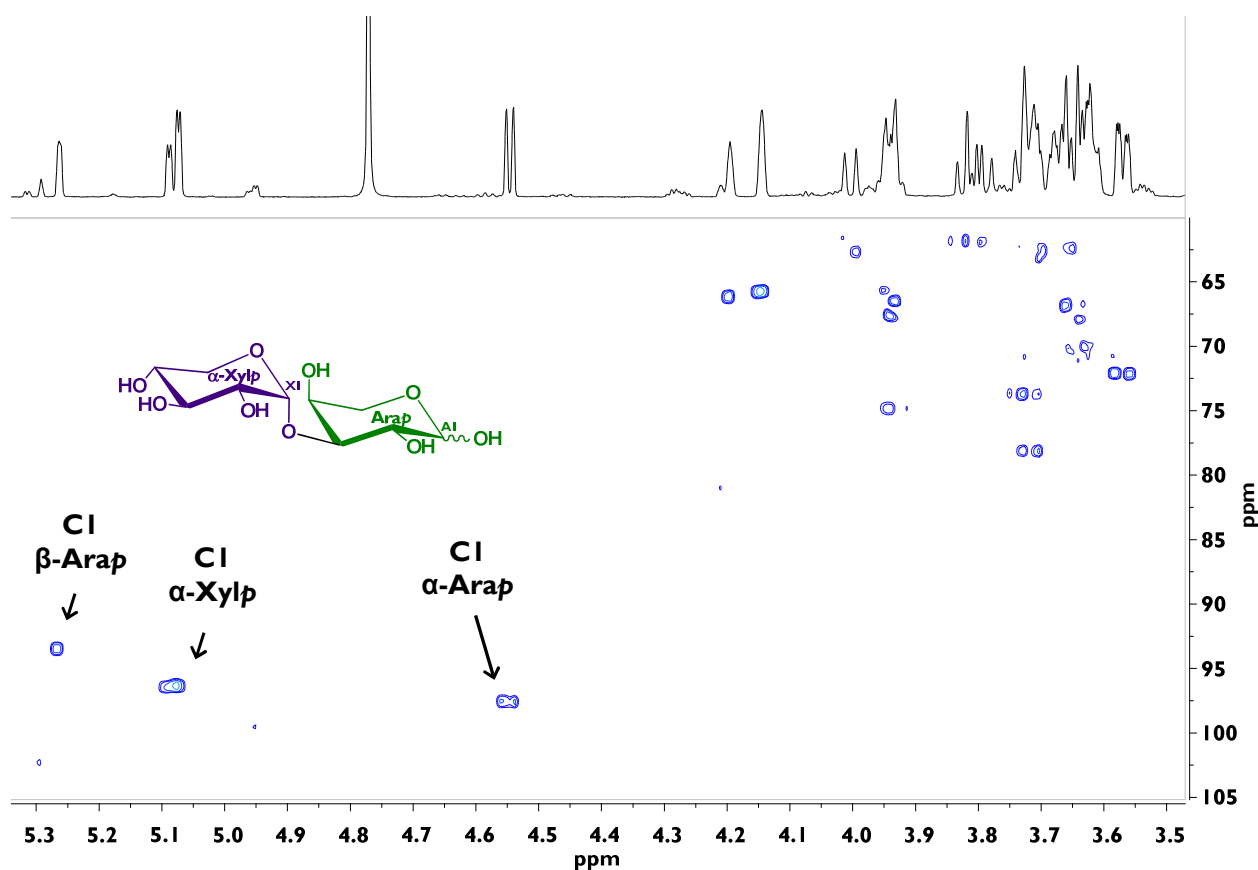


**Figure 32.** HSQC-NMR spectrum and structure of the purified dimeric, non-feruloylated arabinoxylan side-chain purified from maize grain fiber, XA.

Abbreviations used: **Arap**: arabinopyranose; **HSQC**: heteronuclear single quantum coherence spectroscopy; **NMR**: nuclear magnetic resonance. **XA**:  $\alpha$ -D-xylopyranosyl-(1 $\rightarrow$ 3)-L-arabinose; **Xylp**: xylopyranose.

### 7.3. Qualitative screening of cereal grain materials

To confirm that XA is an authentic component of cereal grain AX and not an artefact of the isolation procedure, we hydrolyzed the insoluble fiber of several cereal grains (popcorn maize, oats, and wheat) with a mildly acidic hydrolysis and subjected them to a qualitative screening. The feruloylated oligosaccharides were removed from the hydrolysates with C18-SPE clean-up. To minimize the potential contamination of the aqueous, non-feruloylated SPE eluates with feruloylated compounds, such as FAX, the cartridges were loaded at concentrations below the maximum molar absorption capacity of the C18 material as provided by the manufacturer and elution was performed slowly, in a drop-wise manner. However, the aqueous hydrolysates were not directly screened experimentally for contaminating ferulates. The aqueous hydrolysates were qualitatively screened with HPAEC-PAD for both XA and  $\beta$ -D-xylopyranosyl-(1 $\rightarrow$ 2)-L-arabinose, the side-chain oligosaccharide created upon cleavage of the ester bond in FAX (**Figure 33**). Both XA and  $\beta$ -D-xylopyranosyl-(1 $\rightarrow$ 2)-L-arabinose were present in the hydrolysates of all three cereal grains.

The identification of a novel, non-feruloylated AX side-chain disaccharide whose structure is unique from the oligosaccharide portion of FAX and the subsequent confirmation of the presence of this structure in several cereal grains raises new questions regarding AX biosynthesis. If, as speculated, UDP-feruloyl-Araf is synthesized in the Golgi apparatus before being transferred onto the xylan backbone, do separate xylosyltransferase enzymes then attach the xylose moieties to non-feruloylated Araf substituents on the AX backbone (forming XA) and

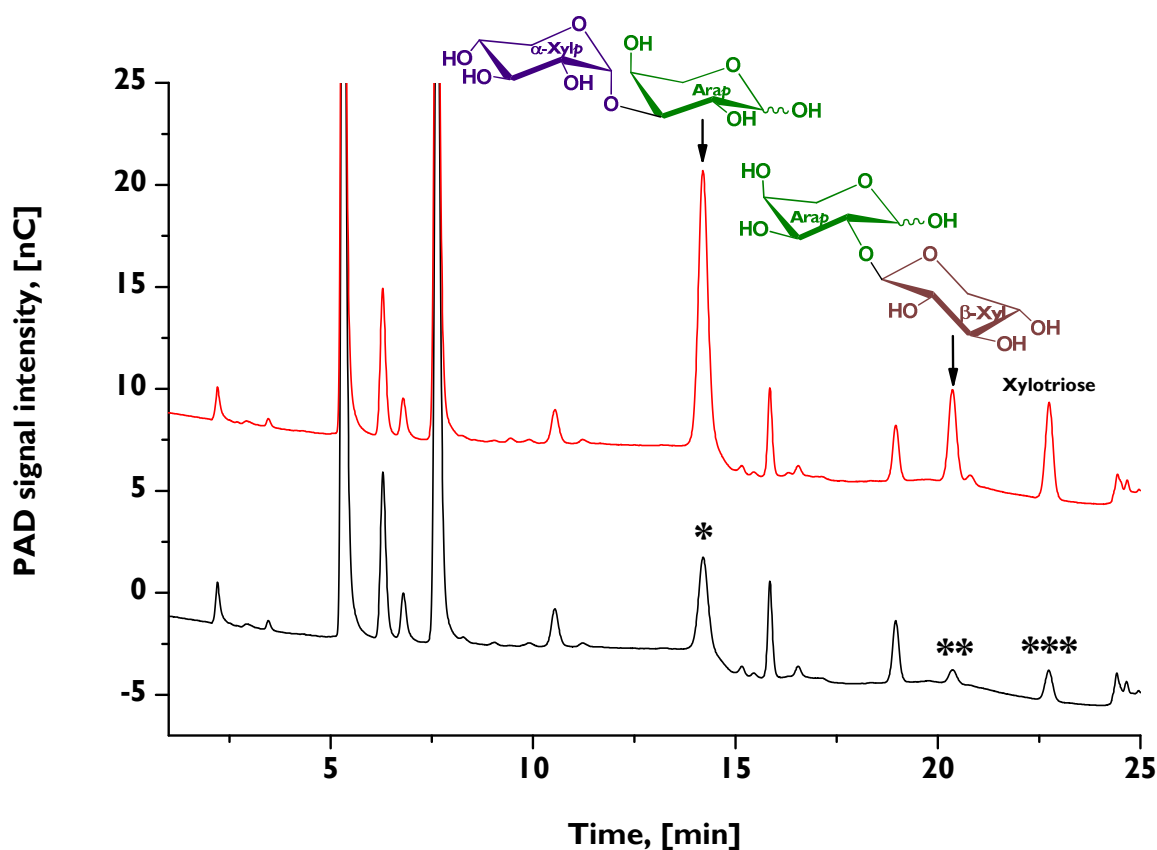


**Figure 33.** HPAEC-PAD chromatogram of a mildly acidic hydrolysate of popcorn maize fiber (bottom, black trace) and the same hydrolysate spiked with standard compounds (top, red trace, standard compound peaks labeled with asterisks). \*Peak label for XA ( $\alpha$ -D-xylopyranosyl-(1 $\rightarrow$ 3)-L-arabinose). \*\*Peak label for  $\beta$ -D-xylopyranosyl-(1 $\rightarrow$ 2)-L-arabinose. \*\*\*Peak label for xylotriose ( $\beta$ -D-xylopyranosyl-(1 $\rightarrow$ 4)- $\beta$ -D-xylopyranosyl-(1 $\rightarrow$ 4)-D-xylopyranose). Note: The HPAEC column and gradient conditions used in these analyses are different from those shown in **Figure 24F**.

Abbreviations used: **Arap**: arabinopyranose; **HPAEC**: high-performance anion-exchange chromatography; **PAD**: pulsed amperometric detection; **Xylp**: xylopyranose.

FA (forming FAX)? Or does xylose substitution of Araf occur prior to feruloylation, with  $\beta$ -(1 $\rightarrow$ 2)-linked xylose units marking the side-chain for feruloylation? The latter theory seems more likely, because down-regulation of XAX, a  $\beta$ -(1 $\rightarrow$ 2)-xylosyl transferase identified in rice was correlated with reduced ferulate contents in the material (Chiniquy et al., 2012). However, because this would mean that feruloylation occurs after Araf substitution of the xylan backbone, the current theory that UDP-Araf serves as an acceptor molecule for feruloyl-CoA is debatable.

The role of XA in the plant is unknown, as well as which factors push the organism to synthesize this compound. Future work will focus on developing quantitative methods for XA and other non-feruloylated side-chains in cereals. This will permit the assessment of structure-function relationships of these substituents in plant physiology, food processing, and human and animal nutrition. Additionally, it will be important to enzymatically isolate an oligosaccharide structure containing the XA moiety attached to a fragment of the xylan backbone to prove XA's attachment to AX polymers.

## 8. Comprehensive Discussion

---

**A**X are a major hemicellulosic component of grasses' cell walls and therefore a substantial part of cereal grains' dietary fiber complex. The structures of AX are built around  $\beta$ -(1 $\rightarrow$ 4)-linked D-xylose backbones to which various substituents are attached: L-Araf and L-Araf-containing oligosaccharides, GlcA, and acetyl groups. The O-5-esterification of some Araf and side-chain oligosaccharide units with hydroxycinnamic acids, especially *trans*-ferulic acid, is a distinguishing characteristic of cereal grain AX. Some of the ester-linked ferulic acid residues undergo free radical-induced oxidative coupling to form ferulate dimers and oligomers, producing cross-links between AX molecules and AX-lignin linkages. However, the majority of the total ferulates remain in monomeric form as feruloylated side-chains.

AX have key functional roles in plant physiology, where, among other effects, they help the plant resist insect and disease pressures. In food processing, AX affect dough and bread outcomes, and in human and animal nutrition, they influence the enzymatic degradability of cereals and display prebiotic properties. Importantly, all of these functional effects are structure-dependent, demonstrating the significance of accurately identifying and quantifying structural differences in feruloylated AX. Therefore, the objective of this work was to identify new structural elements of cereal grain AX and to develop quantitative and qualitative screening methods for both previously-described and newly-discovered structural components.

Multiple insights into the structures of cereal grain AX have been achieved through this work. Qualitative screening of the feruloylated AX from IWG (*Thinopyrum intermedium*) was enabled by two complementary hydrolysis methods: mildly acidic hydrolysis, which semi-selectively cleaves side-chains from the AX backbone and thus reveals the major feruloylated side-chains in a particular material, and enzymatic hydrolysis, which results in cleavage between backbone xylose residues and therefore gives insights into the structural environment surrounding the feruloylated side-chain moieties. Isolation and structural characterization of the released feruloylated AXOS resulted in thirteen feruloylated AXOS. When these structures were taken together with the results of standard carbohydrate analysis methods (monosaccharide composition and methylation analysis of partially methylated alditol acetates), a simple and sparsely-substituted AX structure with similarities to those of wheat and rye emerged. For IWG, which has only limited gluten-forming capabilities, its AX structure could contain the key for potential baking applications. For example, rye flour also has inferior gluten-forming abilities compared to wheat, but the structures of rye AX enable dough formation and are crucial to the baking characteristics of rye-based products. The similar structures of IWG AX to wheat and rye indicate that IWG AX may have similar baking properties.

Some of the isolated feruloylated AXOS structures contained AX structural elements that have not been described before, in particular the substitution of a backbone xylose monomer with a feruloylated side-chain immediately adjacent to another substituted backbone xylose unit (**Figure 34A**). Until now, it was assumed that the biosynthesis of this structural feature was sterically rejected. The ability to uncover new AX structural elements is the main strength of this laborious preparative approach to feruloylated AX study.

The preparative approach revealed only *trans*- and *cis*-FA and FAX as feruloylated side-chains substituting IWG AX, indicating that IWG's feruloylated side-chain profile is relatively simple, and does not contain substantial amounts of the complex, Galp-containing feruloylated

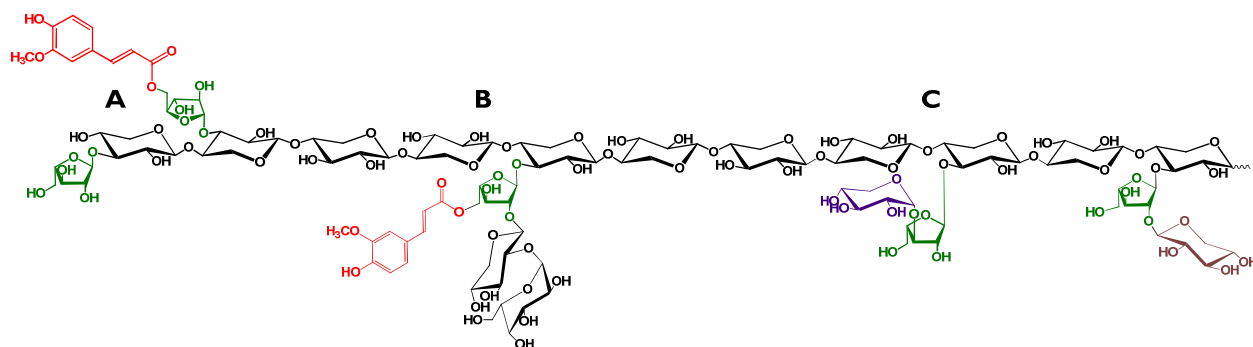


**Figure 34. Arabinoxylan (AX) structural insights gained through this work.** [A]: New structural elements were isolated and characterized from cereal AX which revealed that, among others, the substitution of a backbone xylose unit with a feruloylated side-chain can occur adjacent to another substituted xylose unit. [B]: Two quantitative feruloylated side-chain profile screening methods were developed and applied to cereal grain materials. The FAXG feruloylated side-chain unit ( $\alpha$ -L-galactopyranosyl-(1 $\rightarrow$ 2)- $\beta$ -D-xylopyranosyl-(1 $\rightarrow$ 2)-5-*O*-*trans*-feruloyl-L-arabinofuranose) is ubiquitous to cereal grains. [C]: Non-feruloylated AX side-chain substituents are found in several cereal grains.

side-chains found in maize. However, this method permitted only qualitative comparisons with the feruloylated side-chain profiles of other cereals and, as a preparative approach, lacks sensitivity. Additionally, this preparative method entails 4–6 months of full-time laboratory work and is therefore impractical as a routine method for the rapid comparison of many samples.

In response, we developed, validated, and tested two quantitative screening methods which enabled the rapid screening of the feruloylated side-chain profiles of cereal grain materials (**Figure 34B**). The three most abundant feruloylated side-chains in cereal grains, FA, FAX, and FAXG, were isolated in preparative quantities as standard compounds for method development. For application to cereal grain materials, the feruloylated side-chains were semi-selectively released with the same mildly acidic method used previously and isolated via C18-based SPE. In the first, chromatography-based method, the liberated feruloylated oligosaccharides were reduced to their sugar alcohols with NaBH<sub>4</sub> in the aprotic solvent DMSO, and quantification was performed by external calibration following LC-DAD/MS<sup>2</sup> separation and detection. Reduction to sugar alcohols was necessary because on-column mutarotation of the  $\alpha$ - and  $\beta$ -anomeric configurations of the native compounds occurs under the aqueous conditions of the reversed-phase gradient and results in split, tailing peaks. The use of an aprotic solvent during reduction proved necessary to avoid a base-catalyzed Lobry de Bruyn-van Ekenstein rearrangement of the reducing arabinose to other sugars via an enediol intermediate. For the second, 2D-HSQC-NMR-based method, samples were directly dissolved and measured in DMSO-*d*<sub>6</sub>. Quantification was done via internal calibration (caffeine was used as internal standard) following volume integration of selected cross-peak signals.

Both methods were robust, accurate, and reproducible and revealed distinctive differences in feruloylated side-chain profiles of different cereals, both in terms of quantity of individual side-chains and overall complexity of their profiles. For example, oats had low overall feruloylated side-chain concentrations but high profile complexity, whereas maize displayed both high concentrations and profile complexity. Additionally, using the chromatographic method, we confirmed that the FAXG feruloylated side-chain unit, which until now had only been reported in maize, is ubiquitous to cereal grains.

The determined feruloylated side-chain concentrations showed good correlation between the two methods. Total sample preparation and measurement time was shorter for the NMR-

based method, but the chromatographic method was more sensitive. The sensitivity of the NMR approach could be increased by running more scans, (the time required to obtain a given S/N ratio is proportional to  $(S/N)^2$ ), without, however, reaching the sensitivity of the chromatographic approach given the real-world laboratory limitations on realistic measurement time. Thus, the choice between the NMR and LC-based methods depend on which instruments are available to the analyst and also the sample quantities. The increased sensitivity of the LC-based method compared to the NMR method makes it the better choice for limited sample quantities, whereas the time savings offered by the NMR method make it attractive for samples with sufficient starting material.

Up to 93% of the total esterified monomeric ferulates (as determined by alkaline hydrolysis) were captured in the feruloylated side-chain profiles. Incomplete liberation of feruloylated AX side-chains is the major shortcoming of this approach, because the hydrolysis conditions represent a compromise between maximal cleavage of *Araf*-based side-chains with minimal degradation of ferulate ester bonds. The determined feruloylated side-chain concentrations should therefore not be understood as the absolute concentration in the original material but rather as the portion released under the mildly acidic hydrolysis conditions. However, the method offers the possibility for quantitative comparison between cereal materials, which has not been possible until now. Especially in plant materials with comparatively low recoveries (e.g., millet, oats, etc.), it is also possible that the ferulic acid is involved in structural units that are not covered by the developed profiling approaches.

The developed quantitative screening approaches for feruloylated side-chains will be indispensable for clarifying the structure-function roles of feruloylated side-chains in cereal grain AX. The method may also be expanded to include ferulate dimer side-chains. Although use of the preparative isolation method is still necessary to obtain feruloylated side-chain standard compounds and to isolate novel structural moieties, the use of the preparative method to compare the feruloylated side-chain profiles of cereal grains is now obsolete.

Finally, we investigated cereal grain AX for the presence of non-feruloylated oligosaccharide side-chain substituents. A non-feruloylated disaccharide side-chain from maize AX was isolated and unequivocally characterized. Its structure was uniquely different from the oligosaccharide portion of the comparable feruloylated side-chain compound, FAX (**Figure 34C**). Mildly acidic hydrolysis of cereal grain materials, removal of the feruloylated side-chains by C18-SPE, and HPAEC-PAD-based qualitative screening of the purified hydrolysates showed that this non-feruloylated structure is present in several cereals. This discovery raises questions about the roles and concentrations of these structures *in planta* compared to the feruloylated side-chains as well as their downstream functional effects. To answer these questions, quantitative methods for the non-feruloylated AX side-chains must be developed and validated.

This work provides a foundation for abundant future research. Preparative-scale investigations of cereal grain feruloylated AX remain a valid tool for identifying new structural features. However, for quantitative comparisons of feruloylated AX side-chain profiles, the developed NMR-based or chromatography-based screening approaches will be preferable to the traditional preparative approach. The methods developed in this work can be used to finally answer open questions about the structure-function relationships of feruloylated side-chains, such as their effect on AX enzymatic degradability. Clarifying this issue has far-reaching implications for the fields of human and animal nutrition, second-generation biofuel development, and food processing. Further work is also needed in the area of non-feruloylated AX side-chains, as it is likely that some non-feruloylated side-chain oligosaccharides remain

undiscovered and no quantitative methods have been developed yet for those structures which are known. Additional structural exploration and quantitative method development will be necessary to determine both the role of these structures *in planta* and their downstream effects in food and bioresidue processing and human and animal nutrition.

## 9. Summary

---

Arabinoxylans are the major hemicellulosic component of grasses' cell walls and cereal grains' dietary fiber complex. Their xylan backbones are substituted with L-arabinofuranose and L-arabinofuranose-containing oligosaccharides, and some substituents are acylated with ferulic acid, forming feruloylated side-chains. Substitution differences between arabinoxylans alter their functionality in plant physiology, food and bio-materials processing, and human and animal nutrition. To accurately assess these effects and predict arabinoxylans' physicochemical characteristics, both comprehensive knowledge of the structural elements present and reliable quantification of these elements are required. Therefore, this work's objectives were to identify new arabinoxylan structural elements and to develop qualitative and quantitative screening methods for both previously-described and novel structural components.

The feruloylated arabinoxylans from *Thinopyrum intermedium*, a perennial cereal grain, were structurally screened via partial arabinoxylan hydrolysis and preparative isolation and structural characterization of the released feruloylated arabinoxylan oligosaccharides, which revealed a sparsely-substituted arabinoxylan comparable to those of wheat and rye. Novel arabinoxylan structural elements were identified, such as a backbone xylose unit substituted with a feruloylated side-chain and adjacent to another substituted backbone xylose unit. Until now, it was assumed that this structural feature's biosynthesis was sterically rejected. This approach also showed that the main feruloylated side-chains in *T. intermedium* are relatively simple.

However, this preparative approach to feruloylated arabinoxylan side-chain profile screening is time-consuming and only qualitative. Therefore, two rapid, quantitative methods for feruloylated arabinoxylan side-chain profiles were developed and validated. For application to cereal grain materials, the feruloylated side-chains were semi-selectively released (50 mM trifluoroacetic acid, 2 h, 100°C) and isolated (C18 solid-phase-extraction). Quantification was performed by internal calibration using two-dimensional nuclear magnetic resonance spectroscopy (heteronuclear single quantum coherence experiment) or, after reduction to sugar alcohols, by external calibration using liquid chromatography coupled with diode array and tandem mass-spectrometric detectors. The determined feruloylated side-chain concentrations showed good correlation between the two methods. The nuclear magnetic resonance-based method was faster, but the chromatographic method was more sensitive. Up to 93% of the total esterified monomeric ferulates were captured in the feruloylated side-chain profiles.

Non-feruloylated oligosaccharide side-chains in cereal arabinoxylans were also investigated. A disaccharide side-chain structure different from the comparable feruloylated side-chain disaccharide was isolated and fully characterized. Qualitative screening of cereal grain hydrolysates using high-performance anion-exchange chromatography coupled with pulsed amperometric detection revealed this non-feruloylated side-chain structure in several cereal species.

This work provides a foundation for many future research endeavors. The quantitative feruloylated side-chains screening approach will help clarify the relationship between feruloylated side-chains and arabinoxylan enzymatic degradability. Quantitative methods remain to be developed for the non-feruloylated arabinoxylan side-chains, and other non-feruloylated side-chain oligosaccharides likely remain undiscovered. Continued structural exploration and quantitative method development are needed to clarify these arabinoxylan structures' role *in planta* and their downstream effects on food and bioresidue processing and human and animal nutrition.



# 10. Zusammenfassung

---

**A**rabinoxylane sind Hauptkomponenten der Zellwände von Gräsern und somit wichtige Bestandteile von Getreideballaststoffen. Sie bestehen aus einem Xylanrückgrat, das mit L-Arabinofuranose-Einheiten und mit L-Arabinofuranose enthaltenden Oligosacchariden, die zum Teil mit Ferulasäure verestert sind, substituiert ist. Unterschiede zwischen Arabinoxylanen bezüglich der Art und Häufigkeit der Seitenketten führen zu unterschiedlichen Funktionalitäten im Bereich der Pflanzenphysiologie, der Lebensmittelproduktion und der Ernährungswissenschaften. Ziel dieser Arbeit war es daher, neuartige Strukturelemente von Arabinoxylanen zu identifizieren und qualitative und quantitative Methoden für bekannte als auch für neue Strukturelemente zu entwickeln.

Die Strukturen der mit Ferulasäure veresterten Arabinoxylane aus der mehrjährigen Getreidesorte *Thinopyrum intermedium* wurden mittels partieller Hydrolyse der Arabinoxylane und präparativer Isolierung und Charakterisierung der freigesetzten Verbindungen untersucht. Die Struktur der Arabinoxylane konnte insgesamt als wenig substituiert und als vergleichbar mit den Arabinoxylanen von Weizen und Roggen beschrieben werden. Ebenfalls wurden neuartige Strukturelemente identifiziert, insbesondere ein Oligosaccharid, welches zwei benachbarte Xylose-Einheiten aus dem Xylanrückgrat enthielt, die beide mit Arabinose substituiert waren, wobei eine Arabinose-Einheit zusätzlich mit Ferulasäure verestert vorlag. Bisher wurde die Biosynthese eines solchen Strukturelementes als sterisch ungünstig und daher unwahrscheinlich erachtet. Des Weiteren ergaben diese Studien, dass die mit Ferulasäure veresterten Seitenketten vergleichbar einfache Strukturen aufweisen.

Die auf *T. intermedium* angewandte Methode ist sehr gut geeignet, um das Profil der mit Ferulasäure veresterten Seitenketten aus Getreiden zu bewerten und insbesondere, um neue Strukturen ausfindig zu machen, jedoch zeitaufwendig und nur qualitativer Natur. Daher wurden zwei quantitative Methoden zum schnellen Screening der mit Ferulasäure veresterten Seitenketten entwickelt und validiert. Um die Methoden auf Getreidematrizes anzuwenden, wurden die mit Ferulasäure veresterten Seitenketten gezielt freigesetzt (50 mM Trifluoressigsäure, 2 h, 100°C) und auf einer C18-Festphasenextraktionskartusche gereinigt. Die Quantifizierung erfolgte entweder mittels zweidimensionaler Kernspinresonanzspektroskopie (*Heteronuclear Single Quantum Coherence* Experiment) oder, nach Reduktion zu Zuckeralkoholen, mittels Hochleistungsflüssigkeitschromatographie mit Diodenarray- und Tandem-massenspektrometrischer Detektion. Die Probenvorbereitung nahm bei Anwendung der Kernspinresonanzbasierten Methode weniger Zeit in Anspruch, jedoch war die chromatographische Methode empfindlicher. Vergleichbare Konzentrationen wurden mit beiden Methoden bestimmt, wobei bis zu 93% der gesamten Ferulasäure der Zellwände erfasst wurden.

Ebenfalls wurden nicht mit Ferulasäure veresterte Arabinoxylan-Seitenketten untersucht. Eine Disaccharid-Seitenkette, deren Struktur von der mit Ferulasäure veresterten dimeren Seitenkette abwich, wurde isoliert und charakterisiert. Diese neuartige Struktur wurde in mehreren Getreidesorten mithilfe der Hochleistungsanionenaustauschchromatographie mit gepulst amperometrischer Detektion nachgewiesen.

Diese Arbeit bildet die Basis für eine Reihe zukünftiger Studien. Die quantitative Methode zum Screening auf mit Ferulasäure veresterte Seitenketten kann insbesondere dazu beitragen zu untersuchen, wie diese Strukturelemente die enzymatische Abbaubarkeit von Arabinoxylanen beeinflussen. Weitergehende Forschung im Bereich der nicht mit Ferulasäure veresterten Seitenketten erscheint notwendig, um weitere Strukturelemente zu identifizieren, zu quantifizieren und deren Einfluss auf die Eigenschaften der Arabinoxylane zu untersuchen.



# 11. References

---

- AACCI (2001). The definition of dietary fiber. *Cereal Foods World* 46, 112-126.
- Aerts, G., Broekaert, W., Courtin, C., Delcour, J. Arabinoxyloligosaccharides in beer. US 2010/0040731 A1, 2010.
- Agger, J., Viksø-Nielsen, A., Meyer, A. S. (2010). Enzymatic xylose release from pretreated corn bran arabinoxylan: Differential effects of deacetylation and deferuloylation on insoluble and soluble substrate fractions. *J. Agric. Food Chem.* 58, 6141-6148.
- Albersheim, P., Devins, D. J., English, P. D., Karr, A. (1967). A method for the analysis of sugar in plant cell-wall polysaccharides by gas-liquid chromatography. *Carbohydr. Res.* 5, 340-345.
- Albersheim, P., Darvill, A., Roberts, K., Sederoff, R., Staehelin, A., *Plant Cell Walls*. Garland Science: New York, NY, 2010.
- Allerdings, E., Ralph, J., Schatz, P. F., Gniechwitz, D., Steinhart, H., Bunzel, M. (2005). Isolation and structural identification of diarabinosyl 8-O-4-dehydrodiferulate from maize bran insoluble fibre. *Phytochemistry* 66, 113-124.
- Allerdings, E., Ralph, J., Steinhart, H., Bunzel, M. (2006). Isolation and structural identification of complex feruloylated heteroxylan side-chains from maize bran. *Phytochemistry* 67, 1276-1286.
- Åman, P., Bengtsson, S. (1991). Periodate oxidation and degradation studies on the major water-soluble arabinoxylan in rye grain. *Carbohydr. Polym.* 15, 405-414.
- Anadón, A., Martínez-Larrañaga, M. R., Caballero, V., Castellano, V., Assessment of Prebiotics and Probiotics: An Overview. In *Bioactive Foods in Promoting Health*, Preedy, R. R.; Watson, V. R., Eds. Academic Press: Boston, 2010; pp 19-41.
- Anders, N., Wilkinson, M. D., Lovegrove, A., Freeman, J., Tryfona, T., Pellny, T. K., et al. (2012). Glycosyl transferases in family 61 mediate arabinofuranosyl transfer onto xylan in grasses. *Proc. Natl. Acad. Sci. U.S.A.* 109, 989-993.

- Andersson, A. A. M., Lampi, A.-M., Nyström, L., Piironen, V., Li, L., Ward, J. L., et al. (2008). Phytochemical and dietary fiber components in barley varieties in the HEALTHGRAIN diversity screen. *J. Agric. Food Chem.* 56, 9767-9776.
- Andersson, R., Fransson, G., Tietjen, M., Åman, P. (2009). Content and molecular-weight distribution of dietary fiber components in whole-grain rye flour and bread. *J. Agric. Food Chem.* 57, 2004-2008.
- Andreasen, M. F., Kroon, P. A., Williamson, G., Garcia-Conesa, M. T. (2001a). Intestinal release and uptake of phenolic antioxidant diferulic acids. *Free Radic. Biol. Med.* 31, 304-314.
- Andreasen, M. F., Kroon, P. A., Williamson, G., Garcia-Conesa, M. T. (2001b). Esterase activity able to hydrolyze dietary antioxidant hydroxycinnamates is distributed along the intestine of mammals. *J. Agric. Food Chem.* 49, 5679-5684.
- Andreasen, M. F., Landbo, A.-K., Christensen, L. P., Hansen, Å., Meyer, A. S. (2001c). Antioxidant effects of phenolic rye (*Secale cereale* L.) extracts, monomeric hydroxycinnamates, and ferulic acid dehydrodimers on human low-density lipoproteins. *J. Agric. Food Chem.* 49, 4090-4096.
- Andrewartha, K. A., Phillips, D. H., Stone, B. A. (1979). Solution properties of wheat-flour arabinoxylans and enzymatically modified arabinoxylans. *Carbohydr. Res.* 77, 191-204.
- Angyal, S., Pickles, V. (1967). Equilibria between furanoses and pyranoses. *Carbohydr. Res.* 4, 269-270.
- Anson, N. M., Aura, A.-M., Selinheimo, E., Mattila, I., Poutanen, K., Van den Berg, R., et al. (2011). Bioprocessing of wheat bran in whole wheat bread increases the bioavailability of phenolic acids in men and exerts antiinflammatory effects ex vivo. *J. Nutr.* 141, 137-143.
- Appeldoorn, M. M., Kabel, M. A., Van Eylen, D., Gruppen, H., Schols, H. A. (2010). Characterization of oligomeric xylan structures from corn fiber resistant to pretreatment and simultaneous saccharification and fermentation. *J. Agric. Food Chem.* 58, 11294-11301.
- Appeldoorn, M. M., de Waard, P., Kabel, M. A., Gruppen, H., Schols, H. A. (2013). Enzyme resistant feruloylated xylooligomer analogues from thermochemically treated corn fiber contain large side chains, ethyl glycosides and novel sites of acetylation. *Carbohydr. Res.* 381, 33-42.

- Ardisson Korat, A. V., Willett, W. C., Hu, F. B. (2014). Diet, lifestyle, and genetic risk factors for type 2 diabetes: A review from the Nurses' Health Study, Nurses' Health Study 2, and Health Professionals' Follow-up Study. *Curr. Nutr. Rep.* 3, 345-354.
- Azuma, J., Kato, A., Koshijima, T., K., O. (1990). Arabinosylxylotriase mixedly esterified with acetic and ferulic acids from sugar cane bagasse. *Agric. Biol. Chem.* 54, 2181-2182.
- Bacic, A., Stone, B. A. (1981). Chemistry and organization of aleurone cell wall components from wheat and barley. *Aust. J. Plant Physiol.* 8, 475-495.
- Ballance, G., Hall, R., Manners, D. J. (1986). Studies of some arabinoxylans from barley endosperm walls. *Carbohydr. Res.* 150, 290-294.
- Barberousse, H., Roiseux, O., Robert, C., Paquot, M., Deroanne, C., Blecker, C. (2008). Analytical methodologies for quantification of ferulic acid and its oligomers. *J. Sci. Food Agric.* 88, 1494-1511.
- Bartley, L. E., Peck, M. L., Kim, S.-R., Ebert, B., Manisseri, C., Chiniquy, D. M., et al. (2013). Overexpression of a BAHD acyltransferase, OsAt10, alters rice cell wall hydroxycinnamic acid content and saccharification. *Plant Physiol.* 161, 1615-1633.
- Beaugrand, J., Chambat, G., Wong, V. W. K., Goubet, F., Remond, C., Paes, G., et al. (2004a). Impact and efficiency of GH10 and GH11 thermostable endoxylanases on wheat bran and alkali-extractable arabinoxylans. *Carbohydr. Res.* 339, 2529-2540.
- Beaugrand, J., Crônier, D., Debeire, P., Chabbert, B. (2004b). Arabinoxylan and hydroxycinnamate content of wheat bran in relation to endoxylanase susceptibility. *J. Cereal Sci.* 40, 223-230.
- BeMiller, J. N., Whistler, R. L., Shaw, D. H., *Methods in Carbohydrate Chemistry, Lipopolysaccharides, Separation and Analysis, Glycosylated Polymers.* Wiley: 1993.
- Bengtsson, S., Åman, P. (1990). Isolation and chemical characterization of water-soluble arabinoxylans in rye grain. *Carbohydr. Polym.* 12, 267-277.
- Bengtsson, S., Åman, P., Andersson, R. E. (1992a). Structural studies on water-soluble arabinoxylans in rye grain using enzymatic hydrolysis. *Carbohydr. Polym.* 17, 277-284.

- Bengtsson, S., Andersson, R., Westerlund, E., Åman, P. (1992b). Content, structure and viscosity of soluble arabinoxylans in rye grain from several countries. *J. Sci. Food Agric.* 58, 331-337.
- Bergmans, M. E. F., Beldman, G., Gruppen, H., Voragen, A. G. J. (1996). Optimisation of the selective extraction of (glucurono)arabinoxylans from wheat bran: Use of barium and calcium hydroxide solution at elevated temperatures. *J. Cereal Sci.* 23, 235-245.
- Biely, P., Czigárová, M., Uhliariková, I., Agger, J. W., Li, X.-L., Eijsink, V. G. H., et al. (2013). Mode of action of acetylxyylan esterases on acetyl glucuronoxylan and acetylated oligosaccharides generated by a GH10 endoxylanase. *BBA-Gen. Subjects* 1830, 5075-5086.
- Biely, P., Westereng, B., Puchart, V., de Maayer, P., A. Cowan, D. (2014). Recent progress in understanding the mode of action of acetylxyylan esterases. *J. Appl. Glycosci.* 61, 35-44.
- Björndal, H., Lindberg, B., Svensson, S. (1967a). Mass spectrometry of partially methylated alditol acetates. *Carbohydr. Res.* 5, 433-440.
- Björndal, H., Lindberg, B., Svensson, S. (1967b). Gas-liquid chromatography of partially methylated alditols as their acetates. *Acta Chem. Scand.* 21, 1801-1804.
- Bleton, J., Mejanelle, P., Sansoulet, J., Goursaud, S., Tchaplá, A. (1996). Characterization of neutral sugars and uronic acids after methanolysis and trimethylsilylation for recognition of plant gums. *J. Chromatogr. A* 720, 27-49.
- Bonner, W. A. (1959). C1-C2 Acetyl migration on methylation of the anomeric 1,3,4,6-tetra-O-acetyl-D-glucopyranoses. *J. Org. Chem.* 24, 1388-1390.
- Bowman, M. J., Dien, B. S., Hector, R. E., Sarath, G., Cotta, M. A. (2012). Liquid chromatography–mass spectrometry investigation of enzyme-resistant xylooligosaccharide structures of switchgrass associated with ammonia pretreatment, enzymatic saccharification, and fermentation. *Bioresour. Technol.* 110, 437-447.
- Bowman, M. J., Dien, B. S., Vermillion, K. E., Mertens, J. A. (2014). Structural characterization of (1→2)-β-xylose-(1→3)-α-arabinose-containing oligosaccharide products of extracted switchgrass (*Panicum virgatum*, L.) xylan after exhaustive enzymatic treatment with α-arabinofuranosidase and β-endo-xylanase. *Carbohydr. Res.* 398, 63-71.
- Bowman, M. J., Dien, B. S., Vermillion, K. E., Mertens, J. A. (2015). Isolation and characterization of unhydrolyzed oligosaccharides from switchgrass (*Panicum virgatum*,

- L.) xylan after exhaustive enzymatic treatment with commercial enzyme preparations. *Carbohydr. Res.* 407, 42-50.
- Bradford, M. M. (1976). A rapid and sensitive method for the quantitation of microgram quantities of protein utilizing the principle of protein-dye binding. *Anal. Biochem.* 72, 248-254.
- Brillouet, J.-M., Joseleau, J.-P. (1987). Investigation of the structure of a heteroxylan from the outer pericarp (beeswing bran) of wheat kernel. *Carbohydr. Res.* 159, 109-126.
- Brillouet, J. M., Joseleau, J. P., Utille, J. P., Lelievre, D. (1982). Isolation, purification and characterization of a complex heteroxylan from industrial wheat bran. *J. Agric. Food Chem.* 30, 488-495.
- Broekaert, W. F., Courtin, C. M., Verbeke, K., Van de Wiele, T., Verstraete, W., Delcour, J. A. (2011). Prebiotic and other health-related effects of cereal-derived arabinoxylans, arabinoxylan-oligosaccharides, and xylooligosaccharides. *Crit. Rev. Food Sci. Nutr.* 51, 178-194.
- Buanafina, M. d. O. (2009). Feruloylation in grasses: Current and future perspectives. *Mol. Plant* 2, 861-872.
- Buanafina, M. M. d. O., Fescemyer, H. W. (2012). Modification of esterified cell wall phenolics increases vulnerability of tall fescue to herbivory by the fall armyworm. *Planta* 236, 513-523.
- Buanafina, M. M. d. O., Fescemyer, H. W., Sharma, M., Shearer, E. A. (2015). Functional testing of a PF02458 homologue of putative rice arabinoxylan feruloyl transferase genes in *Brachypodium distachyon*. *Planta* 243, 659-674.
- Buksa, K., Nowotna, A., Ziobro, R., Praznik, W. (2014). Molecular properties of arabinoxylan fractions isolated from rye grain of different quality. *J. Cereal Sci.* 60, 368-373.
- Buksa, K., Nowotna, A., Ziobro, R., Gambuś, H. (2015). Rye flour enriched with arabinoxylans in rye bread making. *Food Sci. Technol. Int.* 21, 45-54.
- Bunzel, M. Monomere und dimere Phenolcarbonsäuren als strukturbildende Elemente in löslichen und unlöslichen Getreideballaststoffen. Doctoral thesis, Universität Hamburg, 2001.

- Bunzel, M., Ralph, J., Marita, J. M., Hatfield, R. D., Steinhart, H. (2001). Diferulates as structural components in soluble and insoluble cereal dietary fibre. *J. Sci. Food Agric.* 81, 653-660.
- Bunzel, M., Allerdings, E., Sinnwell, V., Ralph, J., Steinhart, H. (2002). Cell wall hydroxycinnamates in wild rice (*Zizania aquatica* L.) insoluble dietary fibre. *Eur. Food Res. Technol.* 214, 482-488.
- Bunzel, M., Ralph, J., Funk, C., Steinhart, H. (2003a). Isolation and identification of a ferulic acid dehydrotrimer from saponified maize bran insoluble fiber. *Eur. Food Res. Technol.* 217, 128-133.
- Bunzel, M., Ralph, J., Kim, H., Lu, F., Ralph, S. A., Marita, J. M., et al. (2003b). Sinapate dehydrodimers and sinapate-ferulate heterodimers in cereal dietary fiber. *J. Agric. Food Chem.* 51, 1427-1434.
- Bunzel, M., Ralph, J., Brüning, P., Steinhart, H. (2006). Structural identification of dehydrotriferulic and dehydrotetraferulic acids from insoluble maize bran fiber. *J. Agric. Food Chem.* 54, 6409-6418.
- Bunzel, M., Allerdings, E., Ralph, J., Steinhart, H. (2008). Cross-linking of arabinoxylans via 8-8-coupled diferulates as demonstrated by isolation and identification of diarabinosyl 8-8(cyclic)-dehydrodiferulate from maize bran. *J. Cereal Sci.* 47, 29-40.
- Bunzel, M. (2010). Chemistry and occurrence of hydroxycinnamate oligomers. *Phytochem. Rev.* 9, 47-64.
- Burget, E. G., Verma, R., Mølhøj, M., Reiter, W.-D. (2003). The biosynthesis of L-arabinose in plants: molecular cloning and characterization of a Golgi-localized UDP-D-xylose 4-epimerase encoded by the *MUR4* gene of Arabidopsis. *Plant Cell* 15, 523-531.
- Chambers, R. E., Clamp, J. R. (1971). Assessment of methanolysis and other factors used in analysis of carbohydrate-containing materials. *Biochem. J.* 125, 1009-1018.
- Chanliaud, E., Saulnier, L., Thibault, J.-F. (1995). Alkaline extraction and characterisation of heteroxylans from maize bran. *J. Cereal Sci.* 21, 195-203.
- Cheetham, N. W. H., Sirimanne, P. (1983). Methanolysis studies of carbohydrates, using H.P.L.C. *Carbohydr. Res.* 112, 1-10.

- Chesson, A., Gordon, A. H., Lomax, J. A. (1983). Substituent groups linked by alkali-labile bonds to arabinose and xylose residues of legume, grass and cereal straw cell walls and their fate during digestion by rumen microorganisms. *J. Sci. Food Agric.* 34, 1330-1340.
- Chiniqy, D., Sharma, V., Schultink, A., Baidoo, E. E., Rautengarten, C., Cheng, K., et al. (2012). XAX1 from glycosyltransferase family 61 mediates xylosyltransfer to rice xylan. *Proc. Natl. Acad. Sci. U.S.A.* 109, 17117-17122.
- Chundawat, S. P. S., Beckham, G. T., Himmel, M. E., Dale, B. E. (2011). Deconstruction of lignocellulosic biomass to fuels and chemicals. *Annu. Rev. Chem. Biomol. Eng.* 2, 121-145.
- Ciucanu, I., Kerek, F. (1984). A simple and rapid method for the permethylation of carbohydrates. *Carbohydr. Res.* 131, 209-217.
- Cleemput, G., van Oort, M., Hessing, M., Bergmans, M. E. F., Gruppen, H., Grobe, P. J., et al. (1995). Variation in the degree of D-xylose substitution in arabinoxylans extracted from a European wheat flour. *J. Cereal Sci.* 22, 73-84.
- Cloetens, L., Broekaert, W. F., Delaedt, Y., Ollevier, F., Courtin, C. M., Delcour, J. A., et al. (2010). Tolerance of arabinoxylan-oligosaccharides and their prebiotic activity in healthy subjects: a randomised, placebo-controlled cross-over study. *Br. J. Nutr.* 103, 703-713.
- CODEX, Joint FAO/WHO Food Standards Programme, Secretariat of the CODEX Alimentarius Commission: *CODEX Alimentarius (CODEX) Guidelines on Nutrition Labeling CAC/GL 2-1985 as Last Amended 2010*. Rome: FAO; 2010.
- Coelho, E., Rocha, M. A. M., Moreira, A. S. P., Domingues, M. R. M., Coimbra, M. A. (2016). Revisiting the structural features of arabinoxylans from brewers' spent grain. *Carbohydr. Polym.* 139, 167-176.
- Conner, A. H., Anderson, L. (1972). The tautomerization and mutarotation of  $\beta$ -L-arabinopyranose. Participation of both furanose anomers. *Carbohydr. Res.* 25, 107-116.
- Courtin, C. M., Roelants, A., Delcour, J. A. (1999). Fractionation-reconstitution experiments provide insight into the role of endoxylanases in bread-making. *J. Agric. Food Chem.* 47, 1870-1877.

- Courtin, C. M., Delcour, J. A. (2002). Arabinoxylans and endoxylanases in wheat flour bread-making. *J. Cereal Sci.* 35, 225-243.
- Courtin, C. M., Gys, W., Delcour, J. A. (2006). Arabinoxylans and endoxylanases in refrigerated dough syringing. *J. Sci. Food Agric.* 86, 1587-1595.
- Courtin, C. M., Swennen, K., Verjans, P., Delcour, J. A. (2009). Heat and pH stability of prebiotic arabinoxyloligosaccharides, xylooligosaccharides and fructooligosaccharides. *Food Chem.* 112, 831-837.
- Cox, T. S., Glover, J. D., Van Tassel, D. L., Cox, C. M., DeHaan, L. R. (2006). Prospects for developing perennial grain crops. *BioScience* 56, 649-659.
- Coxon, B. (2009). Developments in the Karplus equation as they relate to the NMR coupling constants of carbohydrates. *Adv. Carbohydr. Chem. Biochem.* 62, 17-82.
- Crepin, V. F., Faulds, C. B., Connerton, I. F. (2004). Functional classification of the microbial feruloyl esterases. *Appl. Microbiol. Biotechnol.* 63, 647-652.
- D'Auria, J. C. (2006). Acyltransferases in plants: a good time to be BAHD. *Curr. Opin. Plant Biol.* 9, 331-340.
- Damen, B., Verspreet, J., Pollet, A., Broekaert, W. F., Delcour, J. A., Courtin, C. M. (2011). Prebiotic effects and intestinal fermentation of cereal arabinoxylans and arabinoxylan oligosaccharides in rats depend strongly on their structural properties and joint presence. *Mol. Nutr. Food Res.* 55, 1862-1874.
- Damen, B., Cloetens, L., Broekaert, W. F., Francois, I., Lescroart, O., Trogh, I., et al. (2012). Consumption of breads containing in situ-produced arabinoxylan oligosaccharides alters gastrointestinal effects in healthy volunteers. *J. Nutr.* 142, 470-477.
- de Munter, J. S. L., Hu, F. B., Spiegelman, D., Franz, M., van Dam, R. M. (2007). Whole grain, bran, and germ intake and risk of type 2 diabetes: a prospective cohort study and systematic review. *PLoS Med.* 48, e261.
- de Vries, R. P., Kester, H. C. M., Poulsen, C. H., Benen, J. A. E., Visser, J. (2000). Synergy between enzymes from *Aspergillus* involved in the degradation of plant cell wall polysaccharides. *Carbohydr. Res.* 327, 401-410.

- Debyser, W., Schooneveld-Bergmans, M. E. F., Derdelinckx, G., Grobet, P. J., Delcour, J. A. (1997). Nuclear magnetic resonance and methylation analysis-derived structural features of water-extractable arabinoxylans from barley (*Hordeum vulgare* L.) malts. *J. Agric. Food Chem.* 45, 2914-2918.
- Delcour, J. A., Van Win, H., Grobet, P. J. (1999). Distribution and structural variation of arabinoxylans in common wheat mill streams. *J. Agric. Food Chem.* 47, 271-275.
- Dervilly-Pinel, G., Saulnier, L., Roger, P., Thibault, J. F. (2000). Isolation of homogeneous fractions from wheat water-soluble arabinoxylans. Influence of the structure on their macromolecular characteristics. *J. Agric. Food Chem.* 48, 270-278.
- Dervilly-Pinel, G., Rimsten, L., Saulnier, L., Andersson, R., Aman, P. (2001a). Water-extractable arabinoxylan from pearled flours of wheat, barley, rye and triticale. Evidence for the presence of ferulic acid dimers and their involvement in gel formation. *J. Cereal Sci.* 34, 207-214.
- Dervilly-Pinel, G., Thibault, J. F., Saulnier, L. (2001b). Experimental evidence for a semi-flexible conformation for arabinoxylans. *Carbohydr. Res.* 330, 365-372.
- Dervilly-Pinel, G., Tran, V., Saulnier, L. (2004). Investigation of the distribution of arabinose residues on the xylan backbone of water-soluble arabinoxylans from wheat flour. *Carbohydr. Polym.* 55, 171-177.
- Dervilly, G., Leclercq, C., Zimmermann, D., Roue, C., Thibault, J. F., Saulnier, L. (2001). Isolation and characterization of high molar mass water-soluble arabinoxylans from barley and barley malt. *Carbohydr. Polym.* 47, 143-149.
- DIN, Deutsches Institut für Normung. Chemische Analytik - Nachweis-, Erfassungs- und Bestimmungsgrenze unter Wiederholbedingungen - Begriffe, Verfahren, Auswertung (DIN 32645:2008-11), 2008.
- Dobberstein, D., Bunzel, M. (2010a). Separation and detection of cell wall-bound ferulic acid dehydrodimers and dehydrotrimers in cereals and other plant materials by reversed phase high-performance liquid chromatography with ultraviolet detection. *J. Agric. Food Chem.* 58, 8927-8935.
- Dobberstein, D., Bunzel, M. (2010b). Identification of ferulate oligomers from corn stover. *J. Sci. Food Agric.* 90, 1802-1810.

- Dohleman, F. G., Long, S. P. (2009). More productive than maize in the Midwest: How does miscanthus do it? *Plant Physiol.* 150, 2104-2115.
- Dornez, E., Verjans, P., Arnaut, F., Delcour, J. A., Courtin, C. M. (2011). Use of psychrophilic xylanases provides insight into the xylanase functionality in bread making. *J. Agric. Food Chem.* 59, 9553-9562.
- Ebert, B., Rautengarten, C., Guo, X., Xiong, G., Stonebloom, S., Smith-Moritz, A. M., et al. (2015). Identification and characterization of a Golgi-localized UDP-xylose transporter family from Arabidopsis. *Plant Cell* 27, 1218-1227.
- Ebringerova, A., Hromadkova, Z., Burchard, W., Dolega, R., Vorweg, W. (1994). Solution properties of water-insoluble rye-bran arabinoxylan. *Carbohydr. Polym.* 24, 161-169.
- Ebringerová, A., Hromádková, Z., Petráková, E., Hricovíni, M. (1990). Structural features of a water-soluble L-arabino-D-xylan from rye bran. *Carbohydr. Res.* 198, 57-66.
- Ebringerová, A., Hromádková, Z., Alföldi, J., Berth, G. (1992). Structural and solution properties of corn cob heteroxylans. *Carbohydr. Polym.* 19, 99-105.
- Egeberg, R., Olsen, A., Loft, S., Christensen, J., Johnsen, N. F., Overvad, K., et al. (2010). Intake of wholegrain products and risk of colorectal cancers in the Diet, Cancer and Health cohort study. *Br. J. Cancer* 103, 730-734.
- El Rassi, Z. (1996). Recent progress in reversed-phase and hydrophobic interaction chromatography of carbohydrate species. *J. Chromatogr. A* 720, 93-118.
- Erkkilä, A. T., Herrington, D. M., Mozaffarian, D., Lichtenstein, A. H. (2005). Cereal fiber and whole-grain intake are associated with reduced progression of coronary-artery atherosclerosis in postmenopausal women with coronary artery disease. *Am. Heart J.* 150, 94-101.
- Evans, D. E., Sheehan, M. C., Stewart, D. C. (1999). The impact of malt derived proteins on beer foam quality. Part II: The influence of malt foam-positive proteins and non-starch polysaccharides on beer foam quality. *J. Inst. Brew.* 105, 171-178.
- Freeman, J., Lovegrove, A., Wilkinson, M. D., Saulnier, L., Shewry, P. R., Mitchell, R. A. C. (2016). Effect of suppression of arabinoxylan synthetic genes in wheat endosperm on chain length of arabinoxylan and extract viscosity. *Plant Biotech. J.* 14, 109-116.

- Fry, S. C., Willis, S. C., Paterson, A. E. J. (2000). Intraprotoplasmic and wall-localised formation of arabinoxylan-bound diferulates and larger ferulate coupling-products in maize cell-suspension cultures. *Planta* 211, 679-692.
- Funk, C., Ralph, J., Steinhart, H., Bunzel, M. (2005). Isolation and structural characterisation of 8-O-4/8-O-4- and 8-8/8-O-4-coupled dehydrotriferulic acids from maize bran. *Phytochemistry* 66, 363-371.
- Gantzer, C. J., Anderson, S. H., Thompson, A. L., Brown, J. R. (1990). Estimating soil erosion after 100 years of cropping on Sanborn Field. *J. Soil Water Conserv.* 45, 641-644.
- Gash, J. H. C., Kabat, P., Monteny, B. A., Amadou, M., Bessemoulin, P., Billing, H., et al. (1997). The variability of evaporation during the HAPEX-Sahel Intensive Observation Period. *J. Hydrol.* 188-189, 385-399.
- Gebruers, K., Dornez, E., Boros, D., F., A., Dynkowska, W., Bedő, Z., et al. (2008). Variation in the content of dietary fiber and components thereof in wheats in the HEALTHGRAIN diversity screen. *J. Agric. Food Chem.* 56, 9740-9749.
- Girhammar, U., Nair, B. M. (1992a). Isolation, separation and characterization of water soluble non-starch polysaccharides from wheat and rye. *Food Hydrocolloids* 6, 285-299.
- Girhammar, U., Nair, B. M. (1992b). Certain physical properties of water soluble non-starch polysaccharides from wheat, rye, triticale, barley and oats. *Food Hydrocolloids* 6, 329-343.
- Glover, J. D., Reganold, J. P., Bell, L. W., Borevitz, J., Brummer, E. C., Buckler, E. S., et al. (2010). Increased food and ecosystem security via perennial grains. *Science* 328, 1638-1639.
- Goesaert, H., Brijs, K., Veraverbeke, W. S., Courtin, C. M., Gebruers, K., Delcour, J. A. (2005). Wheat flour constituents: how they impact bread quality, and how to impact their functionality. *Trends Food Sci. Technol.* 16, 12-30.
- Gottlieb, H. E., Kotlyar, V., Nudelman, A. (1997). NMR chemical shifts of common laboratory solvents as trace impurities. *J. Org. Chem.* 62, 7512-7515.
- Grabber, J. H., Hatfield, R. D., Ralph, J. (1998). Diferulate cross-links impede the enzymatic degradation of non-lignified maize walls. *J. Sci. Food Agric.* 77, 193-200.

- Gray, J., *Dietary fiber - definition, analysis, physiology & health* ILSI Press: Washington, D.C., 2006.
- Gruppen, H., Hamer, R. J., Voragen, A. G. J. (1991). Barium hydroxide as a tool to extract pure arabinoxylans from water-insoluble cell wall material of wheat flour. *J. Cereal Sci.* 13, 275-290.
- Gruppen, H., Hamer, R. J., Voragen, A. G. J. (1992a). Water-unextractable cell wall material from wheat flour. 2. Fractionation of alkali-extracted polymers and comparison with water-extractable arabinoxylans. *J. Cereal Sci.* 16, 53-67.
- Gruppen, H., Hamer, R. J., Voragen, A. G. J. (1992b). Water-unextractable cell wall material from wheat flour. 1. Extraction of polymers with alkali. *J. Cereal Sci.* 16, 41-51.
- Gruppen, H., Hoffmann, R. A., Kormelink, F. J. M., Voragen, A. G. J., Kamerling, J. P., Vliegthart, J. F. G. (1992c). Characterization by <sup>1</sup>H-NMR spectroscopy of enzymatically derived oligosaccharides from alkali-extractable wheat-flour arabinoxylan. *Carbohydr. Res.* 233, 45-64.
- Gruppen, H., Kormelink, F. J. M., Voragen, A. G. J. (1993a). Enzymic degradation of water-unextractable cell wall material and arabinoxylans from wheat flour. *J. Cereal Sci.* 18, 129-143.
- Gruppen, H., Kormelink, F. J. M., Voragen, A. G. J. (1993b). Water-unextractable cell wall material from wheat flour. 3. A structural model for arabinoxylans. *J. Cereal Sci.* 18, 111-128.
- Gubler, F., Ashford, A. E., Bacic, A., Blakeney, A. B., Stone, B. A. (1985). Release of ferulic acid esters from barley aleurone. 2. Characterization of the feruloyl compounds released in response to GA<sub>3</sub>. *Aust. J. Plant Physiol.* 12, 307-317.
- Guillon, F., Thibault, J. F. (1989). Structural investigation of the neutral sugar side-chains of sugar-beet pectins 1. Methylation analysis and mild acid-hydrolysis of the hairy fragments of sugar-beet pectins. *Carbohydr. Res.* 190, 85-96.
- Guo, M., Petrofsky, K., Zhang, L., Chen, P., Hohn, A., Youn, M., et al. (2011). Improving the functionality and bioactivity in wheat bran. *FASEB J.* 25, 581.5.
- Guo, W., Beta, T. (2013). Phenolic acid composition and antioxidant potential of insoluble and soluble dietary fibre extracts derived from select whole-grain cereals. *Food Res. Int.* 51, 518-525.

- Guth, H., Grosch, W. (1994). Quantitative analysis of caffeic and ferulic acids in oatmeal. *Z. Lebensm. Unters. Forsch.* 199, 195-197.
- Gys, W., Courtin, C. M., Delcour, J. A. (2003). Refrigerated dough syruing in relation to the arabinoxylan population. *J. Agric. Food Chem.* 51, 4119-4125.
- Harris, P. J., Trethewey, J. A. K. (2010). The distribution of ester-linked ferulic acid in the cell walls of angiosperms. *Phytochem. Rev.* 9, 19-33.
- Hatfield, R. D., Marita, J. M., Frost, K. (2008). Characterization of *p*-coumarate accumulation, *p*-coumaroyl transferase, and cell wall changes during the development of corn stems. *J. Sci. Food Agric.* 88, 2529-2537.
- Henke, H., *Präparative Gelchromatographie am Sephadex LH 20*. Alpha Druck GmbH: Goldbach, Germany, 1994.
- Hespell, R. B., O'Bryan, P. J. (1992). Purification and characterization of an  $\alpha$ -L-arabinofuranosidase from *Butyrivibrio fibrisolvens* GS113. *Appl. Environ. Microb.* 58, 1082-1088.
- Hoffmann, R. A., Kamerling, J. P., Vliegthart, J. F. G. (1992). Structural features of a water-soluble arabinoxylan from the endosperm of wheat. *Carbohydr. Res.* 226, 303-311.
- Höije, A., Sandström, C., Roubroeks, J. P., Andersson, R., Gohil, S., Gatenholm, P. (2006). Evidence of the presence of 2-O- $\beta$ -D-xylopyranosyl- $\alpha$ -L-arabinofuranose side chains in barley husk arabinoxylan. *Carbohydr. Res.* 341, 2959-2966.
- Holloway, W. D. Extraction, composition and some of the physical and chemical properties of dietary fibre. Doctoral thesis, Massey University, 1985.
- Hopkins, M. J., Englyst, H. N., Macfarlane, S., Furrie, E., Macfarlane, G. T., McBain, A. J. (2003). Degradation of cross-linked and non-cross-linked arabinoxylans by the intestinal microbiota in children. *Appl. Environ. Microbiol.* 69, 6354-6360.
- Hromádková, Z., Kováčiková, J., Ebringerová, A. (1999). Study of the classical and ultrasound-assisted extraction of the corn cob xylan. *Ind. Crops Prod.* 9, 101-109.

- Hsieh, Y. S. Y., Zhang, Q., Yap, K., Shirley, N. J., Lahnstein, J., Nelson, C. J., et al. (2016). Genetics, transcriptional profiles, and catalytic properties of the UDP-arabinose mutase family from barley. *Biochemistry* 55, 322-334.
- Huisman, M. M. H., Schols, H. A., Voragen, A. G. J. (2000). Glucuronoarabinoxylans from maize kernel cell walls are more complex than those from sorghum kernel cell walls. *Carbohydr. Polym.* 43, 269-279.
- Husband, F. A., Jay, A., Faulds, C. B., Waldron, K. W., Wilde, P. J., Extracting Novel Foam and Emulsion Stability Enhancers from Brewers' Grain. In *Total Food: Sustainability of the Agri-Food Chain*, Waldron, K. W.; Moates, G. K.; Faulds, C. B., Eds. The Royal Society of Chemistry: 2009; pp 58-63.
- Ishii, T. (1991). Acetylation at O-2 of arabinofuranose residues in feruloylated arabinoxylan from bamboo shoot cell-walls. *Phytochemistry* 30, 2317-2320.
- Ishii, T. (1997). Structure and functions of feruloylated polysaccharides. *Plant Sci.* 127, 111-127.
- Izydorczyk, M., Biliaderis, C. (1993). Structural heterogeneity of wheat endosperm arabinoxylans. *Cereal Chem.* 70, 641-646.
- Izydorczyk, M. S., Biliaderis, C. G., Bushuk, W. (1990). Oxidative gelation studies of water-soluble pentosans from wheat. *J. Cereal Sci.* 11, 153-169.
- Izydorczyk, M. S., Biliaderis, C. G. (1995). Cereal arabinoxylans: Advances in structure and physicochemical properties. *Carbohydr. Polym.* 28, 33-48.
- Jackson, G. M., Hosney, R. C. (1986a). Fate of ferulic acid in overmixed wheat flour doughs: Partial characterization of a cysteine-ferulic acid adduct. *J. Cereal Sci.* 4, 87-95.
- Jackson, G. M., Hosney, R. C. (1986b). Effect of endogenous phenolic acids on the mixing properties of wheat flour doughs. *J. Cereal Sci.* 4, 79-85.
- Jansson, P.-E., Kenne, L., Liedgren, H., Lindberg, B., Lönngrén, J. (1976). A practical guide to the methylation analysis of carbohydrates. In *Chem. Commun.*, pp 1-74, Stockholm.
- Jennings, A. C. (1961). Determination of the nitrogen content of cereal grain by colorimetric methods. *Cereal Chem.* 38, 467-468.

- Jensen, M. K., Koh-Banerjee, P., Hu, F. B., Franz, M., Sampson, L., Grønbæk, M., et al. (2004). Intakes of whole grains, bran, and germ and the risk of coronary heart disease in men. *Am. J. Clin. Nutr.* 80, 1492-1499.
- Jiang, N. Characterization of TaXPo1-1, a xylan synthase complex from wheat. Doctoral thesis, Ohio University, 2015.
- Jilek, M. L., Bunzel, M. (2013). Dehydrotriferulic and dehydrodiferulic acid profiles of cereal and pseudocereal flours. *Cereal Chem.* 90, 507-514.
- Jones, J. M. (2014). CODEX-aligned dietary fiber definitions help to bridge the ‘fiber gap’. *Nutrition Journal* 13, 1-10.
- Jones, P., Vogt, T. (2001). Glycosyltransferases in secondary plant metabolism: tranquilizers and stimulant controllers. *Planta* 213, 164-174.
- Jung, H.-J. G., Samac, D. A., Sarath, G. (2012a). Modifying crops to increase cell wall digestibility. *Plant Sci.* 185–186, 65-77.
- Jung, H.-J. G., Samac, D. A., Sarath, G. (2012b). Modifying crops to increase cell wall digestibility. *Plant Sci.* 185-186, 65-77.
- Kabel, M. A., Carvalheiro, F., Garrote, G., Avgerinos, E., Koukios, E., Parajó, J. C., et al. (2002). Hydrothermally treated xylan rich by-products yield different classes of xylo-oligosaccharides. *Carbohydr. Polym.* 50, 47-56.
- Kabel, M. A., de Waard, P., Schols, H. A., Voragen, A. G. J. (2003a). Location of *O*-acetyl substituents in xylo-oligosaccharides obtained from hydrothermally treated *Eucalyptus* wood. *Carbohydr. Res.* 338, 69-77.
- Kabel, M. A., Schols, H. A., Voragen, A. G. J., Identification of Structural Features of Various (*O*-Acetylated) Xylo-Oligosaccharides from Xylan-Rich Agricultural By-Products: A Review. In *Hemicelluloses: Science and Technology*, Gatenholm, P.; Tenkanen, M., Eds. American Chemical Society: Washington, DC, 2003b; Vol. 864, pp 107-121.
- Kabel, M. A., van den Borne, H., Vincken, J.-P., Voragen, A. G. J., Schols, H. A. (2007). Structural differences of xylans affect their interaction with cellulose. *Carbohydr. Polym.* 69, 94-105.

- Kamisaka, S., Takeda, S., Takahashi, K., Shibata, K. (1990). Diferulic and ferulic acid in the cell-wall of *Avena* coleoptiles - their relationships to mechanical properties of the cell-wall. *Physiol. Plant.* 78, 1-7.
- Karplus, M. (1959). Contact electron-spin coupling of nuclear magnetic moments. *J. Chem. Phys.* 30, 11-15.
- Kenji, I., Thi, B. T. L., Natsuki, K., Stone, B. A. (1994). Rapid and simple determination of *O*-acetyl groups bound to plant cell walls by acid hydrolysis and <sup>1</sup>H NMR measurement. *Phytochemistry* 35, 959-961.
- Kern, S. M., Bennett, R. N., Mellon, F. A., Kroon, P. A., Garcia-Conesa, M. T. (2003). Absorption of hydroxycinnamates in humans after high-bran cereal consumption. *J. Agric. Food Chem.* 51, 6050-6055.
- Kim, J. B., Carpita, N. C. (1992). Changes in esterification of the uronic acid groups of cell wall polysaccharides during elongation of maize coleoptiles. *Plant Physiol.* 98, 646-653.
- Köhnke, T., Pujolras, C., Roubroeks, J. P., Gatenholm, P. (2008). The effect of barley husk arabinoxylan adsorption on the properties of cellulose fibres. *Cellulose* 15, 537-546.
- Konishi, T., Ono, H., Ohnishi-Kameyama, M., Kaneko, S., Ishii, T. (2006). Identification of a mung bean arabinofuranosyltransferase that transfers arabinofuranosyl residues onto (1, 5)-linked  $\alpha$ -L-arabino-oligosaccharides. *Plant Physiol.* 141, 1098-1105.
- Konishi, T., Takeda, T., Miyazaki, Y., Ohnishi-Kameyama, M., Hayashi, T., O'Neill, M. A., et al. (2007). A plant mutase that interconverts UDP-arabinofuranose and UDP-arabinopyranose. *Glycobiology* 17, 345-354.
- Konishi, T., Aohara, T., Igasaki, T., Hayashi, N., Miyazaki, Y., Takahashi, A., et al. (2011). Down-regulation of UDP-arabinopyranose mutase reduces the proportion of arabinofuranose present in rice cell walls. *Phytochemistry* 72, 1962-1968.
- Kotake, T., Takata, R., Verma, R., Takaba, M., Yamaguchi, D., Orita, T., et al. (2009). Bifunctional cytosolic UDP-glucose 4-epimerases catalyse the interconversion between UDP-D-xylose and UDP-L-arabinose in plants. *Biochem. J.* 424, 169-177.
- Krause, A. Isolierung, Charakterisierung und Screening der Ferulasäure-Oligosaccharide aus Zuckerrübe. Diploma thesis, Karlsruhe Institute of Technology, 2014.

- Kulkarni, A. R., Pattathil, S., Hahn, M. G., York, W. S., O'Neill, M. A. (2012). Comparison of arabinoxylan structure in bioenergy and model grasses. *Ind. Biotechnol.* 8, 222-229.
- Lagaert, S., Pollet, A., Courtin, C. M., Volckaert, G. (2014).  $\beta$ -Xylosidases and  $\alpha$ -L-arabinofuranosidases: Accessory enzymes for arabinoxylan degradation. *Biotechnol. Adv.* 32, 316-332.
- Lam, T. B. T., Iiyama, K., Stone, B. A. (1992). Changes in phenolic-acids from internode walls of wheat and phalaris during maturation. *Phytochemistry* 31, 2655-2658.
- Lam, T. B. T., Iiyama, K., Stone, B. A. (2003). Hot alkali-labile linkages in the walls of the forage grass *Phalaris aquatica* and *Lolium perenne* and their relation to in vitro wall digestibility. *Phytochemistry* 64, 603-607.
- Langos, D., Granvogl, M., Meitingner, M., Schieberle, P. (2015). Development of stable isotope dilution assays for the quantitation of free phenolic acids in wheat and barley and malts produced thereof. *Eur. Food Res. Technol.* 241, 637-645.
- Lee, C., Zhong, R., Ye, Z.-H. (2012). Arabidopsis family GT43 members are xylan xylosyltransferases required for the elongation of the xylan backbone. *Plant Cell Physiol.* 53, 135-143.
- Lemieux, R. U., Kullnig, R. K., Bernstein, H. J., Schneider, W. G. (1958). Configurational effects on the proton magnetic resonance spectra of six-membered ring compounds. *J. Am. Chem. Soc.* 80, 6098-6105.
- Lequart, C., Nuzillard, J.-M., Kurek, B., Debeire, P. (1999). Hydrolysis of wheat bran and straw by an endoxylanase: production and structural characterization of cinnamoyl-oligosaccharides. *Carbohydr. Res.* 319, 102-111.
- Levigne, S. V., Ralet, M.-C. J., Quemener, B. C., Pollet, B. N.-L., Lapierre, C., Thibault, J.-F. J. (2004). Isolation from sugar beet cell walls of arabinan oligosaccharides esterified by two ferulic acid monomers. *Plant Physiol.* 134, 1173-1180.
- Lindsay, S. E., Fry, S. C. (2008). Control of diferulate formation in dicotyledonous and gramineous cell-suspension cultures. *Planta* 227, 439-452.
- Lovegrove, A., Wilkinson, M. D., Freeman, J., Pellny, T. K., Tosi, P., Saulnier, L., et al. (2013). RNA interference suppression of genes in glycosyl transferase families 43 and 47 in wheat starchy endosperm causes large decreases in arabinoxylan content. *Plant Physiol.* 163, 95-107.

- Lowry, O. H., Rosebrough, N. J., Farr, A. L., Randall, R. J. (1951). Protein measurement with the Folin phenol reagent. *J. Biol. Chem.* 193, 265-275.
- Lu, J., Li, Y. (2006). Effects of arabinoxylan solubilization on wort viscosity and filtration when mashing with grist containing wheat and wheat malt. *Food Chem.* 98, 164-170.
- Luonteri, E., Kroon, P. A., Tenkanen, M., Teلمان, A., Williamson, G. (1999). Activity of an *Aspergillus terreus*  $\alpha$ -arabinofuranosidase on phenolic-substituted oligosaccharides. *J. Biotechnol.* 67 41-48.
- Mackie, W., Perlin, A. S. (1966). Pyranose-furanose and anomeric equilibria: influence of solvent and of partial methylation. *Can. J. Chem.* 44, 2039-2049.
- Maes, C., Delcour, J. A. (2002). Structural characterisation of water-extractable and water-unextractable arabinoxylans in wheat bran. *J. Cereal Sci.* 35, 315-326.
- Makaravicius, T., Basinskiene, L., Juodeikiene, G., van Gool, M. P., Schols, H. A. (2012). Production of oligosaccharides from extruded wheat and rye biomass using enzymatic treatment. *Catal. Today* 196, 16-25.
- Maki, K. C., Gibson, G. R., Dickmann, R. S., Kendall, C. W. C., Chen, C. Y. O., Costabile, A., et al. (2012). Digestive and physiologic effects of a wheat bran extract, arabino-xylan-oligosaccharide, in breakfast cereal. *Nutrition* 28, 1115-1121.
- Mandalari, G., Faulds, C. B., Sancho, A. I., Saija, A., Bisignano, G., LoCurto, R., et al. (2005). Fractionation and characterisation of arabinoxylans from brewers' spent grain and wheat bran. *J. Cereal Sci.* 42, 205-212.
- Maness, N. O., Ryan, J. D., Mort, A. J. (1990). Determination of the degree of methyl esterification of pectins in small samples by selective reduction of esterified galacturonic acid to galactose. *Anal. Biochem.* 185, 346-352.
- Marcotuli, I., Hsieh, Y. S. Y., Lahnstein, J., Yap, K., Burton, R. A., Blanco, A., et al. (2016). Structural variation and content of arabinoxylans in endosperm and bran of durum wheat (*Triticum turgidum* L.). *J. Agric. Food Chem.* 64, 2883-2892.
- Marita, J. M., Hatfield, R. D., Rancour, D. M., Frost, K. E. (2014). Identification and suppression of the *p*-coumaroyl CoA:hydroxycinnamyl alcohol transferase in *Zea mays* L. *Plant J.* 78, 850-864.

- Mastrangelo, L. I., Lenucci, M. S., Piro, G., Dalessandro, G. (2008). Evidence for intra- and extra-protoplasmic feruloylation and cross-linking in wheat seedling roots. *Planta* 229, 343-355.
- Mazumder, K., York, W. S. (2010). Structural analysis of arabinoxylans isolated from ball-milled switchgrass biomass. *Carbohydr. Res.* 345, 2183-2193.
- McCallum, J. A., Taylor, I. E. P., Towers, G. H. N. (1991). Spectrophotometric assay and electrophoretic detection of *trans*-feruloyl esterase activity. *Anal. Biochem.* 196, 360-366.
- McCallum, J. A., Walker, J. R. L. (1991). Phenolic biosynthesis during grain development in wheat (*Triticum aestivum* L.) III. Changes in hydroxycinnamic acids during grain development. *J. Cereal Sci.* 13, 161-172.
- McCleary, B. V., DeVries, J. W., Rader, J. I., Cohen, G., Prosky, L., Mugford, D. C., et al. (2012). Determination of insoluble, soluble, and total dietary fiber (CODEX definition) by enzymatic-gravimetric method and liquid chromatography: Collaborative study. *J. AOAC Int.* 95, 824-844.
- McCleary, B. V., Sloane, N., Draga, A. (2015). Determination of total dietary fibre and available carbohydrates: A rapid integrated procedure that simulates *in vivo* digestion. *Starch - Stärke* 67, 860-883.
- Mellen, P. B., Walsh, T. F., Herrington, D. M. (2008). Whole grain intake and cardiovascular disease: A meta-analysis. *Nutr. Metab. Cardiovasc. Dis.* 18, 283-290.
- Meng, X., Slominski, B. A., Nyachoti, C. M., Campbell, L. D., Guenter, W. (2005). Degradation of cell wall polysaccharides by combinations of carbohydrase enzymes and their effect on nutrient utilization and broiler chicken performance. *Poult. Sci.* 84, 37-47.
- Meyer, M. R. Essigsäurekatalysierte Freisetzung von ferulasäurehaltigen Arabinoxylanseitenketten aus Mais. Diplom thesis, Karlsruhe Institute of Technology, 2013.
- Micard, V., Renard, C. M. G. C., Thibault, J. F. (1994). Studies on enzymatic release of ferulic acid from sugar-beet pulp. *Lebensm. Wiss. Technol.* 27, 59-66.

- Mitchell, R. A. C., Dupree, P., Shewry, P. R. (2007). A novel bioinformatics approach identifies candidate genes for the synthesis and feruloylation of arabinoxylan. *Plant Physiol.* 144, 43-53.
- Molinari, H. B. C., Pellny, T. K., Freeman, J., Shewry, P. R., Mitchell, R. A. C. (2013). Grass cell wall feruloylation: distribution of bound ferulate and candidate gene expression in *Brachypodium distachyon*. *Front. Plant Sci.* 4, 1-10.
- Montgomery, R., Smith, F., Srivastava, H. C. (1956). Structure of corn hull hemicellulose. I. Partial hydrolysis and identification of 2-O-( $\alpha$ -D-glucopyranosyluronic acid)-D-xylopyranose. *J. Am. Chem. Soc.* 78, 2837-2839.
- Montgomery, R., Smith, F., Srivastava, H. C. (1957). Structure of corn hull hemicelluloses. Part IV. Partial hydrolysis and identification of 3-O- $\alpha$ -D-xylopyranosyl-L-arabinose and 4-O- $\beta$ -D-galactopyranosyl- $\beta$ -D-xylose. *J. Am. Chem. Soc.* 79, 698-700.
- Mueller-Harvey, I., Hartley, R. D., Harris, P. J., Curzon, E. H. (1986). Linkage of p-coumaroyl and feruloyl groups to cell wall polysaccharides of barley straw. *Carbohydr. Res.* 148, 71-85.
- Müller, P. Vergleich und Anwendungsoptimierung von Methoden zur Bestimmung und Charakterisierung von Proteinen der pflanzlichen Zellwand. Diplom thesis, Karlsruhe Institute of Technology, 2015.
- Mulrone, B., Traeger, J. C., Stone, B. A. (1995). Determination of both linkage position and anomeric configuration in underivatized glucopyranosyl disacchides by electrospray mass spectrometry. *J. Mass Spectrom.* 30, 1277-1283.
- Nardini, M., Cirillo, E., Natella, F., Mencarelli, D., Comisso, A., Scaccini, C. (2002). Detection of bound phenolic acids: prevention by ascorbic acid and ethylenediaminetetraacetic acid of degradation of phenolic acids during alkaline hydrolysis. *Food Chem.* 79, 119-124.
- Nardini, M., Ghiselli, A. (2004). Determination of free and bound phenolic acids in beer. *Food Chem.* 84, 137-143.
- Neumüller, K. G., Carvalho de Souza, A., Van Rijn, J., Appeldoorn, M. M., Streekstra, H., Schols, H. A., et al. (2013). Fast and robust method to determine phenoyl and acetyl esters of polysaccharides by quantitative  $^1\text{H}$  NMR. *J. Agric. Food Chem.* 61, 6282-6287.

- Neumüller, K. G., Streekstra, H., Gruppen, H., Schols, H. A. (2014). *Trichoderma longibrachiatum* acetyl xylan esterase 1 enhances hemicellulolytic preparations to degrade corn silage polysaccharides. *Bioresour. Technol.* 163, 64-73.
- Nguyen, S. K., Sophonputtanaphoca, S., Kim, E., Penner, M. H. (2009). Hydrolytic methods for the quantification of fructose equivalents in herbaceous biomass. *Appl. Biochem. Biotechnol.* 158, 352-361.
- Obel, N., Porchia, A. C., Scheller, H. V. (2003). Intracellular feruloylation of arabinoxylan in wheat: evidence for feruloyl-glucose as precursor. *Planta* 216, 620-629.
- Ohta, T., Yamasaki, S., Egashira, Y., Sanada, H. (1994). Antioxidative activity of corn bran hemicellulose fragments. *J. Agric. Food Chem.* 42, 653-656.
- Oikawa, A., Lund, C. H., Sakuragi, Y., Scheller, H. V. (2013). Golgi-localized enzyme complexes for plant cell wall biosynthesis. *Trends Plant Sci.* 18, 49-58.
- Ordaz-Ortiz, J. J., Devaux, M. F., Saulnier, L. (2005). Classification of wheat varieties based on structural features of arabinoxylans as revealed by endoxylanase treatment of flour and grain. *J. Agric. Food Chem.* 53, 8349-8356.
- Ordaz-Ortiz, J. J., Saulnier, L. (2005). Structural variability of arabinoxylans from wheat flour. Comparison of water-extractable and xylanase-extractable arabinoxylans. *J. Cereal Sci.* 42, 119-125.
- Oscarsson, M., Andersson, R., Salomonsson, A. C., Åman, P. (1996). Chemical composition of barley samples focusing on dietary fibre components. *J. Cereal Sci.* 24, 161-170.
- Panagiotou, G., Topakas, E., Economou, L., Kekos, D., Macris, B. J., Christakopoulos, P. (2003). Induction, purification, and characterization of two extracellular  $\alpha$ -L-arabinofuranosidases from *Fusarium oxysporum*. *Can. J. Microbiol.* 49, 639-644.
- Pastell, H., Virkki, L., Harju, E., Tuomainen, P., Tenkanen, M. (2009). Presence of 1-3-linked 2-O- $\beta$ -D-xylopyranosyl- $\alpha$ -L-arabinofuranosyl side chains in cereal arabinoxylans. *Carbohydr. Res.* 344, 2480-2488.
- Pauli, G. F., Gödecke, T., Jaki, B. U., Lankin, D. C. (2012). Quantitative  $^1\text{H}$  NMR. Development and potential of an analytical method: An update. *J. Nat. Prod.* 75, 834-851.

- Pekkinen, J., Rosa, N., Savolainen, O.-I., Keski-Rahkonen, P., Mykkanen, H., Poutanen, K., et al. (2014). Disintegration of wheat aleurone structure has an impact on the bioavailability of phenolic compounds and other phytochemicals as evidenced by altered urinary metabolite profile of diet-induced obese mice. *Nutr. Metabolism* 11, 1.
- Pellny, T. K., Lovegrove, A., Freeman, J., Tosi, P., Love, C. G., Knox, J. P., et al. (2012). Cell walls of developing wheat starchy endosperm: comparison of composition and RNA-seq transcriptome. *Plant Physiol.* 158, 612-627.
- Petrik, D. L., Karlen, S. D., Cass, C. L., Padmakshan, D., Lu, F., Liu, S., et al. (2014). *p*-Coumaroyl-CoA:monolignol transferase (PMT) acts specifically in the lignin biosynthetic pathway in *Brachypodium distachyon*. *Plant J.* 77, 713-726.
- Pettolino, F. A., Walsh, C., Fincher, G. B., Bacic, A. (2012). Determining the polysaccharide composition of plant cell walls. *Nat. Protoc.* 7, 1590-1607.
- Philippe, S., Tranquet, O., Utile, J.-P., Saulnier, L., Guillon, F. (2007). Investigation of ferulate deposition in endosperm cell walls of mature and developing wheat grains by using a polyclonal antibody. *Planta* 225, 1287-1299.
- Piston, F., Uauy, C., Fu, L., Langston, J., Labavitch, J., Dubcovsky, J. (2009). Down-regulation of four putative arabinoxylan feruloyl transferase genes from family PF02458 reduces ester-linked ferulate content in rice cell walls. *Planta* 231, 677-691.
- Pollet, A., Delcour, J. A., Courtin, C. M. (2010a). Structural determinants of the substrate specificities of xylanases from different glycoside hydrolase families. *Crit. Rev. Biotechnol.* 30, 176-191.
- Pollet, A., Lagaert, S., Eneyskaya, E., Kulminskaya, A., Delcour, J. A., Courtin, C. M. (2010b). Mutagenesis and subsite mapping underpin the importance for substrate specificity of the aglycon subsites of glycoside hydrolase family 11 xylanases. *BBA Proteins Proteom.* 1804, 977-985.
- Porchia, A. C., Sørensen, S. O., Scheller, H. V. (2002). Arabinoxylan biosynthesis in wheat. Characterization of arabinosyltransferase activity in Golgi membranes. *Plant Physiol.* 130, 432-441.
- Puchart, V., Biely, P. (2015). Redistribution of acetyl groups on the non-reducing end xylopyranosyl residues and their removal by xylan deacetylases. *Appl. Microbiol. Biotechnol.* 99, 3865-3873.

- Quemener, B., Ralet, M.-C. (2004). Evidence for linkage position determination in known feruloylated mono- and disaccharides using electrospray ion trap mass spectrometry. *J. Mass Spectrom.* 39, 1153-1160.
- Quemener, B., Ordaz-Ortiz, J. J., Saulnier, L. (2006). Structural characterization of underivatized arabino-xylo-oligosaccharides by negative-ion electrospray mass spectrometry. *Carbohydr. Res.* 341, 1834-1847.
- Rakszegi, M., Lovegrove, A., Balla, K., Láng, L., Bedő, Z., Veisz, O., et al. (2014). Effect of heat and drought stress on the structure and composition of arabinoxylan and  $\beta$ -glucan in wheat grain. *Carbohydr. Polym.* 102, 557-565.
- Ralet, M. C., Faulds, C. B., Williamson, G., Thibault, J. F. (1994a). Degradation of feruloylated oligosaccharides from sugar-beet pulp and wheat bran by ferulic acid esterases from *Aspergillus niger*. *Carbohydr. Res.* 263, 257-269.
- Ralet, M. C., Thibault, J. F., Faulds, C. B., Williamson, G. (1994b). Isolation and purification of feruloylated oligosaccharides from cell-walls of sugar-beet pulp. *Carbohydr. Res.* 263, 227-241.
- Ralph, J., Quideau, S., Grabber, J. H., Hatfield, R. D. (1994). Identification and synthesis of new ferulic acid dehydrodimers present in grass cell walls. *J. Chem. Soc. Perkin Trans. 1* 3485-3498.
- Ralph, J., Grabber, J. H., Hatfield, R. D. (1995). Lignin-ferulate cross-links in grasses: active incorporation of ferulate polysaccharide esters into ryegrass lignins. *Carbohydr. Res.* 275, 167-178.
- Ralph, J., Bunzel, M., Marita, J. M., Hatfield, R. D., Lu, F., Kim, H., et al. (2004). Peroxidase-dependent cross-linking reactions of p-hydroxycinnamates in plant cell walls. *Phytochem. Rev.* 3, 79-96.
- Rancour, D. M., Hatfield, R. D., Marita, J. M., Rohr, N. A., Schmitz, R. J. (2015). Cell wall composition and digestibility alterations in *Brachypodium distachyon* achieved through reduced expression of the UDP-arabinopyranose mutase. *Front. Plant Sci.* 6, 1-20.
- Rao, R. S. P., Muralikrishna, G. (2007). Structural characteristics of water-soluble feruloyl arabinoxylans from rice (*Oryza sativa*) and ragi (finger millet, *Eleusine coracana*): Variations upon malting. *Food Chem.* 104, 1160-1170.

- Ratnayake, S., Beahan, C. T., Callahan, D. L., Bacic, A. (2014). The reducing end sequence of wheat endosperm cell wall arabinoxylans. *Carbohydr. Res.* 386, 23-32.
- Rattan, O., Izydorczyk, M. S., Biliaderis, C. G. (1994). Structure and rheological behaviour of arabinoxylans from Canadian bread wheat flours. *LWT- Food Sci. Technol.* 27, 550-555.
- Rautengarten, C., Ebert, B., Herter, T., Petzold, C. J., Ishii, T., Mukhopadhyay, A., et al. (2011). The interconversion of UDP-arabinopyranose and UDP-arabinofuranose is indispensable for plant development in *Arabidopsis*. *Plant Cell* 23, 1373-1390.
- Remond, C., Boukari, T., Chambat, G., O'Donohue, M. (2008). Action of a GH 51  $\alpha$ -L-arabinofuranosidase on wheat-derived arabinoxylans and arabino-xylooligosaccharides. *Carbohydr. Polym.* 72, 424-430.
- Rennie, E. A., Scheller, H. V. (2014). Xylan biosynthesis. *Curr. Opin. Biotechnol.* 26, 100-107.
- Rhodes, D. I., Sadek, M., Stone, B. A. (2002). Hydroxycinnamic acids in walls of wheat aleurone cells. *J. Cereal Sci.* 36, 67-81.
- Rosler, K.-H., Goodwin, R. S. (1984). A general use of Amberlite XAD-2 resin for the purification of flavonoids from aqueous fractions. *J. Nat. Prod.* 47, 188-188.
- Ruiz-Matute, A. I., Hernandez-Hernandez, O., Rodriguez-Sanchez, S., Sanz, M. L., Martinez-Castro, I. (2011). Derivatization of carbohydrates for GC and GC-MS analyses. *J. Chromatogr. B: Anal. Technol. Biomed. Life Sci.* 879, 1226-1240.
- Russell, W. R., Scobbie, L., Chesson, A. (2005). Structural modification of phenylpropanoid-derived compounds and the effects on their participation in redox processes. *Bioorg. Med. Chem.* 13, 2537-2546.
- Sanchez, J. I., Marzorati, M., Grootaert, C., Baran, M., Craeyveld, V. V., Courtin, C. M., et al. (2009). Arabinoxylan-oligosaccharides (AXOS) affect the protein/carbohydrate fermentation balance and microbial population dynamics of the Simulator of Human Intestinal Microbial Ecosystem. *Microb. Biotech.* 2, 101-113.
- Sasayama, D., Azuma, T., Itoh, K. (2011). Involvement of cell wall-bound phenolic acids in decrease in cell wall susceptibility to expansins during the cessation of rapid growth in internodes of floating rice. *J. Plant Physiol.* 168, 121-127.

- Saulnier, L., Mestres, C., Doublier, J. L., Roger, P., Thibault, J. F. (1993). Studies of polysaccharides solubilized during alkaline cooking of maize kernels. *J. Cereal Sci.* 17, 267-276.
- Saulnier, L., Marot, C., Chanliaud, E., Thibault, J. F. (1995a). Cell wall polysaccharide interactions in maize bran. *Carbohydr. Polym.* 26, 279-287.
- Saulnier, L., Peneau, N., Thibault, J. F. (1995b). Variability in grain extract viscosity and water-soluble arabinoxylan content in wheat. *J. Cereal Sci.* 22, 259-264.
- Saulnier, L., Vigouroux, J., Thibault, J.-F. (1995c). Isolation and partial characterization of feruloylated oligosaccharides from maize bran. *Carbohydr. Res.* 272, 241-253.
- Saulnier, L., Crepeau, M. J., Lahaye, M., Thibault, J. F., Garcia-Conesa, M. T., Kroon, P. A., et al. (1999). Isolation and structural determination of two 5,5'-diferuloyl oligosaccharides indicate that maize heteroxylans are covalently cross-linked by oxidatively coupled ferulates. *Carbohydr. Res.* 320, 82-92.
- Saulnier, L., Sado, P.-E., Branlard, G., Charmet, G., Guillon, F. (2007). Wheat arabinoxylans: Exploiting variation in amount and composition to develop enhanced varieties. *J. Cereal Sci.* 46, 261-281.
- Saulnier, L., Quemener, B., Enzymatic mapping of arabinoxylan structure. In *HEALTHGRAIN Methods: Analysis of Bioactive Components in Small Grain Cereals*, Shewry, P. R.; Ward, J. L., Eds. AACC International Incorporated: Minneapolis, Minnesota, USA, 2010.
- Saulnier, L., Guillon, F., Chateigner-Boutin, A.-L. (2012). Cell wall deposition and metabolism in wheat grain. *J. Cereal Sci.* 56, 91-108.
- Schatz, P. F., Ralph, J., Lu, F., Guzei, I. A., Bunzel, M. (2006). Synthesis and identification of 2,5-bis-(4-hydroxy-3-methoxyphenyl)-tetrahydrofuran-3,4-dicarboxylic acid, an unanticipated ferulate 8-8-coupling product acylating cereal plant cell walls. *Org. Biomol. Chem.* 44, 2801-2806.
- Schatzkin, A., Mouw, T., Park, Y., Subar, A. F., Kipnis, V., Hollenbeck, A., et al. (2007). Dietary fiber and whole-grain consumption in relation to colorectal cancer in the NIH-AARP Diet and Health Study. *Am. J. Clin. Nutr.* 85, 1353-1360.
- Scheller, H. V., Ulvskov, P. (2010). Hemicelluloses. *Annu. Rev. Plant Biol.* 61, 263-289.

- Schooneveld-Bergmans, M. E. F., Beldman, G., Voragen, A. G. J. (1999). Structural features of (glucurono)arabinoxylans extracted from wheat bran by barium hydroxide. *J. Cereal Sci.* 29, 63-75.
- Selig, M. J., Adney, W. S., Himmel, M. E., Decker, S. R. (2009). The impact of cell wall acetylation on corn stover hydrolysis by cellulolytic and xylanolytic enzymes. *Cellulose* 16, 711-722.
- Selig, M. J., Thygesen, L. G., Felby, C., Master, E. R. (2015). Debranching of soluble wheat arabinoxylan dramatically enhances recalcitrant binding to cellulose. *Biotechnol. Lett.* 37, 633-641.
- Selvendran, R. R., March, J. F., Ring, S. G. (1979). Determination of aldoses and uronic acid content of vegetable fiber. *Anal. Biochem.* 96, 282-292.
- Shewry, P. R., Piironen, V., Lampi, A.-M., Edelman, M., Kariluoto, S., Nurmi, T., et al. (2010). Effects of genotype and environment on the content and composition of phytochemicals and dietary fiber components in rye in the HEALTHGRAIN diversity screen. *J. Agric. Food Chem.* 58, 9372-9383.
- Shibuya, N., Misaki, A., Iwasaki, T. (1983). The structure of arabinoxylan and arabinoglucuronoxylan isolated from rice endosperm cell wall. *Agric. Biol. Chem.* 47, 2223-2230.
- Shibuya, N., Iwasaki, T. (1985). Structural features of rice bran hemicellulose. *Phytochemistry* 24, 285-289.
- Shiiba, K., Yamada, H., Hara, H., Okada, K., Nagao, S. (1993). Purification and characterization of two arabinoxylans from wheat bran. *Cereal Chem.* 70, 209-214.
- Snelders, J., Dornez, E., Delcour, J. A., Courtin, C. M. (2013). Ferulic acid content and appearance determine the antioxidant capacity of arabinoxylanoligosaccharides. *J. Agric. Food Chem.* 61, 10173-10182.
- Snelders, J., Dornez, E., Delcour, J. A., Courtin, C. M. (2014a). Impact of wheat bran derived arabinoxylanoligosaccharides and associated ferulic acid on dough and bread properties. *J. Agric. Food Chem.* 62, 7190-7199.

- Snelders, J., Olaerts, H., Dornez, E., Van de Wiele, T., Aura, A.-M., Vanhaecke, L., et al. (2014b). Structural features and feruloylation modulate the fermentability and evolution of antioxidant properties of arabinoxylanoligosaccharides during *in vitro* fermentation by human gut derived microbiota. *J. Funct. Foods* 10, 1-12.
- Søgaard, C., Stenbæk, A., Bernard, S., Hadi, M., Driouich, A., Scheller, H. V., et al. (2012). GO-PROMTO illuminates protein membrane topologies of glycan biosynthetic enzymes in the Golgi apparatus of living tissues. *PLoS ONE* 7, e31324.
- Sørensen, H. R., Pedersen, S., Meyer, A. S. (2007). Characterization of solubilized arabinoxylo-oligosaccharides by MALDI-TOF MS analysis to unravel and direct enzyme catalyzed hydrolysis of insoluble wheat arabinoxylan. *Enzyme Microb. Technol.* 41, 103-110.
- Steinhart, H., Bunzel, M. (2003). Separation techniques in structural analysis of dietary fiber polysaccharides. *Chromatographia* 57, Suppl., S359-S361.
- Supelco (1997). Amberlite XAD-2 polymeric adsorbent. Product specification. Sigma-Aldrich Co.
- Sweet, D. P., Shapiro, R. H., Albersheim, P. (1975). Quantitative analysis by various GLC response-factor theories for partially methylated and partially ethylated alditol acetates. *Carbohydr. Res.* 40, 217-225.
- Szwajgier, D., Pielecki, J., Targonski, Z. (2005). The release of ferulic acid and feruloylated oligosaccharides during wort and beer production. *J. Inst. Brew.* 111, 372-379.
- Szwajgier, D., Wasko, A., Zapp, J., Targonski, Z. (2007). An attempt to identify the low molecular feruloylated oligosaccharides in beer. *J. Inst. Brew.* 113, 185-195.
- Tian, L., Gruppen, H., Schols, H. A. (2015). Characterization of (glucurono)arabinoxylans from oats using enzymatic fingerprinting. *J. Agric. Food Chem.* 63, 10822-10830.
- Tomás-Barberán, F. A., Blázquez, M. A., Garcia-Viguera, C., Ferreres, F., Tomás-Lorente, F. (1992). A comparative study of different Amberlite XAD resins in flavonoid analysis. *Phytochem. Anal.* 3, 178-181.
- Tong, X., Lange, L., Grell, M. N., Busk, P. K. (2015). Hydrolysis of wheat arabinoxylan by two acetyl xylan esterases from *Chaetomium thermophilum*. *Appl. Biochem. Biotechnol.* 175, 1139-1152.

- Toole, G. A., Le Gall, G., Colquhoun, I. J., Drea, S., Opanowicz, M., Bedo, Z., et al. (2012). Spectroscopic analysis of diversity in the spatial distribution of arabinoxylan structures in endosperm cell walls of cereal species in the HEALTHGRAIN diversity collection. *J. Cereal Sci.* 56, 134-141.
- Topping, D. (2007). Cereal complex carbohydrates and their contribution to human health. *J. Cereal Sci.* 46, 220-229.
- Vaidyanathan, S., Bunzel, M. (2012). Development and application of a methodology to determine free ferulic acid and ferulic acid ester-linked to different types of carbohydrates in cereal products. *Cereal Chem.* 89, 247-254.
- Van den Abbeele, P., Venema, K., Van de Wiele, T., Verstraete, W., Possemiers, S. (2013). Different human gut models reveal the distinct fermentation patterns of arabinoxylan versus inulin. *J. Agric. Food Chem.* 61, 9819-9827.
- Van Dongen, F. E. M., Van Eylen, D., Kabel, M. A. (2011). Characterization of substituents in xylans from corn cobs and stover. *Carbohydr. Polym.* 86, 722-731.
- Van Eylen, D., van Dongen, F., Kabel, M., de Bont, J. (2011). Corn fiber, cobs and stover: Enzyme-aided saccharification and co-fermentation after dilute acid pretreatment. *Bioresour. Technol.* 102, 5995-6004.
- Vanbeneden, N., Gils, F., Delvaux, F., Delvaux, F. R. (2007). Variability in the release of free and bound hydroxycinnamic acids from diverse malted barley (*Hordeum vulgare* L.) cultivars during wort production. *J. Agric. Food Chem.* 55, 11002-11010.
- Vanbeneden, N., Van Roey, T., Willems, F., Delvaux, F., Delvaux, F. R. (2008). Release of phenolic flavour precursors during wort production: Influence of process parameters and grist composition on ferulic acid release during brewing. *Food Chem.* 111, 83-91.
- Vanhamel, S., Cleemput, G., Delcour, J. A., Nys, M., Darius, P. L. (1993). Physicochemical and functional properties of rye nonstarch polysaccharides. IV. The effect of high molecular weight water-soluble pentosans on wheat-bread quality in a straight-dough procedure. *Cereal Chem.* 70, 306-311.
- Veličković, D., Ropartz, D., Guillon, F., Saulnier, L., Rogniaux, H. (2014). New insights into the structural and spatial variability of cell-wall polysaccharides during wheat grain development, as revealed through MALDI mass spectrometry imaging. *J. Exp. Bot.* 65, 2079-2091.

- Verbruggen, M. A., Beldman, G., Voragen, A. G. J., Hollemans, M. (1993). Water-unextractable cell wall material from sorghum: Isolation and characterization. *J. Cereal Sci.* 17, 71-82.
- Verbruggen, M. A., Beldman, G., Voragen, A. G. J. (1995). The selective extraction of glucuronoarabinoxylans from sorghum endosperm cell walls using barium and potassium hydroxide solutions. *J. Cereal Sci.* 21, 271-282.
- Verbruggen, M. A., Spronk, B. A., Schols, H. A., Beldman, G., Voragen, A. G., Thomas, J. R., et al. (1998). Structures of enzymically derived oligosaccharides from sorghum glucuronoarabinoxylan. *Carbohydr. Res.* 306, 265-74.
- Verwimp, T., Van Craeyveld, V., Courtin, C. M., Delcour, J. A. (2007). Variability in the structure of rye flour alkali-extractable arabinoxylans. *J. Agric. Food Chem.* 55, 1985-1992.
- Verwimp, T., Courtin, C. M., Delcour, J. A., Rye Constituents and Their Impact on Rye Processing. In *Food Biochemistry and Food Processing*, Wiley-Blackwell: 2012; pp 654-672.
- Viëtor, R. J., Angelino, S. A. G. F., Voragen, A. G. J. (1992). Structural features of arabinoxylans from barley and malt cell wall material. *J. Cereal Sci.* 15, 213-222.
- Viëtor, R. J., Hoffmann, R. A., Angelino, S. A. G. F., Voragen, A. G. J., Kamerling, J. P., Vliegthart, J. F. G. (1994a). Structures of small oligomers liberated from barley arabinoxylans by endoxylanase from *Aspergillus awamori*. *Carbohydr. Res.* 254, 245-255.
- Viëtor, R. J., Kormelink, F. J. M., Angelino, S. A. G. F., Voragen, A. G. J. (1994b). Substitution patterns of water-unextractable arabinoxylans from barley and malt. *Carbohydr. Polym.* 24, 113-118.
- Vinkx, C. J. A., Reynaert, H. R., Grobet, P. J., Delcour, J. A. (1993). Physicochemical and functional properties of rye nonstarch polysaccharides. V. Variability in the structure of water-soluble arabinoxylans. *Cereal Chem.* 70, 311-317.
- Vinkx, C. J. A., Delcour, J. A., Verbruggen, M. A., Gruppen, H. (1995a). Rye water-soluble arabinoxylans also vary in their 2-monosubstituted xylose content. *Cereal Chem.* 72, 227-228.

- Vinkx, C. J. A., Stevens, I., Gruppen, H., Grobet, P. J., Delcour, J. A. (1995b). Physicochemical and functional properties of rye nonstarch polysaccharides. VI. Variability in the structure of water-unextractable arabinoxylans. *Cereal Chem.* 72, 411-418.
- Vinkx, C. J. A., Delcour, J. A. (1996). Rye (*Secale cereale* L) arabinoxylans: A critical review. *J. Cereal Sci.* 24, 1-14.
- Virkki, L., Johansson, L., Ylinen, M., Maunu, S., Ekholm, P. (2005). Structural characterization of water-insoluble nonstarchy polysaccharides of oats and barley. *Carbohydr. Polym.* 59, 357-366.
- Vismeh, R., Humpala, J. F., Chundawat, S. P. S., Balan, V., Dale, B. E., Jones, A. D. (2013). Profiling of soluble neutral oligosaccharides from treated biomass using solid phase extraction and LC-TOF MS. *Carbohydr. Polym.* 94, 791-799.
- Vitaglione, P., Napolitano, A., Fogliano, V. (2008). Cereal dietary fibre: a natural functional ingredient to deliver phenolic compounds into the gut. *Trends Food Sci. Technol.* 19, 451-463.
- Vogel, J. (2008). Unique aspects of the grass cell wall. *Curr. Op. Plant Biol.* 11, 301–307.
- Voragen, A. G. J., Schols, H. A., Pilnik, W. (1986). Determination of the degree of methylation and acetylation of pectins by h.p.l.c. *Food Hydrocolloids* 1, 65-70.
- Voragen, A. G. J., Schols, H. A., Marijs, J., Rombouts, F. M., Angelino, S. A. G. F. (1987). Non-starch polysaccharides from barley: Structural features and breakdown during malting. *J. Inst. Brew.* 93, 202-208.
- Vuletić, M., Hadži-Tašković Šukalović, V., Marković, K., Kravić, N., Vučinić, Ž., Maksimović, V. (2014). Differential response of antioxidative systems of maize (*Zea mays* L.) roots cell walls to osmotic and heavy metal stress. *Plant Biology* 16, 88-96.
- Wagoner, P., Schauer, A., Intermediate wheatgrass as a perennial grain crop. In *Advances in new crops*, Janick, J.; Simon, J. E., Eds. Timber Press: Portland, OR, 1990; pp 143-145.
- Wallace, J. S. (2000). Increasing agricultural water use efficiency to meet future food production. *Agric. Ecosyst. Environ.* 82, 105-119.

- Wang, Y., Azhar, S., Lindström, M. E., Henriksson, G. (2015). Stabilization of polysaccharides during alkaline pre-treatment of wood combined with enzyme-supported extractions in a biorefinery. *J. Wood Chem. Technol.* 35, 91-101.
- Wefers, D., Tyl, C., Bunzel, M. (2014). Novel arabinan and galactan oligosaccharides from dicotyledonous plants. *Front. Chem.* 2, 100.
- Wefers, D., Tyl, C. E., Bunzel, M. (2015). Neutral pectin side chains of amaranth (*Amaranthus hypochondriacus*) contain long, partially branched arabinans and short galactans, both with terminal arabinopyranoses. *J. Agric. Food Chem.* 63, 707-715.
- Wende, G., Fry, S. C. (1997). 2-O- $\beta$ -D-xylopyranosyl-(5-O-feruloyl)-L-arabinose, a widespread component of grass cell walls. *Phytochemistry* 44, 1019-1030.
- Westerlund, E., Andersson, R., Åman, P. (1993). Isolation and chemical characterization of water-soluble mixed-linked  $\beta$ -glucans and arabinoxylans in oat milling fractions. *Carbohydr. Polym.* 20, 115-123.
- Westphal, Y., Schols, H. A., Voragen, A. G. J., Gruppen, H. (2010). Introducing porous graphitized carbon liquid chromatography with evaporative light scattering and mass spectrometry detection into cell wall oligosaccharide analysis. *J. Chromatogr. A* 1217, 689-695.
- Willis, R. B., Montgomery, M. E., Allen, P. R. (1996). Improved method for manual, colorimetric determination of total Kjeldahl nitrogen using salicylate. *J. Agric. Food Chem.* 44, 1804-1807.
- Withers, S., Lu, F., Kim, H., Zhu, Y., Ralph, J., Wilkerson, C. G. (2012). Identification of grass-specific enzyme that acylates monolignols with *p*-coumarate. *J. Biol. Chem.* 287, 8347-8355.
- Wood, T. M., McCrae, S. I. (1996). Arabinoxylan-degrading enzyme system of the fungus *Aspergillus awamori*: purification and properties of an  $\alpha$ -L-arabinofuranosidase. *Appl. Microbiol. Biotechnol.* 45, 538-545.
- Yang, J.-G., Maldonado-Gómez, M. X., Hutkins, R. W., Rose, D. J. (2013). Production and in vitro fermentation of soluble, non-digestible, feruloylated oligo- and polysaccharides from maize and wheat brans. *J. Agric. Food Chem.* 62, 159-166.

- Yoshida-Shimokawa, T., Yoshida, S., Kakegawa, K., Ishii, T. (2001). Enzymic feruloylation of arabinoxylan-trisaccharide by feruloyl-CoA: arabinoxylan-trisaccharide O-hydroxycinnamoyl transferase from *Oryza sativa*. *Planta* 212, 470-474.
- Zaia, J. (2004). Mass spectrometry of oligosaccharides. *Mass Spectrom. Rev.* 23, 161-227.
- Zeng, W., Jiang, N., Nadella, R., Killen, T. L., Nadella, V., Faik, A. (2010). A glucurono(arabino)xylan synthase complex from wheat contains members of the GT43, GT47, and GT75 families and functions cooperatively. *Plant Physiol.* 154, 78-97.
- Zhang, J., Tang, M., Viikari, L. (2012). Xylans inhibit enzymatic hydrolysis of lignocellulosic materials by cellulases. *Bioresour. Technol.* 121, 8-12.
- Zhang, Q., Hrmova, M., Shirley, Neil J., Lahnstein, J., Fincher, Geoffrey B. (2006). Gene expression patterns and catalytic properties of UDP-D-glucose 4-epimerases from barley (*Hordeum vulgare* L.). *Biochem. J.* 394, 115-124.
- Zhang, Q., Shirley, N. J., Burton, R. A., Lahnstein, J., Hrmova, M., Fincher, G. B. (2010). The genetics, transcriptional profiles, and catalytic properties of UDP- $\alpha$ -D-xylose 4-epimerases from barley. *Plant Physiol.* 153, 555-568.
- Zhang, Z., Smith, C., Li, W. (2014). Extraction and modification technology of arabinoxylans from cereal by-products: A critical review. *Food Res. Int.* 65, 423-436.

# 12. Appendices

## 12.1. Instruments

<b>Instrument</b>	<b>Description</b>	<b>Manufacturer</b>
<i>GC-FID</i>	AOC-20i autosampler GC-2010 Plus column oven and FID detector	<b>Shimadzu</b> , Duisburg, Germany
<i>GC-MS</i>	GC-MS QP2010 Ultra system AOC-20i autosampler GC-2010 Plus column oven EI ion source GCMS QP2010 Ultra MS detector	<b>Shimadzu</b>
<i>GC-MS</i>	GC-MS QP2010 SE system AOC-20i autosampler GC-2010 Plus column oven EI ion source GCMS QP2010 SE MS detector	<b>Shimadzu</b>
<i>HPLC-PAD</i>	Thermo Scientific Dionex ICS-5000 system Dionex ICS-5000 dual pump AS-AP autosampler ICS-5000 DC electrochemical (PAD) detector	<b>Thermo Scientific</b> , Waltham, Massachusetts, USA
<i>HPLC, analytical</i>	SIL-20AC autosampler Three LC-20AT pumps DGU-20A3 degasser SPD-M20A DAD detector	<b>Shimadzu</b>
<i>HPLC, preparative</i>	Two LC-8A pumps Manual injection SPD-20A UV-Vis detector Manual fraction collection	<b>Shimadzu</b>
<i>HPLC, analytical, used on a semi-preparative scale</i>	Hitachi L-7100 pump Systec vacuum degasser Manual injection LaChrom RI-detector L-7490 BFO-04 SV column oven	<b>Hitachi</b> , Tokyo, Japan <b>IDEX Health &amp; Science</b> , Lake Forest, Illinois, USA – <b>Hitachi</b> <b>W.O. Electronics</b> , Langenzersdorf, Austria
<i>LC-DAD/MS</i>	Finnigan Surveyor Plus autosampler Finnigan Surveyor Plus pump Finnigan Surveyor Plus DAD detector LXQ linear ion trap MS <sup>n</sup> detector	<b>Thermo Scientific</b>

<b>Instrument</b>	<b>Description</b>	<b>Manufacturer</b>
<i>LC-MS, used only for analysis of non-feruloylated oligosaccharides</i>	Pump: Waters 2690 Separations Module	<b>Waters</b> , Milford, Massachusetts, USA
	Autosampler: Waters 2690 Separations Module	
	Micromass Quattro Micro tandem quadrupole mass spectrometer	<b>W.O. Electronics</b>
	BFO-04 SV column oven	
<i>NMR-Spectrometer (Minnesota NMR Center)</i>	Bruker Ultrashield 700 MHz 5 mm TXI cryoprobe	<b>Bruker</b> , Rheinstetten, Germany
<i>NMR-Spectrometer (KIT)</i>	Bruker Ascend TM 500 MHz	<b>Bruker</b>
<i>Size-exclusion chromatography / gel chromatography (Sephadex LH-20)</i>	Sephadex LH-20 column material (100 × 2.5 cm) packed in an empty column	Column: <b>GE Healthcare Life Sciences</b> , Pittsburgh, Pennsylvania, USA Column packing material (Sephadex LH-20): <b>Sigma</b>
	Jasco 880 pump	<b>Jasco Analytical Instruments</b> , Easton, Maryland, USA
	Phenomenex Degassex D6-4400	<b>Phenomenex</b> , Aschaffenburg, Germany
	FC 204 fraction collector	<b>Gilson</b> , Middleton, Wisconsin, USA
	K2600 UV detector	<b>Knauer</b> , Berlin, Germany
<i>Size-exclusion chromatography / gel chromatography (Bio-Gel P-2)</i>	Bio-Gel P-2 column material (100 × 2.5 cm) packed in a XK 16/20 empty column with cooling jacket	Column: <b>GE Healthcare Life Sciences</b> Column packing material (Bio-Gel P-2): <b>Bio-Rad</b> , Hercules, California, USA
	Julabo VC waterbath/thermostat	<b>Julabo GmbH</b> , Seelbach, Germany
	K-500 Pump	<b>Knauer</b>
	Degasser	<b>Knauer</b>
	Advantec SF-2120 Super Fraction Collector	<b>Advantec MFS, Inc</b> , Dublin, California, USA
	Smartline RI Detector 2300	<b>Knauer</b>
	<i>UV-Vis-Spectrophotometer</i>	Jasco V-550

## 12.2. Chemicals

Chemical name, purity	CAS number	Hazard symbols		Manufacturer
		Hazard (H) statements		
		Other EU hazard (EUH) statements		
		Precautionary (P) statements		
Acetic acid (CH <sub>3</sub> COOH), 100%, p.a.	64-19-7	 		Roth
		<p>H226: Flammable liquid and vapour.            H314: Causes severe skin burns and eye damage.            P280: Wear protective gloves/ protective clothing/ eye protection/ face protection.            P305 + P351 + P338 IF IN EYES: Rinse cautiously with water for several minutes. Remove contact lenses, if present and easy to do. Continue rinsing.            P310: Immediately call a POISON CENTER or doctor/physician.</p>		
Acetic anhydride ((CH <sub>3</sub> CO) <sub>2</sub> O), ≥99%	108-24-7	  		Roth
		<p>H226: Flammable liquid and vapour.            H302: Harmful if swallowed.            H314: Causes severe skin burns and eye damage.            H331: Toxic if inhaled.            P261: Avoid breathing dust/ fume/ gas/ mist/ vapours/ spray.            P280 :Wear protective gloves/ protective clothing/ eye protection/ face protection.            P303 + P361 + P353 IF ON SKIN (or hair): Take off immediately all contaminated clothing. Rinse skin with water/shower.            P304 + P340 + P310: IF INHALED: Remove person to fresh air and keep comfortable for breathing. Immediately call a POISON CENTER or doctor/ physician.            P305 + P351 + P338: IF IN EYES: Rinse cautiously with water for several minutes. Remove contact lenses, if present and easy to do. Continue rinsing.            P403 + P233: Store in a well-ventilated place. Keep container tightly closed.</p>		
Acetone ((CH <sub>3</sub> ) <sub>2</sub> CO), ≥99.8%	67-64-1	 		VWR
Acetone-d <sub>6</sub> , ≥99.80% D (≤0.02% H <sub>2</sub> O)	666-52-4			VWR
		<p>H225: Highly flammable liquid and vapour.            H319: Causes serious eye irritation.            H336: May cause drowsiness or dizziness.            EUH066: Repeated exposure may cause skin dryness or cracking.            P210: Keep away from heat/sparks/open flames/hot surfaces. — No smoking.            P261: Avoid breathing dust/fume/gas/mist/vapours/spray.            P305 + P351 + P338: IF IN EYES: Rinse cautiously with water for several minutes. Remove contact lenses if present and easy to do — continue rinsing.</p>		
Acetonitrile, 99.9%	75-05-8	 		VWR
		<p>H225: Highly flammable liquid and vapour.            H302+H312+H332: Harmful if swallowed, in contact with skin or if inhaled.            H319: Causes serious eye irritation.</p>		

Chemical name, purity	CAS number	Hazard symbols	Manufacturer
		Hazard (H) statements Other EU hazard (EUH) statements Precautionary (P) statements	
		<p>P210: Keep away from heat/sparks/open flames/hot surfaces. — No smoking.</p> <p>P280: Wear protective gloves/protective clothing/eye protection/face protection.</p> <p>P305 + P351 + P338: IF IN EYES: Rinse cautiously with water for several minutes. Remove contact lenses if present and easy to do — continue rinsing.</p>	
Ammonium chloride, ≥99.5 %	12125-02-9	 <p>H302: Harmful if swallowed.</p> <p>H319: Causes serious eye irritation.</p> <p>P305 + P351 + P338: IF IN EYES: Rinse cautiously with water for several minutes. Remove contact lenses, if present and easy to do. Continue rinsing.</p>	Roth
L-(+)-Arabinose, ≥99 %	5328-37-0	None	Sigma
D-(–)-Arabinose, ≥98 %	10323-20-3		Sigma
N,O-Bis-(trimethylsilyl)-trifluoroacetamide (BSTFA), ≥99.0%	25561-30-2	  <p>H226: Flammable liquid and vapour.</p> <p>H314: Causes severe skin burns and eye damage.</p> <p>P280: Wear protective gloves/ protective clothing/ eye protection/ face protection.</p> <p>P305 + P351 + P338: IF IN EYES: Rinse cautiously with water for several minutes. Remove contact lenses, if present and easy to do. Continue rinsing.</p> <p>P310: Immediately call a POISON CENTER or doctor/ physician.</p>	Fluka
tert-Butyl alcohol, 99%	75-65-0	  <p>H225: Highly flammable liquid and vapour.</p> <p>H319: Causes serious eye irritation.</p> <p>H332: Harmful if inhaled.</p> <p>H335: May cause respiratory irritation.</p> <p>H336: May cause drowsiness or dizziness.</p> <p>P210: Keep away from heat, hot surfaces, sparks, open flames and other ignition sources. No smoking.</p> <p>P261: Avoid breathing dust/ fume/ gas/ mist/ vapours/ spray.</p> <p>P305 + P351 + P338: IF IN EYES: Rinse cautiously with water for several minutes. Remove contact lenses, if present and easy to do. Continue rinsing.</p> <p>P370 + P378: In case of fire: Use dry powder or dry sand to extinguish.</p> <p>P403 + P235: Store in a well-ventilated place. Keep cool.</p>	Merck
Caffeic acid, 97%	501-16-6	  <p>H319: Causes serious eye irritation.</p>	Fluka

Chemical name, purity	CAS number	Hazard symbols		Manufacturer
		Hazard (H) statements		
		Other EU hazard (EUH) statements		
		Precautionary (P) statements		
			<p>H351: Suspected of causing cancer.            P281: Use personal protective equipment as required.            P305 + P351 + P338: IF IN EYES: Rinse cautiously with water for several minutes. Remove contact lenses, if present and easy to do. Continue rinsing.</p>	
Caffeine, ≥98.5%	58-08-2		<p>H302: Harmful if swallowed.</p>	Roth
<i>trans-ortho-</i> Coumaric acid, ≥97%	614-60-8		<p>H301: Toxic if swallowed.            H315: Causes skin irritation.            H319: Causes serious eye irritation.            H335: May cause respiratory irritation.            P261: Avoid breathing dust/ fume/ gas/ mist/ vapours/ spray.            P301 + P310: IF SWALLOWED: Immediately call a POISON CENTER or doctor/physician.            P305 + P351 + P338: IF IN EYES: Rinse cautiously with water for several minutes. Remove contact lenses, if present and easy to do. Continue rinsing.</p>	Aldrich
<i>trans-para-</i> Coumaric acid, ≥98%	501-98-4		<p>H315: Causes skin irritation.            H319: Causes serious eye irritation.            H335: May cause respiratory irritation.            P261: Avoid breathing dust/ fume/ gas/ mist/ vapours/ spray.            P305 + P351 + P338: IF IN EYES: Rinse cautiously with water for several minutes. Remove contact lenses, if present and easy to do. Continue rinsing.</p>	Sigma
Deuterium oxide, 99.9%	7789-20-0	None		Deutero GmbH
Diethyl ether, 99.5%	60-29-7	 	<p>H224: Extremely flammable liquid and vapour.            H302: Harmful if swallowed.            H336: May cause drowsiness or dizziness.            EUH019: May form explosive peroxides.            EUH066: Repeated exposure may cause skin dryness or cracking.            P210: Keep away from heat, hot surfaces, sparks, open flames and other ignition sources. No smoking.            P261: Avoid breathing vapours.</p>	Roth
Dichloro-methane, 99.9%	75-09-2	 	<p>H315: Causes skin irritation.            H319: Causes serious eye irritation.            H335: May cause respiratory irritation.            H336: May cause drowsiness or dizziness.            H351: Suspected of causing cancer.            H373: May cause damage to organs (Liver, Blood, Central nervous system) through prolonged or repeated exposure.</p>	VWR

Chemical name, purity	CAS number	Hazard symbols		Manufacturer
		Hazard (H) statements		
		Other EU hazard (EUH) statements		
		Precautionary (P) statements		
		P261: Avoid breathing vapours. P281: Use personal protective equipment as required. P305 + P351 + P338: IF IN EYES: Rinse cautiously with water for several minutes. Remove contact lenses, if present and easy to do. Continue rinsing.		
Dimethyl sulfoxide, ≥99.8%	67-68-5	None		Roth
Dimethyl sulfoxide- <i>d</i> <sub>6</sub> , ≥99.9%	2206-27-1	None		Sigma Aldrich
Disodium phosphate, anhydrous (Na <sub>2</sub> HPO <sub>4</sub> ), ≥99%	7558-79-4	None		Roth
Ethanol, ≥96%, denatured with 1% methyl ethyl ketone	None			Roth
		H225: Highly flammable liquid and vapour. H302: Harmful if swallowed. H319: Causes serious eye irritation. H371: May cause damage to organs. H411: Toxic to aquatic life with long lasting effects. P210: Keep away from heat, hot surfaces, sparks, open flames and other ignition sources. No smoking. P260: Do not breathe dust/ fume/ gas/ mist/ vapours/ spray. P273: Avoid release to the environment. P280: Wear eye protection/ face protection. P308 + P311: IF exposed or concerned: Call a POISON CENTER or doctor/ physician. P337 + P313: If eye irritation persists: Get medical advice/ attention.		
Formic acid, 98-100%	64-18-6			Merck
		H226: Flammable liquid and vapour. H302: Harmful if swallowed. H314: Causes severe skin burns and eye damage. H331: Toxic if inhaled. EUH071: Corrosive to the respiratory tract. P210: Keep away from heat, hot surfaces, sparks, open flames and other ignition sources. No smoking. P280: Wear protective gloves/ protective clothing/ eye protection/ face protection. P303 + P361 + P353 IF ON SKIN (or hair): Take off immediately all contaminated clothing. Rinse skin with water/shower. P304 + P340 + P310 IF INHALED: Remove person to fresh air and keep comfortable for breathing. Immediately call a POISON CENTER or doctor/ physician. P305 + P351 + P338 IF IN EYES: Rinse cautiously with water for several minutes. Remove contact lenses, if present and easy to do. Continue rinsing.		

Chemical name, purity	CAS number	Hazard symbols		Manufacturer
		Hazard (H) statements Other EU hazard (EUH) statements Precautionary (P) statements		
			P403 + P233: Store in a well-ventilated place. Keep container tightly closed.	
<i>trans</i> -Ferulic acid, 99%	537-98-4		H315: Causes skin irritation. H319: Causes serious eye irritation. H335: May cause respiratory irritation. P261: Avoid breathing dust/ fume/ gas/ mist/ vapours/ spray. P305 + P351 + P338: IF IN EYES: Rinse cautiously with water for several minutes. Remove contact lenses, if present and easy to do. Continue rinsing.	Aldrich
<i>iso</i> -Ferulic acid, >98%	25522-33-2	None		Alfa-Aesar
D-(+)-Galactose, ≥99.0%	59-23-4	None		Sigma
D-(+)-Glucose, ≥99.5%	50-99-7	None		Sigma
Hydrochloric acid, 37%, p.a.	7647-01-0		H290: May be corrosive to metals. H314: Causes severe skin burns and eye damage. H335: May cause respiratory irritation. P261: Avoid breathing vapours. P280: Wear protective gloves/ protective clothing/ eye protection/ face protection. P305 + P351 + P338: IF IN EYES: Rinse cautiously with water for several minutes. Remove contact lenses, if present and easy to do. Continue rinsing. P310: Immediately call a POISON CENTER or doctor/ physician.	Roth
Kjeldahl catalyst according to Wieninger	None		H302: Harmful if swallowed. H410 :Very toxic to aquatic life with long lasting effects. P273: Avoid release to the environment. P501: Dispose of contents/ container to an approved waste disposal plant.	Fluka
Lithium chloride, ≥99%	7447-41-8		H302: Harmful if swallowed. H315: Causes skin irritation. H319: Causes serious eye irritation. H335: May cause respiratory irritation. P261: Avoid breathing dust. P305 + P351 + P338: IF IN EYES: Rinse cautiously with water for several minutes. Remove contact lenses, if present and easy to do. Continue rinsing.	Riedel-de-Haen
D-Mannitol, ≥99%	69-65-8	None		Sigma

Chemical name, purity	CAS number	Hazard symbols		Manufacturer
		Hazard (H) statements		
		Other EU hazard (EUH) statements		
		Precautionary (P) statements		
D-(+)-Mannose, ≥99.0%	3458-28-4	None		Sigma
Methanol, LC-MS and HPLC-grade	67-56-1			VWR
		<p>H225: Highly flammable liquid and vapour.  H301 + H311 + H331: Toxic if swallowed, in contact with skin or if inhaled.  H370: Causes damage to organs.  P210: Keep away from heat, hot surfaces, sparks, open flames and other ignition sources. No smoking.  P280: Wear protective gloves/ protective clothing.  P302 + P352 + P312: IF ON SKIN: Wash with plenty of water.  Call a POISON CENTER or doctor/ physician if you feel unwell.  P304 + P340 + P311: IF INHALED: Remove person to fresh air and keep comfortable for breathing. Call a POISON CENTER or doctor/ physician.  P370 + P378: In case of fire: Use dry powder or dry sand to extinguish.  P403 + P235: Store in a well-ventilated place. Keep cool.</p>		
1-Methylimidazole, ≥99%	616-47-7			Roth
		<p>H302: Harmful if swallowed.  H311: Toxic in contact with skin.  H314: Causes severe skin burns and eye damage.  P280: Wear protective gloves/ protective clothing/ eye protection/ face protection.  P301 + P312 + P330: IF SWALLOWED: Call a POISON CENTER or doctor/ physician if you feel unwell. Rinse mouth.  P303 + P361 + P353: IF ON SKIN (or hair): Take off immediately all contaminated clothing. Rinse skin with water/shower.  P304 + P340 + P310: IF INHALED: Remove person to fresh air and keep comfortable for breathing. Immediately call a POISON CENTER or doctor/ physician.  P305 + P351 + P338: IF IN EYES: Rinse cautiously with water for several minutes. Remove contact lenses, if present and easy to do. Continue rinsing.</p>		
Methyl iodide, ≥99%	74-88-4			Sigma
		<p>H301: Toxic if swallowed.  H312: Harmful in contact with skin.  H315: Causes skin irritation.  H331: Toxic if inhaled.  H335: May cause respiratory irritation.  H351: Suspected of causing cancer.  P261: Avoid breathing vapours.  P280: Wear protective gloves/ protective clothing.  P301 + P310: IF SWALLOWED: Immediately call a POISON CENTER or doctor/ physician.  P311: Call a POISON CENTER or doctor/ physician.</p>		

Chemical name, purity	CAS number	Hazard symbols		Manufacturer
		Hazard (H) statements		
		Other EU hazard (EUH) statements		
		Precautionary (P) statements		
Monosodium phosphate dihydrate (NaH <sub>2</sub> PO <sub>4</sub> • 2H <sub>2</sub> O), 99%	13472-35-0	None		Sigma-Aldrich
(R)-(-)-2-Octanol, 99%	5978-70-1			Sigma
		<p>H315: Causes skin irritation.  H319: Causes serious eye irritation.  H335: May cause respiratory irritation.  P261: Avoid breathing dust/ fume/ gas/ mist/ vapours/ spray.  P305 + P351 + P338: IF IN EYES: Rinse cautiously with water for several minutes. Remove contact lenses, if present and easy to do.  Continue rinsing.</p>		
Pyridine, 100%	110-86-1			VWR
		<p>H225: Highly flammable liquid and vapour.  H302 + H312 + H332: Harmful if swallowed, in contact with skin or if inhaled  H315: Causes skin irritation.  H319: Causes serious eye irritation.  P210: Keep away from heat, hot surfaces, sparks, open flames and other ignition sources. No smoking.  P280: Wear protective gloves/ protective clothing.  P305 + P351 + P338: IF IN EYES: Rinse cautiously with water for several minutes. Remove contact lenses, if present and easy to do.  Continue rinsing.</p>		
L-Rhamnose monohydrate, ≥99%	10030-85-0	None		Sigma
Sinapic acid, ≥98%	530-59-6			Fluka
		<p>H315: Causes skin irritation.  H319: Causes serious eye irritation.  H335: May cause respiratory irritation.  P261: Avoid breathing dust/ fume/ gas/ mist/ vapours/ spray.  P305 + P351 + P338: IF IN EYES: Rinse cautiously with water for several minutes. Remove contact lenses, if present and easy to do.  Continue rinsing.</p>		
Sodium acetate, ≥99%	127-09-3	None		Sigma-Aldrich
Sodium borodeuteride, 98% D	15681-89-7			Sigma
		<p>H260: In contact with water releases flammable gases which may ignite spontaneously.  H301: Toxic if swallowed.  H311: Toxic in contact with skin.  H314: Causes severe skin burns and eye damage.  P223: Keep away from any possible contact with water, because of</p>		

Chemical name, purity	CAS number	Hazard symbols		Manufacturer
		Hazard (H) statements		
		Other EU hazard (EUH) statements		
		Precautionary (P) statements		
		<p>violent reaction and possible flash fire.  P231 + P232: Handle under inert gas. Protect from moisture.  P280: Wear protective gloves/ protective clothing/ eye protection/ face protection.  P301 + P310: IF SWALLOWED: Immediately call a POISON CENTER or doctor/physician.  P370 + P378: In case of fire: Use dry sand, dry chemical or alcohol-resistant foam for extinction.  P422: Store contents under inert gas.</p>		
Sodium borohydride, 98%	16940-66-2		<p>H260: In contact with water releases flammable gases which may ignite spontaneously.  H301: Toxic if swallowed.  H314: Causes severe skin burns and eye damage.  H360F: May damage fertility.  EUH014: Reacts violently with water.  P201: Obtain special instructions before use.  P231 + P232: Handle under inert gas. Protect from moisture.  P280: Wear protective gloves/ protective clothing/ eye protection/ face protection.  P308 + P313: IF exposed or concerned: Get medical advice/ attention.  P370 + P378: In case of fire: Use dry powder or dry sand to extinguish.  P402 + P404: Store in a dry place. Store in a closed container.</p>	Sigma-Aldrich
Sodium hydroxide, solid pellets, 98%	1310-73-2		<p>H290: May be corrosive to metals.  H314: Causes severe skin burns and eye damage.  P280: Wear protective gloves/ protective clothing/ eye protection/ face protection.  P305 + P351 + P338: IF IN EYES: Rinse cautiously with water for several minutes. Remove contact lenses, if present and easy to do. Continue rinsing.  P310: Immediately call a POISON CENTER or doctor/ physician.</p>	Roth
Sodium hydroxide solution, 50-52% in water	None		<p>H290: May be corrosive to metals.  H314: Causes severe skin burns and eye damage.  P280: Wear protective gloves/ protective clothing/ eye protection/ face protection.  P303 + P361 + P353: IF ON SKIN (or hair): Take off immediately all contaminated clothing. Rinse skin with water/shower.  P304 + P340 + P310: IF INHALED: Remove person to fresh air and keep comfortable for breathing. Immediately call a POISON CENTER or doctor/ physician.  P305 + P351 + P338: IF IN EYES: Rinse cautiously with water for several minutes. Remove contact lenses, if present and easy to do. Continue rinsing.</p>	Sigma

Chemical name, purity	CAS number	Hazard symbols		Manufacturer
		Hazard (H) statements		
		Other EU hazard (EUH) statements		
		Precautionary (P) statements		
Sodium hypochlorite solution, ≥12% Cl	7681-52-9 (for NaClO)	 	<p>H314: Causes severe skin burns and eye damage.</p> <p>H400: Very toxic to aquatic life.</p> <p>P273: Avoid release to the environment.</p> <p>EUH031: Contact with acids liberates toxic gas.</p> <p>P280: Wear protective gloves/ protective clothing/ eye protection/ face protection.</p> <p>P305 + P351 + P338: IF IN EYES: Rinse cautiously with water for several minutes. Remove contact lenses, if present and easy to do. Continue rinsing.</p> <p>P310: Immediately call a POISON CENTER or doctor/ physician.</p>	Roth
Sodium salicylate, 99%	54-21-7		<p>H302: Harmful if swallowed.</p> <p>H319: Causes serious eye irritation.</p> <p>P305 + P351 + P338: IF IN EYES: Rinse cautiously with water for several minutes. Remove contact lenses, if present and easy to do. Continue rinsing.</p>	Fluka
Sodium nitroprusside dihydrate (Na <sub>2</sub> [Fe(CN) <sub>5</sub> N O] · 2 H <sub>2</sub> O), ≥99%	13755-38-9		<p>H301: Toxic if swallowed.</p> <p>P301 + P310: IF SWALLOWED: Immediately call a POISON CENTER or doctor/physician.</p>	Roth
Sodium thiosulfate, anhydrous, ≥99%	7772-98-7	none		Roth
Sulfuric acid (H <sub>2</sub> SO <sub>4</sub> ), 96%	7664-93-9		<p>H290: May be corrosive to metals.</p> <p>H314: Causes severe skin burns and eye damage.</p> <p>P280: Wear protective gloves/ protective clothing/ eye protection/ face protection.</p> <p>P305 + P351 + P338: IF IN EYES: Rinse cautiously with water for several minutes. Remove contact lenses, if present and easy to do. Continue rinsing.</p> <p>P310: Immediately call a POISON CENTER or doctor/ physician.</p>	VWR
Trifluoroacetic acid (CF <sub>3</sub> COOH), ≥99.8%	76-05-1	 	<p>H314: Causes severe skin burns and eye damage.</p> <p>H332: Harmful if inhaled.</p> <p>H412: Harmful to aquatic life with long lasting effects.</p> <p>P261: Avoid breathing dust/ fume/ gas/ mist/ vapours/ spray.</p> <p>P273: Avoid release to the environment.</p> <p>P280: Wear protective gloves/ protective clothing/ eye protection/ face protection.</p> <p>P303 + P361 + P353: IF ON SKIN (or hair): Take off immediately all contaminated clothing. Rinse skin with water/shower.</p>	Merck

Chemical name, purity	CAS number	Hazard symbols	Manufacturer
		Hazard (H) statements Other EU hazard (EUH) statements Precautionary (P) statements	
		P304 + P340 + P310 IF INHALED: Remove person to fresh air and keep comfortable for breathing. Immediately call a POISON CENTER or doctor/ physician. P305 + P351 + P338: IF IN EYES: Rinse cautiously with water for several minutes. Remove contact lenses, if present and easy to do. Continue rinsing.	
Trisodium phosphate •12 H <sub>2</sub> O, 98%	10101-89-0	 H315: Causes skin irritation. H319: Causes serious eye irritation. P305 + P351 + P338: IF IN EYES: Rinse cautiously with water for several minutes. Remove contact lenses, if present and easy to do. Continue rinsing.	Sigma Aldrich
D-(+)-Xylose, ≥99.0%	58-86-6	None	Sigma Aldrich
L-(-)-Xylose, ≥99%	609-06-03		Sigma

### 12.3. Enzymes

Enzyme name	Manufacturer	Activity	Source
$\alpha$ -Amylase (Termamyl 120 L)	Novozymes	$\geq 500$ units <sup>a</sup> /mg protein, $\geq 10$ mg protein/mL solution	<i>Bacillus globigii</i> ( <i>Bacillus licheniformis</i> ), Type XII-A
$\alpha$ -Amylase (Mats-L-Classic)	DSM	$\geq 8.150$ TAU <sup>b</sup> /g	
Amyloglucosidase (AMG 300L)	Novozymes	$\geq 300$ units <sup>c</sup> /mL solution	<i>Aspergillus niger</i>
Amyloglucosidase (Amigase Mega L)	DSM	$\geq 16000$ AGI <sup>d</sup> /g	
Driselase	Sigma	–	<i>Basidiomycetes</i> sp.
Protease (Alcalase 2.5L)	Novozymes	$\geq 2.4$ Anson units <sup>e</sup> /g	Proteinase from <i>Bacillus licheniformis</i> , Subtilisin A
Protease (Maxzyme NNP-DS)	DSM	$\geq 184000$ PCU <sup>f</sup> /g	<i>Bacillus amyloliquefaciens</i>
<i>endo</i> -1,4- $\beta$ -Xylanase (E-XYLATM)	Megazymes	3750 units <sup>g</sup> /mL	<i>Thermotoga maritima</i>
<i>endo</i> -1,4- $\beta$ -Xylanase (E-XYLNP)	Megazymes	10,000 units <sup>g</sup> /mL	<i>Neocallimastix patriciarum</i>

<sup>a</sup> One unit is defined as the amount of enzyme required to release 1.0 mg of maltose from starch in 3 min (pH 6.9, 20°C).

<sup>b</sup> Thermostable amylase units (TAU) are defined as the amount of enzyme which will convert under standardized conditions 1 mg of starch per minute into a product with an equal absorption to a reference color at 620 nm following reaction with iodine.

<sup>c</sup> One unit = the amount of enzyme capable of hydrolyzing 1  $\mu$ mol maltose per min in acetate buffer (pH 4.3) at 25°C.

<sup>d</sup> One unit of amyloglucosidase activity (AGI) is defined as the amount of enzyme that releases 1 pmole of glucose from soluble starch under defined conditions (pH 4.3, 60°C).

<sup>e</sup> Anson units (AU) are defined as the enzyme amount which, under defined conditions, “digests urea-denatured hemoglobin at an initial rate such that there is liberated an amount of TCA-soluble product per minute which gives the same color with Folin-Ciocalteu Phenol reagent as one milliequivalent of tyrosine at 25°C at pH 7.50.” (Source: Sigma-Aldrich website, accessed April 17, 2016: <http://www.sigmaaldrich.com/life-science/metabolomics/enzyme-explorer/analytical-enzymes/subtilisin.html>)

<sup>f</sup> PCU is a protease-specific activity unit defined as the amount of enzyme which, with a hydrolysis time of 1 min and under specific test conditions, produces a hydrolysate with the same absorbance at 275 nm as a tyrosine solution with the concentration 1.50  $\mu$ g/mL.

<sup>g</sup> One unit is defined as the amount of enzyme needed to release 1  $\mu$ mole of “xylose reducing-sugar equivalents per minute from wheat arabinoxylan (5 mg/mL) in sodium acetate buffer (100 mM) pH 5.0.” (Source: Megazyme).

## 12.4. Prepared reagents and solutions

Solution/reagent	Preparation
Ammonium chloride stock solution for protein measurement calibration (1000 mg N/L)	Dissolve 328 mg ammonium chloride in 100 mL pure water.
Caffeine in DMSO- <i>d</i> <sub>6</sub> , 4.407 mM (for quantitative NMR method)	Weigh in 85.6 mg caffeine. Bring up to 10 mL with pure water. Remove exactly 1 mL of this solution and transfer to a 15-mL Pyrex tube. Freeze, then freeze-dry. When dry, add exactly 10 mL DMSO- <i>d</i> <sub>6</sub> . Cap tightly.
Color reagent for colorimetric protein measurement	Weigh 3.2 g sodium salicylate, 18.54 g trisodium phosphate • 12 H <sub>2</sub> O, 0.05 g sodium nitroprusside into a 100 mL volumetric flask. Add pure water (not up to volume). Sonicate with heating (40-50°C) until dissolved (15-20 min). Cool to room temperature and bring up to volume.
Formic acid, 0.1%	In a fume hood, add 1 mL of formic acid to pure water and bring up to 1 L.
HCl solution, 0.325 M	Fill a 1 L volumetric flask partway full with pure water. In fume hood, add 15.625 mL concentrated HCl (37%). Bring up to 1 L.
HPAEC eluents	<b>Eluent 1:</b> Fill eluent bottle with 2 L deionized H <sub>2</sub> O. Degas with helium for 15 min. <b>Eluent 2:</b> Fill eluent bottle with 2 L deionized H <sub>2</sub> O. Degas with helium for 15 min.
1. Water	<b>Eluent 2:</b> Fill eluent bottle with 2 L deionized H <sub>2</sub> O. Degas with helium for 15 min.
2. 100 mM NaOH	Add 5.2 mL 50% NaOH solution (must use solution designated for ion chromatography).
3. 100 mM NaOH + 0.2 mM NaOAc	<b>Eluent 3:</b> Dissolve 16.4 g NaOAc in 1 L deionized H <sub>2</sub> O. Degas for 15 min. Add 5.2 mL 50% NaOH solution (must use solution designated for ion chromatography).
NaBH <sub>4</sub> in DMSO, 30 mg/mL	<u>Quickly</u> weigh 600 mg NaBH <sub>4</sub> into a large (25 mL) Pyrex vial. Cap tightly after weighing to prevent moisture absorption. Add 20 mL DMSO. Cap tightly. Sonicate (40°C) until dissolved (15-20 min). Prepare solution immediately before use—do not store.
NaOH solution, 0.275 M	Dissolve 11 g of NaOH pellets in pure water and bring up to 1 L.
NaOH solution, 2 M	Dissolve 40 g of NaOH pellets in pure water and bring up to 500 mL.
Sodium hypochlorite solution (0.25%)	Add 2.5 mL sodium hypochlorite solution (12.5%) to distilled H <sub>2</sub> O and bring up to 100 mL.
Sodium phosphate buffer, 0.08 M, pH 6.2	Prepare separate 0.8M solutions of NaH <sub>2</sub> PO <sub>4</sub> • 2 H <sub>2</sub> O and Na <sub>2</sub> HPO <sub>4</sub> . (For NaH <sub>2</sub> PO <sub>4</sub> • 2 H <sub>2</sub> O: Dissolve 12.48 g NaH <sub>2</sub> PO <sub>4</sub> • 2 H <sub>2</sub> O in pure water and bring up to 1 L.) (For Na <sub>2</sub> HPO <sub>4</sub> : Dissolve 11.36 g Na <sub>2</sub> HPO <sub>4</sub> in pure water and bring up to 1 L.) Mix two solutions to achieve pH 6.2 (approximately 81.5 mL NaH <sub>2</sub> PO <sub>4</sub> • 2 H <sub>2</sub> O solution + 19.5 mL Na <sub>2</sub> HPO <sub>4</sub> solution).
TFA solution, 1 mM	In fume hood, add 77 μL of TFA to pure water and bring up to 1 L.
TFA solution, 50 mM	Fill a 500 mL volumetric flask partway full with pure water. In fume hood, add 1.914 mL concentrated TFA. Bring up to 500 mL.
TFA solution, 2 M	Fill a 100 mL volumetric flask partway full with pure water. In fume hood, add 15.4 mL concentrated TFA. Bring up to 100 mL.

## 12.5. Experimental methods

### 12.5.1. Preparative isolation of insoluble dietary fiber from cereal grains

- Mill grains to 1 mm diameter.
- Wash with three volumes of acetone (200 g flour, 3 × 200 mL acetone). Dry.
- Mill acetone-washed flour to <0.5 mm diameter.
- Suspend 20 g flour in 200 mL phosphate buffer (0.08, pH 6.2). Add 1.5 mL thermostable  $\alpha$ -amylase (Termamyl 120 L, Novozymes).
- Incubate for 20 min at 92°C. Swirl flask every five minutes.
- Cool the sample to room temperature over ice and adjust pH to 7.5 with 0.275 M NaOH solution
- Add 700  $\mu$ L protease (Alcalase 2.5L, Novozymes).
- Incubate for 30 min at 60°C in a shaking water bath.
- Cool the sample to room temperature over ice and adjust pH to 4.5 with 0.325 M HCl.
- Add 700  $\mu$ L amyloglucosidase (AMG 300 L, Novozymes).
- Incubate for 30 min at 60°C in a shaking water bath.
- Centrifuge the warm solution for 15 min at 5000 rpm.
- Carefully decant off supernatant.
- Wash pellet with 2 × 100 mL and 1 × 50 mL warm water (60°C). Centrifuge after every wash and discard supernatant between washing steps.
- Wash pellet with 1 × 100 mL and 1 × 50 mL 96% EtOH. Centrifuge after every wash and discard supernatant between washing steps.
- Wash pellet with 1 × 100 mL and 1 × 50 mL acetone. Centrifuge after every wash and discard supernatant between washing steps.
- Dry residue overnight in a 60°C drying oven.

### 12.5.2. Drying isolated insoluble fiber samples

- Spread fiber samples in a thin layer in a shallow beaker. Cover with filter paper and fasten with a rubber band to prevent sample loss while pulling and releasing vacuum.
- Place in vacuum oven at 70°C and pull a vacuum of at least 90 mbar.
- Dry for 22 h or longer.
- Store dried samples in a desiccator. Use for all other analyses requiring insoluble fiber samples.

### 12.5.3. Methods for characterization of dietary fiber samples

#### 12.5.3.1. *Ash correction of insoluble fiber samples*

- Heat crucibles for ashing for >6 h in muffle furnace at 520°C. Cool to room temperature in a desiccator.
- Weigh at least 300 mg of completely dry insoluble fiber samples into crucibles. Record weight.
- Heat crucibles for 9 h at 520°C in muffle furnace.
- Remove from furnace, cool, and add 1 mL H<sub>2</sub>O<sub>2</sub> solution (30%).
- Return to furnace and heat for another 3 h.
- Remove from furnace overnight. If samples are still coal-black, continue ashing on next day until light gray or white in color.
- Remove from furnace, cool, and record weight.
- Clean crucibles with 4 M H<sub>2</sub>SO<sub>4</sub>. (Let stand overnight.)

#### 12.5.3.2. *Colorimetric protein correction of insoluble fiber samples*

- **NOTE:** For best results, prepare color reagent and 0.25% sodium hypochlorite solution on day of

analysis. Calibration must also be performed daily.

- Prepare solutions (ammonium chloride stock solution, color reagent, and 0.25% sodium hypochlorite solution). See **Section 12.4** for preparation methods for these solutions.
- Prepare calibration solutions according to **Table 20**. Bring indicated volume of stock solution up to 50 mL in a volumetric flask.

**Table 20. Preparation of calibration curve solutions for colorimetric quantification of nitrogen in Kjeldahl hydrolysates.**

Volume of 1000 mg/mL ammonium chloride stock solution, mL	0.2	0.6	1.0	1.4	1.8	2.0
Nitrogen concentration, mg/L	4	12	20	28	36	44

- Weigh 50 mg of completely dry insoluble fiber samples into Kjeldahl flasks. Record weights. Add 10 glass beads.
- Add 500 mg Kjeldahl catalyst (Wieninger) and 5 mL concentrated H<sub>2</sub>SO<sub>4</sub>.
- Heat on Kjeldahl digestion block in fume hood until residue is completely dissolved and solution is no longer turbid. (A green color may develop. This is not an issue, so long as the solution is clear.)
- Cool samples and carefully add 10 mL distilled water (samples will become very warm again).
- *Note:* At this point, some cereal samples may turn bright pink. This is not a problem for the analysis.
- Cool samples again and quantitatively transfer (without glass beads) into a 50 mL volumetric flask. Bring up to volume.
- Wash Kjeldahl flasks. If residue remains that resists soap and water, freshly prepared aqua regia usually does the trick (conc. HNO<sub>3</sub>/ conc. HCl, v/v, 1/3; **Caution! Very corrosive!**).
- Add 0.1 mL sample and 4 mL color reagent to a reagent glass vial with stopper. Shake well.
- Quickly add 1 mL 0.25% sodium hypochlorite solution and shake well.
- After 10 min, measure the extinction at 685 nm (pipette solution into plastic cuvettes).
- Measurement of the calibration solutions is performed in the same way as the sample.
- Create linear standard curve and check that samples are within the calibration curve range. If not, dilute with water as necessary.

#### 12.5.3.3. Determination of ester-linked phenolic acids

- Weigh in dry insoluble fiber material (100 mg) into a large Pyrex glass (25 mL) with Teflon-lined caps. Check vial for chips around the rim. Record weight.
- Add 50  $\mu$ L 5 mM *trans-o*-coumaric acid (internal standard, dissolved in 50/50 MeOH/H<sub>2</sub>O, v/v).
- Add 5 mL 2 M NaOH and a stir bar. Cap tightly. Vortex until all material is wetted. Wrap tightly with aluminum and stir for 18 h in the dark at room temperature.
- Acidify hydrolysates with 0.95 mL 37 % HCl. Check pH with pH paper (must be less than 2—add more HCl as necessary).
- Extract with diethyl ether (3  $\times$ , 6 mL, 5 mL, and 5 mL). For each ether extraction: Add ether to hydrolysate, mix carefully, yet thoroughly. Centrifuge at 2000 rpm. Carefully pipette off ether layer. Combine extracts from three extractions.
- Dry combined ether extracts under a N<sub>2</sub> stream.
- Dissolve residues in 1 mL MeOH/H<sub>2</sub>O (50/50, v/v).
- Analyze solutions with Shimadzu analytical HPLC-DAD system, using the conditions, column, and gradient provided in **Table 21**.
- Linear, five-point, equidistant internal calibration curves should be prepared for caffeic, sinapic, *trans-p*-coumaric, and *iso*-ferulic acids (concentration range 5–500  $\mu$ M) and measured under the same chromatographic conditions, using *trans-o*-coumaric acid as an internal standard (concentration of 250  $\mu$ M in all samples).

<b>Table 21. Analytical parameters for separation of phenolic acids</b>			
Column	Phenomenex phenyl-hexyl column (250 × 4.6 mm, 5 μm, 100 Å)		
Injection volume	10 μL		
Flow rate	1 mL/min		
Column temperature	45°C		
Quantification wavelength	325 nm		
<b>Gradient program</b>			
Gradient time [min]	TFA (1 mM), [%]	Acetonitrile/1 mM TFA in water, 90/10, v/v, [%]	MeOH/1 mM TFA in water, 90/10, v/v, [%]
0	87	13	0
11	87	13	0
23	85	15	0
28	84	16	0
32	25	50	25
33	87	13	0
42	87	130	0

- *cis*-Ferulic acid and *cis*-coumaric acid are prepared by exposing a stock solution containing *trans*-ferulic acid and *trans*-coumaric acid (prepared in 50/50 MeOH/H<sub>2</sub>O, v/v) to UV radiation (366 nm) overnight (covering sample with plastic wrap permits UV light transmission but prevents sample evaporation). Afterwards the sample should be brought up to a known volume and then diluted to create an equidistant, 5-point calibration curve. The concentrations of the *cis*-compounds in the UV-exposed stock solution are determined via the loss of *trans*-compounds in the stock solution.
- Correct values for residual protein and ash contents of the insoluble fibers. Each replicate is corrected individually using its unique values for protein and ash contents.

#### 12.5.3.4. Determination of monosaccharide composition of insoluble fiber materials (Saeman hydrolysis)

- Weigh in dried insoluble fiber material (100 mg; may be down-scaled) in a 15 mL Pyrex tube with a Teflon-lined cap. Check vial for chips around the rim. Add glass beads.
- Add 1.5 mL 12 M H<sub>2</sub>SO<sub>4</sub> and vortex vigorously for 1 min.
- Allow to stand in ice for 30 min, with vigorous vortexing for 1 min every 10 min.
- Let sample stand at room temperature for 2 h. Vortex every 30 min.
- Dilute sample by adding 9.75 mL water. Heat in a 100 °C oven for 3 h.
- Cool to room temperature, and filter an aliquot through a PTFE syringe filter (0.20 μm porosity).
- Neutralize 100 μL of the filtrate by mixing with 75 μL 4 M NaOH and 825 μL water.
- Mix a 20 μL aliquot of the neutralized solution with 20 μL 1 μM mannitol solution (injection standard) and 160 μL of water. This solution is then analyzed via HPAEC-PAD, using the conditions, column, and gradient provided in **Table 22**.
- Five-point, equidistant calibration curves may be created for two concentration ranges (1–24 μM and 25–125 μM) for arabinose, apiose, fucose, galactose, glucose, and rhamnose. Galacturonic and glucuronic acid may also be calibrated in these ranges, although uronic acids are quite resistant to cleavage under the Saeman hydrolysis conditions.
- Calibration data are fitted to a quadratic curve.
- Correct values for residual protein and ash contents of the insoluble fibers. Each replicate is corrected individually using its unique values for protein and ash contents.

**Table 22. Analytical parameters for HPAEC-PAD separation and detection of monosaccharides**

Column	CarboPac PA 20 (150 × 3 mm) anion-exchange column
Injection volume	25 µL
Flow rate	0.25 mL/min
Column temperature	25°C
Detection mode, waveform name, electrode	PAD detector (IntAmp), Carbohydrates (Standard Quad), AgCl

**Gradient program**

Gradient time [min]	Water	100 mM NaOH	100 mM NaOH + 0.2 mM NaOAc
-20.0	0	100	0
-10.0	0	100	0
-9.9	90	10	0
0.0 (injection)	90	10	0
1.5	96	4	0
22.0	96	4	0
32.0	0	100	0
32.1	0	0	100
42.0	0	0	100

Abbreviations used: **HPAEC-PAD**: high-performance anion-exchange chromatography coupled with a pulsed amperometric detector.

### 12.5.3.5. Methylation analysis of insoluble fiber samples (linkage analysis via partially methylated alditol acetates)

- As a precautionary measure, dry insoluble fiber material (60 mg) overnight in a vacuum oven (40 °C).
- Solubilize in 2 mL DMSO for 30 min with sonication (<40 °C, add ice to water bath if it becomes too warm).
- Add 40 mg freshly powdered (performed under N<sub>2</sub> with a glass mortar and pestle that has been previously dried) NaOH pellets.
- Sonicate for 90 min, and allow to stand for another 90 min at room temperature.
- Put sample on ice and add 1 mL methyl iodide. Allow to react for 30 min under sonication (<40 °C), followed by 30 min without sonication (room temperature). **Caution! Methyl iodide is extremely toxic! All steps must be carried out in fume hood!**
- Extract the methylated polysaccharides into dichloromethane (3 mL).
- Add 5 mL 0.1 M sodium thiosulfate, and remove and dispose the water phase.
- Wash the organic phase with water (2 × 5 mL).
- Rotary evaporate sample under vacuum and dry overnight in a vacuum oven at 40 °C.
- On the following morning (Day 2), solubilize the dry residue in 2 mL DMSO, sonicate for 15 min, and allow to stand overnight.
- On the following morning (Day 3), methylate the residue again according to the previous procedure to reduce under-methylation.
- Following the second methylation, dry residues overnight in a 40 °C vacuum oven.
- On the following morning (Day 4), hydrolyze the methylated polysaccharides in 2 mL 2 M TFA for 90 min at 120 °C.
- Rotary evaporate to dryness under reduced pressure.
- Add NaBD<sub>4</sub> (20 mg) and 0.3 mL ammonia to the dry sample.
- After 1 h, stop reduction by adding 0.1 mL of glacial acetic acid.
- Cool sample on ice, and add 1-methylimidazole (0.45 mL) and acetic anhydride (3 mL).

- After 30 min, add 3 mL of water, and extract the partially methylated alditol acetates into 5 mL dichloromethane.
- Wash organic phase with water (3 × 5 mL).
- Freeze residual water out of organic phase.
- Partially methylated alditol acetates were analyzed with both the Shimadzu GC-MS QP-2010 SE and the Shimadzu GC-2010 Plus (GC-FID) systems. Parameters are described in **Table 23**.
- Partially methylated alditol acetates are identified by comparing retention times and fragmentation with standard compounds and literature data.
- Quantification is performed by GC-FID according to the molar response factors described by Sweet et al. (1975).

**Table 23. Analytical parameters for GC separation of partially methylated alditol acetates and their MS or FID detection**

Column	GC-MS: Agilent DB 225 MS capillary column (30 m × 0.25 mm i.d., 0.25 μm film thickness). GC-FID: Agilent DB 225 capillary column (same dimensions as above)	
Injection volume	1 μL (GC-MS) or 3 μL (GC-FID)	
Split ratio	1:10	
Carrier gas	Helium	
Flow rate (linear velocity)	37.0 cm/sec	
MS detection parameters	interface temperature = 220 °C; ion source temperature = 200 °C; ionization voltage = 70 eV; scan range = $m/z$ 41– 350; scan time = 0.2 sec; detector voltage = 1.33 kV	
FID detection parameters	Detector temperature = 240 °C	
<b>GC temperature program</b>		
Heating rate [°C/min]	Final temperature [°C]	Hold time [min]
-	140	1
20	170	0
2	200	0
20	220	20

*Abbreviations used: FID: flame ionization detector; GC: gas chromatography; MS: mass spectrometry.*

#### 12.5.4. Methods for release and isolation of feruloylated oligosaccharides

##### 12.5.4.1. Mild acid degradation (semi-selective side-chain hydrolysis method for preparative quantities)

- Heat insoluble fiber material (20 g) with 400 mL TFA solution (50 mM in water) for 2 h at 100 °C under reflux.
- Cool on ice, adjust pH to 5.0 with 0.275 M NaOH.
- Centrifuge suspension and save supernatant, or filter through glass wool.

##### 12.5.4.2. Enzymatic degradation (Driselase method)

- Suspend insoluble fiber material (9 g) with Driselase (1 g) in water (900 mL) in a large Erlenmeyer flask. Replicate incubations may be performed simultaneously.  
*NOTE: If Sephadex LH-20 separation is the end goal for the hydrolysate, incubation with 15-20 g of insoluble cereal fiber material will produce a hydrolysate amount which does not completely overflow the detector cell.*
- Incubate at 40 °C for 48 h under gentle shaking.
- Heat suspension in a 92 °C water bath for 15 min and then centrifuge (5000 rpm, 12 min).
- Filter suspension through glass wool.
- If desired, filtrate volume may be reduced with a rotary evaporator (maximum water bath

temperature of 40 °C).

#### 12.5.4.3. *Amberlite XAD-2 separation of feruloylated oligosaccharides from acidic or enzymatic hydrolysates*

- Apply hydrolysates to an Amberlite XAD-2 column (300 mL column volume) which has been preconditioned beforehand (wash thoroughly with several column volumes of MeOH, then condition with three column volumes of pure water).
- Wash the column with water (600 mL); water wash contains non-feruloylated monosaccharides and oligosaccharides. Maintain a moderate column flow rate.
- Elute mono-feruloylated oligosaccharides with 600–900 mL MeOH/water (50/50, v/v).
- Wash remaining hydrolysate material from the column pure MeOH (600–900 mL).
- Concentrate 50/50 MeOH/water eluate under vacuum to approximately 10 mL with a rotary evaporator

#### 12.5.4.4. *Sephadex LH-20 separation of feruloylated oligosaccharides*

- Inject concentrated aqueous solution of feruloylated oligosaccharides (for example, the concentrated 50/50 MeOH/H<sub>2</sub>O Amberlite XAD-20 eluate from **Section 12.5.4.4**) onto the Sephadex LH-20 column (100 × 2.5 cm).
- Pure water is used as eluent (0.5 mL/min).
- Monitor column eluate with the UV detector.  
*NOTE: For maximum sensitivity, 325 nm can be used, but it is sometimes preferable to choose an absorption minimum from trans-ferulic acid's UV-absorption spectrum (for example 360 nm) to avoid overflowing the detector.)*
- Collect fractions at 6-min intervals and pool based on detected peaks.
- Concentrate under vacuum with a rotary evaporator (maximum water bath temperature of 40°C).
- When all peaks have eluted (up to 4000 min), switch eluent to 70-30 MeOH-H<sub>2</sub>O to wash column. Wash with
- Store column in 20-80 MeOH-H<sub>2</sub>O (too much MeOH will weaken the column's seals).

#### 12.5.4.5. *Semi-preparative/preparative chromatography clean-up of feruloylated oligosaccharide fractions*

- When necessary, feruloylated oligosaccharide fractions (for example, pooled Sephadex LH-20 fractions) may be further purified on a (semi-)preparative RP-C18 column.
- RP-HPLC-UV parameters are described below in **Table 24**.
- Label a rack-full of 8-mL glass vials in advance (always have extra labeled vials on hand in case unexpected peaks appear in the chromatogram).
- Collect fractions manually. Cut peaks aggressively (i.e. collect peak shoulders into separate vials than the middle of the peak), but save everything initially in case shoulders turn out to be peak tails or split peaks instead of a contaminant.  
*NOTE: When separated in the aqueous conditions of RP-HPLC, many feruloylated oligosaccharide peaks are very broad due to on-column mutarotation between the  $\alpha$ - and  $\beta$ -anomers of the reducing sugar). These peaks generally take two shapes: either a single peak with major tailing or a partially split peak (see **Figure 15** in **Section 3.4.2.3**).*
- Screen collected fractions with LC-DAD-MS (use method from **Section 12.5.6.1**); combine identical fractions.

Table 24. Analytical parameters for (semi-)preparative clean-up of feruloylated oligosaccharides		
Column	<u>Preparative separations</u> : Phenomenex Luna C18 column (250 × 25 mm, 5 μm, 100 Å) <u>Semi-preparative separations</u> : Phenomenex Luna C18 column (250 × 8 mm, 5 μm, 100 Å)	
Injection volume	manual injection, 1.1 to 1.8 mL (2 mL loop volume)	
Flow rate	8 mL/min (preparative) or 4 mL/min (semi-preparative)	
Column temperature	room temperature	
Detection wavelength	325 nm	
Gradient program		
Gradient time [min]	0.1% formic acid in H <sub>2</sub> O, [%]	MeOH, [%]
0	75	25
5	70	25
25	62	38
30	0	100
32	0	100
33	75	25
40	75	25

### 12.5.5. Methods for release and isolation of non-feruloylated side-chain oligosaccharides

#### 12.5.5.1. Mild acid degradation (semi-selective side-chain hydrolysis method for preparative quantities)

- Heat insoluble fiber material (10 g) with 500 mL TFA solution (50 mM in water) for 3 h at 100 °C under reflux.
- Cool on ice, adjust pH to 7.0 with 0.325 M NaOH.
- Filter suspension through a paper filter.
- Concentrate under vacuum with a rotary evaporator to 50 mL.

#### 12.5.5.2. Amberlite XAD-2 separation of non-feruloylated oligosaccharides from acidic hydrolysate

- Apply hydrolysate to an Amberlite XAD-2 column (300 mL column volume) which has been preconditioned beforehand (wash thoroughly with several column volumes of MeOH, then condition with three column volumes of pure water).
- Elute non-feruloylated oligosaccharides and monosaccharides from the column with water (600 mL); collect all aqueous eluates. Maintain a moderate column flow rate.
- Wash column with MeOH (600 mL).
- Concentrate aqueous eluate under vacuum to approximately 50 mL with a rotary evaporator.
- Add four volumes of EtOH to solution to precipitate soluble polysaccharides.
- Centrifuge, collect supernatant. Evaporate supernatant under vacuum with a rotary evaporator. Remove stubborn water residue by freeze-drying.

#### 12.5.5.3. Bio-Gel P-2 separation of non-feruloylated oligosaccharides

- Heat Bio-Gel P-2 column (100 × 2.5 cm) to 45°C using water jacket.
- Start flow rate (pure water) at 1 mL/min, turn on RI detector and equilibrate for at least 1 h.
- Dissolve ≈750 mg of dried residue (from **Section 12.5.5.2**) in 10 mL of water and inject onto the Bio-Gel P-2 column
- Pure water is used as eluent (1.0 mL/min).
- Monitor column eluate with the RI detector.

- Collect fractions at 2.5-min intervals and pool based on detected peaks.
- Dry pooled fractions via freeze-drying.

#### 12.5.5.4. *Semi-preparative/preparative chromatography clean-up of non-feruloylated oligosaccharide fractions*

- RP-HPLC-RI parameters are described below in **Table 25**.
- Label a rack-full of 8-mL glass vials in advance (always have extra labeled vials on hand in case unexpected peaks appear in the chromatogram).
- Dissolve collected fractions in water ( $\approx 10$  mg/mL).
- Collect fractions manually.
- Check fraction purity by injecting a diluted aliquot (1:100) onto the HPAEC-PAD system.

**Table 25. Analytical parameters for semi-preparative clean-up of non-feruloylated oligosaccharides**

Column	<u>Semi-preparative separations</u> : Knauer Europher-100 C18 column (250 $\times$ 8 mm, 5 $\mu$ m)
Injection volume	manual injection, 200-1000 $\mu$ L (1 mL loop volume)
Flow rate	1.5 mL/min, 100% water
Column temperature	5°C (chill column)
Detection	RI
<b>Gradient program: None</b>	
<i>Abbreviations used: RI: refractive index.</i>	

### 12.5.6. Methods for characterization of isolated (feruloylated)-oligosaccharides

#### 12.5.6.1. *Molecular weight determination of feruloylated oligosaccharides*

- Analyze an aliquot of the isolated compounds using the parameters in **Table 26**.

**Table 26. Analytical parameters for RP-HPLC separation and DAD/ESI-MS detection and analysis of feruloylated oligosaccharides (Thermo system)**

Column	Phenomenex Luna C18 column (250 $\times$ 4.6 mm, 5 $\mu$ m particle size)	
Injection volume	20 $\mu$ L	
Flow rate	0.5 mL/min	
Column temperature	room temperature	
DAD monitoring wavelength	325 nm	
MS ionization	ESI positive mode	
MS parameters	capillary temperature = 350°C; spray voltage = 4 kV; capillary voltage = 47V	
<b>Gradient program</b>		
Gradient time [min]	0.1% formic acid in H <sub>2</sub> O, [%]	MeOH, [%]
0	88	12
5	88	12
30	0	100
35	0	100
36	88	12
40	88	12
<i>Abbreviations used: DAD: diode-array detector; ESI: electrospray ionization; MS: mass spectrometry; RP-HPLC: reversed-phase high-performance liquid chromatography.</i>		

- Feruloylated oligosaccharides readily form a range of quasi-molecular ions, in particular  $[M+H]^+$ ,  $[M+NH_4]^+$ ,  $[M+Na]^+$ ,  $[M+K]^+$ , and  $[2M+Na]^+$ .

### 12.5.6.2. PGC-ESI-MS analysis of non-feruloylated oligosaccharides

- Analyze an aliquot of the isolated compounds using the parameters in **Table 27**.

Table 27. Analytical parameters for PGC-HPLC separation and ESI-MS (or MS/MS) detection and analysis of non-feruloylated oligosaccharides (Waters system)		
Column	Hypercarb PGC column (100 × 4.6 mm, 3 μM particle size)	
Injection volume	25 μL	
Flow rate	0.4 mL/min	
Column temperature	80°C	
MS ionization	ESI positive mode	
MS parameters	desolvation temperature = 450°C; source temperature = 120°C; desolvation gas = 800 L/h; cone gas = 60 L/h; cone voltage = 40 kV; capillary voltage = 4V	
MS/MS parameters	Same except collision voltage = 26 V	
Gradient program		
Gradient time [min]	25 μM LiCl in H <sub>2</sub> O, [%]	Acetonitrile, [%]
0	100	0
5	100	0
20	95	5
22	20	80
27	20	80
28	100	0
33	100	0
<i>Abbreviations used: ESI: electrospray ionization; MS: mass spectrometry; PGC: porous graphitized carbon.</i>		

### 12.5.6.3. NMR spectroscopy for structural characterization

- Dry isolated compounds (preferably by freeze-drying).
- Deuterium-exchange samples by dissolving dried sample in D<sub>2</sub>O (200 μL), freezing sample, and freeze-drying.
- Deuterium-exchange sample again.
- After removing dry sample from freeze-dryer, immediately cap it tightly with an air-tight cap to prevent the hygroscopic samples from absorbing moisture.
- Dissolve sample in 520 μL of D<sub>2</sub>O. Cap sample quickly.
- With a GC-syringe, add 0.5 μL acetone to the sample, or (if samples contain acetyl groups) *tert*-butanol.

**NOTE:** *tert-butyl alcohol is solid at room temperature, so both the solvent and the GC syringe must be heated to successfully transfer an aliquot.*

- With a long Pasteur pipette, transfer the sample to a clean and dry 5-mm NMR tube. Cap tube quickly.
- NMR experiments (1H, H,H-COSY; HMQC or HSQC; HMBC; TOCSY; and HSQC-TOCSY) were standard Bruker implementations (see **Section 12.6.1.1–6** for sample NMR parameters).
- Spectra calibration is performed against acetone or *tert*-butyl alcohol using the chemical shifts published by Gottlieb et al. (1997): acetone, <sup>1</sup>H = δ 2.22 ppm, methyl carbon = δ 30.89 ppm; *tert*-butyl alcohol, <sup>1</sup>H = δ 1.24 ppm, methyl carbon = δ 30.29 ppm.

### 12.5.6.4. Determination of monosaccharide composition of soluble oligosaccharides (TFA hydrolysis)

- Aliquot a sample volume containing 75-150 μg of sample into a 1.5 mL glass vial with cap. Dry down.
- Add 500 μL 2 M TFA. Cap tightly (vials must contain septa).
- Heat in a 121 °C oven for 1 h.

- Evaporate samples to dryness in a SpeedVac centrifugal evaporator.
- Add 200  $\mu\text{L}$  EtOH to residue to dissolve remaining traces of TFA and evaporate again.
- Repeat EtOH addition and evaporate to dryness again.
- Dissolve residue in 180  $\mu\text{L}$  deionized water and add 20  $\mu\text{L}$  1mM D-mannitol solution.
- Analyze via HPAEC-PAD using the parameters described in **Table 22**.

#### 12.5.6.5. Determination of D/L-configuration of monosaccharides

- Aliquot a sample volume containing 15-20  $\mu\text{g}$  of sample into a 1.5 mL glass vial with cap. Dry down.
- Hydrolyze according to TFA hydrolysis method (see **Section 12.5.6.4**).
- Add 150  $\mu\text{L}$  (R)-(-)-2-octanol and 5  $\mu\text{L}$  concentrated TFA to evaporated hydrolysate. Seal tightly.
- Heat 8 h at 130°C in drying oven.
- Evaporate solvent.
- Add 200  $\mu\text{L}$  EtOH to residue to dissolve remaining traces of solvent and evaporate again. Repeat two more times.
- Silylate samples for GC-MS analysis: Add 80  $\mu\text{L}$  BSTFA and 20  $\mu\text{L}$  pyridine. Seal tightly and heat for 30 min at 60°C.
- Dilute 1/10 with acetonitrile.
- Analyze via GC-MS using the parameters described in **Table 28**.

Table 28. Analytical parameters for GC separation of silylated (-)-2-octyl glycosides and their MS detection		
Column	Rtx-5MS capillary column (30 m $\times$ 0.25 mm i.d., 0.25 $\mu\text{m}$ film thickness)	
Injection volume	1 $\mu\text{L}$	
Split ratio	1:10	
Carrier gas	Helium	
Flow rate (linear velocity)	40.0 cm/sec	
MS detection parameters	interface temperature = 275 °C; ion source temperature = 250 °C; ionization voltage = 70 eV; detector start time = 16 min; scan range = $m/z$ 100– 700; scan time = 0.3 sec; detector voltage = 1.30 kV	
GC temperature program		
Heating rate [°C/min]	Final temperature [°C]	Hold time [min]
-	150	0
1	200	0
15	300	0
<i>Abbreviations used: GC = gas chromatography; MS = mass spectrometry.</i>		

- Each derivatized sugar will result in up to four peaks resulting from the respective  $\alpha$ - and  $\beta$ -furanose and pyranose derivatives. Derivatives (silylated (-)-2-octyl glycosides) are identified by comparing retention times with those resulting from authentic chiral monosaccharide standards.

### 12.5.7. Feruloylated side-chain profiling methods

#### 12.5.7.1. LC-DAD/MS-based determination of feruloylated side-chain profiles

##### **Mildly acidic hydrolysis and hydrolysate clean-up**

- Weigh in 200 mg dry cereal fiber (100 mg is sufficient for maize materials) into a 15-mL Pyrex tube. Record exact weight.
- Add exactly 5 mL 50 mM TFA solution and a small stir-bar. Vortex thoroughly.
- Incubate for 2 h at 100°C in a boiling water bath while stirring and protecting samples from light. (Wrap tightly in aluminum foil.)

- Cool on ice.
- Centrifuge and remove an aliquot of the supernatant (as much as possible; record aliquot volume).
- Apply aliquot to a preconditioned C18-SPE cartridge (500 mg C18 material).  
*NOTE: Preconditioning cartridges by washing with 6 mL MeOH, then 6 mL pure water. Do not allow cartridge material to dry out between washing steps or sample application.*
- Pass aliquot through cartridge slowly (dropwise). Wash loaded cartridge slowly with water (6 mL).
- Elute feruloylated side-chains from cartridge with MeOH (6 mL) into a small Pyrex tube (15 mL).
- Evaporate MeOH from samples. Ensure residues are completely dry (vacuum drying oven at 40°C).

#### **Reduction of feruloylated side-chains**

- Add 2 mL freshly prepared NaBH<sub>4</sub> in DMSO solution (30 mg NaBH<sub>4</sub>/mL DMSO; *NOTE: See preparation instructions in Section 12.4.*)
- Add a small stir bar and immediately cap samples tightly to prevent moisture contamination.
- Wrap sample racks in aluminum foil to protect from light and heat for 18 h at 30°C with stirring.
- Remove samples from heat, cool on ice.
- Quickly add 2 mL of 1M HCl (aqueous) solution.  
*NOTE: Some plant samples will foam vigorously at this step. The acid should be added as quickly as possible without allowing the samples to foam over. Step-wise addition of the acid works best: 500 µL of acid solution; cap immediately, vortex lightly, release gas (caution: H<sub>2</sub> gas!), and repeat. After all the acid has been added, vortex the sample thoroughly to break any foam, and check the pH with pH paper (should be mildly acidic—pH 4-5). If sample is still alkaline, add an additional 200 µL of acid. Record the exact volume of acid added.*
- Analyze directly with LC-DAD/MS (Thermo system) using the parameters described in **Table 29**.

**Table 29. Analytical parameters for RP-HPLC separation and DAD/ESI-MS detection and analysis of reduced feruloylated side-chain oligosaccharides (Thermo system)**

Column	Phenomenex Luna C18 column (250 × 4.6 mm, 5 µM particle size)
Injection volume	25 µL
Flow rate	0.5 mL/min
Column temperature	room temperature
DAD monitoring wavelength	325 nm
MS ionization	ESI positive mode
MS parameters	capillary temperature = 350°C; spray voltage = 4 kV; capillary voltage = 47 V

#### **Gradient program**

Gradient time [min]	0.1% formic acid in H <sub>2</sub> O, [%]	Acetonitrile, [%]
0	95	5
4	95	5
8	90	10
10	90	10
14	84	16
23	84	16
33	50	50
34	5	95
36	5	95
37	95	5
42	95	5

*Abbreviations used: DAD: diode-array detector; ESI: electrospray ionization; MS: mass spectrometry; RP-HPLC: reversed-phase high-performance liquid chromatography.*

#### **External calibration**

- Prepare stock solutions of FA, FAX, and FAXG in MeOH.

- Dilute if necessary, carefully pipette increasing aliquot volumes into 15-mL Pyrex tubes (calculate the end concentration of the sample based on its end volume after reduction: 2 mL DMSO solution and 2 mL acid). Recommended FA concentration range for calibration = 10–250  $\mu\text{M}$ ; Recommended FAX concentration range for calibration = 5–25  $\mu\text{M}$ ; Recommended FAXG concentration range for calibration = 5–25  $\mu\text{M}$ .
- Create 5-point calibration curves in triplicate (create separate stock solutions for each calibration curve). Standard compounds may be calibrated together.
- Dry down aliquots completely.
- Reduce following method above and analyze on LC-DAD-MS system (Thermo). NOTE: *Standard samples do not foam as excessively as cereal samples.*

#### 12.5.7.2. HSQC-NMR-based determination of feruloylated side-chain profiles

##### **Mildly acidic hydrolysis and hydrolysate clean-up**

- Weigh in 200 mg dry cereal fiber (100 mg is sufficient for maize materials) into a 15-mL Pyrex tube. Record exact weight.
- Follow method described in **Section 12.5.7.1** (up until Reduction).

##### **NMR analysis**

- Dissolve dried residues in 550  $\mu\text{L}$  of DMSO-*d*<sub>6</sub> containing caffeine internal standard (4.407 mM; see **Section 12.4** for preparation method). Transfer to an NMR tube (5 mm diameter)
- Measure using Bruker standard pulse program HSQCETGP with 20 scans (see **Section 12.6.2** for measurement and data processing parameter).
- Calibrate spectrum shifts against residual DMSO (<sup>1</sup>H = 2.50 ppm; <sup>13</sup>C = 39.52 ppm).
- Identify quantification signals by overlaying spectra from standard compounds.
- Integrate the internal standard signal generously (cut deeply and take the entire volume).

##### **Internal calibration**

- Prepare stock solutions of FA, FAX, and FAXG in MeOH.
- Dilute if necessary, carefully pipette increasing aliquot volumes into vials (calculate the end concentration of the sample based on its end volume dissolving in NMR solvent: 550  $\mu\text{L}$  DMSO-*d*<sub>6</sub>). Recommended FA concentration range for calibration = 500–2500  $\mu\text{M}$ ; Recommended FAX concentration range for calibration = 250–750  $\mu\text{M}$ ; Recommended FAXG concentration range for calibration = 250–750  $\mu\text{M}$ .
- Dry down aliquots completely.
- Dissolve dried residues in 550  $\mu\text{L}$  of DMSO-*d*<sub>6</sub> containing caffeine internal standard (4.407 mM). Transfer to an NMR tube (5 mm diameter).
- Measure using NMR analysis method described above.

#### 12.5.8. Qualitative HPAEC-PAD screening of cereal materials for non-feruloylated side-chain oligosaccharides

- Weigh in 200 mg dry cereal fiber (100 mg is sufficient for maize materials) into a 15-mL Pyrex tube.
- Add 5 mL 50 mM TFA solution and a small stir-bar. Vortex thoroughly.
- Incubate for 2 h at 100°C in a boiling water bath while stirring.
- Cool on ice.
- Centrifuge and remove an aliquot of the supernatant (as much as possible; record aliquot volume).
- Apply aliquot to a preconditioned C18-SPE cartridge (500 mg C18 material).  
NOTE: *Preconditioning cartridges by washing with 6 mL MeOH, then 6 mL pure water. Do not allow cartridge material to dry out between washing steps or sample application.*
- Pass aliquot through cartridge slowly (dropwise). Wash loaded cartridge slowly with water (6 mL). Collect all aqueous eluate. Freeze eluate and freeze-dry.

- Dissolve residues in a defined volume of pure water. Remove two aliquots of each sample. Dilute one aliquot with an aqueous solution containing standard compounds of interest. Dilute other aliquot with same volume of water.
- Analyze samples on HPAEC system using the parameters described in **Table 30**.

**Table 30. Analytical parameters for qualitative HPAEC-PAD screening of non-feruloylated side-chain oligosaccharides**

Column	CarboPac PA 200 (150 × 3 mm) anion-exchange column
Injection volume	25 µL
Flow rate	0.45 mL/min
Column temperature	25°C
Detection mode, waveform name, electrode	PAD detector (IntAmp), Carbohydrates (Standard Quad), AgCl

**Gradient program**

Gradient time [min]	Water	100 mM NaOH	100 mM NaOH + 0.5 mM NaOAc
-30.0	0	0	100
-20.0	0	0	100
-19.9	90	10	0
0.0 (injection)	90	10	0
10	90	10	0
10.1	50	50	0
55	34	34	32
55.1	0	0	100
65.0	0	0	100

*Abbreviations used: HPAEC-PAD: high-performance anion-exchange chromatography coupled with a pulsed amperometric detector.*

## 12.6. NMR parameters

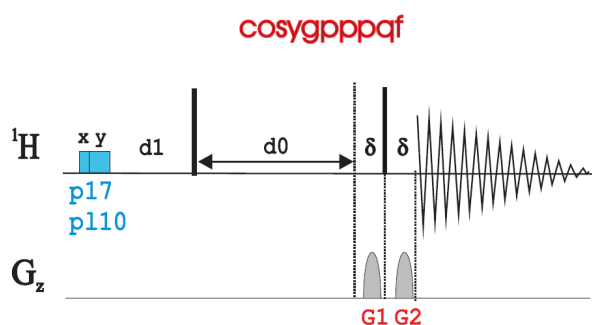
### 12.6.1. Measurement and processing parameters for structural characterization

#### 12.6.1.1. <sup>1</sup>H-NMR measurement and processing parameters

Table 31. <sup>1</sup> H-NMR measurement and processing parameters	
Measurement parameters (Bruker abbreviation)	Value
Pulse program	zg30
Time-domain data points (TD)	65536
Solvent	D <sub>2</sub> O
Number of scans (NS)	16
Number of dummy scans (DS)	2
Spectral width (SWH), Hz	10.000
FID resolution (FIDRES), Hz	0.152588
Acquisition time (AQ), sec	3
Receiver gain (RG)	31.06
Dwell time (DW), μsec	50
Pre-scan delay (DE), μsec	10
Temperature (TE), K	295.1
Relaxation delay (D1), 1	1
Number of cycles (TD0)	1
f1 Channel	
Irradiation frequency for channel 1 (SFO1), MHz	500.1331
Nucleus observed	<sup>1</sup> H
90° pulse (P1), μsec	12
Pulse power level (PLW1), W	14
Processing parameters (Bruker abbreviation)	
Data points for Fourier transform (SI)	65536
Frequency (SF), MHz	500.1300
Type of window function (WDW)	Exponential multiplication
Line-broadening (LB), Hz	0.3

### 12.6.1.2. $^1\text{H}, ^1\text{H}$ -COSY measurement and processing parameters

Table 32. $^1\text{H}, ^1\text{H}$ -COSY measurement and processing parameters	
Measurement parameters (Bruker abbreviation)	Value
Pulse program	cosygpppqf magnitude (qf) COSY with gradients (gp) and purge pulses



Pulse program figure from  
Parella, Teodor. 2006. *Pulse Program Catalogue: 1D & 2D NMR experiments*. Bruker Biospin GmbH.

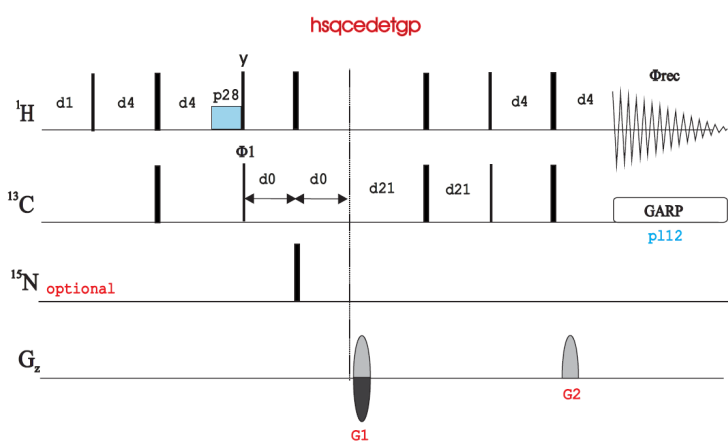
Time-domain data points (TD)	2048
Solvent	D <sub>2</sub> O
Number of scans (NS)	16
Number of dummy scans (DS)	8
Spectral width (SWH), Hz	4237.288
FID resolution (FIDRES), Hz	2.068988
Acquisition time (AQ), sec	0.241664
Receiver gain (RG)	15.94
Dwell time (DW), $\mu\text{sec}$	118
Pre-scan delay (DE), $\mu\text{sec}$	10
Temperature (TE)	295.1
Incremented delay (D0), sec	0,000003
Relaxation delay (D1), sec	1.91152596
Short delay (D13), sec	0.000004
Recovery delay after gradient pulse (D16), sec	0.0002
<b>F1 Channel measurement parameters</b>	
Radiation frequency, MHz	500.132281
Nucleus	$^1\text{H}$
First 90° pulse (P0), $\mu\text{sec}$	12
Second 90° pulse (P1), $\mu\text{sec}$	12
F1 Channel-trim pulse at pl10 or pl15 (P17), $\mu\text{sec}$	2500
Pulse 1 power (PLW1), W	14
F1 channel, power level for spinlock (PLW10), W	2.98219991
<b>Gradient channel parameters</b>	
Gradient file name	SMSQ10.100
Gradient level for z-axis gradient 1 (GPZ1), % of maximum	10
Gradient pulse (P16), $\mu\text{sec}$	1000
<b>F1 Acquisition parameters</b>	

<b>Table 32. <sup>1</sup>H, <sup>1</sup>H-COSY measurement and processing parameters</b>	
Time domain data points (TD)	128
Irradiation frequency, MHz	500.1323
FID resolution (FIDRES), Hz	33.103813
Sweep width (SW), ppm	8.472
Acquisition mode for indirect detections (FnMODE)	QF (successive FID w/o phase program)
<b>F2 Processing parameters</b>	
Data points for Fourier transform (SI)	1024
Frequency (SF), MHz	500.13
Type of window function (WDW)	QSINE (squared sine)
Shift of the sine function (SSB)	0 (perfect sine)
Line broadening (LB), Hz	0
<b>F1 Processing parameters</b>	
Data points for Fourier transform (SI)	1024
Type of F1 data transformation (MC2)	QF (complex 2-quadrant transformation)
frequency	500.13
type of window function	QSINE (squared sine)
Shift of the sine function (SSB)	0 (perfect sine)
Line broadening (LB), Hz	0

### 12.6.1.3. $^1\text{H},^{13}\text{C}$ -HSQC measurement and processing parameters

**Table 33.  $^1\text{H},^{13}\text{C}$ -HSQC measurement and processing parameters**

Measurement parameters (Bruker abbreviation)	Value
Pulse program	hsqcedetgp Phase-sensitive ge-2D multiplicity-edited HSQC using echo-antiecho



Pulse program figure from  
Parella, Teodor. 2006. *Pulse Program Catalogue: 1D & 2D NMR experiments*.  
Bruker Biospin GmbH.

Time-domain data points (TD)	1024
Solvent	D <sub>2</sub> O
Number of scans (NS)	32
Number of dummy scans (DS)	16
Spectral width (SWH), Hz	4237.288
FID resolution (FIDRES), Hz	4.137977
Acquisition time (AQ), sec	0.120832
Receiver gain (RG)	197.51
Dwell time (DW), $\mu\text{sec}$	118
Pre-scan delay (DE), $\mu\text{sec}$	10
Temperature (TE)	295.1
Default $^{13}\text{C}$ - $^1\text{H}$ coupling constant (CNST2)	145
Incremented delay (D0), sec	0.000003
Relaxation delay (D1), sec	1.45801604
[1/(4J)(XH)] delay (D4), sec	0.00172414
Short delay (D13), sec	0.000004
Recovery delay after gradient pulse (D16), sec	0.0002
1/(2J(XH)) delay for multiplicity editing (D21), sec	0.00345
<b>F1 Channel measurement parameters</b>	
Radiation frequency, MHz	500.132281
Nucleus	$^1\text{H}$
F1 channel— $90^\circ$ high power pulse (P1), $\mu\text{sec}$	12
F1 channel— $180^\circ$ high power pulse (P2), $\mu\text{sec}$	24
F1 Channel-trim pulse (P28), $\mu\text{sec}$	0
Pulse 1 power (PLW1), W	14
<b>F2 Channel measurement parameters</b>	

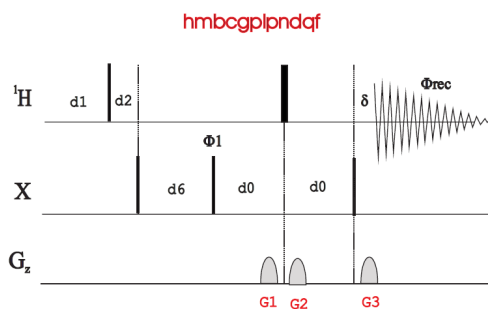
**Table 33. <sup>1</sup>H, <sup>13</sup>C-HSQC measurement and processing parameters**

Radiation frequency, MHz	125.7671682
Nucleus	<sup>13</sup> C
Multiple pulse decoupling scheme/heteronuclear broadband decoupling (CPDPRGG)	GARP (globally-optimized, alternating phase, rectangular pulses)
F2 channel – 90° high power pulse (P3), μsec	10
F2 channel – 180° high power pulse (P4), μsec	20
90° pulse for decoupling sequence (PCPD2), μsec	70
F2 channel pulse power (PLW2), W	65
Power level for CDP/BB decoupling (PLW12), W	1.32650006
<b>Gradient channel parameters</b>	
Gradient file name	SMSQ10.100
Gradient level for z-axis gradient 1 (GPZ1), % of maximum	80
Gradient level for z-axis gradient 2 (GPZ2), % of maximum	20.1
Gradient pulse (P16), μsec	1000
<b>F1 Acquisition parameters</b>	
Time domain data points (TD)	256
Irradiation frequency, MHz	125.7672
FID resolution (FIDRES), Hz	81.380211
Sweep width (SW), ppm	165.65
Acquisition mode for indirect detections (FnMODE)	Echo-antiecho (forward quad complex, phase sensitive 4-quadrant transformation for gradient enhanced spectroscopy)
<b>F2 Processing parameters</b>	
Data points for Fourier transform (SI)	1024
Frequency (SF), MHz	500.13
Type of window function (WDW)	QSINE (squared sine)
Shift of the sine function (SSB)	2 (perfect cosine)
Line broadening (LB), Hz	0
<b>F1 Processing parameters</b>	
Data points for Fourier transform (SI)	1024
Type of F1 data transformation (MC2)	Echo-antiecho (phase sensitive 4-quadrant transformation for gradient enhanced spectroscopy)
frequency	500.13
type of window function	QSINE (squared sine)
Shift of the sine function (SSB)	2 (perfect cosine)
Line broadening (LB), Hz	0

### 12.6.1.4. HMBC measurement and processing parameters

**Table 34. HMBC measurement and processing parameters**

Measurement parameters (Bruker abbreviation)	Value
Pulse program	hmbcgp1pndqf Magnitude-mode ge-2D HMBC using low-pass J-filter



Pulse program figure from  
Parella, Teodor. 2006. *Pulse Program Catalogue: 1D & 2D NMR experiments*. Bruker Biospin GmbH.

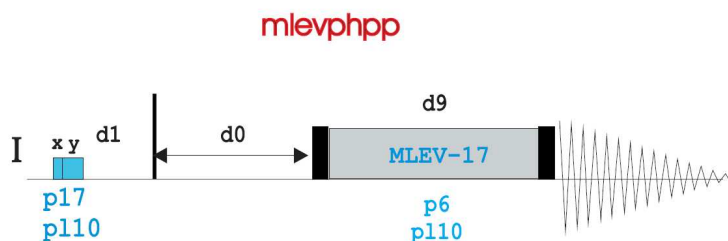
Time-domain data points (TD)	2048
Solvent	D <sub>2</sub> O
Number of scans (NS)	64
Number of dummy scans (DS)	16
Spectral width (SWH), Hz	4237.288
FID resolution (FIDRES), Hz	2.068988
Acquisition time (AQ), sec	0.241664
Receiver gain (RG)	197.51
Dwell time (DW), μsec	118
Pre-scan delay (DE), μsec	10
Temperature (TE)	295.1
Default <sup>13</sup> C- <sup>1</sup> H coupling constant (CNST2)	145
Default long-range <sup>13</sup> C- <sup>1</sup> H coupling constant (CNST3)	10
Incremented delay (D0), sec	0.000003
Relaxation delay (D1), sec	1.41603196
[1/(2J)XH] delay (D1), sec	0.00344828
Delay for development of long-range couplings (D6), sec	0.05
Recovery delay after gradient pulse (D16), sec	0.0002
<b>F1 Channel measurement parameters</b>	
Radiation frequency, MHz	500.132281
Nucleus	<sup>1</sup> H
F1 channel—90° high power pulse (P1), μsec	12
F1 channel—180° high power pulse (P2), μsec	24
Pulse 1 power (PLW1), W	14
<b>F2 Channel measurement parameters</b>	
Radiation frequency, MHz	125.7703
Nucleus	<sup>13</sup> C
F2 channel – 90° high power pulse (P3), μsec	10
F2 channel pulse power (PLW2), W	65

<b>Table 34. HMBC measurement and processing parameters</b>	
Power level for CDP/BB decoupling (PLW12), W	1.32650006
<b>Gradient channel parameters</b>	
Gradient file name	SMSQ10.100
Gradient level for z-axis gradient 1 (GPZ1), % of maximum	50
Gradient level for z-axis gradient 2 (GPZ2), % of maximum	30
Gradient level for z-axis gradient 3 (GPZ3), % of maximum	40.1
Gradient pulse (P16), $\mu$ sec	1000
<b>F1 Acquisition parameters</b>	
Time domain data points (TD)	128
Irradiation frequency, MHz	125.7703
FID resolution (FIDRES), Hz	218.226257
Sweep width (SW), ppm	222.095
Acquisition mode for indirect detections (FnMODE)	QF (complex 2-quadrant transformation)
<b>F2 Processing parameters</b>	
Data points for Fourier transform (SI)	2048
Frequency (SF), MHz	500.13
Type of window function (WDW)	SINE (sine)
Shift of the sine function (SSB)	0 (perfect sine)
Line broadening (LB), Hz	0
<b>F1 Processing parameters</b>	
Data points for Fourier transform (SI)	1024
Type of F1 data transformation (MC2)	QF (complex 2-quadrant transformation)
Frequency (SF)	125.757789
Type of window function (WDW)	SINE (sine)
Shift of the sine function (SSB)	0 (perfect sine)
Line broadening (LB), Hz	0

### 12.6.1.5. TOCSY measurement and processing parameters

**Table 35. TOCSY measurement and processing parameters**

Measurement parameters (Bruker abbreviation)	Value
Pulse program	mlevphpp Phase-sensitive 2D TOCSY using MLEV with purge pulses before d1



Pulse program figure from  
Parella, Teodor. 2006. *Pulse Program Catalogue: 1D & 2D NMR experiments*.  
Bruker Biospin GmbH.

Time-domain data points (TD)	2048
Solvent	D <sub>2</sub> O
Number of scans (NS)	32
Number of dummy scans (DS)	16
Spectral width (SWH), Hz	3205.128
FID resolution (FIDRES), Hz	1.565004
Acquisition time (AQ), sec	0.319488
Receiver gain (RG)	31.06
Dwell time (DW), μsec	156
Pre-scan delay (DE), μsec	10
Temperature (TE)	289.3
Incremented delay (D0), sec	0.00014436
Relaxation delay (D1), sec	1.88531196
TOCSY mixing time (D9), sec	0.08

#### F1 Channel measurement parameters

Radiation frequency, MHz	500.132402
Nucleus	<sup>1</sup> H
F1 channel – 90° high power pulse (P1), μsec	12
F1 channel – 60° low power pulse (P5), μsec	17.34
F1 channel – 90° low power pulse (P6), μsec	26
F1 channel – 180° shaped pulse (H <sub>2</sub> O on resonance) (P7), μsec	52
F1 channel - trim pulse at p110 (P7), μsec	2500
Pulse 1 power (PLW1), W	14
F1 channel, power level for TOCSY spinlock (PLW10), W	2.98219991

#### F1 Acquisition parameters

Time domain data points (TD)	256
Irradiation frequency, MHz	500.1324
FID resolution (FIDRES), Hz	12.520032
Sweep width (SW), ppm	6.409
Acquisition mode for indirect detections (FnMODE)	States-TPPI (successive FID w/alt. time interval @ 0, 90, 180, 270°)

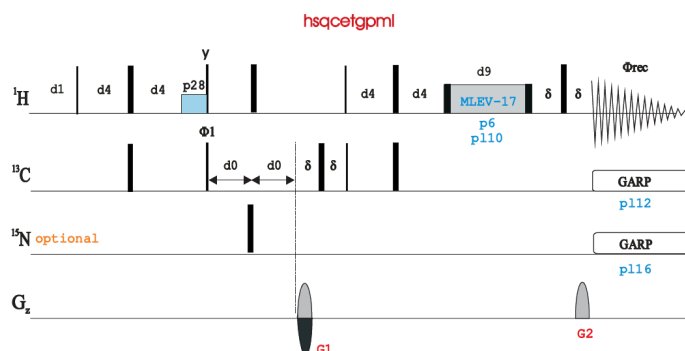
#### F2 Processing parameters

<b>Table 35. TOCSY measurement and processing parameters</b>	
Data points for Fourier transform (SI)	1024
Frequency (SF), MHz	500.13
Type of window function (WDW)	QSINE (squared sine)
Shift of the sine function (SSB)	2 (perfect cosine)
Line broadening (LB), Hz	0
<b>F1 Processing parameters</b>	
Data points for Fourier transform (SI)	1024
Type of F1 data transformation (MC2)	QF (complex 2-quadrant transformation)
Frequency (SF), MHz	500.13
Type of window function (WDW)	QSINE (squared sine)
Shift of the sine function (SSB)	2 (perfect cosine)
Line broadening (LB), Hz	0

### 12.6.1.6. HSQC-TOCSY measurement and processing parameters

**Table 36. HSQC-TOCSY measurement and processing parameters**

Measurement parameters (Bruker abbreviation)	Value
Pulse program	hsqcetgpm1 Phase-sensitive ge-2D HSQC-TOCSY with MLEV using echo-antiecho



Pulse program figure from  
Parella, Teodor. 2006. *Pulse Program Catalogue: 1D & 2D NMR experiments*.  
Bruker Biospin GmbH

Time-domain data points (TD)	1024
Solvent	D <sub>2</sub> O
Number of scans (NS)	410
Number of dummy scans (DS)	16
Spectral width (SWH), Hz	4950.495
FID resolution (FIDRES), Hz	4.834468
Acquisition time (AQ), sec	0.103424
Receiver gain (RG)	197.51
Dwell time (DW), μsec	101
Pre-scan delay (DE), μsec	10
Temperature (TE)	298
Default <sup>13</sup> C- <sup>1</sup> H coupling constant (CNST2)	145
Incremented delay (D0), sec	0.000003
Relaxation delay (D1), sec	1.47542405
[1/(4J)(XH)] delay (D4), sec	0.00172414
TOCSY mixing time (D9), sec	0.08
Short delay (D13), sec	0.000004

#### F1 Channel measurement parameters

Radiation frequency, MHz	500.132281
Nucleus	<sup>1</sup> H
F1 channel-90° high power pulse (P1), μsec	12
F1 channel-180° high power pulse (P2), μsec	24
F1 channel-60° low power pulse (P5), μsec	17.34
F1 channel-90° low power pulse (P6), μsec	26
F1 channel-180° low power pulse (P7), μsec	52
F1 channel-trim pulse at pl10 (P17), μsec	2500
F1 Channel-trim pulse at pl1 (P28), μsec	0
Pulse 1 power (PLW1), W	14
Power for TOCSY spinlock (PLW10), W	2.98219991

#### F2 Channel measurement parameters

<b>Table 36. HSQC-TOCSY measurement and processing parameters</b>	
Radiation frequency, MHz	125.7671682
Nucleus	<sup>13</sup> C
Multiple pulse decoupling scheme/heteronuclear broadband decoupling (CPDPRGG)	GARP (globally-optimized, alternating phase, rectangular pulses)
F2 channel – 90° high power pulse (P3), μsec	10
F2 channel – 180° high power pulse (P4), μsec	20
90° pulse for decoupling sequence (PCPD2), μsec	70
F2 channel pulse power (PLW2), W	65
Power level for CDP/BB decoupling (PLW12), W	1.32650006
<b>Gradient channel parameters</b>	
Gradient file name	SMSQ10.100
Gradient level for z-axis gradient 1 (GPZ1), % of maximum	80
Gradient level for z-axis gradient 2 (GPZ2), % of maximum	20.1
Gradient pulse (P16), μsec	1000
<b>F1 Acquisition parameters</b>	
Time domain data points (TD)	256
Irradiation frequency, MHz	125.7672
FID resolution (FIDRES), Hz	81.380211
Sweep width (SW), ppm	165.65
Acquisition mode for indirect detections (FnMODE)	Echo-antiecho (phase sensitive 4-quadrant transformation for gradient enhanced spectroscopy)
<b>F2 Processing parameters</b>	
Data points for Fourier transform (SI)	1024
Frequency (SF), MHz	500.13
Type of window function (WDW)	QSINE (squared sine)
Shift of the sine function (SSB)	2 (perfect cosine)
Line broadening (LB), Hz	0
<b>F1 Processing parameters</b>	
Data points for Fourier transform (SI)	1024
Type of F1 data transformation (MC2)	Echo-antiecho (phase sensitive 4-quadrant transformation for gradient enhanced spectroscopy)
frequency	500.13
type of window function	QSINE (squared sine)
Shift of the sine function (SSB)	2 (perfect cosine)
Line broadening (LB), Hz	0

## 12.6.2. Measurement and processing parameters for quantitative NMR ( $^1\text{H}$ , $^{13}\text{C}$ -HSQC)

**Table 37.  $^1\text{H}$ ,  $^{13}\text{C}$ -HSQC measurement and processing parameters for quantitative measurements**

Measurement parameters (Bruker abbreviation)	Value
Pulse program	hsqcetgp Phase-sensitive ge-2D HSQC using echo-antiecho
Time-domain data points (TD)	1024
Solvent	DMSO
Number of scans (NS)	20
Number of dummy scans (DS)	16
Spectral width (SWH), Hz	4424.779
FID resolution (FIDRES), Hz	4.321073
Acquisition time (AQ), sec	0.115712
Receiver gain (RG)	197.51
Dwell time (DW), $\mu\text{sec}$	113
Pre-scan delay (DE), $\mu\text{sec}$	10
Temperature (TE)	298
Default $^{13}\text{C}$ - $^1\text{H}$ coupling constant (CNST2)	145
Incremented delay (D0), sec	0.000003
Relaxation delay (D1), sec	1.46313596
[1/(4J)(XH)] delay (D4), sec	0.0172414
Recovery delay after gradient pulse (D16), sec	0.0002
<b>F1 Channel measurement parameters</b>	
Radiation frequency, MHz	500.132281
Nucleus	$^1\text{H}$
F1 channel— $90^\circ$ high power pulse (P1), $\mu\text{sec}$	12
F1 channel— $180^\circ$ high power pulse (P2), $\mu\text{sec}$	24
F1 Channel-trim pulse (P28), $\mu\text{sec}$	0
Pulse 1 power (PLW1), W	14
<b>F2 Channel measurement parameters</b>	
Radiation frequency, MHz	125.7671682
Nucleus	$^{13}\text{C}$
Multiple pulse decoupling scheme/heteronuclear broadband decoupling (CPDPRGG)	GARP (globally-optimized, alternating phase, rectangular pulses)
F2 channel – $90^\circ$ high power pulse (P3), $\mu\text{sec}$	10
F2 channel – $180^\circ$ high power pulse (P4), $\mu\text{sec}$	20
$90^\circ$ pulse for decoupling sequence (PCPD2), $\mu\text{sec}$	70

Pulse program figure from  
Parella, Teodor. 2006. *Pulse Program Catalogue: 1D & 2D NMR experiments*. Bruker Biospin GmbH.

<b>Table 37. <sup>1</sup>H, <sup>13</sup>C-HSQC measurement and processing parameters for quantitative measurements</b>	
F2 channel pulse power (PLW2), W	65
Power level for CDP/BB decoupling (PLW12), W	1.32650006
<b>Gradient channel parameters</b>	
Gradient file name	SMSQ10.100
Gradient level for z-axis gradient 1 (GPZ1), % of maximum	80
Gradient level for z-axis gradient 2 (GPZ2), % of maximum	20.1
Gradient pulse (P16), μsec	1000
<b>F1 Acquisition parameters</b>	
Time domain data points (TD)	256
Irradiation frequency, MHz	125.7672
FID resolution (FIDRES), Hz	81.380211
Sweep width (SW), ppm	165.65
Acquisition mode for indirect detections (FnMODE)	Echo-antiecho (phase sensitive 4-quadrant transformation for gradient enhanced spectroscopy)
<b>F2 Processing parameters</b>	
Data points for Fourier transform (SI)	1024
Frequency (SF), MHz	500.13
Type of window function (WDW)	QSINE (squared sine)
Shift of the sine function (SSB)	2 (perfect cosine)
Line broadening (LB), Hz	0
<b>F1 Processing parameters</b>	
Data points for Fourier transform (SI)	1024
Type of F1 data transformation (MC2)	Echo-antiecho (phase sensitive 4-quadrant transformation for gradient enhanced spectroscopy)
frequency	500.13
type of window function	QSINE (squared sine)
Shift of the sine function (SSB)	2 (perfect cosine)
Line broadening (LB), Hz	0

## 12.7. Additional data tables

**Table 38.** <sup>1</sup>H NMR data of feruloylated oligosaccharides/monosaccharides (in D<sub>2</sub>O) isolated from intermediate wheatgrass (*Thinopyrum intermedium*). Coupling constants *J* in Hz; chemical shifts δ<sub>H</sub> in ppm; spectra calibrated against acetone (0.5 μL, δ<sub>H</sub> = 2.22 ppm, δ<sub>C</sub> = 30.89 ppm).

	H1 ( <i>J</i> <sub>1,2</sub> )	H2	H3	H4	H5 ( <i>J</i> <sub>5,6</sub> )		H6 ( <i>J</i> <sub>7,8</sub> )	H7	H8	OMe
					H5 <sub>eq</sub>	H5 <sub>ax</sub>				
<b>(A4.1):</b> β-xylopyranosyl-(1→4)-[5- <i>O</i> - <i>trans</i> -feruloyl-α-arabinofuranosyl-(1→3)]-β-xylopyranosyl-(1→4)-xylopyranose										
α-Xylose, reducing	5.18 (3.6)	3.53	3.76	3.91	3.85	3.74				
β-Xylose, reducing	4.57 (7.7)	3.24	nd	3.74	4.04	3.36	-	-	-	-
β-Xylose <sup>I</sup>	4.41 (7.8)	3.27	3.40	3.59	3.91	3.25				
β-Xylose <sup>II</sup>	4.51 (8.0)	3.44	3.71	3.81	4.13	3.40				
α-Arabinose, reducing	5.39 (1.7)	4.20	3.98	4.55	4.52	4.34	-	-	-	-
<i>trans</i> -Ferulic acid	-	7.33	-	-	6.93 (8.5)	7.22	7.74 (16.1)	6.48	3.91	
<b>(A7):</b> 5- <i>O</i> - <i>cis</i> -feruloyl-L-arabinofuranose										
β-Arabinose, reducing	5.29	nd	nd	nd	nd	nd	-	-	-	-
α-Arabinose, reducing	5.20 (2.3)	nd	nd	nd	nd	nd	-	-	-	-
<i>cis</i> -Ferulic acid	-	7.35	-	-	6.90 (8.5)	7.07	7.07 (12.6)	5.94	3.86	
<b>(A8):</b> β-D-xylopyranosyl-(1→2)-5- <i>O</i> - <i>trans</i> -feruloyl-L-arabinofuranose										
β-Xylose ( <i>side-chain</i> )	4.56 (7.71)	3.27	nd	nd	nd	nd	-	-	-	-
β-Arabinose, reducing	5.37	nd	nd	nd	nd	nd	-	-	-	-
α-Arabinose, reducing	5.42	4.18	nd	nd	nd	nd	-	-	-	-
<i>trans</i> -Ferulic acid	-	7.25	-	-	6.83 (7.8)	7.17	7.71 (16.1)	6.39	3.86	
<b>(A10):</b> 5- <i>O</i> - <i>trans</i> -feruloyl-L-arabinofuranose										
β-Arabinose, reducing	5.32 (4.9)	4.13	4.16	4.04	4.48	4.27	-	-	-	-
α-Arabinose, reducing	5.29	4.08	4.07	4.34	4.45	4.30	-	-	-	-
<i>trans</i> -Ferulic acid	-	7.18	-	-	6.90 (8.3)	7.11	7.61 (16.1)	6.36	3.86	
<b>(E2):</b> 5- <i>O</i> - <i>trans</i> -feruloyl-α-arabinofuranosyl-(1→3)-β-xylopyranosyl-(1→4)-xylopyranose										
α-Xylose, reducing	5.21 (3.4)	3.55	3.77	3.69	3.78	3.75	-	-	-	-
β-Xylose, reducing	4.60 (8.5)	3.28	3.56	3.74	4.04	3.37	-	-	-	-
β-Xylose <sup>I</sup>	4.36 (8.6)	3.39	3.48	3.63	3.97	3.26	-	-	-	-
α-Arabinose	5.30	4.24	4.03	4.35	4.39	4.16	-	-	-	-
<i>trans</i> -Ferulic acid	-	6.72	-	-	6.69 (7.0)	6.76	7.22 (15.4)	5.97	3.66	

**Table 38. <sup>1</sup>H NMR data of feruloylated oligosaccharides/monosaccharides (in D<sub>2</sub>O) isolated from intermediate wheatgrass (*Thinopyrum intermedium*).** Coupling constants *J* in Hz; chemical shifts  $\delta_{\text{H}}$  in ppm; spectra calibrated against acetone (0.5  $\mu\text{L}$ ,  $\delta_{\text{H}} = 2.22$  ppm,  $\delta_{\text{C}} = 30.89$  ppm).

	H1 ( <i>J</i> <sub>1,2</sub> )	H2	H3	H4	H5 ( <i>J</i> <sub>5,6</sub> )		H6 ( <i>J</i> <sub>7,8</sub> )	H7	H8	OMe
					H5 <sub>eq</sub>	H5 <sub>ax</sub>				
<b>(E5.1):</b> $\beta$ -xylopyranosyl-(1 $\rightarrow$ 4)-[5- <i>O</i> - <i>trans</i> -feruloyl- $\alpha$ -arabinofuranosyl-(1 $\rightarrow$ 3)]- $\beta$ -xylopyranosyl-(1 $\rightarrow$ 4)-xylopyranose										
$\alpha$ -Xylose, reducing	5.19 (3.4)	3.54	3.75	3.77	3.78	3.72	-	-	-	-
$\beta$ -Xylose, reducing	4.58 (8.0)	3.25	3.55	3.74	4.03	3.35	-	-	-	-
$\beta$ -Xylose <sup>I</sup>	4.41 (7.8)	3.27	3.41	3.60	3.90	3.26	-	-	-	-
$\beta$ -Xylose <sup>II</sup>	4.43 (7.6)	3.42	3.72	3.78	4.09	3.35	-	-	-	-
$\alpha$ -Arabinose	5.44 (3.6)	4.22	4.00	4.54	4.45	4.30	-	-	-	-
<i>trans</i> -Ferulic acid	-	7.00	-	-	6.81 (8.1)	6.98	7.47 (16.0)	6.23	3.78	

<sup>I, II, III</sup> Roman numeral notation is used to differentiate non-reducing xylose moieties originating from the arabinoxylan backbone (compare **Figure 13**).

Abbreviations used: **nd**: not determined; **NMR**: nuclear magnetic resonance.

**Table 39.**  $^{13}\text{C}$  NMR data of feruloylated oligosaccharides/monosaccharides (in  $\text{D}_2\text{O}$ ) isolated from intermediate wheatgrass (*Thinopyrum intermedium*). Chemical shifts  $\delta_{\text{C}}$  in ppm; spectra calibrated against acetone (0.5  $\mu\text{L}$ ,  $\delta_{\text{H}} = 2.22$  ppm,  $\delta_{\text{C}} = 30.89$  ppm); data taken from HSQC<sup>1</sup>.

	C1	C2	C3	C4	C5	C6	C7	C8	C9	OMe
<b>(A4.1):</b> $\beta$ -xylopyranosyl-(1 $\rightarrow$ 4)-[5- <i>O</i> - <i>trans</i> -feruloyl- $\alpha$ -arabinofuranosyl-(1 $\rightarrow$ 3)]- $\beta$ -xylopyranosyl-(1 $\rightarrow$ 4)-xylopyranose										
$\alpha$ -Xylose, reducing	92.6	74.5	71.2	71.4	59.5	-	-	-	-	-
$\beta$ -Xylose, reducing	97.3	74.0	nd	77.1	63.7	-	-	-	-	-
$\beta$ -Xylose <sup>I</sup>	102.4	73.4	76.3	69.9	66.0	-	-	-	-	-
$\beta$ -Xylose <sup>II</sup>	102.3	73.9	78.7	74.5	63.5	-	-	-	-	-
$\alpha$ -Arabinose	108.7	81.5	78.4	82.5	64.9	-	-	-	-	-
<i>trans</i> -Ferulic acid	126.8	112.3	148.4	149.9	116.4	124.4	147.5	114.7	169.8	56.7
<b>(A8):</b> $\beta$ -D-xylopyranosyl-(1 $\rightarrow$ 2)-5- <i>O</i> - <i>trans</i> -feruloyl-L-arabinofuranose										
$\beta$ -Xylose, ( <i>side-chain</i> )	103.43 104.40	89.97	nd	nd	nd	-	-	-	-	-
$\beta$ -Arabinose, reducing	95.83	nd	nd	nd	nd	-	-	-	-	-
$\alpha$ -Arabinose, reducing	101.17	nd	nd	nd	nd	-	-	-	-	-
<i>trans</i> -Ferulic acid	129.7	112.0	149.4	153.5	117.4	125.1	147.9	113.1	169.9	56.6
<b>(A10):</b> 5- <i>O</i> - <i>trans</i> -feruloyl-L-arabinofuranose										
$\beta$ -Arabinose, reducing	95.5	76.0	75.1	79.0	65.3	-	-	-	-	-
$\alpha$ -Arabinose, reducing	101.6	80.9	77.2	81.1	64.2	-	-	-	-	-
<i>trans</i> -Ferulic acid	126.9	111.7	147.9	nd	115.9	124.3	146.2	114.5	169.5	56.6
<b>(E2):</b> 5- <i>O</i> - <i>trans</i> -feruloyl- $\alpha$ -arabinofuranosyl-(1 $\rightarrow$ 3)]- $\beta$ -xylopyranosyl-(1 $\rightarrow$ 4)-xylopyranose										
$\alpha$ -Xylose, reducing	92.7	72.1	71.8	77.4	59.5	-	-	-	-	-
$\beta$ -Xylose, reducing	97.2	74.7	74.6	77.3	63.7	-	-	-	-	-
$\beta$ -Xylose <sup>I</sup>	102.4	73.4	83.0	68.6	65.8	-	-	-	-	-
$\alpha$ -Arabinose	109.0	81.7	77.6	81.9	64.9	-	-	-	-	-
<i>trans</i> -Ferulic acid	127.0	111.3	147.8	nd	116.0	124.0	147.1	113.8	169.4	56.0
<b>(E5.1):</b> $\beta$ -xylopyranosyl-(1 $\rightarrow$ 4)-[5- <i>O</i> - <i>trans</i> -feruloyl- $\alpha$ -arabinofuranosyl-(1 $\rightarrow$ 3)]- $\beta$ -xylopyranosyl-(1 $\rightarrow$ 4)-xylopyranose										
$\alpha$ -Xylose, reducing	92.8	72.0	71.8	74.4	59.6	-	-	-	-	-
$\beta$ -Xylose, reducing	97.3	74.4	74.6	77.5	63.6	-	-	-	-	-
$\beta$ -Xylose <sup>I</sup>	102.5	74.0	76.4	69.9	65.8	-	-	-	-	-
$\beta$ -Xylose <sup>II</sup>	102.3	74.2	78.1	74.5	63.5	-	-	-	-	-
$\alpha$ -Arabinose	108.8	81.4	78.4	82.9	64.9	-	-	-	-	-
<i>trans</i> -Ferulic acid	127.0	111.6	148.2	nd	116.0	124.3	147.5	114.2	169.6	56.2

<sup>1</sup>When reported, C1, C3, C4, and C9 phenolic acid shifts were taken from HMBC.

<sup>I, II, III</sup> Roman numeral notation is used to differentiate non-reducing xylose moieties originating from the arabinoxylan backbone (compare **Figure 13**).

Abbreviations used: **HSQC**: heteronuclear single quantum coherence spectroscopy; **nd**: not determined; **NMR**: nuclear magnetic resonance.

## 12.8. Additional figures: Chromatograms

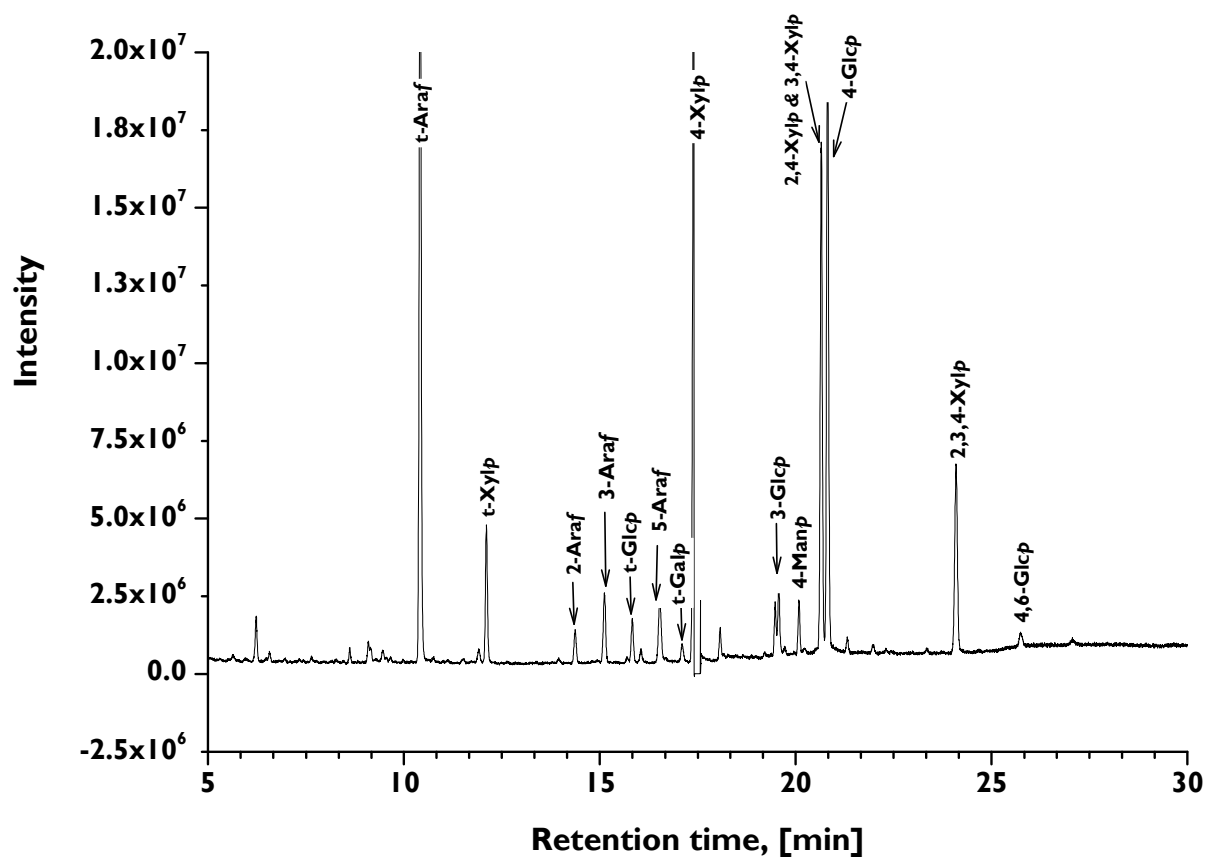


Figure 35. GC-MS chromatogram of partially-methylated alditol acetates arising from methylation analysis of intermediate wheatgrass insoluble fiber.

Abbreviations used: 2-, etc: *O*-2-glycosidically linked; **Araf**: arabinopyranose; **Galp**: galactopyranose; **Glcp**: glucopyranose; **Manp**: mannopyranose; **t**: terminal; **Xylp**: xylopyranose.

## 12.9. Additional figures: Spectra

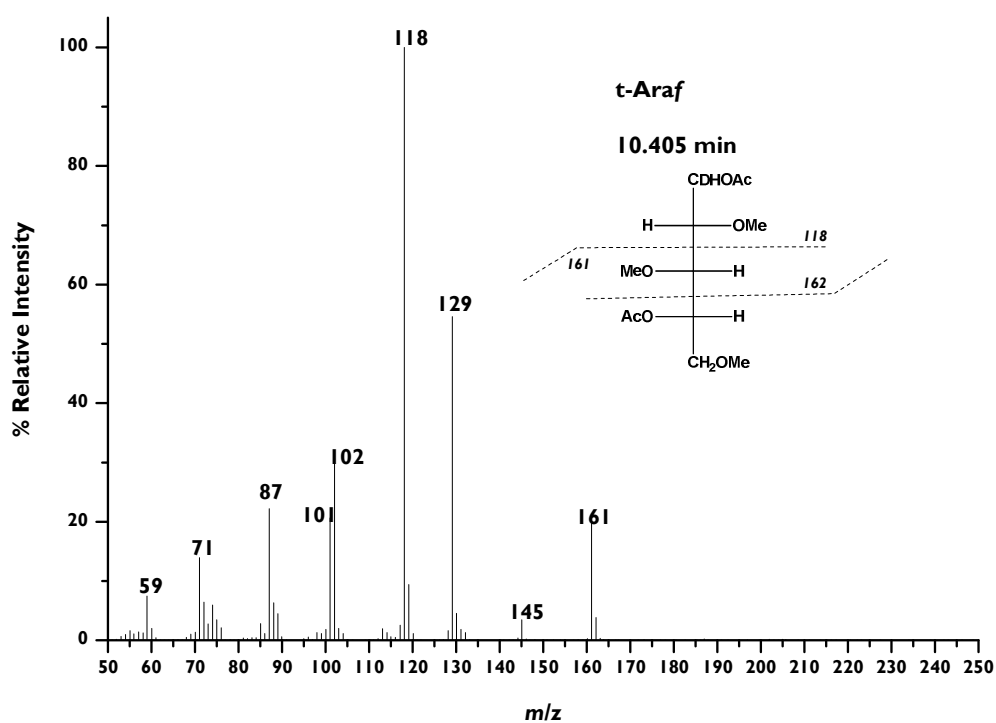


Figure 36. Electron impact (EI) mass spectrum of partially methylated alditol acetate of terminal arabinofuranose (t-Araf).

Abbreviations used:  $m/z$ : mass-to-charge ratio.

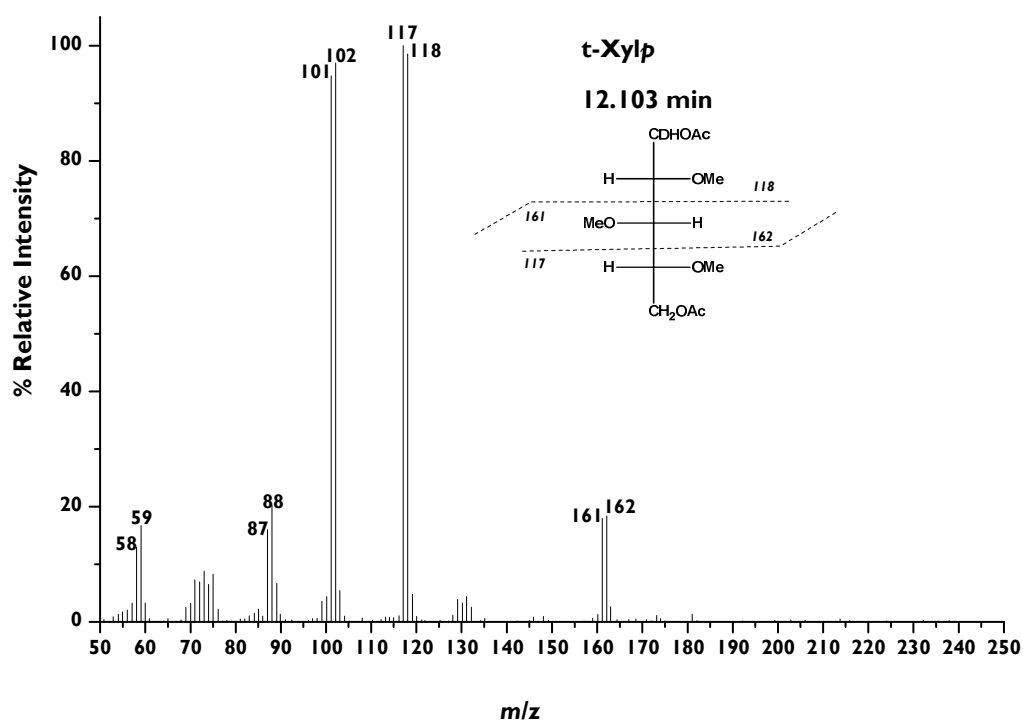


Figure 37. Electron impact (EI) mass spectrum of partially methylated alditol acetate of terminal xylopyranose (t-Xylp).

Abbreviations used:  $m/z$ : mass-to-charge ratio.

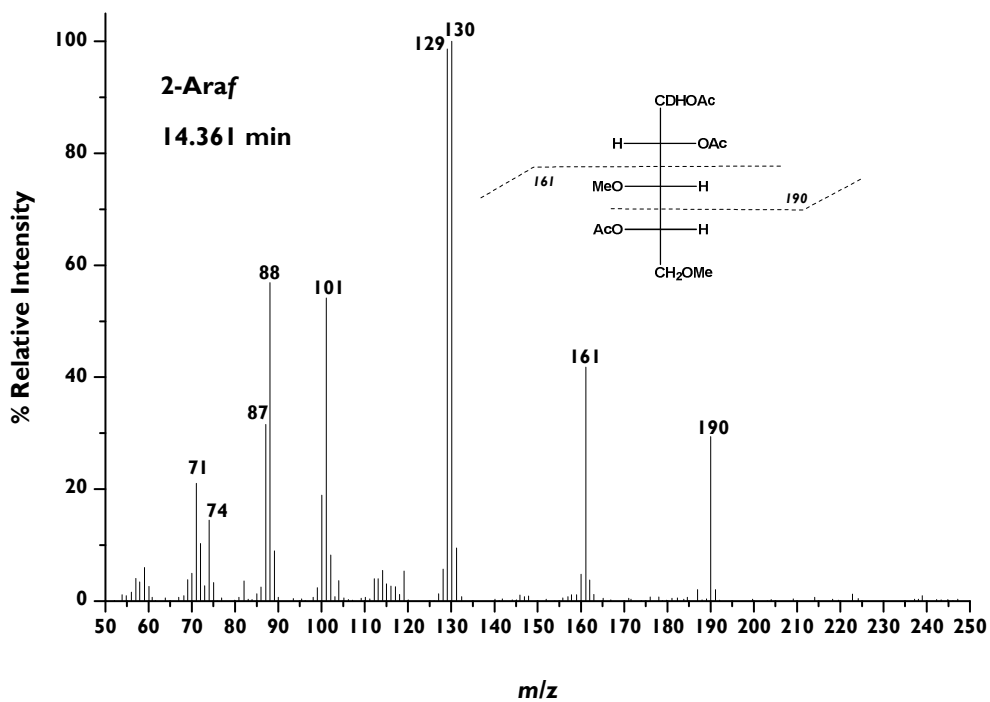


Figure 38. Electron impact (EI) mass spectrum of partially methylated alditol acetate of 1,2-linked arabinofuranose (2-Araf).

Abbreviations used:  $m/z$ : mass-to-charge ratio.

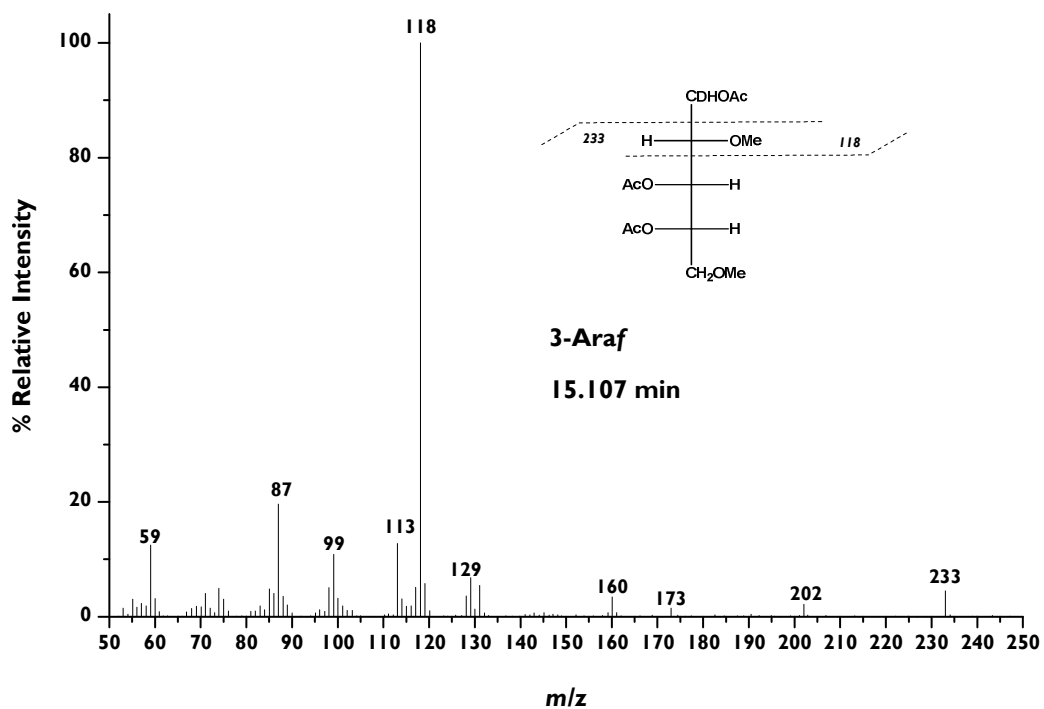


Figure 39. Electron impact (EI) mass spectrum of partially methylated alditol acetate of 1,3-linked arabinofuranose (3-Araf).

Abbreviations used:  $m/z$ : mass-to-charge ratio.

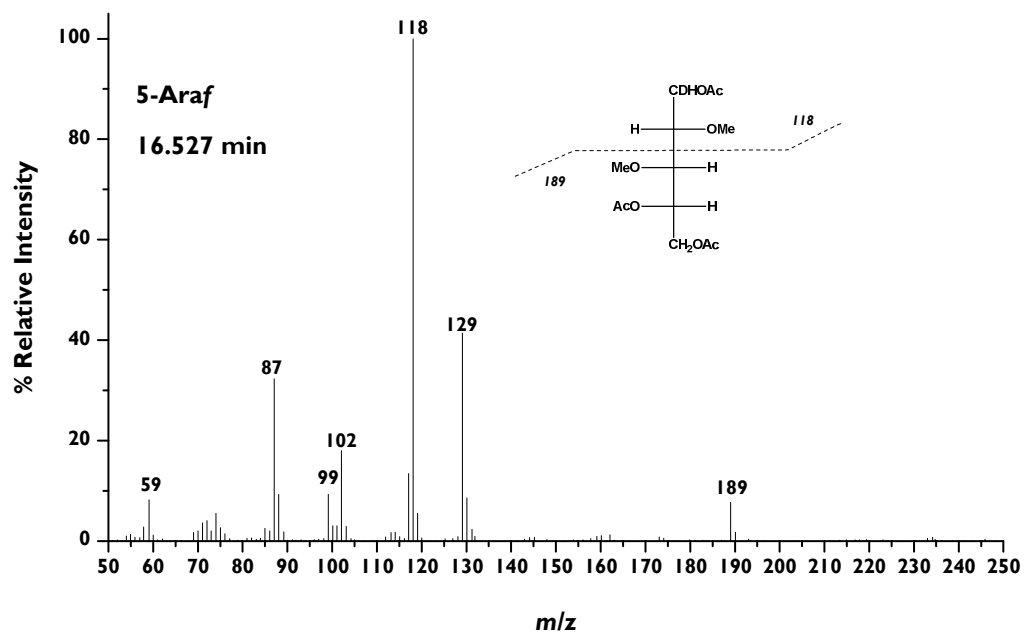


Figure 40. Electron impact (EI) mass spectrum of partially methylated alditol acetate of 1,5-linked arabinofuranose (5-Araf).

Abbreviations used: *m/z*: mass-to-charge ratio.

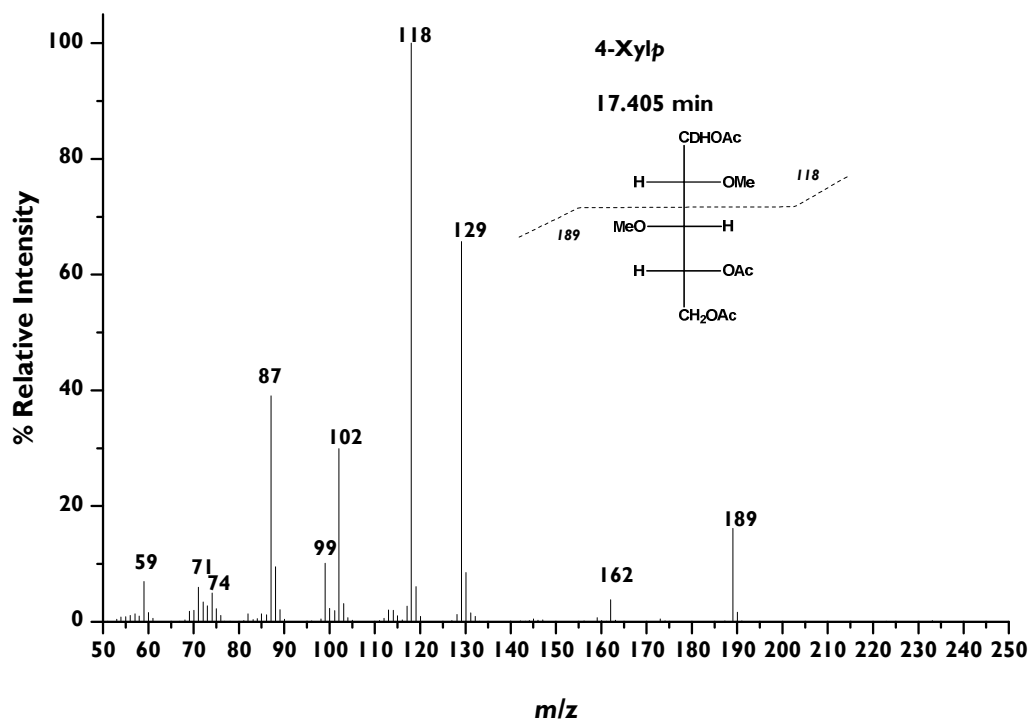


Figure 41. Electron impact (EI) mass spectrum of partially methylated alditol acetate of (1,4)-glycosidically linked xylopyranose (4-Xylp).

Abbreviations used: *m/z*: mass-to-charge ratio.

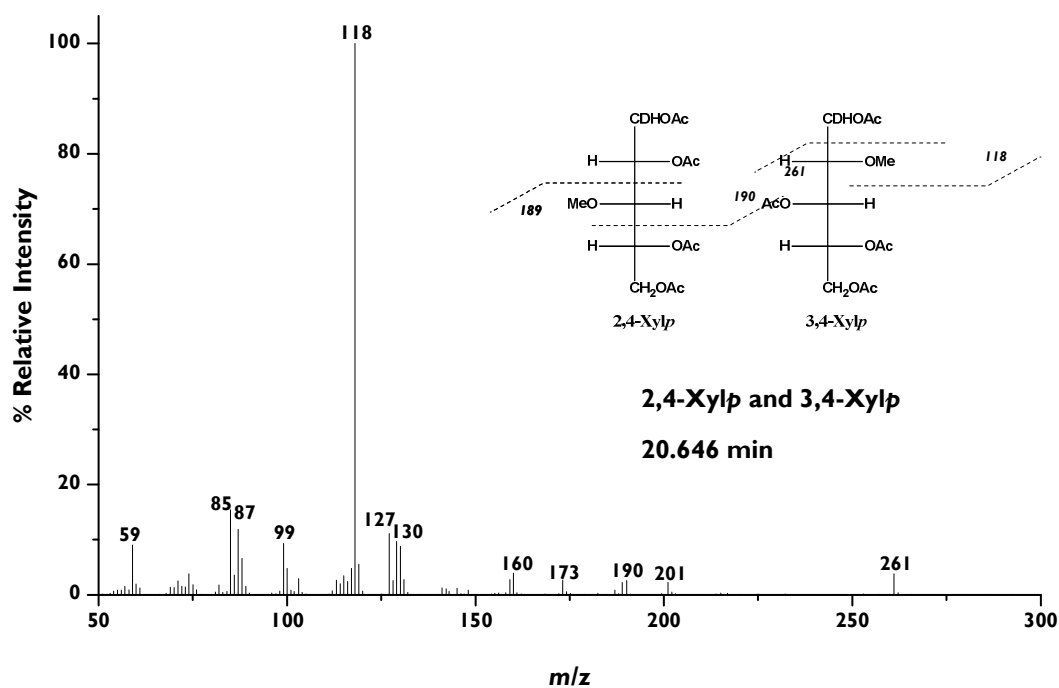


Figure 42. Electron impact (EI) mass spectrum of the partially methylated alditol acetates of (1,2,4)-linked xylopyranose (2,4-Xylp) and (1,3,4)-linked xylopyranose (3,4-Xylp).

Compounds were coeluted.

Abbreviations used:  $m/z$ : mass-to-charge ratio.

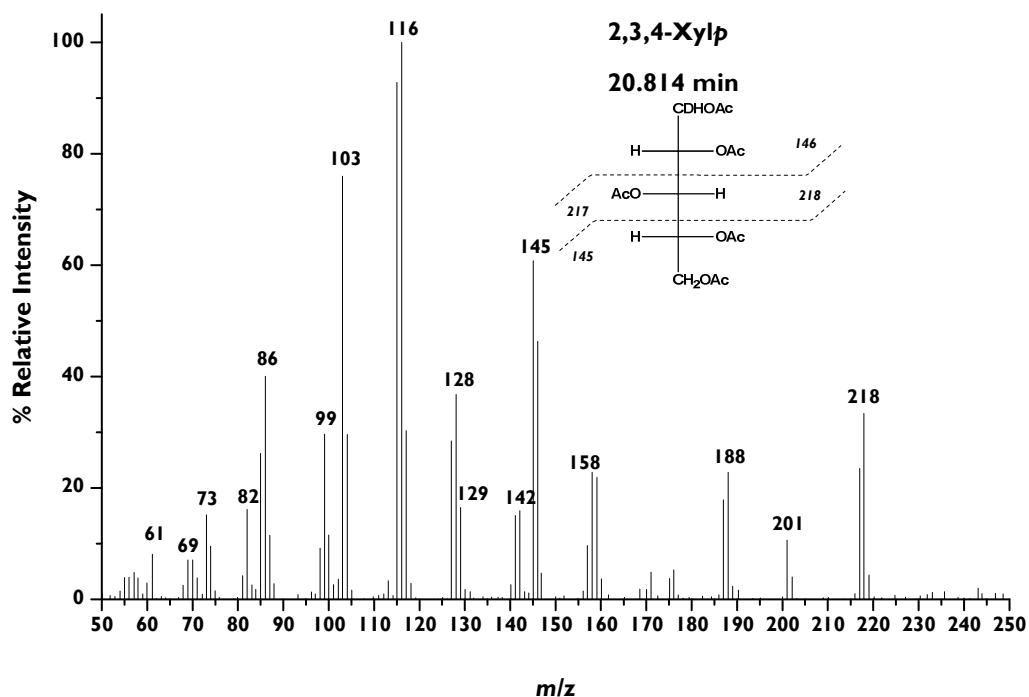
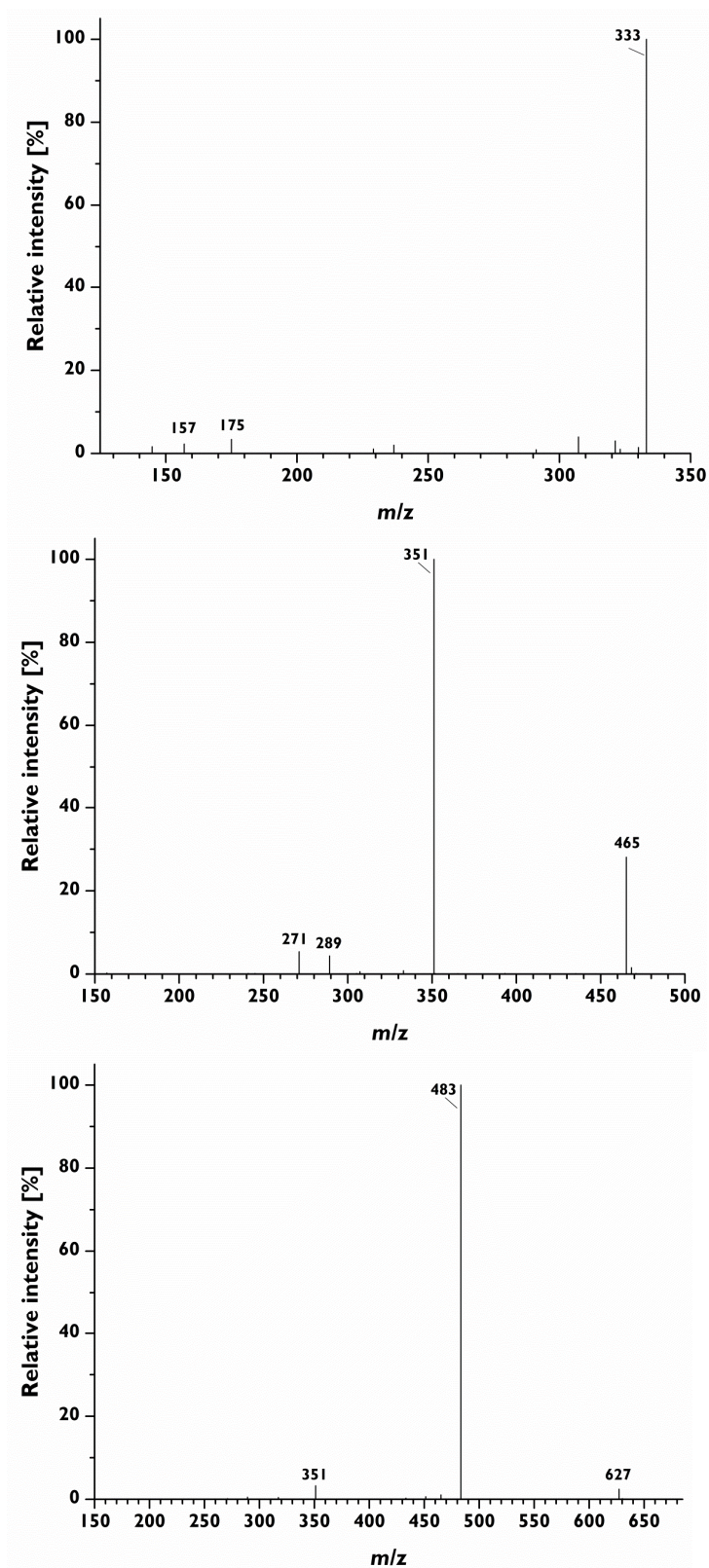


Figure 43. Electron impact (EI) mass spectrum of partially methylated alditol acetate of (1,2,3,4)-linked xylopyranose (2,3,4-Xylp).

Abbreviations used:  $m/z$ : mass-to-charge ratio.



**Figure 44. MS/MS spectra of the sodium adducts of feruloylated side-chain standard compounds following reduction. [Top]:** Reduced FA ( $[M + Na]^+$   $m/z$  351); **[Middle]:** Reduced FAX ( $[M + Na]^+$   $m/z$  483); **[Bottom]:** Reduced FAXG ( $[M + Na]^+$   $m/z$  645).

*Abbreviations used:* **FA:** 5-*O*-*trans*-feruloyl-L-arabinofuranose; **FAX:**  $\beta$ -D-xylopyranosyl-(1 $\rightarrow$ 2)-5-*O*-*trans*-feruloyl-L-arabinofuranose; **FAXG:**  $\alpha$ -L-galactopyranosyl-(1 $\rightarrow$ 2)- $\beta$ -D-xylopyranosyl-(1 $\rightarrow$ 2)-5-*O*-*trans*-feruloyl-L-arabinofuranose.

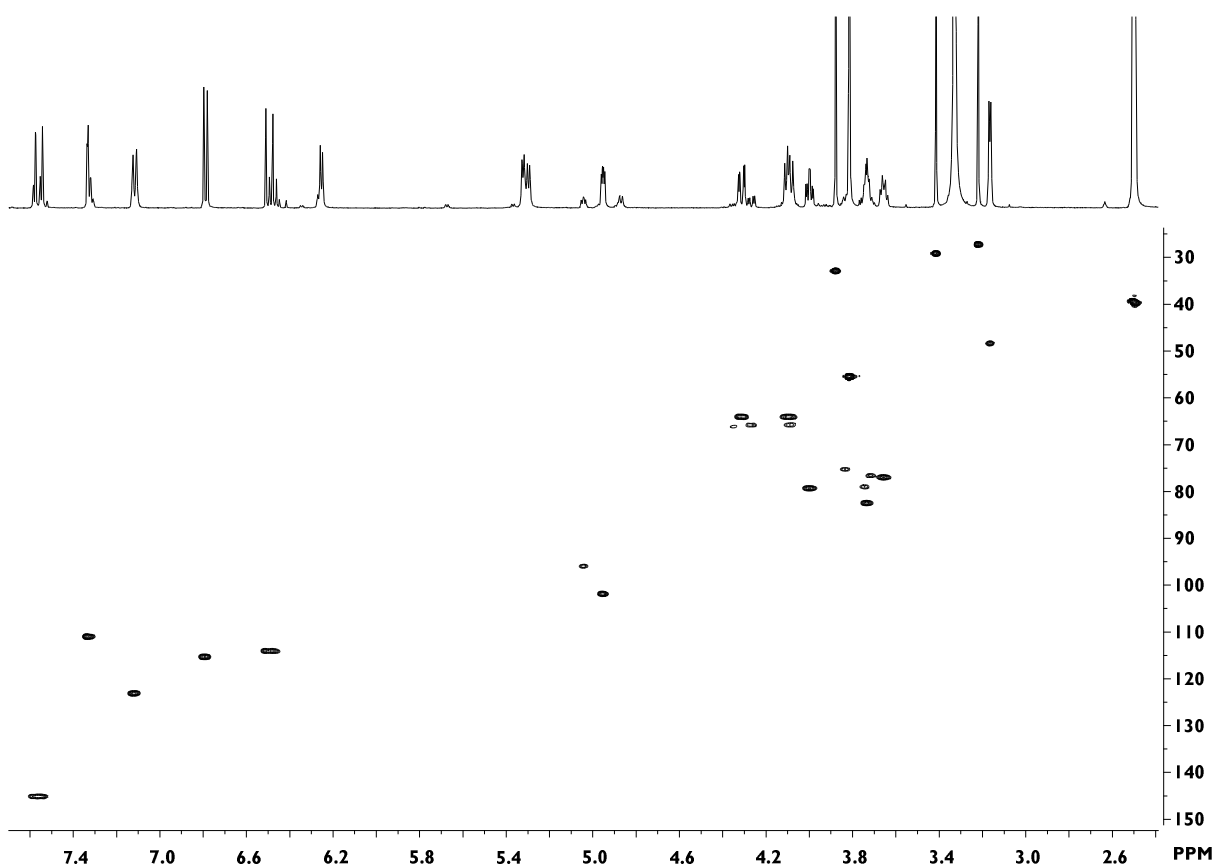


**Figure 45. HSQC-NMR spectrum of FA and caffeine.** Spectrum was measured in DMSO-*d*<sub>6</sub> and calibrated against residual DMSO signal ( $^1\text{H} = 2.50$  ppm;  $^{13}\text{C} = 39.52$  ppm)..

*Abbreviations used:* **FA:** 5-*O-trans*-feruloyl-L-arabinofuranose; **HSQC:** heteronuclear single quantum coherence spectroscopy; **NMR:** nuclear magnetic resonance.

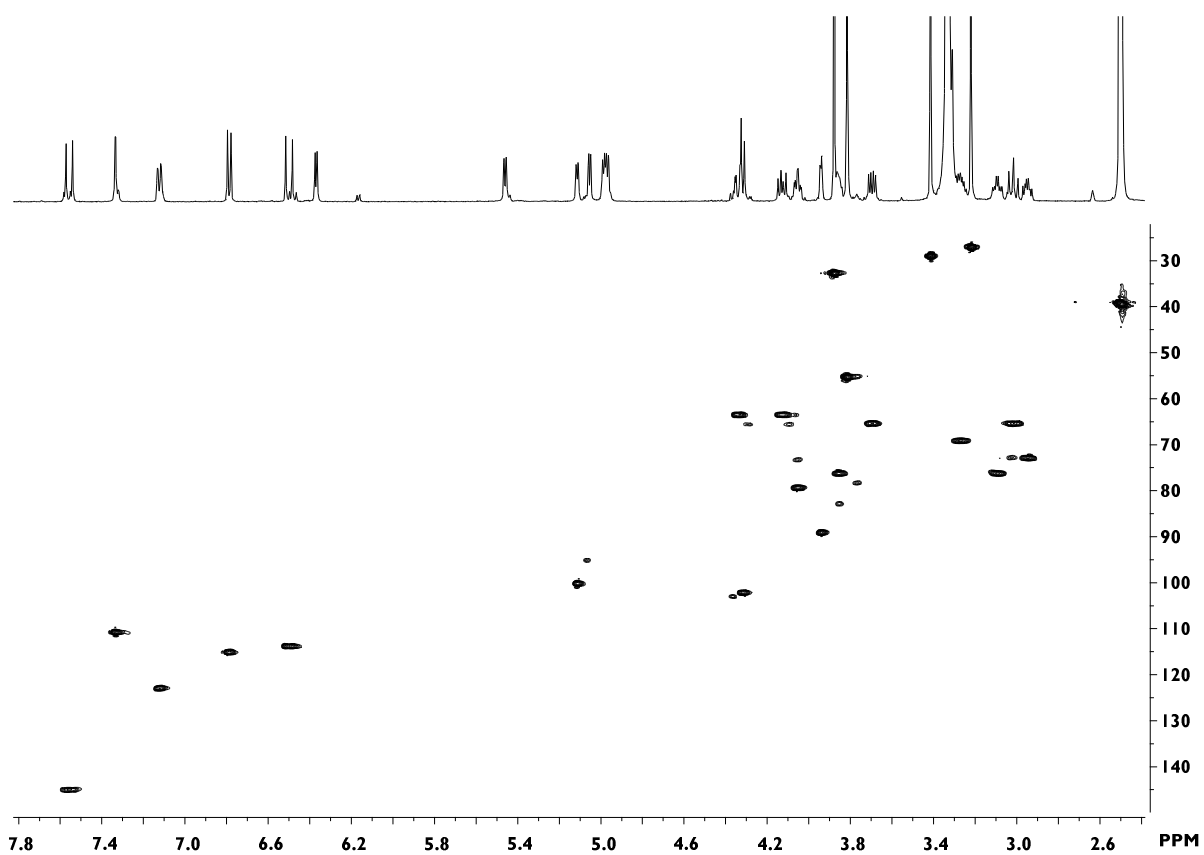


**Figure 46. HSQC-NMR spectrum of FAX and caffeine.** Spectrum was measured in DMSO-*d*<sub>6</sub> and calibrated against residual DMSO signal (<sup>1</sup>H = 2.50 ppm; <sup>13</sup>C = 39.52 ppm).

*Abbreviations used:* **FAX:** β-D-xylopyranosyl-(1→2)-5-*O*-*trans*-feruloyl-L-arabinofuranose; **HSQC:** heteronuclear single quantum coherence spectroscopy; **NMR:** nuclear magnetic resonance.

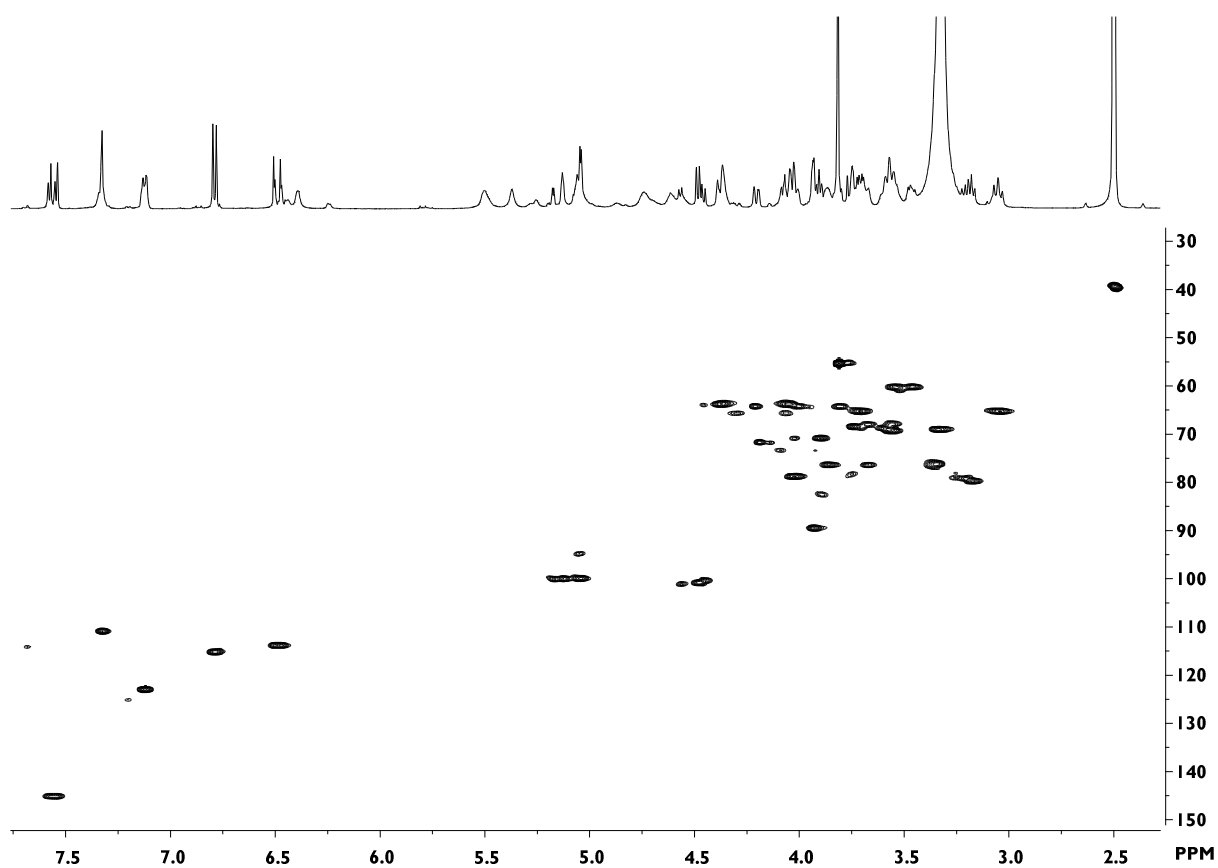


**Figure 47. HSQC-NMR spectrum of FAXG.** Spectrum was measured in DMSO-*d*<sub>6</sub> and calibrated against residual DMSO signal (<sup>1</sup>H = 2.50 ppm; <sup>13</sup>C = 39.52 ppm).

*Abbreviations used:* **FAXG:**  $\alpha$ -L-galacto-pyranosyl-(1 $\rightarrow$ 2)- $\beta$ -D-xylopyranosyl-(1 $\rightarrow$ 2)-5-*O*-*trans*-feruloyl-L-arabinofuranose; **HSQC:** heteronuclear single quantum coherence spectroscopy; **NMR:** nuclear magnetic resonance.

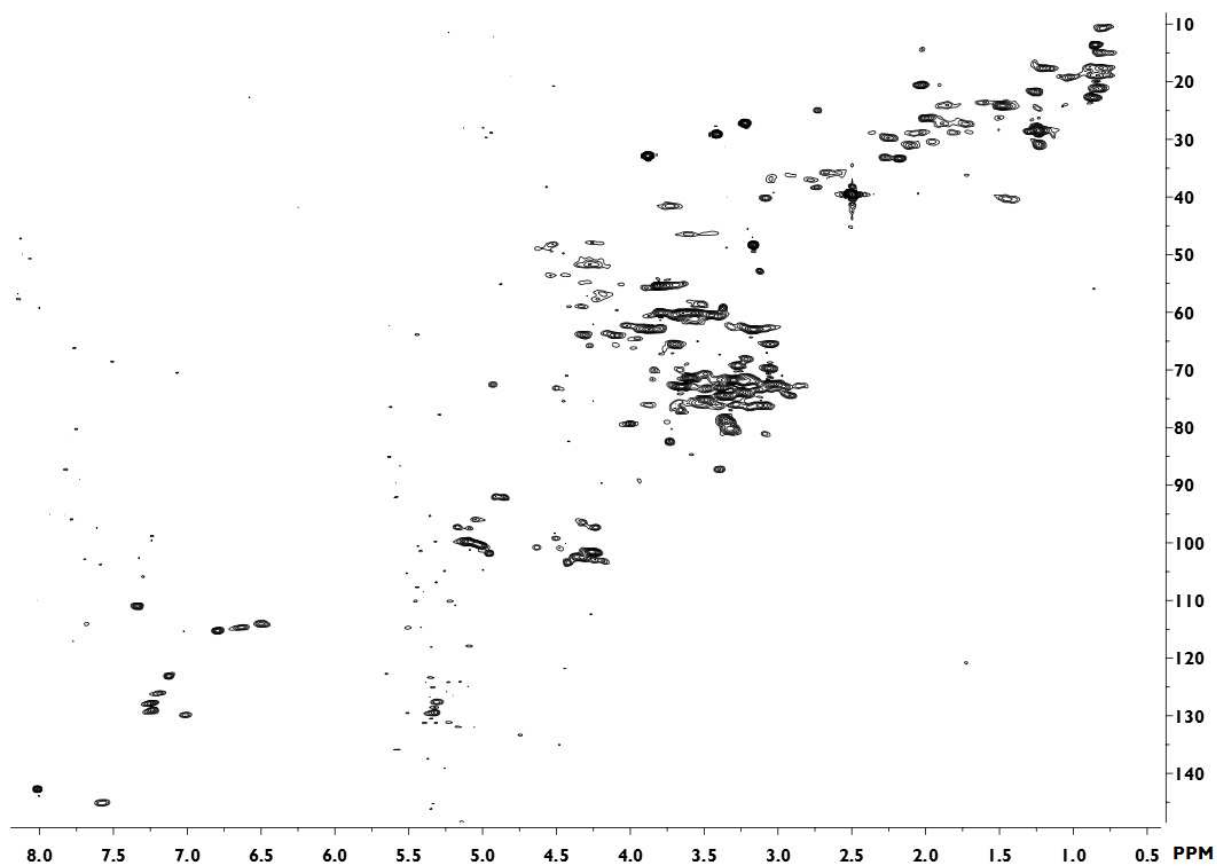


**Figure 48. HSQC-NMR spectrum of the mildly acidic hydrolysate from insoluble oat fiber.** Spectrum was measured in DMSO-*d*<sub>6</sub> and calibrated against residual DMSO signal (<sup>1</sup>H = 2.50 ppm; <sup>13</sup>C = 39.52 ppm).

*Abbreviations used:* **HSQC:** heteronuclear single quantum coherence spectroscopy; **NMR:** nuclear magnetic resonance.

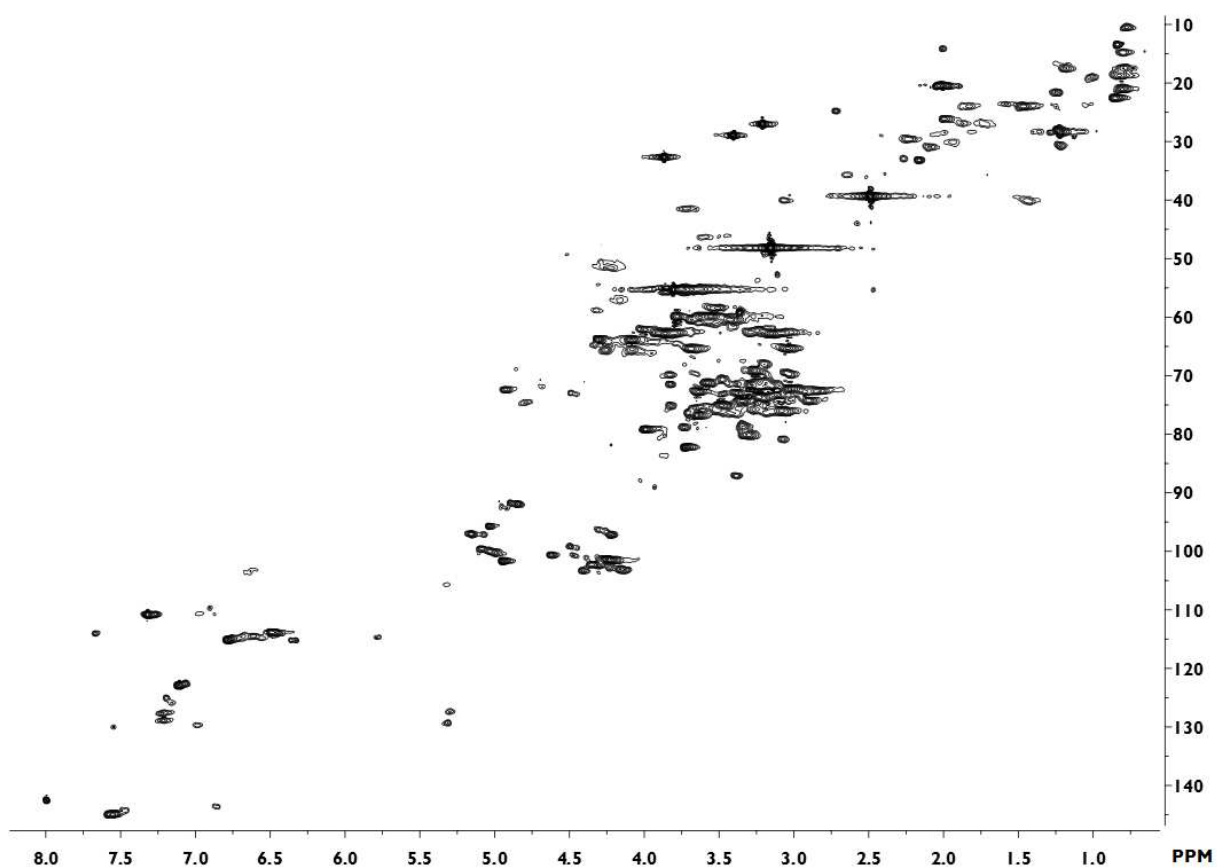


**Figure 49. HSQC-NMR spectrum of the mildly acidic hydrolysate from insoluble wheat fiber.** Spectrum was measured in DMSO-*d*<sub>6</sub> and calibrated against residual DMSO signal (<sup>1</sup>H = 2.50 ppm; <sup>13</sup>C = 39.52 ppm).

*Abbreviations used:* **HSQC:** heteronuclear single quantum coherence spectroscopy; **NMR:** nuclear magnetic resonance.

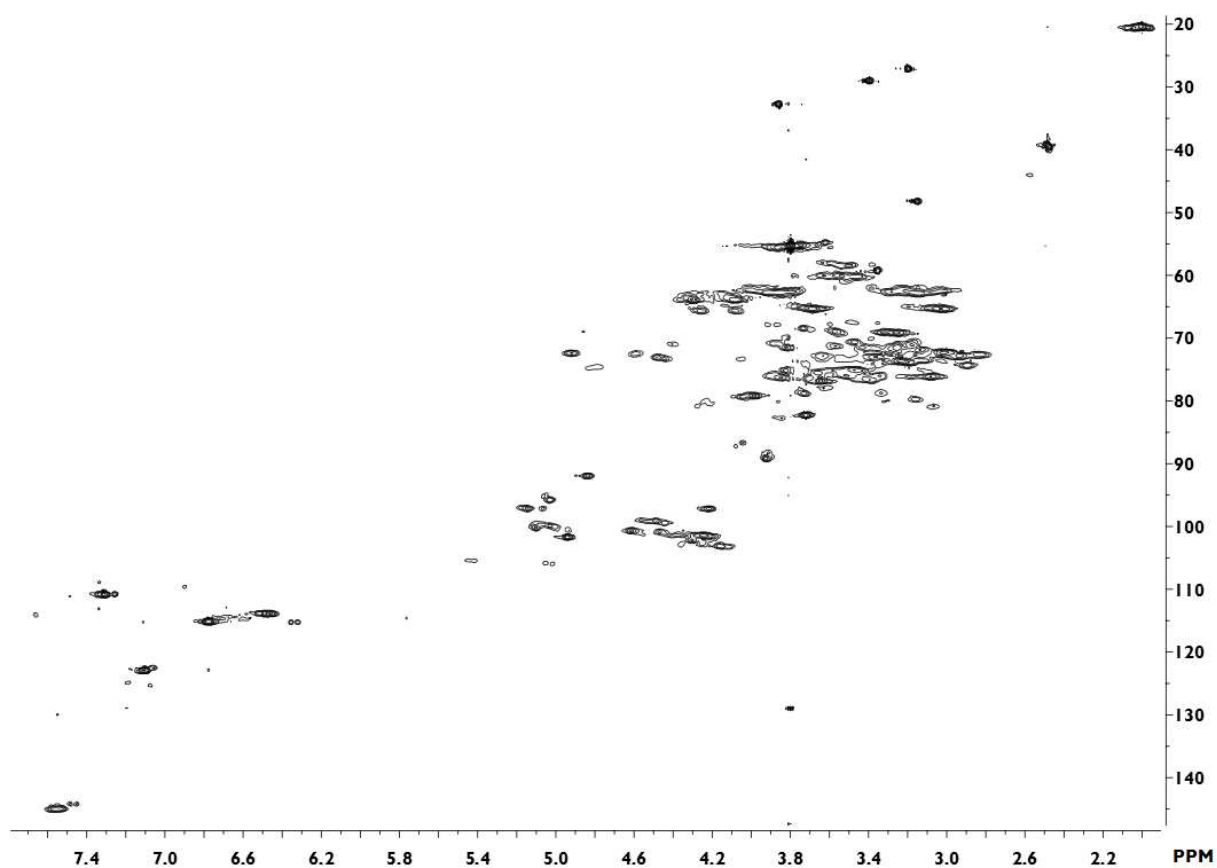


**Figure 50. HSQC-NMR spectrum of the mildly acidic hydrolysate from insoluble popcorn fiber.** Spectrum was measured in DMSO-*d*<sub>6</sub> and calibrated against residual DMSO signal (<sup>1</sup>H = 2.50 ppm; <sup>13</sup>C = 39.52 ppm).

*Abbreviations used:* **HSQC:** heteronuclear single quantum coherence spectroscopy; **NMR:** nuclear magnetic resonance.

## 12.10. Additional data figures

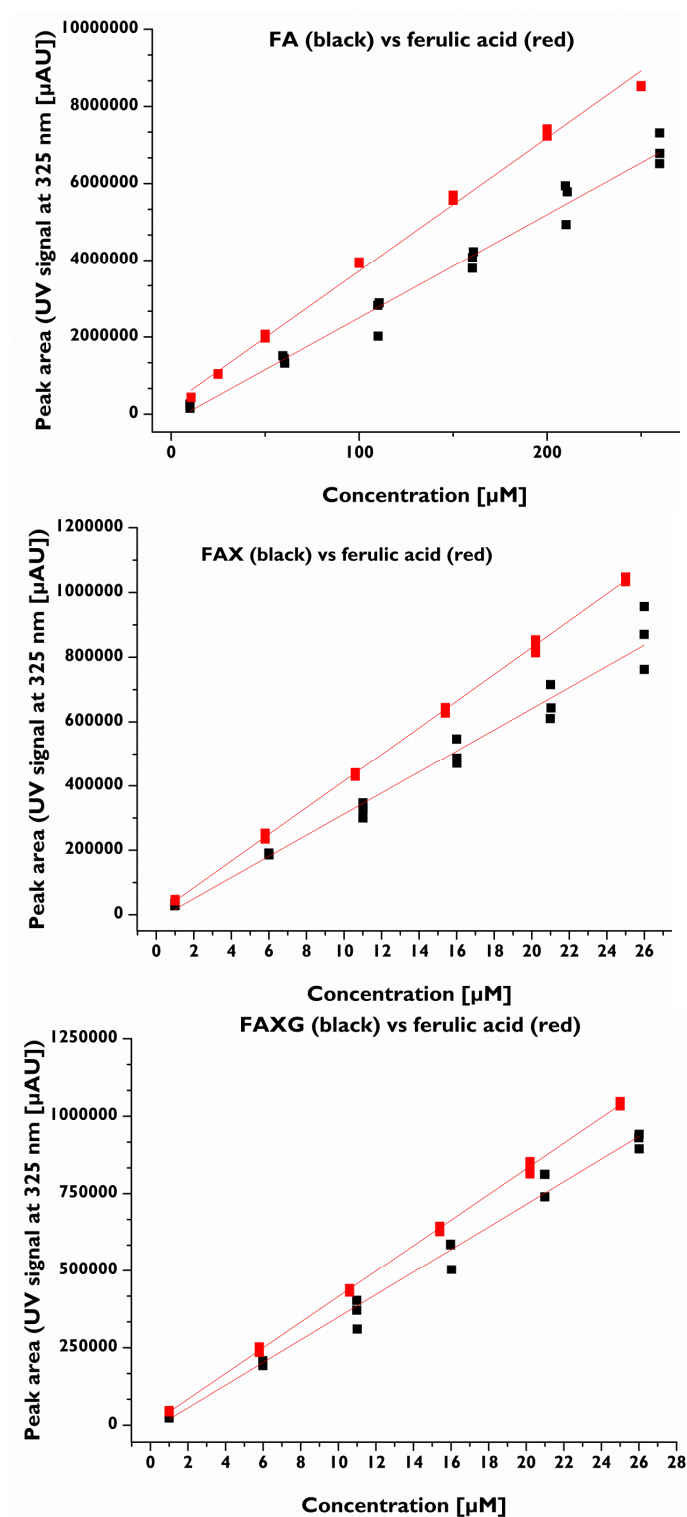


Figure 51. Linear response of FA (top), FAX (middle), and FAXG (bottom) compared to ferulic acid.

Abbreviations used: FA: 5-*O*-*trans*-feruloyl-L-arabinofuranose; FAX:  $\beta$ -D-xylopyranosyl-(1 $\rightarrow$ 2)-5-*O*-*trans*-feruloyl-L-arabinofuranose; FAXG:  $\alpha$ -L-galactopyranosyl-(1 $\rightarrow$ 2)- $\beta$ -D-xylopyranosyl-(1 $\rightarrow$ 2)-5-*O*-*trans*-feruloyl-L-arabinofuranose.

# Curriculum Vitae

---

**Name** Rachel Renae Schendel (maiden name Kylo)  
**Birthdate, Birthplace** 06.06.1986, Rochester, Minnesota, United States of America

## Education

---

09/2012-present **Karlsruhe Institute of Technology (KIT)**  
Doctoral studies at the Institute of Applied Biosciences,  
Department of Food Chemistry and Phytochemistry (Prof.  
Dr. Mirko Bunzel)

01/2011-08/2012 **University of Minnesota-Twin Cities**, Minneapolis,  
MN, USA  
Major: „Food Science“  
Degree: Master of Science

09/2007-12/2010 **University of Minnesota-Twin Cities**, Minneapolis,  
MN, USA  
Major: „Food Science“  
Major: „Nutrition Science“  
Degree: Bachelor of Science

08/2006-05/2007 **Rochester Community and Technical College**,  
Rochester, MN, USA

09/2004-05/2006 **Association Free Lutheran Bible School**, Plymouth,  
MN, USA  
Degree: Certificate of Biblical Studies

08/2000-05/2004 **Oxbow Academy (Home school)**, Byron, MN, USA  
Degree: High School Diploma

## Awards and Scholarships

---

06/2015 Institut Danone Travel Scholarship  
2013-2014 American Association of Cereal Chemists International  
Endowment Fund Fellowship  
2012-2013 American Association of Cereal Chemists International,  
Elvira A. Tarleton Fellowship  
2012 MN-Institute of Food Technologists graduate scholarship  
2011 MN-Institute of Food Technologists graduate scholarship  
13. Mai 2011 Student speaker at the University of Minnesota's College of  
Food, Agricultural, and Natural Resource Sciences graduation  
ceremony  
08/2007-12/2010 University of Minnesota College of Food, Agricultural and  
Natural Resource Sciences Dean's List  
09/2010 University of MN Women's Club scholarship  
09/2010 Federal National SMART Grant



# Publications List

---

## PUBLICATIONS IN PEER-REVIEWED JOURNALS

- R.R. Schendel**, A. Becker, C.E. Tyl, M. Bunzel. Isolation and characterization of feruloylated arabinoxylan oligosaccharides from the perennial cereal grain intermediate wheat grass (*Thinopyrum intermedium*). *Carbohydr. Res.* **2015**, 407:16-25. Submitted October 16, 2014.
- R.R. Schendel**, C. Karrer, D. Bunzel, M. Huch, A.A. Hildebrand, S.E. Kulling, M. Bunzel. Structural Transformation of 8-5-Coupled Dehydrodiferulates by Human Intestinal Microbiota. *J. Agric. Food Chem.* **2015**, 63:7975-7985. Submitted July 1, 2015.
- R.R. Schendel**, M.R. Meyer, M. Bunzel. Quantitative profiling of feruloylated arabinoxylan side chains from graminaceous cell walls. *Front. Plant Sci.* **2015**, 6:1249 (11 pages). Submitted November 18, 2015.
- R.R. Schendel**, A. Puchbauer, N. Britscho, M. Bunzel. Feruloylated wheat bran arabinoxylans: Isolation and characterization of acetylated and *O*-2-monosubstituted structures. *Cereal Chem.* **2016**, (Accepted, in press). Submitted December 18, 2015.
- R.R. Schendel**, A. Puchbauer, M. Bunzel. Glycoside hydrolase family 51  $\alpha$ -L-arabinofuranosidases from *Clostridium thermocellum* and *Cellvibrio japonicas* release *O*-5-feruloylated arabinose. *Cereal Chem.* **2016**, (Accepted, in press). Submitted January 20, 2016.
- M.B. Kantar, C.E. Tyl, K. Dorn, X. Zhang, J. Jungers, J.M. Kaser, **R.R. Schendel**, J. Eckberg, B.C. Runck, M. Bunzel, N.R. Jordan, R.M. Stupar, M.D. Marks, J.A. Anderson, G.A. Johnson, C.C. Sheaffer, T. Schoenfuss, B. Ismail, G.E. Heimpel, D. Wyse. Perennial grain and oilseed crops. *Annu. Rev. Plant Biol.* **2016**, 67:703-729. Submitted August 15, 2015.

## BOOK CHAPTERS

- M. Bunzel, **R.R. Schendel**. Determination of (Total) Phenolics and Antioxidant Capacity in Food and Ingredients. In *Food Analysis*, 5<sup>th</sup> edition. S.S. Nielsen, Ed. Submitted January 30, 2016.

## PRESENTATIONS AT SCIENTIFIC CONFERENCES

### ORAL PRESENTATIONS

Conversion of 8-5-coupled dehydrodiferulates by human intestinal microbiota. **AACC International Centennial Meeting**, Minneapolis, MN, USA, October 2015.

Feruloylated arabinoxylans as cell wall components of cereal grains. **1. KIT Rice Symposium**, Karlsruhe, Germany, October 2015.

Metabolism of 8-5-coupled dehydrodiferulates by human intestinal microbiota. **6th International Dietary Fibre Conference 2015**, Paris, France, June 2015.

Charakterisierung der mit Ferulasäure veresterten Arabinoxylane aus der mehrjährigen Getreidesorte *Thinopyrum intermedium* – Characterization of the feruloylated arabinoxylans from the perennial grain *Thinopyrum intermedium*. **Arbeitstagung des Regionalverbandes Südwest der Lebensmittelchemischen Gesellschaft**, Neustadt an der Weinstraße, Germany. March 2014.

#### **POSTER PRESENTATIONS**

**R.R. Schendel**, U. Schmitt, M. Bunzel. Quantitative HSQC-NMR screening of feruloylated arabinoxylan side-chain profiles in cereal grains. **XIII International Conference on the Applications of Magnetic Resonance in Food Science**, Karlsruhe, Germany, June 2016.

**R.R. Schendel**, A. Puchbauer, M. Bunzel. Comparison of the action of three GH 51  $\alpha$ -L-arabinofuranosidases on feruloylated arabinoxylan-oligosaccharides. **AACC International Centennial Meeting**, Minneapolis, Minnesota, USA, October 2015.

**R.R. Schendel**, I. Sackmann, M. Bunzel. Isolation and identification of  $\alpha$ -xylopyranosyl-(1 $\rightarrow$ 3)-arabinose as an oligomeric side chain from maize arabinoxylans. **AACC International Centennial Meeting**, Minneapolis, Minnesota, USA, October 2015.

**R.R. Schendel**, N. Britscho, I. Sackmann, M. Bunzel. New structural characteristics from wheat and maize arabinoxylans. **2015 Deutscher Lebensmittelchemikertag**, Karlsruhe, Germany, September 2015.

**R.R. Schendel**, M. Meyer, M. Bunzel. Development of a quantitative screening method for comparison of feruloylated arabinoxylan side chain profiles in cereal grains. **6th International Dietary Fibre Conference 2015**, Paris, France, June 2015.

**R.R. Schendel**, A. Becker, M. Bunzel. Characterization of feruloylated arabinoxylans from the perennial grain species intermediate wheat grass (*Thinopyrum intermedium*). **AACC International Centennial Meeting**, Providence, RI, USA, October 2014.

**R.R. Schendel**, M. Meyer, M. Bunzel. Entwicklung einer HPLC-DAD Methode zum Screening und zur Quantifizierung der mit Ferulasäure veresterten Seitenketten von Arabinoxylanen – Development of an HPLC-DAD method for quantitative screening of feruloylated side chains from arabinoxylans. **2014 Deutscher Lebensmittelchemikertag**, Gießen, Germany, September 2014.

**R.R. Kylo**, M. Bunzel. Effect of cereal grains on the formation of heterocyclic aromatic amines in fried beef patties. **2012 Deutscher Lebensmittelchemikertag**, Münster, Germany, September 2012.